

A Systemic Approach to Palmprint Identification

A thesis submitted during March 2015 to the University of Hyderabad in partial
fulfillment of the award of Ph.D. degree

by

Kalluri Hemantha Kumar



School of Computer & Information Sciences

University of Hyderabad

(P.O.) Central University, Gachibowli

Hyderabad – 500 046

Telangana

India



CERTIFICATE

This is to certify that the thesis entitled **A Systemic Approach to Palmprint Identification** submitted by **Kalluri Hemantha Kumar** bearing Reg. No. 07MCPC01 in partial fulfillment of the requirements for the award of **Doctor of Philosophy in Computer Science** is a bonafide work carried out by him under our supervision and guidance, which is a plagiarism free thesis.

The thesis has not been submitted previously in part or in full to this or any other University or Institution for the award of any degree or diploma.

Dr M. V. N. K. Prasad
Associate Professor
IDRBT
Castle Hills, Masab Tank
Hyderabad – 500057.

Prof. Arun Agarwal
Professor
School of Computer and Information Sciences
University of Hyderabad
Hyderabad – 500046.

Dean
School of Computer and Information Sciences
University of Hyderabad
Hyderabad – 500046

DECLARATION

I, **Kalluri Hemantha Kumar**, hereby declare that this thesis entitled **A Systemic Approach to Palmprint Identification** submitted by me under the guidance and supervision of **Dr M.V.N.K. Prasad and Prof. Arun Agarwal** is a bonafide research work, which is also free from plagiarism. I also declare that it has not been submitted previously in part or in full to this University or any other University or Institution for the award of any degree or diploma. I hereby agree that my thesis can be deposited in Shodganga / INFLIBNET.

Date:

Name: Kalluri Hemantha Kumar

Signature of the student

Reg. No: 07MCPC01

ABSTRACT

Biometrics play an important role in personal authentication/identification. Palmprint identification is one of the emerging areas in biometrics. Region of Interest (ROI) extraction is an important task for palmprint identification. Earlier reported works used fixed size ROI for the recognition of palmprints. When the fixed size ROI is used, the palm area taken up for recognition is less compared to dynamic ROI extraction. The proposed method focuses on extraction of maximum possible rectangular shape ROI compared to existing fixed and dynamic ROI extraction techniques. The experimental results demonstrate that the proposed approach extracts better ROI on three databases, 1. The PolyUPalmprint Database, 2. CASIA Palmprint Image Database and 3. IIT Delhi Touchless Palmprint Database, when compared to the existing fixed size and dynamic ROI extraction techniques.

Feature selection plays a vital role in the performance of the palmprint identification system. We proposed two feature extraction techniques such as Wide Principal Line Features (WPLF) and Statistical Features (SF). A set of wide principal line extractors are devised to extract WPLF. Later these wide principal line extractors are used to extract the wide principal lines from ROI. To generate the SF, the ROI is segmented into overlapping segments by six schemes and the features are extracted directly from the segments. The proposed approach focuses on extraction of SF based on standard deviation and coefficient of variation.

We proposed palmprint verification and two-phase palmprint identification algorithms can be applied on WPLF and SF. We proposed an algorithm to determine the parameters required for verification and identification. To test the effectiveness of the proposed system, conducted several experiments with the data sets used by the previous researchers. The results show that the Correct Identification Rate (CIR) of the

proposed approach is better than existing methods.

ACKNOWLEDGEMENTS

I owe my deepest gratitude to my supervisors **Prof. Arun Agarwal and Dr M. V. N. K. Prasad** whose valuable guidance and support from preliminary to concluding level enabled me to develop an understanding of the subject. I am thankful to them for their patience and constant encouragement in motivating me with the words of hope throughout this work. It is pleasure to thank DRC committee **Prof. C. Raghavendra Rao and Prof. Chakravarthy Bhagyati** for their valuable suggestions in completing this work.

I wish to thank Dean, School of Computer and Information Sciences, **Prof. Arun K. Pujari** for providing me with the facilities. I would like to express my sincere thanks to all the faculty and staff members, for providing me the support whenever I need.

I wish to thank **VFSTR management and administration** for providing me with the facilities. I would like to avail this opportunity to thank my family members whose good wishes enabled me to pursue and achieve my goal.

Kalluri Hemantha Kumar

TABLE OF CONTENTS

ABSTRACT	i
ACKNOWLEDGEMENTS	iii
LIST OF FIGURES	xvi
LIST OF TABLES	xix
LIST OF ALGORITHMS	xx
GLOSSARY	xxii
1 Introduction	1
1.1 What is Pattern Recognition ?	2
1.2 Approaches to Pattern Recognition	2
1.3 Applications of Pattern Recognition	4
1.4 Biometric Recognition System based on Physical Characteristics . . .	4
1.4.1 Fingerprint Recognition System	6
1.4.2 Iris Recognition System	8
1.4.3 Face Recognition System	8
1.5 Palmprint Recognition System	9
1.5.1 Description of palmprint	9

1.5.2	Palmprint Scanners	9
1.5.3	Block Diagram of Palmprint Recognition System	12
1.5.4	Advantages of Palmprint Recognition System	13
1.5.5	Benchmark Databases	14
1.6	Motivation for the present work	14
1.7	Contributions	15
1.8	Organization of the thesis	16
2	Literature Survey	17
2.1	ROI Extraction Techniques	17
2.1.1	Static ROI Extraction	17
2.1.2	Dynamic ROI Extraction	20
2.2	Feature Extraction Techniques	21
2.2.1	Structural Features	21
2.2.2	Statistical Features	25
2.2.3	Other Features	27
2.3	Recognition Strategies	31
2.4	Fusion Techniques	36
2.5	Justification for the present work	40
3	Dynamic ROI Extraction	42
3.1	Binarization of the Palmprint Image	43
3.2	Localization of Key Points	46

3.3	Maximizing ROI	51
3.4	Registration	60
3.5	Experimental Results	61
3.5.1	Experiments on PolyUPalmprint Database	61
3.5.2	Experiments on CASIA Palmprint Image Database	64
3.5.3	Experiments on IIT Delhi Touchless Palmprint Database	67
3.6	Summary	70
4	Feature Extraction	71
4.1	Wide Principal Line Feature Extraction	72
4.1.1	Mask construction for line and curve extraction	73
4.1.2	Energy of ROI	76
4.1.3	Post-processing	78
4.1.4	WPLF extraction algorithm	81
4.1.5	WPLI database generation	82
4.2	Statistical Features Extraction	90
4.2.1	Segmentation of ROI region into blocks	90
4.2.2	Block feature extraction	92
4.2.3	Statistical feature extraction algorithm	93
4.3	Summary	95
5	Verification and identification	96
5.1	Palmprint Verification	98

5.2	Two-Phase Palmprint Identification	106
5.2.1	Generation of Feature Database	108
5.2.2	Palmprint Identification	115
5.3	Summary	119
6	Experimental Design & Analysis	120
6.1	Data Sets	120
6.2	Experiments using WPLF	121
6.2.1	Experiments on data set I	121
6.2.2	Experiments on data set II	123
6.2.3	Experiments on data set III	125
6.2.4	Experiments on data set IV	127
6.2.5	Experiments on data set V	129
6.3	Experiments using SF on ROI	132
6.3.1	Standard deviation as a feature	132
6.3.2	Coefficient of variation as a feature	138
6.3.3	Standard deviation and coefficient of variation as features . .	145
6.4	Experiments using SF on WPLI	152
6.4.1	Standard deviation as a feature	152
6.4.2	Coefficient of variation as a feature	160
6.4.3	Standard deviation and coefficient of variation as features . .	166
6.5	Summary	173

7	Conclusions and Future Directions	175
7.1	Conclusion	175
7.1.1	Papers Published	176
7.2	Future Directions	177

LIST OF FIGURES

1.1	An illustration of Biometric Recognition System.	5
1.2	Sample images of Biometrics (i)Fingerprint (ii) Eyes (Iris) (iii) Face. .	7
1.3	Sample Palmprint image.	10
1.4	The outlook of the multispectral palmprint image acquisition device.	11
1.5	The outlook of the scanners (i) hyperspectral palmprint image acquisition device (ii) LSCAN 1000PX.	11
1.6	An illustration of palmprint recognition system.	13
3.1	(i)&(iii) Sample palmprint images (ii)&(iv) binarized palmprint images.	44
3.2	Sample palmprint image to illustrate the size of the Structuring Element (SE) to be dynamic (i) palmprint image (ii) binarized image with SE size is 3 (iii) binarized image with SE size is 6.	45
3.3	(i) Sample palmprint image (ii) binarized image with SE is 3 (iii) binarized image with SE is 1.	45
3.4	Illustration of the Key Points (KPs) $P_1(x_1, y_1)$, $P_2(x_2, y_2)$ and $P_3(x_3, y_3)$ for the Right-Hand Palmprint.	46
3.5	Illustration of r_1 row, r_2 row, c column and Mid-Point (MP).	47
3.6	Non palmprint pixel is identified as MP (i)&(iii) palmprint images (ii)&(iv) binarized palmprint images.	48

3.7	Distance distribution diagram using n-coordinate values of border pixels.	49
3.8	Distance distribution diagram of the energy values.	49
3.9	Sample palmprint having very small portion of the finger (i) Palmprint image (ii) Binarized palmprint image.	50
3.10	Palmprint images to illustrate the KPs: P_1 and P_3 are aligned vertically (i) palmprint before alignment (ii) palmprint after alignment.	51
3.11	Sample palmprint image after applying the LocalizeROI algorithm. .	55
3.13	(i)&(iv) palmprint images (ii)&(vi) Static ROIs (iii)&(vii) Dynamic ROIs.	58
3.12	Sample ROIs before and after applying the MaximizeROI algorithm (i)&(iv) palmprint images (ii)&(v) ROIs before applying MaximizeROI algorithm (iii)&(vi) ROIs after applying MaximizeROI algorithm.	59
3.14	Illustration of the reference points DX and DY.	60
3.15	Schematic diagram for dynamic ROI registration.	61
3.16	The ROIs extracted using [16, 21] and proposed method on PolyU-Palmprint database.	63
3.17	The ROIs extracted using [16, 21] and proposed method on CASIA palmprint image database.	65
3.18	The ROIs extracted using [16, 21] and proposed method on IIT Delhi touchless palmprint database.	69
4.1	Palmprint image labelling with life line, head line and heart line. . .	72
4.2	Wide Principal Line Extractors with different orientations.	74
4.3	Wide Principal Line Extractors to extract curve region.	76
4.4	Sample ROIs.	77

4.5	Sample Energy_images.	77
4.6	Sample Lines_images.	78
4.7	Sample skeleton_images after applying the morphological skeleton operation.	79
4.8	Sample thin_line_images after eliminating noise pixels.	79
4.9	Sample thick_line_images after applying dilate operation with structuring element size 2.	80
4.10	Sample thick_line_images after applying dilate operation with structuring element size 3.	80
4.11	Sample thick_line_images after applying dilate operation with structuring element size 4.	80
4.12	Sample thick_line_images after applying dilate operation with structuring element size 5.	81
4.13	Sample thick_line_images after applying dilate operation with structuring element size 6.	81
4.14	Sample WPLIs.	82
4.15	Schematic diagram for dynamic WPLI database generation.	84
4.17	Number of pixels (average) extracted using WPLeS on Dynamic ROI database and sample number of values of sample ROIs.	84
4.16	Pixels extracted using each extractor of sample images	89
4.18	Schematic diagrams for segmenting the ROI into 128 x 128.	91
4.19	Schematic diagrams for segmenting the ROI into (i)&(ii) 16 x 16 (iii)&(iv) 8 x 8 blocks.	92

5.1	Thread diagram representing the palmprint verification and two-phase palmprint identification.	98
5.2	Common region of the two dynamic ROIs of the same palm (i)& (iii) dynamic ROIs (ii)& (iv) selected common regions from dynamic ROIs.	99
5.3	Schematic diagram for palmprint verification.	106
5.4	Schematic diagram for feature database generation.	113
5.5	Schematic diagram for palmprint identification.	116
6.1	FAR & FRR representation on data set I using WPLF.	122
6.2	ROC curve on data set I using WPLF.	123
6.3	FAR & FRR representation on data set II using WPLF.	124
6.4	ROC Curve on data set II using WPLF.	125
6.5	FAR & FRR representation on data set III using WPLF.	126
6.6	ROC Curve on data set III using WPLF.	126
6.7	FAR & FRR representation on data set IV using WPLF.	128
6.8	ROC Curve on data set IV using WPLF.	128
6.9	FAR & FRR representation on data set V using WPLF.	130
6.10	ROC Curve on data set V using WPLF.	130
6.11	FAR & FRR representation on data set I using STD as a feature.	133
6.12	ROC curve on data set I using STD as a feature.	134
6.13	FAR & FRR representation on data set II using STD as a feature.	134
6.14	ROC curve on data set II using STD as a feature.	135
6.15	FAR & FRR representation on data set III using STD as a feature.	135

6.16	ROC curve on data set III using STD as a feature.	136
6.17	FAR & FRR representation on data set IV using STD as a feature. . .	136
6.18	ROC curve on data set IV using STD as a feature.	137
6.19	FAR & FRR representation on data set V using STD as a feature. . .	137
6.20	ROC curve on data set V using STD as a feature.	138
6.21	FAR & FRR representation on data set I using CV as a feature. . . .	140
6.22	ROC curve on data set I using CV as a feature.	141
6.23	FAR & FRR representation on data set II using CV as a feature. . . .	141
6.24	ROC curve on data set II using CV as a feature.	142
6.25	FAR & FRR representation on data set III using CV as a feature. . . .	142
6.26	ROC curve on data set III using CV as a feature.	143
6.27	FAR & FRR representation on data set IV using CV as a feature. . . .	143
6.28	ROC curve on data set IV using CV as a feature.	144
6.29	FAR & FRR representation on data set V using CV as a feature. . . .	144
6.30	ROC curve on data set V using CV as a feature.	145
6.31	FAR & FRR representation on data set I using STD & CV as a feature.	147
6.32	ROC curve on data set I using STD & CV as a feature.	147
6.33	FAR & FRR representation on data set II using STD & CV as a feature.	148
6.34	ROC curve on data set II using STD & CV as a feature.	148
6.35	FAR & FRR representation on data set III using STD & CV as a fea- ture.	149
6.36	ROC curve on data set III using STD & CV as a feature.	149

6.37 FAR & FRR representation on data set IV using STD & CV as a feature.	150
6.38 ROC curve on data set IV using STD & CV as a feature.	150
6.39 FAR & FRR representation on data set V using STD & CV as a feature.	151
6.40 ROC curve on data set V using STD & CV as a feature.	151
6.41 FAR & FRR representation on data set I of WPLI database using STD as a feature.	154
6.42 ROC curve on data set I of WPLI database using STD as a feature.	154
6.43 FAR & FRR representation on data set II of WPLI database using STD as a feature.	155
6.44 ROC curve on data set II of WPLI database using STD as a feature.	155
6.45 FAR & FRR representation on data set III of WPLI database of WPLI database using STD as a feature.	156
6.46 ROC curve on data set III of WPLI database using STD as a feature.	156
6.47 FAR & FRR representation on data set IV of WPLI database using STD as a feature.	157
6.48 ROC curve on data set IV of WPLI database using STD as a feature.	157
6.49 FAR & FRR representation on data set V of WPLI database using STD as a feature.	158
6.50 ROC curve on data set V of WPLI database using STD as a feature.	158
6.51 FAR & FRR representation on data set I of WPLI database using CV as a feature.	161
6.52 ROC curve on data set I of WPLI database using CV as a feature.	162

6.53 FAR & FRR representation on data set II of WPLI database using CV as a feature.	162
6.54 ROC curve on data set II of WPLI database using CV as a feature. . .	163
6.55 FAR & FRR representation on data set III of WPLI database using CV as a feature.	163
6.56 ROC curve on data set III of WPLI database using CV as a feature. .	164
6.57 FAR & FRR representation on data set IV of WPLI database using CV as a feature.	164
6.58 ROC curve on data set IV of WPLI database using CV as a feature. .	165
6.59 FAR & FRR representation on data set V of WPLI database using CV as a feature.	165
6.60 ROC curve on data set V of WPLI database using CV as a feature. . .	166
6.61 FAR & FRR representation on data set I of WPLI database using STD & CV as a feature.	168
6.62 ROC curve on data set I of WPLI database using STD & CV as a fea- ture.	168
6.63 FAR & FRR representation on data set II of WPLI database using STD & CV as a feature.	169
6.64 ROC curve on data set II of WPLI database using STD & CV as a feature.	169
6.65 FAR & FRR representation on data set III of WPLI database using STD & CV as a feature.	170
6.66 ROC curve on data set III of WPLI database using STD & CV as a feature.	170

6.68	ROC curve on data set IV of WPLI database using STD & CV as a feature.	171
6.67	FAR & FRR representation on data set IV of WPLI database using STD & CV as a feature.	171
6.69	FAR & FRR representation on data set V of WPLI database using STD & CV as a feature.	172
6.70	ROC curve on data set V of WPLI database using STD & CV as a feature.	172

LIST OF TABLES

2.1	ROI Extraction Techniques	22
2.2	Structural feature extraction techniques	25
2.3	Transformations applied before extracting statistical features	27
2.4	Feature extraction techniques	30
2.5	Recognition Techniques	35
2.6	Fusion Techniques	40
3.1	Number of ROIs with background information using proposed approach, static approach [21] and dynamic approach [16] on PolyUPalmprint database	62
3.2	Maximum, minimum and average height, width for ROI extraction and percentage of background in ROI using Proposed approach, Static approach [21] and Dynamic approach [16] on PolyUPalmprint database	62
3.3	Maximum, minimum and average time in seconds for dynamic ROI extraction of the proposed approach on PolyUPalmprint database . .	64
3.4	Number of ROIs with background information using proposed approach, static approach [21] and dynamic approach [16] on CASIA palmprint image database	66
3.5	Maximum, minimum and average height, width for ROI extraction and percentage of background in ROI using proposed approach, static approach [21] and dynamic approach [16] on CASIA palmprint image database	66

3.6	Maximum, minimum and average time in seconds for dynamic ROI extraction of the proposed approach on CASIA palmprint image database	66
3.7	Number of ROIs with background information using proposed approach, static approach [21] and dynamic approach [16] on IIT Delhi touchless palmprint database	68
3.8	Maximum, minimum and average Height, Width for ROI extraction and percentage of background in ROI using proposed approach, static approach [21] and dynamic approach [16] on IIT Delhi touchless palmprint database	68
3.9	Maximum, minimum and average time in seconds for dynamic ROI extraction of the proposed approach on IIT Delhi touchless palmprint database	68
4.1	Maximum, minimum and average time in seconds for WPLF extraction on dynamic ROI of PolyUPalmprint database	90
4.2	Sample statistical feature vector sizes of dynamic ROIs / WPLIs	94
4.3	Maximum, minimum and average time in seconds for statistical feature extraction on dynamic ROI of PolyUPalmprint database	95
5.1	Sample images of common region of Dynamic ROI	111
5.2	Sample images of common region of WPLI	112
6.1	Decidability Index (DI) and Equal Error Rate (EER) analysis using WPLF on PolyUPalmprint database	123
6.2	Performance comparison of approaches [23, 24, 61, 62, 95, 99, 101] and proposed approach using WPLF on PolyUPalmprint database	129
6.3	Time required for identification using WPLF (in seconds)	129

6.4	Performance comparison of approach [66] and proposed approach using WPLF and SF on Data Set V of PolyUPalmprint database	131
6.5	Decidability index (DI) and equal error rate (EER) analysis using SF .	138
6.6	Performance comparison (CIR) of approaches [23, 24, 61, 62, 95, 99, 101] and the proposed approach using SF on PolyUPalmprint database	139
6.7	Time required for identification using SF (in seconds)	152
6.8	Performance (DI) comparison of the proposed approach using SF on ROI and WPLI databases	159
6.9	Performance (EER) comparison of the proposed approach using SF on ROI and WPLI databases	159
6.10	Performance (CIR) comparison of the proposed approach using SF on ROI and WPLI databases	160
6.11	Time required for identification on WPLI using SF (in seconds)	173

List of Algorithms

3.1	KPsExtract(F_1): To identify Key Points (KPs) position	52
3.2	LocalizeROI(BP, y_1 , v_1 , v_3): To identify the location of the ROI . . .	54
3.3	MaximizeROI(X_T , X_B , R_1 , R_2 , x_2 , y_1): To extract maximum possible ROI	57
4.4	WPLFExtract(ri, T_1 , T_3): To generate Wide Principal Line Image(WPLI)	83
4.5	SFExtract(ri, T_1 , T_2): To extract statistical features	93
5.6	CommonRegExtract(r_1 , r_2 , d_{x1} , d_{y1} , d_{x2} , d_{y2}) : To extract common region of two dynamic ROIs (or) WPLIs	100
5.7	EERExtract(ISS , GSS , $ISScount$, $GSScount$) : To identify EER and $threshold_c$ from genuine and imposter similarity scores	103
5.8	PALMVER($database$, $query\ palmprint$, $Palmprint_{Id}$, $Threshold_c$): To perform palmprint verification	105
5.9	FDBGGENERATE($database$,u): To generate the feature database .	110
5.10	ParamID($FeatureDatabase$): To identify the parameters, to be used in palmprint identification algorithm	114
5.11	PalmID($Query\ Palmprint$, $FeatureDatabase$, $database$): To identify the palmprint from the database images	117

GLOSSARY

BP	Border Pixel
CD	Canberra Distance
CI	Correct Identification
CIR	Correct Identification Rate
CV	Coefficient of Variation
DCT	Discrete Cosine Transform
DI	Decidability Index
DD	Dissimilarity Distance
EER	Equal Error Rate
EM	Expectation Maximization
EV	Energy Value
FAR	False Acceptance Rate
FRAT	Finite Radon Transform
FRR	False Rejection Rate
KPs	Key Points
GSS	Genuine Similarity Score
ISS	Imposter Similarity Score
IT	Number of Iterations
MDD	Minimum Dissimilarity Distance
MFRAT	Modified Finite Radon Transform
MP	Mid Point
MS	Matching Score
ROI	Region of Interest

SD	Standard Deviation
SDD	Sorted Dissimilarity Distances
SE	Structuring Element
SF	Statistical Features
SS	Similarity Score
TH	Threshold
WPLE	Wide Principal Line Extractor
WPLF	Wide Principal Line Features
WPLI	Wide Principal Line Image

CHAPTER 1

Introduction

Automatic recognition of humans is a very essential for law enforcement (e.g., criminal investigation), government (e.g., border control, R & D labs), commercial (e.g., logical and physical access control) applications, industries, educational institutions, public places such as airports, ports and shopping complexes etc. With increased emphasis on national and global security, there is a growing and urgent need to automatically identify humans both locally and remotely on a routine basis. Traditionally documents used for human identification are pass ports, pan cards, voter cards, ration cards, driving licences, employee identification cards, bank pass books etc. But these are susceptible for forgery. Biometric based systems are possibly the best solution to overcome the above problem for human recognition [1, 2].

Further, the relevance of biometrics [3] in modern society is reinforced by the need for large-scale identity management systems whose functionality relies on the accurate determination of an individual's identity in the context of several different applications. Examples of these applications include sharing networked computer resources, granting access to nuclear facilities, performing remote financial transactions or boarding a commercial flight. The proliferation of web-based services (e.g., online banking, e-transactions) and the deployment of decentralized customer service centers (e.g., credit cards) have further underscored the need for reliable identity management systems that can accommodate a large number of individuals.

In order to understand the biometric system we briefly digress and discuss the definition and the basic approaches to pattern recognition.

1.1 What is Pattern Recognition ?

Pattern is a real time data such as images of face, fingerprint, palmprint, sound data, text data etc. Pattern Recognition [4] is automatic (machine) recognition, classification, description and grouping of patterns. Pattern Recognition is widely used in engineering and scientific disciplines. There are two types of recognition algorithms, such as verification and identification. Verification is used for checking whether the pattern meets requirements, specifications and that it fulfils its intended purpose. In identification, the system performs a one-to-many comparison against a pattern database, to establish the identity of an unknown pattern. The system will succeed in identifying the pattern, if the comparison of the pattern sample to a template in the pattern database falls within a previously set threshold.

Pattern recognition [5] also involves classification and clustering of patterns. Assign an appropriate class label to a pattern based on an abstraction that is generated using a set of training patterns or domain knowledge is called classification. Partition the data to perform decision making, is called clustering.

1.2 Approaches to Pattern Recognition

Statistical Pattern Recognition

To determine the category / class label for a given sample belongs to [feature vector] through observation and measurements. The statistical pattern recognition [4] has been most intensively studied and used in practice. The most widely used approaches [6] are Bayes decision theory, optimal rules, density estimation, decision boundary construction, linear discriminant analysis, non-linear discriminant analysis such as kernel methods and projection methods, tree-based methods, and cluster analysis. In these approaches each pattern is represented as a feature set or measurements and viewed as a feature space. Based on the training patterns, decision boundaries in the feature space is determined using probabilistic distribution. These decision boundaries separates

patterns belong to different classes.

Structural Pattern Recognition

The comparison is made by a symbolic match that computes a measure of similarity between the unknown input and a number of prototype models. The patterns are represented using strings, graphs, digraphs. String kernel functions and graph kernel functions are available to effectively represent the patterns. General kernel theory is used for effective classification and clustering.

The structural methods [4, 7] are based on explicit or implicit representation of a pattern's structure, where structure conceptually represents the characteristic way sub-patterns of a pattern related together. The quantitative measures are structural complexity, structural distance between class, structural information content. The structured pattern recognition is widely used in unsupervised classification and clustering algorithms.

Syntactic Pattern Recognition

A parser checks an unknown input whether it is accordance with the rules of a grammar that desemles all members of a pattern class. Syntactic pattern recognition [4, 7] can be used if there is a clear structure in the patterns. One way to present such structure is by means of strings of symbols from a formal language. In this case the differences in the structures of the classes are encoded as different grammars.

One of the syntactic pattern recognition approach [8] is to relate the structure of patterns with the syntax of a formally defined language.

Artificial Neural Networks

Artificial Neural Networks [9] has been an enabling methodology for pattern recognition and practice. Neural networks [4] have been used to solve a wide variety of tasks in pattern recognition that are hard to solve using ordinary rule-based programming. The neural network techniques and methods from statistical learning theory

have been increasing attention. The most widely used neural networks for pattern classification are feed-forward neural network, radial-basis function (RBF) networks. Self-organising map (SOM) and Kohonen-network (KN) are the most popular neural networks for data clustering and feature mapping. Combine Artificial Neural Networks [12] with other well established paradigms, like evolutionary computation , fuzzy logic, rough sets etc., is one of the emerging research area.

1.3 Applications of Pattern Recognition

Pattern Recognition [5] is used in a wide variety of areas including bioinformatics, data mining, document classification, document image analysis, industrial automation, multimedia, biometrics, remote sensing, speech processing, transportation, finance, agriculture, education, military, medicine and entertainment.

Specific applications of pattern recognition [4] are DNA sequence analysis, searching for meaningful patterns from huge data, internet search for semantic categories, reading machine for the blind (ex. Adobe reader), printed circuit board inspection for industries and diagnosing diseases. Biometrics is widely used for personal recognition such as face recognition, iris recognition, fingerprint recognition, palmprint recognition and multimodal recognition systems. Pattern recognition is also used to forecast whether, crop yield based on the growth patterns of crops, telephone directory enquiry without operator assistance and expert systems.

1.4 Biometric Recognition System based on Physical Characteristics

Biometric Recognition System [1] is basically pattern recognition system consisting of four modules, such as i) data acquisition ii) signal/ image pre-processing iii) feature extraction and iv) feature matching. The block diagram of a generic biometric recog-

nition system is shown in Figure 1.1.

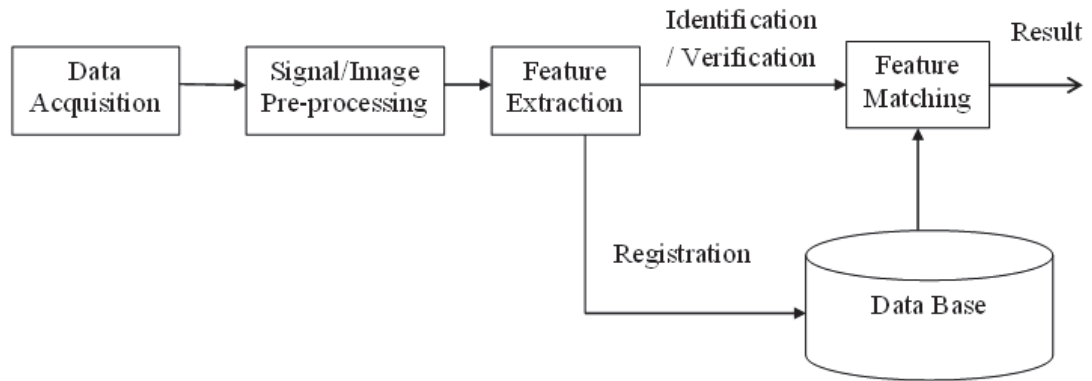


Figure 1.1: An illustration of Biometric Recognition System.

The sensors or transducers are used for data acquisition. The most widely used sensors are camera, voice recorders etc. Sensor configuration depends on the application. For example, fingerprint recognition requires high resolution sensors whereas palmprint recognition requires low resolution sensors. Signal / image pre-processing is the next important step in biometric recognition system. At the time of data acquisition, there is a possibility of inclusion of noise, unwanted background information and foreign objects inclusion etc. In pre-processing, various filters (such as low pass, high pass filters) are used to remove the noise. Segmentation is used to remove the background and foreign objects. Histogram equalisation, normalization etc., are used for illumination adjustment.

Proper feature selection is the crucial step in biometric recognition system. The features may be local features or global features. The most widely used features are statistical features and structural features. Number of features to be used may vary, based on the application, i.e. in some applications only one feature is sufficient and in some other applications may require more number of features. The chosen feature must satisfy the universality and distinguishable. For every database pattern, extract the features and stored in the database. Based on the database information, the system

generates knowledge, later, the generated knowledge is used for matching. Feature matching is used for verification and identification. In feature matching, the query pattern features are compared with database features.

Biometrics [3] is the science of establishing the identity of an individual based on the physical or behavioural attributes of the person. Physical attributes or characteristics are fingerprint, iris, face recognition, palmprint recognition etc. Behavioural characteristics are related to pattern of a person like gait, voice etc.

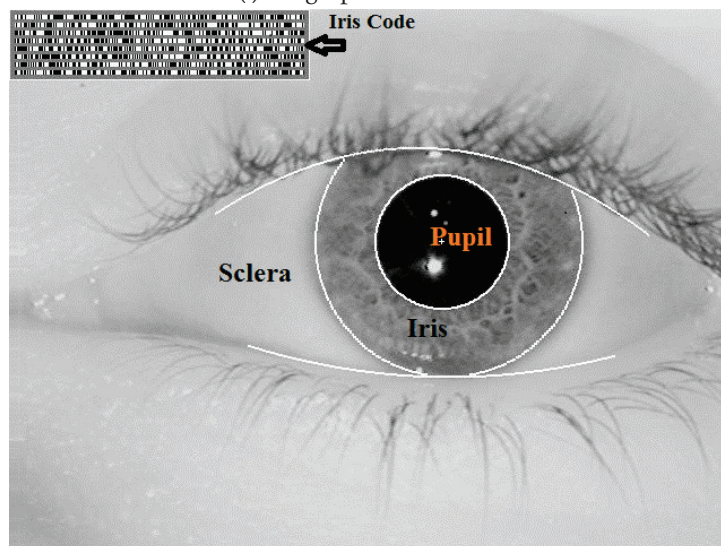
We now provide a short description of biometric system based on physical characteristics and discuss in more detail about palmprint recognition system.

1.4.1 Fingerprint Recognition System

The popular biometric trait is the fingerprint. Fingerprint [3] consists of ridges and valleys on the surface of a fingertip whose formation is determined during the first seven months of fetal development. It has been experimentally determined that the fingerprints of identical twins are different and so are the prints on each finger of the same person [10]. Fingerprints are widely used in physical access control, logical access control, transaction authentication, device access control, civil control, forensic identification. Now a days small organisations are also using the fingerprint recognition systems for monitoring the punctuality and regularity (i.e. enter to the organisation and leave from the organisation) of employees. Some of the operating systems (windows 7, windows 8) are using fingerprint for user authentication. Fingerprints are also been used in "Aadhaar Card" for authenticating individuals. A sample fingerprint image is shown in Figure 1.2(i).



(i) Fingerprint



(ii) Eye



(iii) Face

Figure 1.2: Sample images of Biometrics (i)Fingerprint (ii) Eyes (Iris) (iii) Face.

1.4.2 Iris Recognition System

Iris [11] is the protected internal organ of the eye. Each iris has a unique structure which is stable and unchanging throughout life. The iris image is captured in a controlled environment. The iris recognition is accurate and widely used biometric trait, but it has limitations. The iris acquisition devices [3] are expensive and create inconvenience to the user. However, recently iris biometric is widely been used in public distribution system and Aadhaar authentication system etc. A sample iris image and its iris code is shown in Figure 1.2(ii).

1.4.3 Face Recognition System

Face Recognition System is used for automatic identification or authentication of a person in a digital image or video frame from a video source. Facial recognition algorithms are used to extract facial features by extracting landmarks or features from the subject's face. Face Recognition algorithms are classified into two types one is geometric approach [13]; it is mostly depending upon the identification of landmarks and also relation among pose variations. The second one is statistical or template matching approach; in this a face can be treated as a pattern and uses general pattern matching / classification algorithms for face recognition. A sample face image is shown in Figure 1.2(iii).

While the authentication performance of the commercial face recognition systems is reasonable, but they impose a number of restrictions [11] on how the facial images are obtained, often requiring a fixed and simple background with controlled illumination. These systems also have difficulty in matching face images captured from two different views, under different illumination conditions, and at different times. It is questionable whether the face itself is a sufficient basis for recognizing a person from a large number of identities with an extremely high level of confidence.

1.5 Palmprint Recognition System

1.5.1 Description of palmprint

Palmprint is a region between the wrist and the fingers, contains information [1] like principal lines, wrinkles, ridges, minutiae points, datum points etc. These details provide more information when compared to fingerprints and so palmprint is considered as the better biometric for human identification. Palmprint images are classified into two categories [14], such as low resolution palmprint images and high resolution palmprint images. Low resolution palmprint images (around 500 or less dpi) are widely used in online personal authentication and identification. High resolution palmprint images (around 1000 dpi) are used in forensics and law enforcement. Palmprints can be used for fortune telling, health diagnosis, personal recognition such as criminal, forensic and commercial applications.

A sample palmprint image is shown in Figure 1.3, it shows the principal lines such as life line, head line and heart line, wrinkles and ridges. Principal lines [1] structure and thicknesses are vary from person to person. In the principal lines, life line is the first line developed in the embryo. Some wrinkles are congenital, while others are acquired by life time grip/grasp activities of a hand. Ridges are raised above general level of the skin.

1.5.2 Palmprint Scanners

Palmprint recognition is a newly emerging area. Various research groups have tried to collect palmprint data using scanners, digital cameras and even inked image. However, there has been a great disparity between the palmprints captured by those devices. A brief review of a few popular palmprint acquisition devices is as follows:

- The Biometric Research Centre (UGC/CRC) at the Hong Kong Polytechnic University has developed the following scanners :

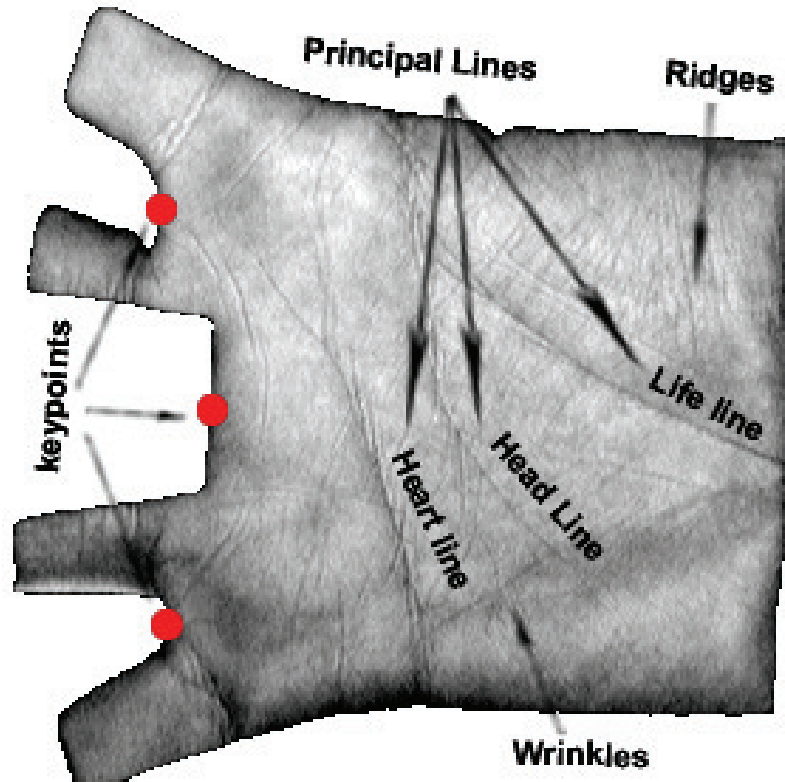


Figure 1.3: Sample Palmprint image.

1. A real time palmprint capture device has used it to construct a large-scale palmprint database.
2. A real time multispectral palmprint capture device which can capture palmprint images under blue, green, red and near-infrared (NIR) illuminations, and has used it to construct a large-scale multispectral palmprint database. The outlook of the multispectral palmprint image acquisition device is shown in Figure 1.4.
3. A hyperspectral palmprint capture device can capture palmprint images from 420 nm-1100 nm, and has used it to construct a large-scale hyperspectral palmprint database. The outlook of the hyperspectral palmprint image acquisition device is shown in Figure 1.5(i).

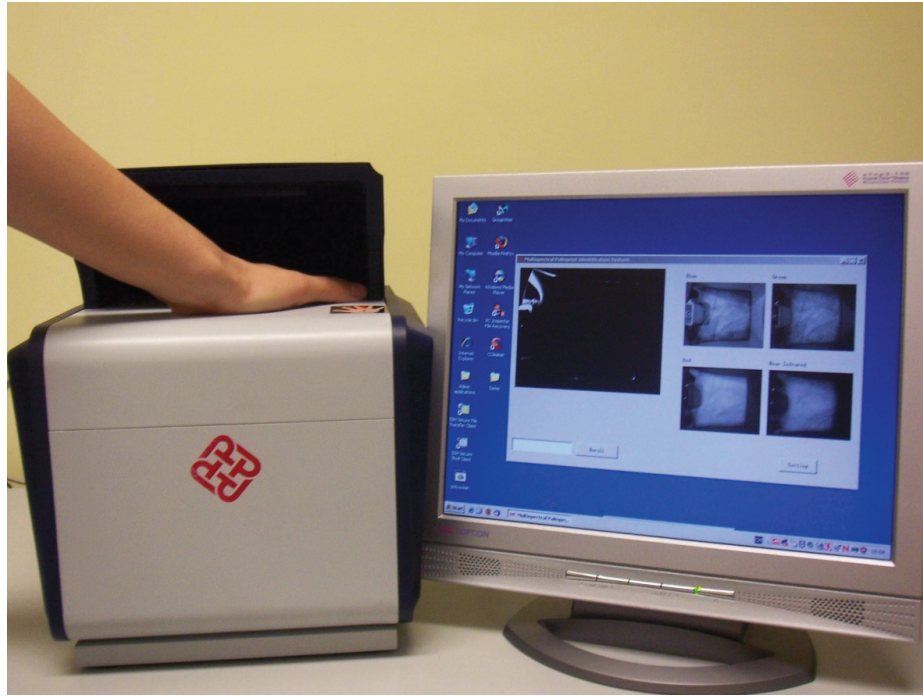
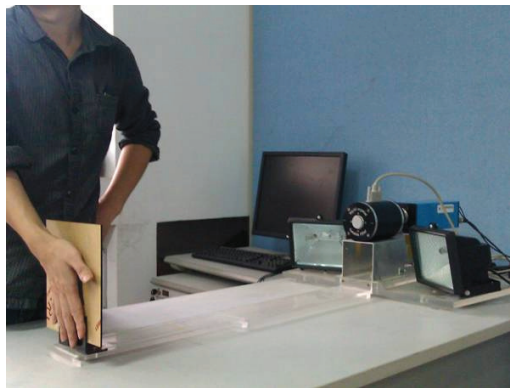


Figure 1.4: The outlook of the multispectral palmprint image acquisition device.



(i) hyperspectral palmprint image acquisition device



(ii) LSCAN 1000PX

Figure 1.5: The outlook of the scanners (i) hyperspectral palmprint image acquisition device (ii) LSCAN 1000PX.

- The real time applications using palmprints, LSCAN 1000PX is available in market, it is one of the fastest and smallest palmprint scanner and it generates the images with resolution 1000 pixels per inch. The LSCAN 1000PX is shown in Figure 1.5(ii). LSCAN 500P is an optical palmprint and fingerprint scanner with IEEE 1394 (FireWire) interface. The scanner is able to scan:
 - Palmprints - upper, lower and writer's palms (ANSI/NIST compliant).
 - Flat fingerprints - up to 4 fingers can be scanned simultaneously, allowing capture of all 10 fingers as 4+4+2 scans.
 - Rolled fingerprints - single rolled fingerprints can be captured.
 - Resolution was 500 ppi, and image capturing area 5.0" x 5.1".

1.5.3 Block Diagram of Palmprint Recognition System

The block diagram of the palmprint recognition system is shown in Figure 1.6. Palmprint scanner is used to acquire the palmprint image. The acquired palmprint image is pre-processed. In pre-processing, various filters (such as low pass, high pass filters), histogram equalization, normalization may be used to enhance the palmprint image. Most of the researchers also use segmentation to remove the background and foreign objects. Later, features are extracted from the pre-processed palmprint image. Extracted features are stored in the database for registration otherwise compared with database for recognition.

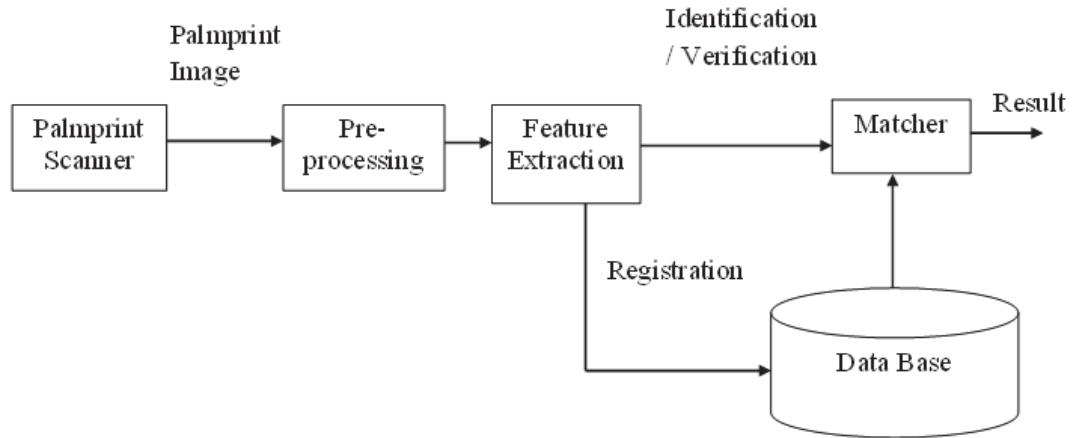


Figure 1.6: An illustration of palmprint recognition system.

1.5.4 Advantages of Palmprint Recognition System

Compared to all these biometric features, the use of palmprint has the following advantages [1].

1. Compared with the fingerprint, the palmprint provides a larger surface area so that more features can be extracted.
2. An individual is less likely to damage a palm than a finger, and the line features of a palm are stable throughout one's lifetime.
3. Small amounts of dirt or grease sometimes appear on an individual's finger adversely affecting the performance of fingerprint verification. This problem does not arise in palmprint verification / identification.
4. Compared with the 3D hand geometry, palmprints have more unique features that can be used for personal identification, so a better performance can be expected.

1.5.5 Benchmark Databases

Benchmark databases are used by the most of the researchers to test the effectiveness of their proposed algorithms. Generally, these databases are available online with free of cost. Standard databases available are PolyUPalmprint Database [17], CASIA Palmprint Image Database [18] and IIT Delhi Touchless Palmprint Database [19].

PolyUPalmprint Database contains 7752 gray scale images corresponding to 386 different palms in BMP image format. Around 20 images from each palm are collected in two sessions. The average interval between the first and second session was 69 days. In the second session, the light source was changed and adjusted the focus of the CCD camera so that the images collected in the first and the second session could be regarded as being captured by different palmprint acquisition devices. The images are acquired by placing pegs and using CCD at a spatial resolution of 75 dpi and 256 gray levels.

CASIA Palmprint Image Database contains 5502 images captured from 312 individuals in 8bit JPEG image format.

IIT Delhi Touchless Palmprint Database [19] contains 2760 images captured from 233 individuals in 8bit JPEG image format.

1.6 Motivation for the present work

The central region of the palmprint is referred as Region of Interest (ROI) [15]. The central region of the palmprint contains core features and thus has become focus of interest for palmprint analysts. Therefore, ROI extraction must be a primary step in palmprint registration, verification and identification process. Static Region of Interest (ROI), commonly referred to as a fixed size ROI used for palmprint identification has some inherent limitations. When a fixed size ROI is used for the palm area it may lead to extraction of unnecessary data like background area. For example in case palmprint size of a child being less than the size of static ROI, the ROI includes background or ROI size is smaller than an adult palm may lead to omission of some valuable data.

A more generalized rectangular shape dynamic ROI is needed that would mitigate the disadvantages listed.

Selection of a proper feature set and its extraction plays an important role in the palmprint verification and identification. The palmprint features can be extracted either from principal lines or using some statistical measures on the image. Principal lines extraction is an established step for palmprint verification and identification. Thin principal lines are sometimes similar for different users. Therefore, Wide Principal Line Feature (WPLF) extraction has to be explored. Statistical Features (SF) are extracted after applying transformation such as Gabor filter, Fourier transform etc. Hence, Statistical Features (SF) extraction without using transformations has to be explored. We need to explore a suitable palmprint verification & identification algorithm that can use either Wide Principal Line Features (WPLF) or Statistical Features (SF).

Motivation is to develop a palmprint identification system through dynamic ROI extraction using WPLF and SF techniques.

1.7 Contributions

This thesis presents the following contributions made in palmprint recognition.

1. Dynamic ROI extraction algorithm is proposed to extract maximum possible rectangular shape ROI and reference point information from palmprint.
2. Proposed an algorithm to extract maximum possible common region from given Dynamic ROIs.
3. Wide principle line extractors are proposed to extract wide principal lines contained in dynamic ROI.
4. Proposed a local statistical feature extraction method based on the sliding window concept.

5. Proposed an architecture of a complete system. It shows interaction between different components to perform palmprint verification and identification using two-phase model.

1.8 Organization of the thesis

The rest of the chapters in the thesis are organized as follows: Chapter 2 presents a survey of various approaches used for ROI extraction, features extraction and matching methods for palmprint identification. Chapter 3 explains the technique for extraction of Dynamic Region of Interest and an algorithm to maximize the ROI. Dynamic ROI extraction results are discussed on the PolyUPalmprint Database, CASIA Palmprint Image Database and IIT Delhi Palmprint Database.

Chapter 4 defines the Wide Principal Line Features and explains the process of a Wide Principal Line Features extraction. Statistical Features extraction based on standard deviation and coefficient of variation is also discussed in Chapter 4. Chapter 5 proposed an algorithm to establish the correspondence between two dynamic ROIs (i.e. query image dynamic ROI and database image dynamic ROI). The palmprint authentication based on Wide Principal Line Features and Statistical Features is also discussed. This chapter also elucidates the process of a two-phase palmprint identification based on Wide Principal Line Features and Statistical Features.

Chapter 6 presents exhaustive experiments conducted and shows effectiveness of the proposed approaches along with the comparative study with earlier works. Chapter 7 concludes the thesis with future directions.

CHAPTER 2

Literature Survey

This chapter describes recent works to give an insight into the latest advancements related to palmprint verification/recognition.

2.1 ROI Extraction Techniques

The central region of the palmprint is referred to as Region of Interest (ROI) [15]. ROI extraction can be performed in different ways like static/dynamic, and in shapes like square, circle etc. Most researchers [20–28] have used static ROI for palmprint recognition/authentication. In these approaches, mainly square shaped ROIs were used. In [29] circle shaped ROIs had been used. Very few researchers [30–34] have not extracted ROI, because they have processed the entire palmprint images.

2.1.1 Static ROI Extraction

Kong et al. [15] applied a low pass filter for smoothing the palmprint, later a threshold was used to obtain binary image. The boundaries of the gaps between little finger and ring finger, ring finger and middle finger, middle finger and index finger were extracted. For each gap, computed the center of gravity and constructed a line that passes through the center of gravity and the middle point between the starting point and ending point of the gap. The line intersection with the gap boundary was considered as a key point. Based on these key points, palmprint was aligned and a fixed size ROI was extracted.

Zhang et al. [20] applied low pass Gaussian filter for smoothing, later a threshold was used to obtain binary image. Boundary tracking algorithm was used to obtain the boundary of the gaps between fingers. Later he used the tangent based approach to

identify the reference points. The tangent based approach considered two boundaries: one from index finger and middle finger and the other from ring finger and little finger and computed the tangent of these two gaps. The intersections were considered as reference points for establishing the coordinate system. The reference points were used to align the palmprint image and extracted a sub image of a fixed size based on the coordinate system. To extract ROI most of the researchers [26, 35–51] have used this approach.

Kumar et al. [52] used the Otsu's method to obtain the threshold. The obtained threshold was used for binarization of the palmprint image. The binarized palmprint image was approximated by an ellipse. The parameters of the best-fitting ellipse were computed. The orientation of the binarized palmprint image was estimated by the major axis of the ellipse. Based on the orientation palmprint was aligned. Using the morphological operations, fixed size square shape ROI was extracted.

Wu et al. [53] applied a low-pass filter to smooth the palmprint image and used a threshold to convert palmprint image to a binary image. Palmprints boundary pixels were extracted. Four straight lines were constructed to fit the segments of the boundary of the indexing finger, middle finger, ring finger and little finger. Computed the bisectors of the angles formed by the constructed lines and the intersection of bisectors and the boundary were considered as key points. These identified key points were used to align the palmprint image and extracted a fixed size (128 x 128) ROI from the center of the palmprint image.

Lin et al. [21] applied the median filter on the input palmprint image to reduce the noise. Mode method was applied to determine the suitable threshold, to binarize the palmprint image. The inner border tracing was used to find the palmprint border pixels. The middle point of the intersection line that was formed by the wrist and bottom margin of a palmprint image was located. Euclidean distance was calculated between border pixels and middle point. Using the Euclidean distance, finger-webs were identified. The finger-webs were then used to align the palmprint image and

extracted a fixed size ROI based on the established coordinate system.

Pan et al. [54] applied a low pass filter on the palmprint image and converted the filtered image into the binary image. The boundaries of the gaps between fingers were obtained. The middle point of gaps of index-middle fingers and ring-little fingers were located. These two points were considered as key points and used to align as the palmprint image. Later, he extracted 128 x 128 sub-image from palmprint image for feature extraction.

Shang et al. [55] applied a lowpass filter on the palmprint image and converted it into binary image. Linear searching was used along the boundary of the palm, to find the middle point of the root of middle finger and the middle point of the wrist. These identified points were joined to form Y-axis of the right angle coordination system and the origin was defined as the middle point of line segment. A sub-image of 128 x 128 was extracted as the ROI. Yue et al. [56] used Gaussian filtering to smooth the palmprint image and performed the binarization on the resultant image. Morphological operations were applied to fill the gaps and remove noise pixels. Boundary pixels were identified using boundary tracking. Using the boundary pixels, identified the reference points. Using the reference points established the coordinate system, and extracted a fixed size ROI.

Chen et al. [57] applied a fixed threshold to convert the palmprint image to a binary image. Morphological operations were used to remove isolated pixels, spurs and leaks on the binary image. Later boundary tracking algorithm was used to obtain the boundary. The maximum curvature points were obtained using the curvature maxima finding. These identified points were used to extract a fixed size 135 x 135 ROI. To enhance the palmprint texture non-uniform illumination correction was performed.

2.1.2 Dynamic ROI Extraction

Connie et al. [58] applied an image thresholding technique to segment the hand image from the background. To obtain three valley points between the adjacent fingers, applied the salient-point detection algorithm. Based on these three points, the palmprint was aligned and Dynamic (Square Shape) ROI was obtained. The ROIs vary from hand to hand, so the ROIs were resized to 150 x 150 pixels by using bicubic interpolation.

Savic et al. [59] applied global threshold for binarizing the palmprint image. To extract the hand contour, contour following algorithm was applied on the binary image. Reference points were identified using the local maxima and local minima from the hand contour. Dynamic (Square Shaped) ROI was extracted based on the reference points. The obtained ROIs were normalized to 128 x 128 pixels. Michael et al. [60] used the skin-color thresholding method to segment the hand image from the background. A valley detection algorithm was used to find the valleys of the fingers. These valleys were considered the base points to locate the Dynamic (Square Shape) ROI. Later, the Dynamic ROIs were resized to 150 x 150 by using bicubic interpolation.

Kong et al. [16] located the valley points among little finger, ring finger, middle finger and index finger by using the algorithm proposed by Lin et al. [23]. These points were used to establish a coordinate system and extracted a Dynamic (Square Shape) ROI. To enhance the contrast of the ROI, applied the Laplacian transform.

Badrinath et al. [61] applied the global threshold to extract the palmprint from the background. Palmprint image was processed with standard morphological operations to remove the isolated small blobs or holes. Contour tracing algorithm was applied to extract the contour of the hand image from binarized hand image. Four valley points between the fingertips are determined using local minima on the contour of hand image. These points were used to establish the coordinate system and extracted a square shape dynamic ROI. Later the extracted ROIs were normalized to 176 x 176,

to generate the equivalent size features.

Different ROI sizes are reported in the existing literature. Some of the researchers [53, 54] have used an ROI size of 128 x 128 and some researchers [61, 62] have used an ROI of size 176 x 176 with PolyUPalmprint Database [17]. Very few researchers [16, 58–61] have used the square shape Dynamic ROI. The researchers [58–61] normalised the Dynamic ROI to fixed size for comparison. The square shape ROI used in these approaches again has certain inherent disadvantages that may limit its applicability. A summary of ROI extraction techniques is shown in Table 2.1.

2.2 Feature Extraction Techniques

For feature extraction, several approaches like Line based features [21, 22, 25–28], Statistical features [63, 64], Geometrical features [16], Datum points [21, 65], Delta points [65] etc., were used by the researchers. Some of the researchers used directly the pixel values of a palmprint as a features, Zhang et al. [66] named it as the holistic based approach.

2.2.1 Structural Features

Lines and wrinkles are the basic features of palmprint. Thus, line based approaches play an important role in palmprint recognition/authentication field. Kung et al. [30] extracted edge feature from the palmprint image and down sample it to 18 x 16 feature vector. Boles et al. [31] applied histogram equalisation followed by edge detection using the Sobel masks. Thresholding was applied on the resulting image followed by thinning to obtain the life line, heart line and head line. Hough transforms were applied to extract the parameters of the six lines with highest densities in the accumulator array for matching. Shu et al. [33] defined the principal lines as the life line, head line and heart line on palmprint. The authors extracted geometrical features such as length, width and area of the palm and structural features such as principal lines and ridges

Table 2.1: ROI Extraction Techniques

Author Name	Filters used to smooth the Palmprint Image	Techniques Used		Size of the ROI
		threshold selection for binarization & pre-processing after binarization & to identify the boundary pixels	Key points identification / align the palmprint image	
Kong et al. [15]	low pass filter	The boundaries of the gaps between fingers were extracted	Constructed a line that passes through the center of gravity and the middle point between the starting point and ending point of the gap. The line intersection with the gap boundary was considered as a key point.	Fixed Size
Zhang et al. [20]	low pass Gaussian filter	Boundary tracking algorithm	Tangent based approach	Fixed Size
Kumar et al. [52]		Otsus method	best-fitting ellipse was used to align and morphological operations were used to extract ROI	square shape ROI
Wu et al. [53]	low-pass filter		bisectors based method	128 x 128
Lin et al. [21]	Median filter	Mode method was used for binarization. Inner border tracing algorithm was used to extract border pixels	Euclidean distance was calculated between border pixels and middle point. Using the Euclidean distance, finger-webs were identified.	Fixed Size
Pan et al. [54]			key points are used to align the palmprint image	128 x 128
Shang et al. [55]	Low-pass filter		Linear searching was used along the boundary to find key points	128 x 128
Yue et al. [56]	Gaussian filtering, Morphological operations were applied to fill the gaps and remove noise pixels	boundary tracking		Fixed Size
Chen et al. [57]		Morphological operations to remove isolated pixels. boundary tracking	Curvature maxima finding	135 x 135
Connie et al. [58]			salient-point detection algorithm	Dynamic (Square Shape) ROI, Later ROIs were resized to 150 x 150 pixels by using bicubic interpolation
Savic et al. [59]		global threshold. contour following algorithm was applied on the binary image	the local maxima and local minima from the hand contour	Dynamic (Square Shaped) ROI was Extracted, ROIs were normalized to 128 x 128 pixels
Michael et al. [59]		skin-color threshold method	valley detection algorithm	Dynamic (Square Shape) ROI. Later, the Dynamic ROIs were resized to 150 x 150.
Kong et al. [16]			Used the algorithm proposed by Lin et al. [14]	Dynamic (Square Shape) ROI
Badrinath et al. [61]		Global threshold method. Morphological operations are used to remove the isolated small blobs or holes. Contour tracing algorithm was applied to extract the contour of the hand image	local minima on the contour of hand image	square shape dynamic ROI. Later, the extracted ROIs were normalized to 176 x 176.

from palmprint images. Geometrical features were used to eliminate some palmprints, and principal line features were used to process the remaining palmprints for identification. Zhang et al. [65] defined datum points as the end points of the principal lines. Templates were defined and used to extract principal lines. The resultant images were post processed to clear the short lines.

Duta et al. [34] smoothed the palmprint image by replacing each pixel value with the average of its original value and the values of its four immediate neighbours. The smoothed image was binarized by applying an interactively chosen threshold "T". All pixels whose values were greater than "T" were regarded as palm line pixels while the remaining ones were considered as the background. A set of successive morphological erosions, dilations and subtractions were performed in order to remove the compact regions, misclassified as palm lines. The remaining foreground pixel locations were subsampled in order to obtain a set of 200 to 400 pixel locations which were considered as feature points. Wu et al. [67] used the Canny edge operator to detect the lines on the palmprint image. Global Fuzzy Directional Element Energy (GFDEE) was calculated in four directions (0° , 45° , 90° and 135°). GFDEE reflected the strength of lines in four directions in a whole palmprint image.

Wu et al. [53] used Sobel masks (0° , 45° , 90° and 135°) to compute the magnitude of palm lines. These magnitudes were projected along both X and Y directions to form 128 histograms. Wu et al. [68] used, the morphological operators such as dilation, erosion, opening, closing to extract principal lines. For each extracted line, a recursive process was devised to further extract and trace the principal lines using the local information. Wu et al. [69] proposed a set of line detectors and used these detectors to extract the principal lines. Later, palmprints were classified into six categories according to the number of the principal lines and the number of principal line intersections.

Wu et al. [70] proposed a set of line detectors based on 1^{st} and 2^{nd} order derivatives. These line detectors were used to obtain the directional line magnitude images.

Each directional line magnitude image was divided into 32×32 sub images. To generate the feature vector, the directional line energy was computed for each sub image along each direction. The directional line energy represents the strength of the line in that block and direction. The feature vector was normalised and it was called as Directional Line Energy Feature (DLEF). Zhang et al. [25] used complete wavelet expansion and directional context modelling technique to extract principal lines and wrinkles like features. The palmprint was first transformed into the wavelet domain, and the directional context of each wavelet sub band was defined and computed in order to collect the predominant coefficients of its principal lines and wrinkles. A set of statistical signatures, which includes gravity center, density and energy were defined to characterize the palmprint with the selected directional context values.

Lin et al. [21] applied the hierarchical decomposition mechanism to extract principal palmprint features, which includes directional and multi-resolution decompositions. Applied the Sobel operator to extract edges, later applied the morphological operators such as clean and dilate to trim the short principal lines. Dominant point filters were defined to extract dominant points. Wu et al. [26] proposed a set of directional line detectors using the 1^{st} and the 2^{nd} order derivatives to extract palm lines. They used the zero-crossings of the first-order derivatives on $(0^\circ, 45^\circ, 90^\circ \text{ and } 135^\circ)$ to identify the edge points. The magnitude of the corresponding second-order derivative was considered as the magnitude of the lines. Positive signs of magnitude represent valleys, whereas minus signs of magnitude represent peaks. They retained only the positive magnitude because palm lines were valleys. Palm lines were much thicker than ridges. For that reason, one or more thresholds were used to remove ridges from magnitude image to a binary image, which was called the 0° -directional line image. The sum of all the directional line images were regarded as line image. Extracted palm lines were represented using chain code to reduce the storage space.

Negi et al. [71] used the Sobel operator to extract the heart line. Liu et al. [27] proposed wide line detector based on the isotropic responses via circular masks. These wide line detectors were applied to detect the wide lines on palmprints, aerial images,

X-ray images and tongue images. Modified Finite Radon Transform (MFRAT) was proposed by Huang et al. [22] to extract line features. Cook et al. [72] used internal image seams to represent principal lines. Internal image seams were identified by using the energy value of the pixels, the energy value was calculated by using Laplacian pyramid. A summary of structural feature extraction techniques is shown in Table 2.2.

Table 2.2: Structural feature extraction techniques

Author names with reference numbers	Approach
Boles et al. [31], Wu et al. [53], Lin et al. [21], Negi et al. [71]	used Sobel masks
Wu et al. [67]	used Canny edge operator
Wu et al. [26, 70]	proposed line detectors based on 1 st and 2 nd order derivatives
Zhang et al. [25]	used complete wavelet expansion and directional context modelling technique
Liu et al. [27]	proposed wide line detector based on the isotropic responses via circular masks
Huang et al. [22]	proposed Modified Finite Radon Transform (MFRAT)
Cook et al. [72]	used Laplacian pyramid

2.2.2 Statistical Features

Kong et al. [35] gave the quantitative evidence to demonstrate that the three principal lines were genetically dependent. This evidence supports the usage of the principal lines for genetic research. The authors also said that some weak lines were also genetically related. Generally, in statistical approaches transformations such as Gabor filters, wavelets, Contourlets and Fourier transforms etc., were applied on palmprint images.

Later, divided the transformed images into several small regions. Local statistics such as mean, standard deviation and variance of each small region were calculated and regarded as features. The small regions were commonly square but some were elliptical and circular.

Wu et al. [67] proposed wavelet based palmprint recognition system. Decompose the ROI into J scale by wavelet transform. Each detail image was divided into $S \times S$ non overlapping blocks. Computed the energy of the each block along horizontal, vertical and diagonal directions respectively.

C. C. Han et al. [28] applied Sobel operator to extract feature points. Later morphological operators such as dilation, erosion, open and close operations applied to enhance the features. The ROI was uniformly divided into several small grids. The mean values of pixels in the grids were calculated to obtain the feature values. These values were sequentially arranged row by row to formulate the feature vectors. In the experiments, three different grid sizes 32×32 , 16×16 and 8×8 were adopted to obtain the multi-resolution feature vectors. Dale et al. [63] extracted 128×128 ROI from palmprints. The ROI was resized to 64×64 and the resized image was divided into four non overlapping sub-images. The two dimensional discrete cosine transform (2-D DCT) was applied on each sub-image separately. The DCT transformed coefficients were grouped into nine frequency bands. For each block the standard deviation was calculated. i.e. for each ROI, obtained 36 standard deviations to form a feature vector.

Pan et al. [73] applied the Gabor filter and divided the resultant image into two level non overlapping partitions and calculated the mean and standard deviation as features. For every level the partition was divided into four equal partitions and computed the local relevance variance on each partition which was considered as a feature.

Mu et al. [74] used the Gabor filter to generate Gabor Magnitude (GM) features. Logarithm transform was applied to generate LogGM features. The LogGM feature image was divided into sub-blocks. Mean and standard deviation of LogGM feature of all the blocks was considered as feature vector. Fisher linear discrimination was used

to reduce the dimensionality. GUO et al. [64] partitioned the palmprint image into several smaller sub-images, and then the feature vectors were extracted by five methods: mean and variance, Fourier transform, DCT transform, Gabor transform and Local Binary Pattern (LBP). The feature vectors of all the sub-images were combined together to form the feature vector of the palmprint image. A summary of transformations applied before extracting statistical feature extraction is shown in Table 2.3.

Table 2.3: Transformations applied before extracting statistical features

Author names with reference numbers	Transformations
Wu et al. [67]	wavelet transform
C. C. Han et al. [28]	Sobel operator
Dale et al. [63]	Discrete Cosine Transform (DCT)
Pan et al. [73], Mu et al. [74]	Gabor filter
GUO et al. [64]	Fourier transform, DCT transform, Gabor filter and Local Binary Pattern (LBP)

2.2.3 Other Features

Zhang et al. [20] and Kong et al. [75] used the Gabor filter to extract the features. Lu et al. [76] transformed the ROIs of palmprints into eigenpalms which were eigenvectors of the training set. The eigenpalm features were extracted by projecting a new palmprint image into the eigenpalms. Pong et al. [77] proposed the Zernike movement invariant to extract the features. Lu et al. [78] applied the wavelets to extract features.

Li et al. [79] proposed translation invariant Zernike movements for feature extraction. Wu et al. [38] devised directional templates to obtain the orientation of the pixels. The ROI was resized from 128 x 128 into 32 x 32. To identify the orientation of the each pixel, applied the devised templates. The orientation image was called Palmprint Orientation Code (POC). Zuo et al. [80] proposed the Bidirectional Prin-

Principal Component Analysis (PCA) to overcome the over fitting problem of PCA. The authors also proposed an Assembled Matrix Distance (AMD) metric to calculate the distance between two feature matrices and then apply the AMD metric in the implementation of Nearest Neighbor classifier and Nearest Feature Level classifier.

Zhang et al. [42] used wavelets to extract the features for recognition. Feng et al. [81] used the Kernel PCA to make the data as linearly separable as possible in feature space. Later Locality Preserving Projections (LPP) were used to generate feature vectors. Wang et al. [82] extracted Local Binary Patterns. Shang et al. [83] proposed the Fast Independent Component Analysis for feature extraction. Hu et al. [84] proposed a Two-dimensional Locality Preserving Projection (2DLPP) for feature extraction. Chen et al. [85] used the dual tree complex wavelets for feature extraction. Zhao et al. [47] used the 2DPCA to extract the features. PCA was applied to reduce the dimensionality. Pan et al. [86] used the Gabor filters to extract features and $(2D)^2$ PCA for dimensionality reduction.

Masood et al. [87] used the wavelets to extract the feature vector. Pan et al. [88] used the Gabor filters to generate the feature vectors. Lu et al. [43] used the discrete wavelet transformation to extract features followed by PCA and LPP were used for dimensionality reduction. Butt et al. [89] used the Contourlet transforms to generate feature vectors. Nanni et al. [90] used the wavelet transforms to generate features and Sequential Forward Floating Selection (SFFS) method was used to select the most useful sub-bands for recognition. Kong et al. [48, 91] used the Gabor filters to generate features called as Competitive Code. Michael et al. [60] wavelet transforms were used to decompose the ROI image into lower resolution images. Sobel operator was applied to identify the edges. Edge images were partitioned into 9 non overlapping partitions. For each partition, obtained the local binary patterns were considered as features.

Yue et al. [56] proposed a modified fuzzy C-means clustering algorithm to determine the orientation of each Gabor filter. Wan et al. [92] proposed Two-Dimensional Local Graph Embedding Discriminant Analysis (2DLGEDA), for feature extraction.

Su et al. [93] used the characteristic matrix to generate the various discriminators. The transformed signals were fed to the characteristic matrix to generate various discriminators.

Chen et al. [94] applied Contourlet transform to generate a number of decomposition levels, performed a 2D Fourier transform on each wavelet subband, and took the spectrum magnitude of the Fourier coefficient of each decomposition subband as a feature. Badrinath et al. [95] divided ROI into equal size 25 sub images. Low-order Zernike moments were computed for all sub-images. Yue et al. [96] used the competitive code and ordinal code to represent the features. Zhang et al. [97] proposed Local Kernel Feature Analysis (LKFA). For each ROI Gabor filters were applied to extract Gabor magnitude. These Gabor magnitudes were given to LKFA for classification.

Mansoor et al. [23] used the Contourlet transforms to extract local and global details as feature vector. Mu et al. [24] applied the complex directional filter banks followed by local binary patterns to extract the feature vectors. Badrinath et al. [61] proposed to use the binarized instantaneous phase differences of overlapping circular-strips as features of palmprint. The Stockwell transform was applied to obtain instantaneous phase which was the phase of user image in resolution of time. Lai et al. [98] proposed a sparse two dimensional locality discriminant projections (S2DLDP), which was a sparse extension of graph based image feature extraction method.

Badrinath et al. [62] divided each ROI into 25 square (44 x 44) overlapping blocks. Reconstruction error using PCA was used to classify these blocks into either a good block or a non-palmprint block. Features from each good block of a ROI were obtained by binarizing the phase difference of vertical and horizontal phase. Xuan et al. [99] proposed that, palmprint images were normalized in the orientation, position and illumination, and then the normalized images were decomposed into several multiscale and directional subbands using the Gabor filters. PCNN was employed to decompose each Gabor subband into a series of binary images. Entropies for these binary images were calculated and regarded as features.

Table 2.4: Feature extraction techniques

Author names with reference numbers	Approach
Zhang et al. [20], Kong et al. [75], Pan et al. [86], Pan et al. [88], Kong et al. [48, 91], Zhang et al. [97]	Gabor filter
Lu et al. [78], Zhang et al. [42], Masood et al. [87], Lu et al. [35] lu2008a, Nanni et al. [90], Michael et al. [60], Imtiaz et al. [100], Chen et al. [85]	applied wavelets
Butt et al. [89], Chen et al. [94], Mansoor et al. [23]	used the Contourlet transforms
Wu et al. [38]	devised directional templates
Lu et al. [76]	proposed eigenpalms
Pong et al. [77], Li et al. [79], Badrinath et al. [95]	Zernike movements
Feng et al. [81]	used the Kernel PCA
Zuo et al. [80]	proposed the bidirectional PCA
Wang et al. [82]	extracted Local Binary Patterns
Wan et al. [92]	proposed Two-Dimensional Local Graph Embedding Discriminant Analysis (2DLGEDA)
Shang et al. [83]	proposed the Fast Independent Component Analysis
Hu et al. [84]	proposed a Two-dimensional Locality Preserving Projection (2DLPP)
Zhao et al. [47]	used the 2DPCA
Badrinath et al. [61]	proposed stockwell transform
Yue et al. [96]	used the competitive code and ordinal code
Mu et al. [24]	applied the complex directional filter banks

Imtiaz et al. [100] segmented the ROI into several small spatial modules and extracted the dominant wavelet features from each of the modules. Xuan et al. [101] used the adaptive lifting scheme to decompose the ROI into several subbands and employed pulse coupled neural networks to decompose each subband into a series of binary images. The entropies of these binary images were considered as features. A summary of feature extraction approaches is shown in Table 2.4.

2.3 Recognition Strategies

Kung et al. [30] used the Decision Based Neural Networks (DBNN) for recognition. Zhang et al. [65] used the slope, intercept, angle and Euclidean distance between the datum points (Principal line end points) to perform principal line matching. Wu et al. [67] used city block distance for matching. Wu et al. [67, 70] used the Euclidean distance to measure the similarity between the query and database image feature vectors. The label of the minimum distance palmprint was considered as the identified palmprint. Kong et al. [15] used the normalized Hamming distance to perform matching.

Zhang et al. [20] used normalized Hamming distance to determine the similarity measurement for palmprint matching. Pong et al. [77] used Euclidean distance to perform verification. Wu et al. [53] used the Hidden Markov Models (HMMs) for identification. Kong et al. [75] used the normalized hamming distance to perform matching. Lu et al. [76] measured the Euclidean distance between query eigenpalm features and database image eigenpalm features to perform recognition. Han et al. [28] used the correlation function to measure the similarity between query image feature vector (x) and template image feature vector (y). Later, back propagation neural network was used for verification.

Lu et al. [78] used the Independent Component Analysis to perform identification. Connie et al. [58] used the PCA, fisher discriminant analysis (FDA) and Independent Component Analysis (ICA) for classification. In order to analyse the palmprint images in multi-resolution-multi-frequency representation, wavelet transformation was also adopted. Li et al. [56, 79] used the modular neural networks for classification. Lin et al. [21] used the correlation function for verification. Wu et al. [38] used the hamming distance to measure the similarity of the two Palmprint Orientation Codes (POCs). Negi et al. [71] divided the ROI into 8 regions. Based on the number of heart line pixels in the regions the palmprints were classified.

Wu et al. [26] defined the matching score as the proportion of matched points obtained by superimposition of two images. Feng et al. [81] used the nearest neighbor classifier to perform the recognition. Wang et al. [82] used the AdaBoost for classification. Chen et al. [102] proposed palmprint classification based on dual tree complex wavelets and SVM. Shang et al. [83] proposed and used radial basis probabilistic neural network for palmprint classification. Chen et al. [85] used the SVM to perform the classification. Zhao et al. [47] used the modular neural networks for classification. Wang et al. [103] used the dual tree complex wavelet transform and local binary pattern histogram for palmprint recognition. Masood et al. [87] used the Euclidean distance to measure the similarity for authentication. Pan et al. [86] used the Euclidean distance and the nearest neighbor classifier for classification.

Michael et al. [60] used the probabilistic neural networks for classification. Pan et al. [88] constructed the nearest neighbor graph, in which each node corresponds to a column inside the matrix, instead of the whole image, to better model the intrinsic manifold structure. 2DPCA was implemented in the row direction prior to 2DLPP in the column direction, to reduce the calculation complexity and the final feature dimensions. Lu et al. [43] used the single hidden layer feed forward neural networks for classification. Butt et al. [89] used the normalized Euclidean distance to perform matching. Kong et al. [16] used two stage neural networks i.e. SOM neural network and BP neural networks. Huang et al. [22] proposed and used the pixel to area matching for palmprint verification. Nanni et al. [90] used the Euclidean distance to measure the similarity between the query image and database image. The nearest neighbor classifier was used for identification.

Pan et al. [73] used the city block distance to measure the similarity between the query image and database image. The nearest neighbor classifier was used for identification. Wan et al. [92] used the Euclidean distance and the nearest neighbor classifier for identification. Dale et al. [63] used the Canberra distance to find out the minimum distance match between feature vectors of database image and query image. Kong et al. [48, 91] used the angular distance to measure the dissimilarity between the com-

petitive codes of query image and database image. Su et al. [93] used the pixel-to-pixel comparisons. To deal the image shifting problem, one pixel in sample image is compared with the surrounding pixels in unknown image to locate the closest matching. Chen et al. [94] used the AdaBoost to perform the classification. Yue et al. [96] used Hamming distance for verification. To speed up the identification process, authors constructed a tree for each subject to utilize the intrinsic characteristics of the templates. Nearest neighbor searching was used in the tree structure for identification. Zuo et al. [104] applied the Gaussian function followed by post processing of LDA to generate the feature vectors. The nearest neighbor classifier was used for recognition. Cook et al. [72] used the k-d tree nearest neighbour searching for identification.

Badrinath et al. [61] proposed a palmprint based verification system which used low-order Zernike moments of palmprint sub-images. Euclidean distance was used to match the Zernike moments of corresponding sub-images of query and enrolled palmprints. The matching scores of sub-images were fused using a weighted fusion strategy. Guo et al. [105] proposed a unified distance measure, of which both SUM-XOR (angular distance) and OR-XOR (Hamming distance) were considered as special cases, and provide some principles for determining the parameters of the unified distance.

Lu et al. [106] used the Diagonal Discriminant Locality Preserving Projections (Dia-DLPP) and Weighted Two-Dimensional Discriminant Locality Preserving Projections (W2D-DLPP) for palmprint recognition. To perform the classification used the nearest neighbor classifier based on the Euclidean distance. Lai et al. [98] used the nearest neighbor classifier based on the Euclidean distance for classification. Badrinath et al. [95] used the Euclidean distance to match the Zernike moments of corresponding sub-images of query and database palmprints. These matching scores of sub-images were fused using a weighted fusion strategy for computing the distance and the distance was used for verification. Mansoor et al. [23] used normalized Euclidean distance for matching. Mu et al. [24] applied the Fisher Linear Discriminant analysis for dimensionality reduction followed by nearest neighbor classification using Euclidean distance.

Badrinath et al. [62] adopted Hamming distance to measure the matching score. Guo et al. [64] performed verification using nearest neighbor classifier in which Euclidean distance was used for matching. Xuan et al. [99] used the support vector machine for classification. Yin et al. [107] proposed a kernel sparse representation based classification algorithm. Samples were mapped into a high dimensional feature space and then Sparse representation based classification was performed. To measure the dissimilarity average sum square distance was proposed by Imtiaz et al. [100] which was similar to Hamming distance. Xu et al. [50] proposed nonnegative sparse representation based fuzzy similar neighbor classifier for identification. Xuan et al. [101] used the support vector machine based classifier for palmprint identification.

Connie et al. [108] proposed cancellable biometrics using PalmHashing. Wu et al. [40] proposed a palmprint cryptosystem. Palmprint was used to generate 128 bit symmetric key to perform the encryption. At the time of decryption, the same palmprint was used to generate the key. Instead of remembering the secret key, palmprint was used for key generation. Yue et al. [109] proposed consistent orientation pattern (COP) hashing to enforce the fast searching. Hong et al. [110] used the Chi-square distance for palmprint identification. Wu et al. [111] extracted the SIFT features from palmprint images. Later, Euclidean distance was used for verification. Guo et al. [112] used the normalized correlation classifier for palmprint identification. A summary of recognition techniques is shown in Table 2.5.

Table 2.5: Recognition Techniques

Approach	Author names with reference numbers
Neural Networks	Kung et al. [30], Han et al. [28], Li et al. [56, 79], Shang et al. [83], Zhao et al. [47], Michael et al. [60], Lu et al. [43], Kong et al. [16]
Euclidean distance	Zhang et al. [65], Wu et al. [67, 70], Pong et al. [77], Lu et al. [76], Masood et al. [87], Pan et al. [86], Butt et al. [89], Nanni et al. [90], Wan et al. [92], Badrinath et al. [61], Lu et al. [106], Lai et al. [98], Badrinath et al. [95], Mansoor et al. [23], Mu et al. [24], Guo et al. [64]
City block distance	Wu et al. [67], Pan et al. [73]
Hamming distance	Kong et al. [15], Zhang et al. [20], Kong et al. [75], Wu et al. [38], Yue et al. [96], Badrinath et al. [62]
Chi-square distance	Hong et al. [110]
Angular distance	Kong et al. [48, 91]
Canberra distance	Dale et al. [63]
Support Vector Machine (SVM)	Chen et al. [102], Chen et al. [85], Xuan et al. [99], Xuan et al. [101]
Hidden Markov Models (HMMs)	Wu et al. [53]
AdaBoost	Wang et al. [82], Chen et al. [94]
Independent Component Analysis (ICA)	Lu et al. [78]
LDA	Zuo et al. [104]
PCA, FDA and ICA	Connie et al. [58]

2.4 Fusion Techniques

Ribaric et al. [113] used the geometrical, fingerprint and palmprint features for identification. Fusion was performed at matching stage. Kumar et al. [52] extracted line features and the resultant image was divided into overlapping blocks. The standard deviation of these blocks was considered as feature vector. Geometrical features such as finger length, finger widths, palm length, palm width and palm area were considered as features. Fusion was performed at the feature level. The normalized correlation was used as the similarity measure.

Feng et al. [37] proposed a feature level fusion strategy for personal identification using face and palmprint. PCA and ICA were used for dimensionality reduction and perform fusion. Later, Nearest Neighbor Classifier was used for classification. Han et al. [114] used the hand geometrical features for coarse level verification. In coarse level verification, the tolerance was considered as looser threshold. If the query palmprint passes the above looser criterion, then it was rechecked by the palmprint feature in the fine level verification. You et al. [36] proposed the hierarchical approach for identification. The authors used the geometrical distance between the key points, global texture energy, fuzzy interested lines and the local texture energy for identification. Poon et al. [115] extracted three feature vectors using Gabor filter, line detectors and Harr wavelet transforms. For matching, the authors computed the mean of the absolute difference between the feature vectors. Fusion was performed at score level and decision level. Kong et al. [39] applied the Gabor filters in 0° , 45° , 90° , 135° orientations, calculated the magnitude and phase values. For every pixel, FusionCode was defined based on the phase having maximum magnitude. To measure the similarity, normalized Hamming distance was used.

Li et al. [116] extracted the ROI, hand shape and knuckleprint from the palmprint image. Decision level fusion was performed. Kumar et al. [117] extracted Gabor features, line features and PCA features. To compute the matching score three distance measures were used, one of the distance measures was Euclidean distance. Fusion was

performed at decision level and product of sum rule was proposed for identification. In the product of sum rule, first applied the sum of the matching scores of Gabor and Line features followed by the product of the matching score of PCA features. To perform the classification used the nearest neighbor classifier. Ribaric et al. [118] extracted fixed size fingerprints (five) and palmprint (ROI) from input image. Eigen palm and Eigen finger features were extracted. Euclidean distance was used to compute the matching score. Fusion was performed at matching score level to take decision.

Kong et al. [44] applied the elliptical Gabor filter on different orientations. For every orientation calculated the phase values. Fusion Code was defined by merging of phase information based on fusion rule. To measure the similarity normalized hamming distance was used. Kumar et al. [119] proposed a system, to acquire an image consisting of palmprint and hand geometry. The authors obtained the hand features like finger length, palm length, hand length, finger width and palm width. ROI was obtained from the palmprint image and applied line detectors proposed in [120] to extract principal lines. The resultant ROI was divided into non overlapping sub-blocks. The standard deviation of these blocks was considered as feature vector. The authors observed that the matching score level fusion scheme, with max rule, achieved better performance than those with fusion at the representation level.

Kumar et al. [121] divided ROI into overlapping sub blocks. For each sub block discrete cosine transforms were applied and calculated the standard deviation of DCT coefficients to compute the feature vector. Hand shape features like finger length, finger width, palm length and palm width etc., were used and several classifiers like Naive Bayes, KNN, SVM and Decision Trees were compared. Shang et al. [122] used the Winner take all network for feature extraction. Radial Basis Probabilistic Neural Network (RBPNN) was used for classification. Wu et al. [41] proposed an approach with fusion of palmprint and iris for personal authentication. The features of the palmprint and the iris were first extracted and matched respectively. Gabor filter was applied to extract feature vector from iris. Palmprints were smoothed by applying Gaussian filter followed by differences in the horizontal direction was computed to obtain the feature

vector. The feature vector was called as DiffCode. Hamming distances were adopted to measure the similarity. Then these matching distances were normalized. Finally, the normalized distances were fused using sum strategy, maximum strategy, minimum strategy, and product strategy for authentication.

Yang et al. [123] used geometrical, fingerprint and palmprint features for identification. The authors decomposed the fingerprint and palmprint into four sub images. Statistical values mean and standard deviation were calculated from each sub image to present a feature vector. Fusion was performed at feature level and score level. Yao et al. [124] used face and palmprint features for recognition. Gabor filter was applied to obtain feature vector followed by PCA was applied to obtain discriminant features followed by Euclidean distance based nearest neighbour classifier for verification. Feature level fusion was performed. Savic et al. [59] extracted a set of 14 geometrical parameters of the hand, the palmprint, four digitprints, and four fingerprints. The features were extracted using the Linear Discriminant Analysis (LDA) appearance-based feature-extraction approach, the templates were matched using the normalized correlation and Euclidean distance, the matching scores were normalized using the linear 3-segment normalization technique and combined using the matcher weighting fusion rule, and finally the best fusion score was compared with the experimentally determined decision threshold to perform recognition.

Jing et al. [46] combined two kinds of biometrics, the face feature and the palmprint feature. Gabor transform was applied on face and palmprint images and combined them at the pixel level. To classify the fused biometric images used the Kernel Discriminative Common Vectors (KDCV) and Radial Base Function (RBF) neural network. Jia et al. [45] used the modified finite radon transforms to extract principal lines. Based on the orientation, wrinkles and ridges were removed from the Line Images. To perform line matching pixel to area comparison was used. In the pixel to area comparison, for every principal line pixel in the query image was compared with the corresponding pixel in the database image and its horizontal and vertical neighbours, if any one of the comparing database image pixel was principal line pixel then

it was considered as a match. LPP was used to retain the texture features. Two fusion approaches were proposed. In the first fusion method, the query image extracted principal lines first. Then the query principal line image was compared with all the database principal line images to calculate the matching scores. Based on the matching scores, the authors selected a subset of database images having largest matching scores. For all database images, calculated the LPP vectors. Query image was mapped to LPP to generate LPP_{query} . The Euclidean distance between LPP_{query} and LPP vectors of selected database images was calculated. The distances were normalized so that greater the similarity images would have larger the matching scores. Fusion was performed by product rule of the matching scores of principal lines distance and LPP distance. Classification was performed by using Nearest Neighbour classifier. In the second fusion method, LPP was performed first to select the most similar ROIs in database images. Later using Principal line matching calculated the matching scores for selected images. Fusion was performed by product rule of the matching scores of principal lines distance and LPP distance. Classification was performed by using Nearest Neighbour classifier.

Wang et al. [125] proposed a multimodal personal identification system using palmprint and palmvein images. The palmprint and palmvein images were fused by an edge-preserving and contrast-enhancing wavelet fusion method in which the modified multiscale edges of the palmprint and palmvein images were combined. Laplacian palm feature was extracted from the fused images by the locality preserving projections (LPP). Later, nearest neighbor classifier was used to perform identification.

Bhatnagar et al. [126] divided ROI into overlapping sub-blocks of size 24 x 24. For each subblock discrete cosine transforms are applied and calculated the standard deviation of DCT coefficients to compute the feature vector. Hand geometry features like finger length, finger width, palm length and palm width etc., were used and Euclidean distance was used for classification. Xu et al. [49] proposed matrix-based complex PCA (MCPCA), a feature level fusion method for bimodal biometrics that used a complex matrix to denote two biometric traits from one subject. The method

took the two images from two biometric traits of a subject as the real part and imaginary part of a complex matrix. MCPCA applied a novel and mathematically tractable algorithm for extracting features directly from complex matrices.

Zhang et al. [127] extracted the palmprint and palmvein features based on Gaussian filters. Fusion was performed at score level by proposing the dynamic weighted by sum fusion scheme. Xu et al. [51] used the feature level fusion by combining the samples of two biometric traits through sparse representation. 2D palmprint, 3D palmprint and Multispectral palmprint databases were used for experiments. A summary of fusion techniques is shown in Table 2.6.

Table 2.6: Fusion Techniques

Fusion at	Author names with reference numbers
Feature level	Kumar et al. [52], Feng et al. [37], Kong et al. [39], Kong et al. [44], Yao et al. [124], Jing et al. [46], Wang et al. [125], Xu et al. [49], Xu et al. [51]
Decision Level	Ribaric et al. [113], Poon et al. [115], Li et al. [116], Kumar et al. [117], Ribaric et al. [118], Kumar et al. [119], Wu et al. [41], Yang et al. [123], Savic et al. [59], Zhang et al. [127]

2.5 Justification for the present work

Based on the literature survey there are three categories of palmprint recognition: holistic based, feature based and hybrid methods. Our contribution in the thesis is feature based palmprint recognition. It is seen that there is also a need of dynamic ROI extraction that extracts maximum possible rectangular-shape ROIs. We have proposed a Dynamic ROI extraction algorithm to extract maximum possible rectangular shape ROI.

Literature survey reveals that the principal lines are distinguishable features of

palmprint and these are stable throughout the life time. Thus, principal line based approaches play a vital role in palmprint recognition and not much research work has been reported using wide principal lines. We have refined principal line feature extraction through the proposed wide principal line extractors. We have proposed a WPLF extraction algorithm to generate WPLI (Wide Principal Line Image).

Literature survey also reveals that statistical features are extracted after performing some transformations. However, we have proposed a local statistical feature extraction without applying any transformations. We have also proposed palmprint verification and a two-phase palmprint identification system that can be applied to Wide Principal Line Features and Statistical Features.

CHAPTER 3

Dynamic ROI Extraction

Region of Interest (ROI) extraction is an important task for palmprint verification and identification. Earlier reported works used fixed size ROI for the verification and identification of palmprints. If the palmprint size is less than the size specified in the ROI, the system will extract unnecessary data like background areas. Similarly, the use of small ROI for large size palms leads to missing of some valuable data. The literature survey establishes the need of a dynamic ROI extraction process for palmprint verification and identification. The survey also highlights the nature of complexity of different techniques available for identifying the key points and also the techniques available for identifying the size of ROI.

Our proposed method focuses on extraction of maximum possible rectangular shape ROI compared to existing fixed and dynamic ROI extraction techniques and the chapter is organized as follows: Section 3.1 gives the binarization of the palmprint image. Section 3.2 gives localization of key points and an algorithm is developed to extract key points. Establishing a coordinate system, localize ROI algorithm and maximize ROI algorithm are developed in section 3.3 and present an illustrative demonstration of the same. Section 3.3 also explains the process of establishing reference point information. Registration of dynamic ROI and its reference point information is described in section 3.4. Section 3.5 presents experimental results and demonstrate that the proposed approach extracts better ROI on three databases, (1) The PolyU-Palmprint Database, (2) CASIA Palmprint Image Database and (3) IIT Delhi Palmprint Database, when compared to the existing fixed and dynamic size ROI extraction techniques.

3.1 Binarization of the Palmprint Image

As palmprints are gray-scale images, they can be represented by the following image model: $f(m, n)$ where $m = 0, 1, 2, \dots, M-1$ and $n = 0, 1, 2, \dots, N-1$ and $0 \leq f(m, n) \leq L-1$ where L is the number of gray-scale levels. Consider a palmprint image of size $M \times N$ as depicted in Figure 3.1(i). Threshold selection to perform the binarization of the palmprint image is an important factor in palmprint verification and identification. We are using the existing mode method [128] to determine the suitable threshold for binarizing the palmprint image. The selected threshold T is used to binarize the palmprint image. The binarized palmprint image is represented by the following image model:

$$f_b(m, n) = \begin{cases} 1 & \text{if } f(m, n) \geq T \\ 0 & \text{otherwise} \end{cases} \quad (3.1)$$

The resulting binarized palmprint image is depicted in Figure 3.1(ii).

Because of improper selection of threshold T , it is seen that a gap appears between the finger and palmprint region as shown in Figure 3.1(iv). Morphological operators [128, 130, 131] such as dilate and erode operations can be applied to eliminate such a problem. The resulting image can be represented by the image model. $A(m, n)$ where $m = 0, 1, 2, \dots, M-1$ and $n = 0, 1, 2, \dots, N-1$ and $0 \leq A(m, n) \leq 1$.

The size of the structuring element used to perform the dilation and erosion needs to be determined dynamically. For example, after the binarization of the palmprint image of Figure 3.2(i), with the structuring element of size 3, the resultant binarized image is shown in Figure 3.2(ii). The finger part is still disconnected from palmprint region. Now if we consider, the structuring element size of 6, the resultant binarized image is shown in Figure 3.2(iii). Now the finger is connected to palmprint region.

For some other palmprint image shown in Figure 3.3(i), if we apply binarization followed by morphological operation with the structuring element (SE) size 3, the re-

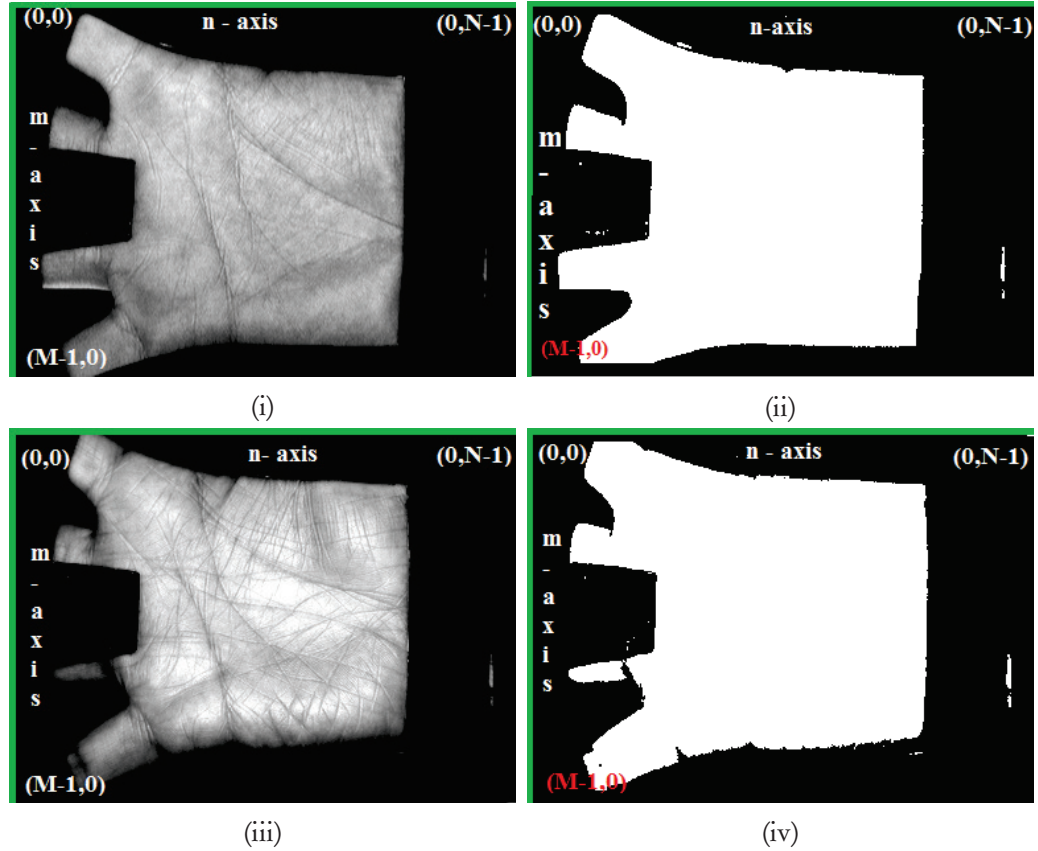


Figure 3.1: (i)&(iii) Sample palmprint images (ii)&(iv) binarized palmprint images.

sultant binarized image is shown in Figure 3.3(ii). It is seen that the middle finger and the ring finger are connected in the middle region. However, if we consider the SE of size one, then the resultant binarized image is shown in Figure 3.3(iii), where the middle and the ring fingers are not connected at the middle. Initialise the structuring element (SE) size is 3. The procedure to determine the size of SE dynamically is explained in localization of key points, i.e. section 3.2.



Figure 3.2: Sample palmprint image to illustrate the size of the Structuring Element (SE) to be dynamic (i) palmprint image (ii) binarized image with SE size is 3 (iii) binarized image with SE size is 6.

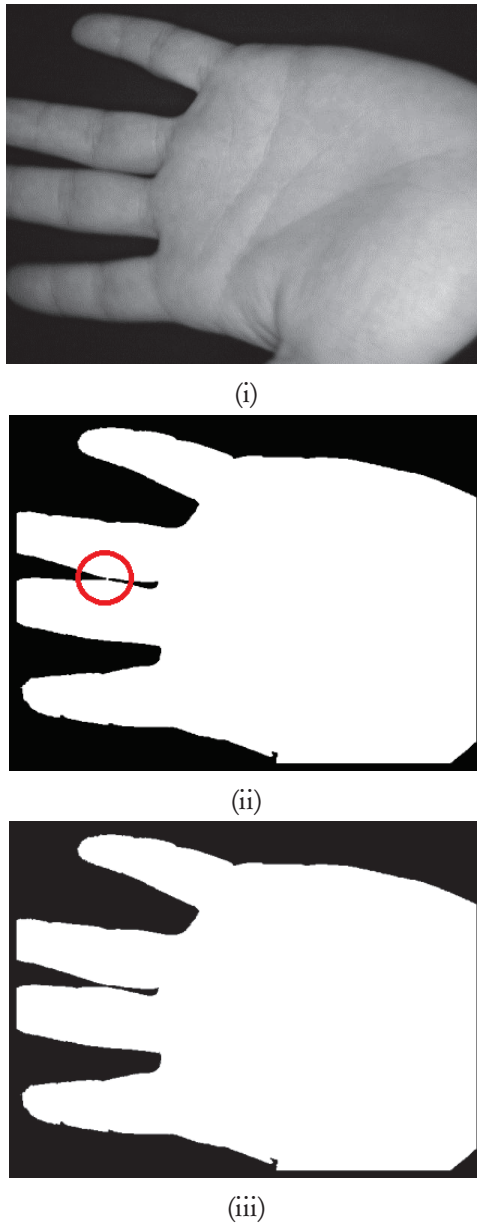


Figure 3.3: (i) Sample palmprint image (ii) binarized image with SE is 3 (iii) binarized image with SE is 1.

3.2 Localization of Key Points

To extract rotation invariant ROI, proper alignment of palmprint is required. To facilitate this, Key Points (KPs) are to be extracted from the palmprint. KP is a point in the valley of the adjacent fingers. For left hand palmprints the KPs between index finger and middle finger, middle finger and ring finger, and ring finger and little finger are named as P_1 , P_2 and P_3 respectively. Similarly, for right hand palmprints, the KPs between little finger and ring finger, ring finger and middle finger, middle finger and index finger are named as P_1 , P_2 and P_3 respectively. The KPs P_1 , P_2 and P_3 for the right-hand palmprint along with the "height" & "width" of the palmprint are depicted in Figure 3.4.

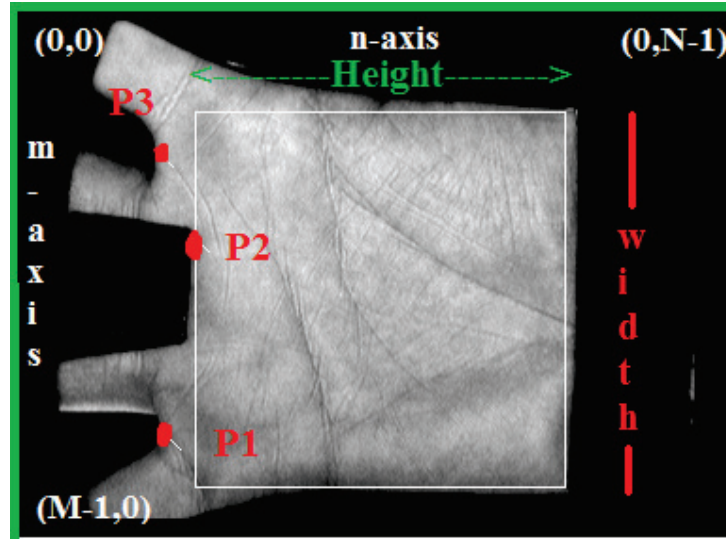


Figure 3.4: Illustration of the Key Points (KPs) $P_1(x_1, y_1)$, $P_2(x_2, y_2)$ and $P_3(x_3, y_3)$ for the Right-Hand Palmprint.

To get the boundary pixels of the binary image $A(m,n)$, Mid-Point (MP) of the "width" is identified by using the following procedure: Let H_1 be a vector of length M . Initialize $H_1(i) = 0 \forall i = 1 \dots M$. H_1 can be calculated by using equation (3.2). $H_1(i) = k$ indicates i^{th} row is having k number of palmprint pixels.

$$H_1(i) = H_1(i) + 1 \text{ if } A(i, j) = 1 \quad \forall i = 0 \dots M-1, j = 0 \dots N-1 \quad (3.2)$$

Observing the palmprint images, the average height of the ROI is equivalent to K_1 where K_1 is the two third of the maximum value of H_1 . Now find the topmost row having K_1 number of palmprint pixels using equation (3.3) and its value be assigned to r_1 . The bottommost row having K_1 number of palmprint pixels is named as r_2 . Its value is calculated by using equation (3.4). The middle row of r_1 and r_2 is named as r and it is calculated by using equation (3.5). The column of rightmost palmprint pixel in r^{th} row is named as c and its value is calculated by using equation (3.6). Now Mid-Point (MP) is (r, c) . MP is depicted in Figure 3.5.

$$r_1 = \{\min(k) \mid H_1(k) > K_1 \quad \forall k = 0, \dots, M-1\} \quad (3.3)$$

$$r_2 = \{\max(l) \mid H_1(l) > K_1 \quad \forall l = 0, \dots, M-1\} \quad (3.4)$$

$$r = \left\lceil \frac{(r_1 + r_2)}{2} \right\rceil \quad (3.5)$$

$$c = \{\max(m) \mid A(r, m) = 1 \quad \forall m = 0, \dots, N-1\} \quad (3.6)$$

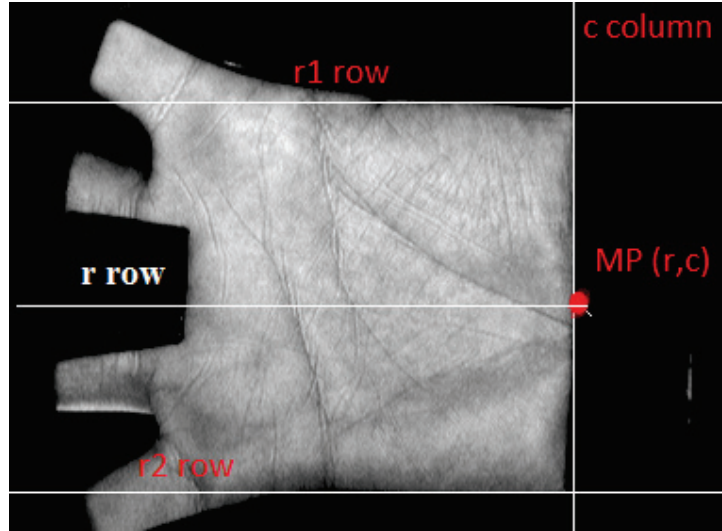


Figure 3.5: Illustration of r_1 row, r_2 row, c column and Mid-Point (MP).

Very few palmprint images of the identified MP may be a foreign object (not belonging to the palmprint pixel). In the entire PolyUPalmprint Database only two palmprints out of 7752 have foreign object as a MP. These palmprints are shown in

the Figure 3.6. These foreign object pixels are identified as the predecessor columns of the same row pixels as background pixels. If MP is a foreign object pixel, then repeatedly reducing the c value by one until correct MP is identified.

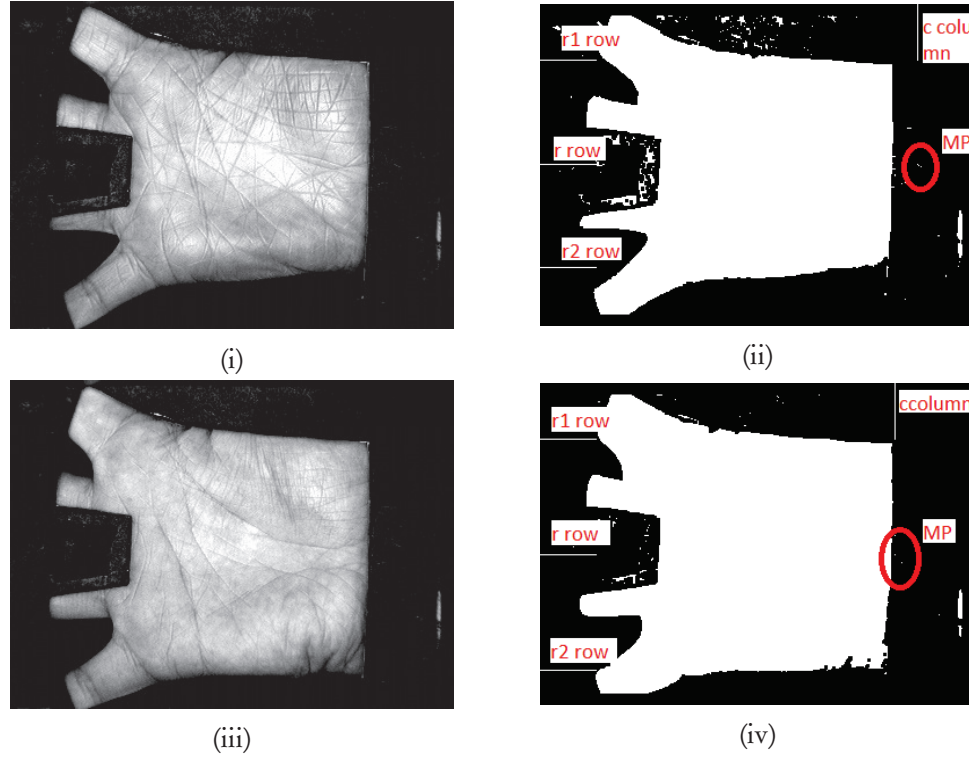


Figure 3.6: Non palmprint pixel is identified as MP (i)&(iii) palmprint images (ii)&(iv) binarized palmprint images.

Inner boundary tracing algorithm [128] is used to extract border pixels starting from MP in anti-clockwise direction. Border pixels are stored in BP (border pixel) 2-dimensional array. Assume BP an array of size u , first column represents m-coordinate values of border pixels, and second column represents n-coordinate values of border pixels and u represents the number of border pixels. Lin et al. [21] used the Euclidean distance from MP to border pixel points to identify finger-webs, but in the proposed approach location of the KPs are identified based on n-coordinate information of border pixels. The n-coordinate values are plotted and the result is depicted in Figure 3.7. The peaks in the curve detects the KPs.

Due to the curve nature of the border pixels at the KP position, the determination of exact peak location is difficult. For example consider KP at location 'A' in the Fig-

ure 3.7. Therefore, to localize the KPs, we need to find the derivative of the border pixel curve. For this, energy values are calculated between points K_2+1 and $u-K_2$ using equation (3.7) where K_2 value is $\max(H_1)/k_3$ and the result is stored in EV. The value of K_2 is nearly equivalent to the finger size, if K_2 value is more than the finger size, it is not possible to identify the key points and if K_2 value is too small, small curves are also considered as a key points. To overcome these problems, the value of K_2 is determined dynamically based on the palmprint image. Further, based on the observation, through the experiments k_3 is determined to have value equal to 10. EV values are plotted and the result is depicted in Figure 3.8. In Figure 3.8 "negative to positive" changes represent KPs. The KPs are named as P_1 , P_2 and P_3 and are depicted in Figure 3.4.

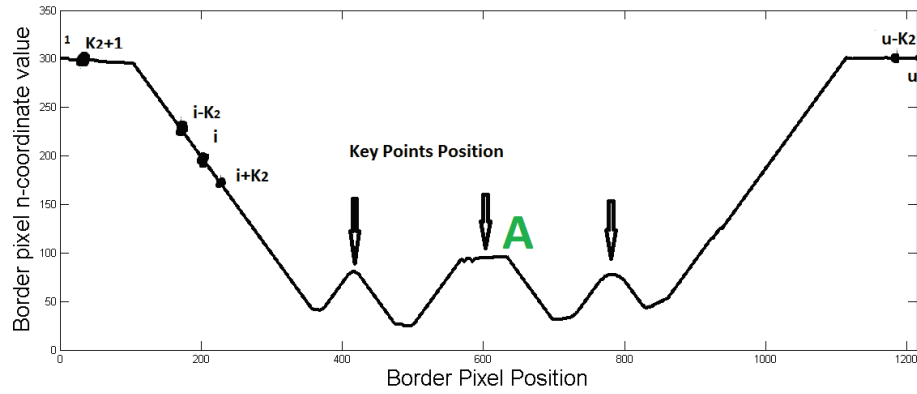


Figure 3.7: Distance distribution diagram using n-coordinate values of border pixels.

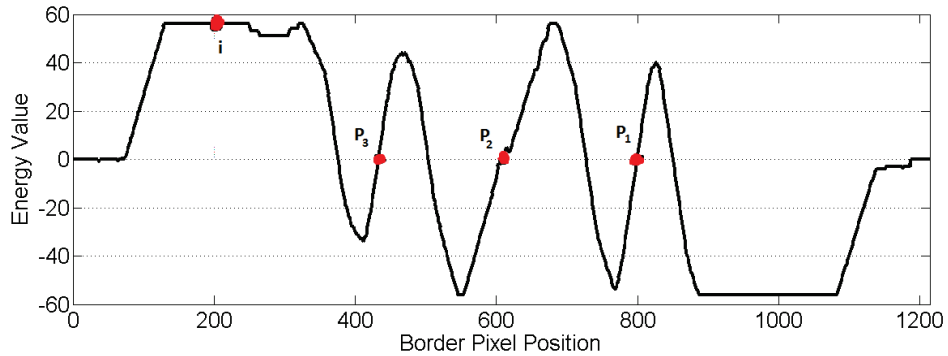


Figure 3.8: Distance distribution diagram of the energy values.

$$EV(i) = BP(i - K_2, 2) - BP(i + K_2, 2) \quad \forall i \text{ between } K_2 + 1 \text{ and } u - K_2 \quad (3.7)$$

For some of the palmprint images finger size is very small, in these palmprints all the KPs are not identified. The sample image is shown in Figure 3.9. In this image the top finger and the second finger from the top side are small. For this reason with $k_3 = 10$, we could identify only two KPs. For these palmprint images increase the k_3 value by 3. If k_3 value greater than 20 then increase SE value by 3 and assign 10 to k_3 . If SE is greater than 20 then assign 1 to SE. The above approach is repeated until all the KPs are obtained. For the palmprint image in Figure 3.9, the three KPs are identified at $k_3 = 13$.

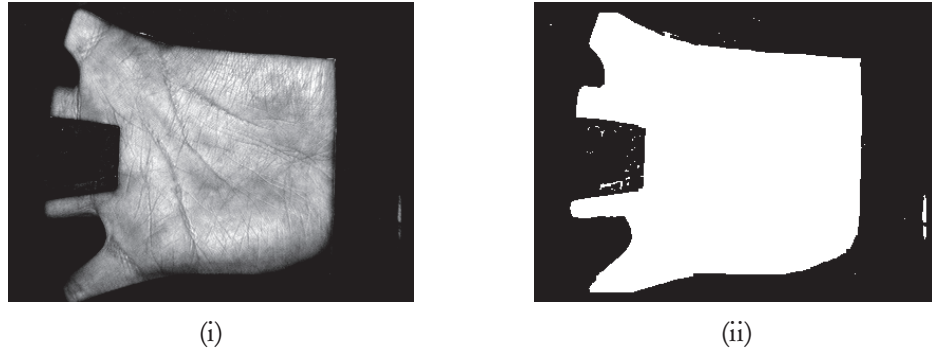


Figure 3.9: Sample palmprint having very small portion of the finger (i) Palmprint image (ii) Binarized palmprint image.

NOTE:

Palmprints in CASIA Palmprint Image Database and IIT Delhi Palmprint Database have five fingers, i.e. these palmprints have 4 valleys between fingers. So the above approach returns 4 KPs. We need to select 3 KPs for which city-block distances between the 1^{st} and 2^{nd} KPs and the 3^{rd} and 4^{th} KPs are calculated and results are assumed as d_1 and d_2 respectively. If $d_1 < d_2$ then the palmprint belongs to left hand and 1^{st} , 2^{nd} and 3^{rd} KPs are considered as required KPs: P_3 , P_2 and P_1 respectively. Otherwise it is right hand palmprint and 2^{nd} , 3^{rd} and 4^{th} KPs are considered as required KPs: P_3 , P_2 and P_1 respectively.

To align P_1 and P_3 points vertically [21], the angle between the points P_1 and P_3 is calculated using equation (3.8).

$$\theta = \tan^{-1}\left(\frac{y_3 - y_1}{x_3 - x_1}\right) \quad (3.8)$$

To perform pivot point rotation with pivot point P_1 , padding is done to the left and the bottom sides of the palmprint image that makes P_1 as the center of the palmprint image. $2 * P_1(x_1) - M$ blank columns are added to the left of the palmprint image and $N - 2 * P_1(y_1)$ rows are added to the bottom of the palmprint image (where $P_1(x_1)$ is the m-coordinate value of P_1 and $P_1(y_1)$ is the n-coordinate value of P_1). After performing the padding, the resulting image size is $(2 * P_1(x_1), 2 * P_1(y_1))$ and $P_1(x_1, y_1)$ is the center of the image. Now rotate the palmprint image with angle θ in clockwise direction if θ is "positive value" otherwise rotate the palmprint image with angle θ in anti-clockwise direction. After performing the rotation, y_1 is equal to y_3 . The resultant palmprint image is shown in Figure 3.10. The step by step procedure to extract the KPs and its position is explained in algorithm 3.1.

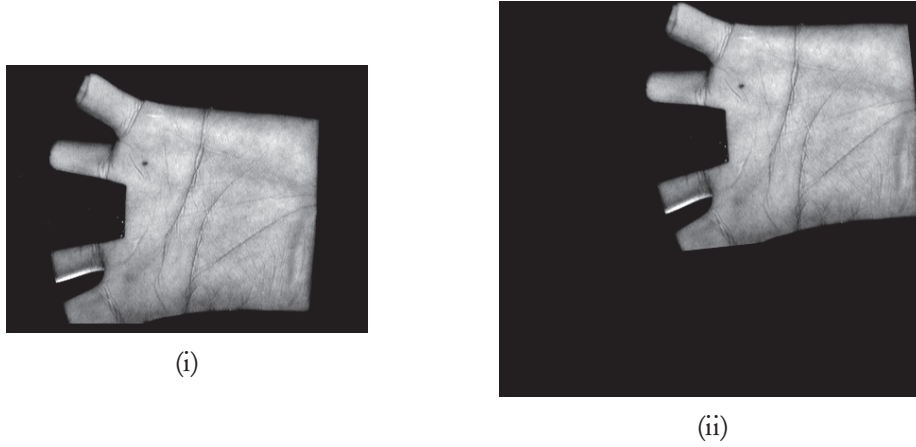


Figure 3.10: Palmprint images to illustrate the KPs: P_1 and P_3 are aligned vertically (i) palmprint before alignment (ii) palmprint after alignment.

3.3 Maximizing ROI

To extract the ROI from the palmprint image, first we need to identify its position. To facilitate this, we proposed the ROI localization algorithm, based on the border pixel information and key points P_1, P_3 . ROI localization algorithm is named as LocalizeROI. Algorithm 3.2 explains the step by step procedure for localization of the ROI. The algorithm takes the BP, P_1 and P_3 as input. In this algorithm, the border

Algorithm 3.1 KPsExtract(F_1): To identify Key Points (KPs) position

//Algorithm for identifying the positions of Key Points//

Input:

F_1 : Input palmprint image of size $M \times N$

Output:

F_2 : Aligned palmprint image of size $M \times N$

BP : Palmprint border pixel information

u : Number of border pixels

x_1, x_2, x_3 : m-coordinate value of the Key Points P_1, P_2 and P_3 respectively

y_1, y_2, y_3 : n-coordinate value of the Key Points P_1, P_2 and P_3 respectively

v_1, v_2, v_3 : positions of the Key Points P_1, P_2 and P_3 in BP

Method:

1. Identify the threshold is used to binarize the palmprint image F_1 . Perform binarization, the binarized image is named as A.
 2. Initialise the structuring element (SE) size is 3.
 3. Apply the morphological operations such as dilate and erode on A, the result image is named as B.
 4. Identify the Mid-Point (MP) in the middle of the Width. Extract border pixels starting from MP in anti-clock wise direction. Border pixels are stored in BP (border pixel) 2-dimensional array. Assume BP an array of size u , first column represents m-coordinate values of border pixels, and second column represents n-coordinate values of border pixels and u represents the number of border pixels.
 5. Calculate the energy values based on n-coordinate information of border pixels.
 6. Identify the position where the energy values changing from negative to positive. These positions represent the KPs. If the number of KPs is greater than or equal to 3 go to next step. Otherwise increase the k_3 value by 3. If k_3 value less than 20 then Go to Step 5, otherwise increase SE value by 3 and assign 10 to k_3 . If SE is greater than 20 then assign 1 to SE. Go to Step 3.
 7. If the number of KPs is 3 then KP_1, KP_2 and KP_3 are considered as P_3, P_2 and P_1 respectively.
 8. If the number of KPs is 4 then
 - Calculate the City-block distance between KP_1 and KP_2 , the result is assigned to d_1 .
 - Calculate the City-block distance between KP_3 and KP_4 , the result is assigned to d_2 .
 - if $d_1 < d_2$ then KP_1, KP_2 and KP_3 are considered as P_3, P_2 and P_1 respectively. Otherwise KP_2, KP_3 and KP_4 are considered as P_3, P_2 and P_1 respectively.
-

-
9. Calculate angle θ between the points P_1 and P_3 .
 10. *if* $\theta > 0$ then rotate the F_1 image with angle θ in clock wise direction, the resultant image is named as F_2 . Re-calculate BP, P_1 , P_2 and P_3 coordinates.
 11. *if* $\theta < 0$ then rotate the F_1 image with angle θ in anti-clock wise direction, the resultant image is named as F_2 . Re-calculate BP, P_1 , P_2 and P_3 coordinates.
 12. Assign P_1 , P_2 and P_3 coordinates to x_1, y_1 , x_2, y_2 , x_3 and y_3 respectively. Assign the positions of KPs in BP: P_1 , P_2 and P_3 to v_1 , v_2 and v_3 .
-

Computational Complexity of KPsExtract	
Steps 1 to 4	$O(MN)$
Step 5 & 6	$O(u)$
Step 8 & 9	$O(u)$
Step 10&11	$O(MN)$
Algorithm Complexity: $O(MN)$	

pixel on the top and bottom on y_1 column in BP are named as T and B respectively. The half of the Euclidean distance between the points T and B is defined as d. The bottommost pixel on border pixels between T-d and T points is identified and its m-coordinate value is assigned to X_T . The topmost pixel on border pixels between B and B+d points is identified and its m-coordinate value is assigned to X_B . ROIs rightmost column position in X_T and X_B rows is assigned in R_1 and R_2 respectively. R_1 holds the rightmost palmprint pixel n-coordinate value in X_T^{th} row. R_2 holds the rightmost palmprint pixel n-coordinate value in X_B^{th} row. The n-coordinate maximum value on the border pixels between P_3 and P_1 is consider as ROI n-coordinate minimum value and it is assigned to Y_L . Minimum of R_1 and R_2 is consider as ROI n-coordinate maximum value and it is assigned to Y_R . The algorithm returns X_T , X_B , Y_L , Y_R , R_1 and R_2 values. The points (X_T, Y_L) , (X_T, Y_R) represents the north-west and north-east corner point of the ROI respectively. Similarly the points (X_B, Y_L) and (X_B, Y_R) represents the south-west and south-east corner point of the ROI respectively. These points are shown in Figure 3.11. The complexity of the algorithm is $O(u)$ where u is the number of border pixels.

Algorithm 3.2 LocalizeROI(BP, γ_1 , v_1 , v_3): To identify the location of the ROI

//Algorithm for extraction of Region of Interest//

Input:

BP : Palmprint border pixel Information
 γ_1 : n-coordinate value of the Key Point P_1
 v_1, v_3 : KPs P_1, P_3 positions in BP

Output:

X_T : m-coordinate Minimum value of the ROI
 X_B : m-coordinate Maximum value of the ROI
 Y_L : n-coordinate Minimum value of the ROI
 Y_R : n-coordinate Maximum value of the ROI
 R_1 : ROI's maximum possible n-coordinate value in North-East corner
 R_2 : ROI's maximum possible n-coordinate value in South-East corner

Method:

1. The border pixel on the top on γ_1 column is named as T. Identify the T value

$$T \leftarrow \{ \min(e) \mid BP[e, 2] = \gamma_1 \ \forall e = 1 \text{ to } u \}$$
 2. The border pixel on the bottom on γ_1 column is named as B. Identify the B value

$$B \leftarrow \{ \max(f) \mid BP[f, 2] = \gamma_1 \ \forall f = 1 \text{ to } u \}$$
 3. Compute $d \leftarrow \left\lceil \frac{(B-T)}{2} \right\rceil$
 4. Identify the m-coordinate value of the bottom most pixel on boarder pixels between T-d and T

$$X_T \leftarrow \max_{T-d \leq i \leq T} BP[i, 1]$$
 5. Identify the m-coordinate top most pixel on boarder pixels between B and B+d

$$X_B \leftarrow \min_{B \leq j \leq B+d} BP[j, 1]$$
 6. Compute the ROI's rightmost column position in X_T row

$$R_{11} \leftarrow \{ \min(k) \mid BP[k, 1] = X_T \ \forall k = 1 \text{ to } T \}$$
 7. Compute the ROI's maximum possible n-coordinate value in North-East corner

$$R_1 \leftarrow BP[R_{11}, 2]$$
 8. Compute the ROI's rightmost column position in X_B rows

$$R_{22} \leftarrow \{ \max(k) \mid BP[k, 1] = X_B \ \forall k = B \text{ to } u \}$$
 9. Compute the ROI's maximum possible n-coordinate value in South-East corner

$$R_2 \leftarrow BP[R_{22}, 2]$$
-

increase the height of the ROI. The step by step procedure to extract maximum possible ROI is given in algorithm 3.3. The algorithm takes X_T , X_B , R_1 , R_2 , x_2 , y_1 as inputs. In this algorithm verify whether the height of the ROI increases if X_T value is increased (or) X_B value is decreased. If the height is increases then automatically update the X_T , X_B , R_1 and R_2 values. This process repeated until obtain the maximum possible ROI. The algorithm returns the enhanced values of X_T , X_B , R_1 and R_2 . The algorithm time complexity is $O(qu)$ where q is the $\max((x_2-T_1), (B_1-x_2))$ and u is the number of border pixels of the binarized palmprint image.

Rightmost column of ROI is considered as minimum of R_1 and R_2 , and it is calculated using equation (3.9) and stored in Y_R . The maximum value of n-coordinate values of border pixels between P_3 and P_1 points, and it is calculated using equation (3.10) and the result is stored in Y_L . Now width of the ROI is the difference of X_B and X_T , and it is calculated using equation (3.11) and stored in W . Height is the difference between Y_R and Y_L , and it is calculated using equation (3.12) and stored in H .

$$Y_R = \min(R_1, R_2) \quad (3.9)$$

$$Y_L = \max_{P_3 \leq i \leq P_1} BP[i, 2] \quad (3.10)$$

$$Width \ W = X_B - X_T \quad (3.11)$$

$$Height \ H = Y_R - Y_L \quad (3.12)$$

Sample ROIs without applying the MaximizeROI algorithm and applying the MaximizeROI algorithm are shown in Figure 3.12. The green colour represents the boarder of ROI without applying the MaximizeROI algorithm and red colour represents the boarder of ROI after applying the MaximizeROI algorithm.

To extract Static ROI, identify the Key Points (KPs) and align the palmprint image using the algorithm 3.1 and then establish the coordinate system based on [21]. The samples of Static and Dynamic ROIs are shown in Figure 3.13.

Algorithm 3.3 MaximizeROI($X_T, X_B, R_1, R_2, x_2, y_1$): To extract maximum possible ROI

//Algorithm for extraction of maximum possible ROI//

Input:

BP : ROI boarder pixel information
 X_T : ROI m-coordinate minimum value
 X_B : ROI m-coordinate maximum value
 R_1 : ROI north-east corner point
 R_2 : ROI south-east corner point
 x_2 : m-coordinate value of the key point P_2
 y_1 : n-coordinate value of the key point P_1

Output:

X_T : Enhanced ROI m-coordinate minimum value
 X_B : Enhanced ROI m-coordinate maximum value
 R_1 : Enhanced ROI north-east corner point
 R_2 : Enhanced ROI south-east corner point

Method: if we reduce a small value of width then height may increase

1. Initialize T_1 and B_1
 $T_1 \leftarrow X_T - 1$
 $B_1 \leftarrow X_B - 1$
 2. while $T_1 < x_2$ or $B_1 > x_2$ do
 3. begin
 4. Compute the width of the ROI
 $W \leftarrow X_B - X_T$
 5. Compute the height on Right portion of ROI
 $H_1 \leftarrow R_1 - y_1$
 6. Compute the height on Left portion of ROI
 $H_2 \leftarrow R_2 - y_1$
 7. Compute the height of the ROI
 $H \leftarrow \min(H_1, H_2)$
 8. if width is less than height then stop the process
if $W < H$ *then* Return X_T, X_B, R_1, R_2
 9. *else begin*
 10. $r \leftarrow \frac{H}{W}$
 11. *if* $R_1 < R_2$ *then begin*
 $R_{33} \leftarrow \{\min(k) | BP[k, 1] = T_1 \quad \forall k = 1 \text{ to } T\}$
 $r_3 = BP[R_{33}, 2]$
if $R_3 - R_1 > (r * (T_1 - X_T))$ *then begin*
 $R_1 \leftarrow R_3$ $X_T \leftarrow T_1$ *end*
 $T_1 \leftarrow T_1 + 1$
end
-

```

12.      else begin
            $R_{44} \leftarrow \{\max(k) \mid BP[k, 1] = X_B \ \forall k = B \text{ to } u\}$ 
            $r_4 = BP[R_{44}, 2]$ 
           if  $R_4 - R_2 > (r * (X_B - B_1))$  then begin
                $R_2 \leftarrow R_4$ 
                $X_B \leftarrow B_1$ 
           end
            $B_1 \leftarrow B_1 - 1$ 
       end

13.      end

14. end

15. Return  $X_T, X_B, R_1, R_2$ 

```

Computational Complexity of MaximizeROI	
q is the $\max((x_2 - T_1), (B_1 - x_2))$ and	
u is the number of border pixels of the binarized palmprint image	
Steps 11 and 12	$O(u)$
Steps 3 to 12 repeated at maximum q times	
Algorithm Complexity: $O(qu)$	

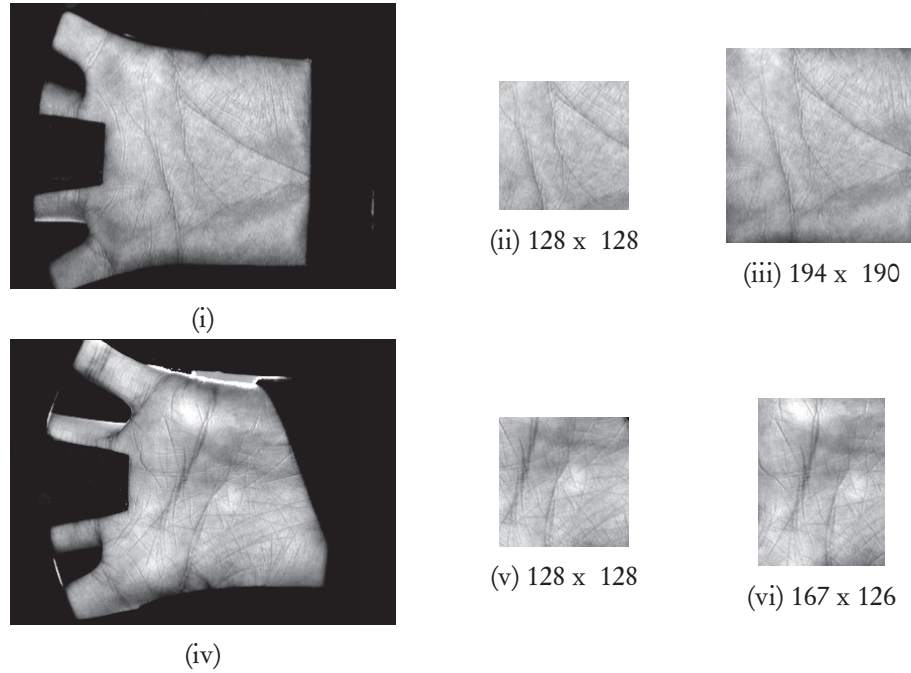


Figure 3.13: (i)&(iv) palmprint images (ii)&(vi) Static ROIs (iii)&(vii) Dynamic ROIs.

In the proposed maximized dynamic ROI extraction approach, the ROIs sizes of the same palm may be different. So, the dynamic ROIs must be aligned before per-

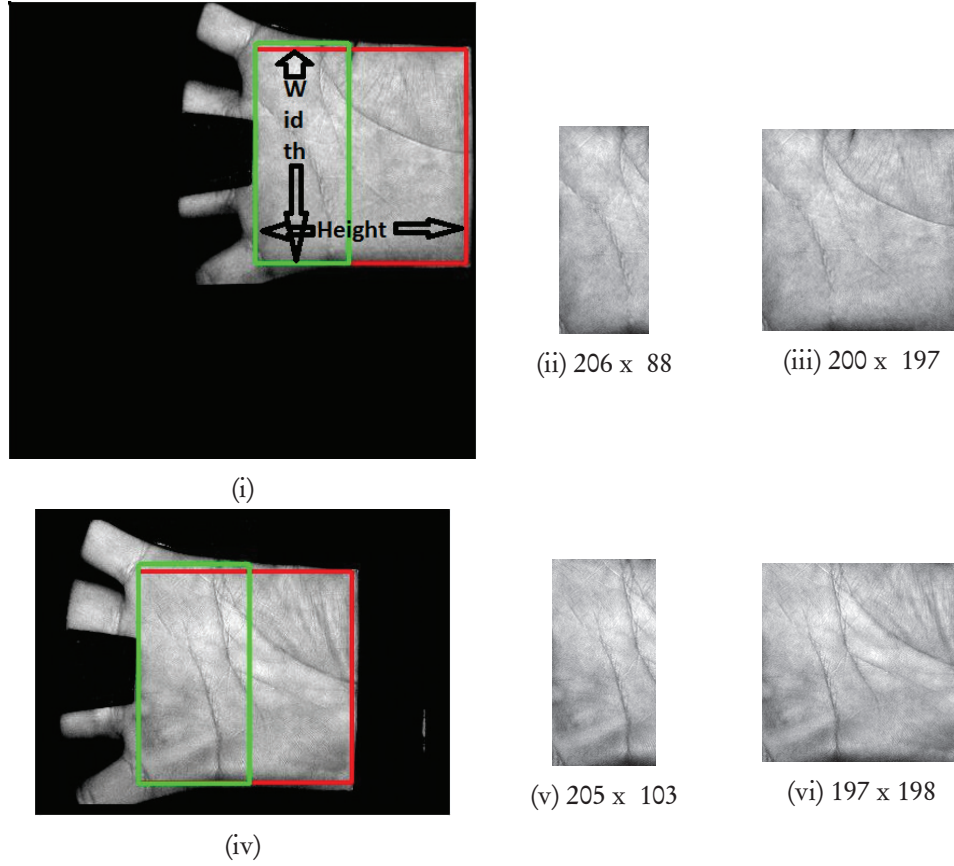


Figure 3.12: Sample ROIs before and after applying the MaximizeROI algorithm (i)&(iv) palmprint images (ii)&(v) ROIs before applying MaximizeROI algorithm (iii)&(vi) ROIs after applying MaximizeROI algorithm.

forming the matching (comparison). To align the palmprint images at the time of comparison, obtain the reference point information for every ROI using equations (3.13) and (3.14). DX and DY are shown in Figure 3.14.

$$DX = \left\lceil \frac{(x_1 + x_3)}{2} \right\rceil - X_T \quad (3.13)$$

$$DY = Y_L - y_1 \quad (3.14)$$

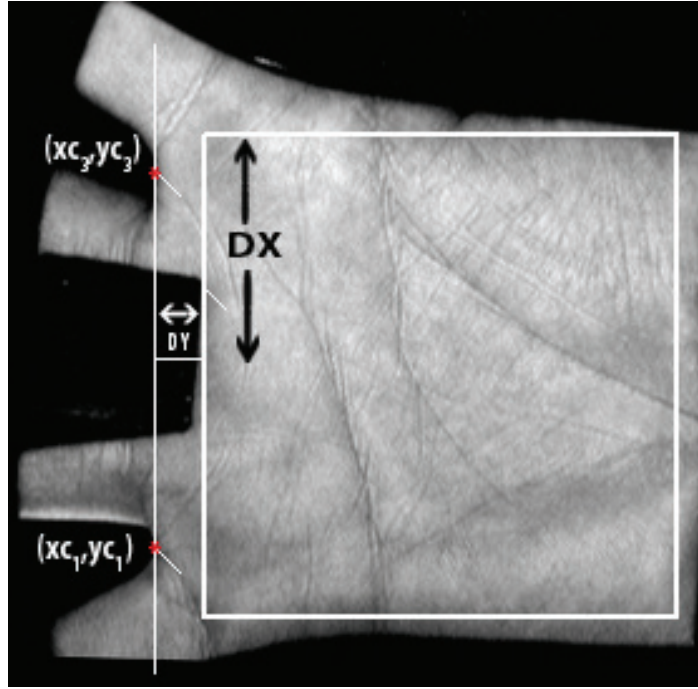


Figure 3.14: Illustration of the reference points DX and DY.

3.4 Registration

In registration, for every palmprint in the database images extract the dynamic ROI and its reference point information. Store the dynamic ROI and its reference point information in dynamic ROI database. The block diagram is shown in Figure 3.15.

Dynamic ROIs are stored in a folder. To store the reference point information, four two dimensional vectors are defined and these are named as FDX, FDY, SDX, SDY. If the registered palmprint represents the first session i^{th} palm j^{th} image, then it's DX and DY values are stored in i^{th} row of j^{th} column in FDX and FDY respectively. Similarly, if the registered palmprint represents the second session i^{th} palm j^{th} image, then it's DX and DY values are stored in i^{th} row of j^{th} column in SDX and SDY respectively.

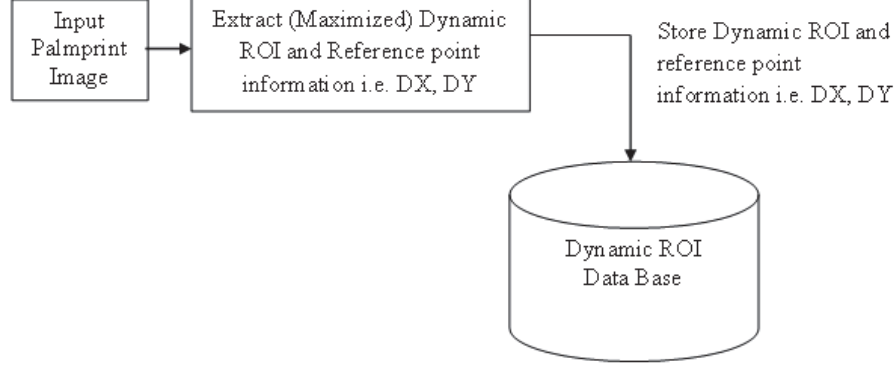


Figure 3.15: Schematic diagram for dynamic ROI registration.

3.5 Experimental Results

To test the proposed ROI extraction algorithm, experiments were performed on the PolyUPalmprint Database, CASIA Palmprint Image Database and IIT Delhi Palmprint Database. The experiments on these three databases were conducted on a system with an Intel Core i3 processor (2.4 GHz) and 2GB RAM configured with Windows 7 and MATLAB R2012b with image processing toolbox.

3.5.1 Experiments on PolyUPalmprint Database

Most of the researchers [14, 20–22, 30, 35, 66, 109, 129] used the PolyUPalmprint database [17] and they extracted fixed size ROI. This database contained 7752 grayscale images corresponding to 386 different palms in BMP image format. Around 20 images from each palm are collected in two sessions. The images are acquired by placing pegs and using CCD at a spatial resolution of 75 dpi and 256 gray levels. Results are depicted in Figure 3.16. The proposed approach extracted ROIs having the minimum, maximum and average widths as 148, 202, and 188 respectively. Minimum, maximum and average heights are 119, 200 and 184 respectively. The ROIs extracted using dynamic approach [16] having the minimum, maximum and average widths (same as heights) are 165, 214 and 192 respectively. The number of ROIs having background using the

fixed size approach [21], dynamic approach [16], and the proposed approach are 47, 7214, and 0 respectively. The analysis of the background information of ROI is given in Table 3.1. The analysis of the ROI sizes and time required to extract ROI are given in Table 3.2 and Table 3.3 respectively.

The experiments demonstrated that fixed size ROI [21] covers a small area and valuable information is missed whereas dynamic size ROI of [16] extracts maximum size ROI but 93.04% ROIs have unwanted background information. In Figure 3.16(i) the ROI extracted using [16] is 197 x 197 and it has 4482 background pixels i.e. background is 12%. Using [21] extracted ROI size is 128 x 128 and it has 647 background pixels i.e. background is 4%. Using the proposed algorithm ROI extracted in Figure 3.16(iv) ROI size is 166 x 163 without the background information. So compared to the fixed size approach [21] and dynamic size approach [16], the proposed algorithm extracts maximum size ROI without background information.

Table 3.1: Number of ROIs with background information using proposed approach, static approach [21] and dynamic approach [16] on PolyUPalmprint database

	Static approach [21]	Dynamic approach [16]	Proposed approach
No of ROIs with background information	47	7214	0

Table 3.2: Maximum, minimum and average height, width for ROI extraction and percentage of background in ROI using Proposed approach, Static approach [21] and Dynamic approach [16] on PolyUPalmprint database

Property	Minimum			Maximum			Average		
	Static approach [21]	Dynamic approach [16]	Proposed approach	Static approach [21]	Dynamic approach [16]	Proposed approach	Static approach [21]	Dynamic approach [16]	Proposed approach
Height	128	165	119	128	214	200	128	192	184
Width	128	165	148	128	214	202	128	192	188
Background%	0	0	0	4	14	0	0.0096	2.42	0

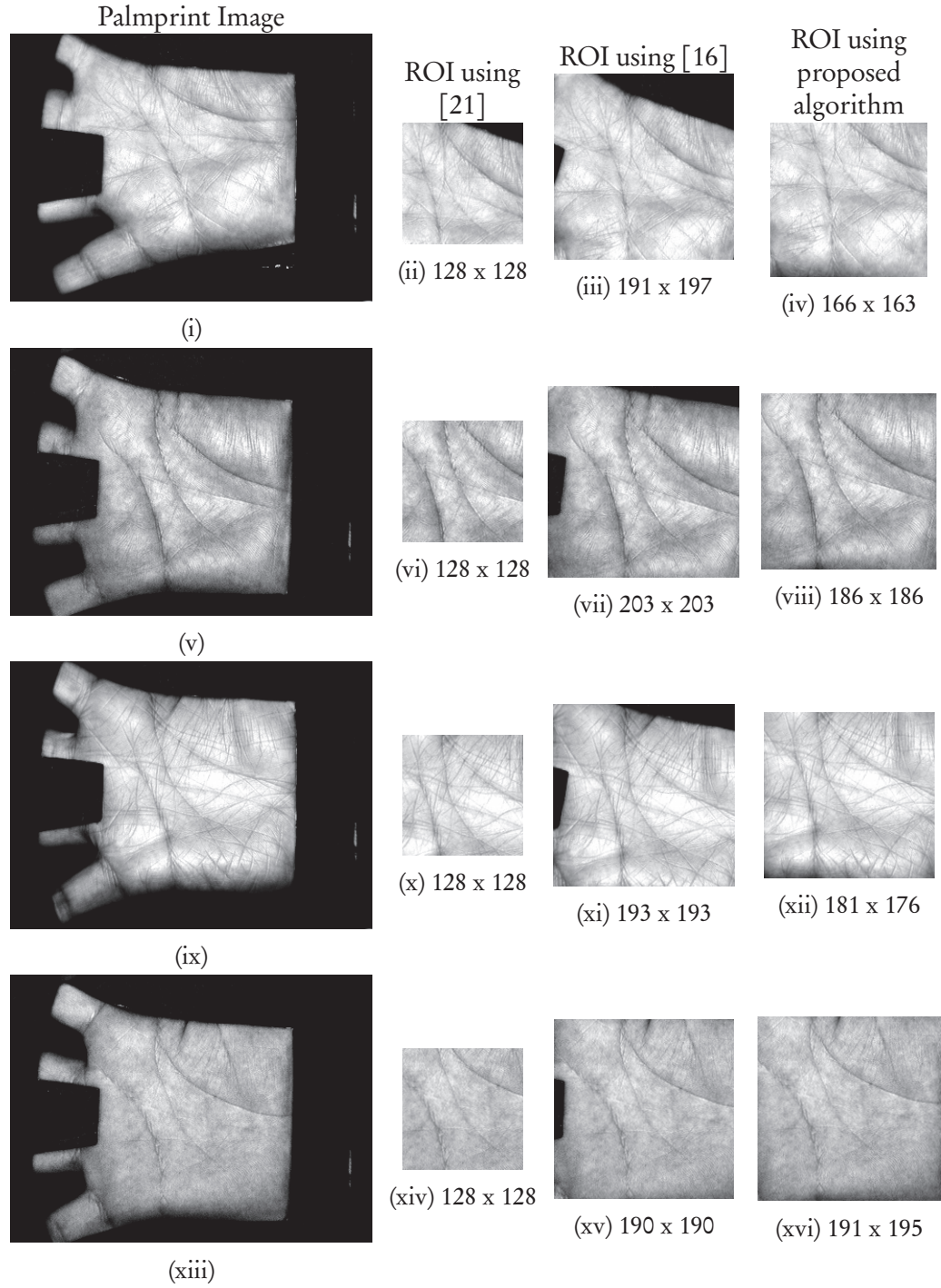


Figure 3.16: The ROIs extracted using [16, 21] and proposed method on PolyUPalm-print database.

Table 3.3: Maximum, minimum and average time in seconds for dynamic ROI extraction of the proposed approach on PolyUPalmprint database

	Minimum	Maximum	Average
Time in seconds	0.0204	0.7192	0.0919

3.5.2 Experiments on CASIA Palmprint Image Database

Another popular database is CASIA palmprint image database [18] contains 5502 images captured from 312 individuals in 8bit JPEG image format. The proposed algorithm was applied on this database. The proposed approach extracted ROIs having the minimum, maximum and average widths are 150, 395, and 300 respectively. Minimum, maximum and average heights are 152, 436 and 325 respectively. The ROIs extracted using dynamic approach [16] having the minimum, maximum and average widths (same as heights) are 172, 365 and 273 respectively. The number of ROIs having background using the fixed size approach [21], dynamic approach [16], and the proposed approach are 0, 218, and 0 respectively. The experiments on the CASIA palmprint image database demonstrated that fixed size ROI [21] covers small area with valid information missing. ROI extraction method of [16] is suitable for this database. However, some of the images of ROI retain background while the images produced through our approach gives maximum size ROI without background. The analysis of the background information of ROI is given in Table 3.4. The analysis of the ROI sizes and time required for extraction of ROI are given in Table 3.5 and Table 3.6 respectively.

Results of the proposed algorithm are compared with fixed size ROI [21] extraction algorithm and dynamic ROI extraction algorithm [16]. Results are depicted in Figure 3.17. The experiments demonstrated that fixed size ROI [21] covers small area with valid information missing. In Figure 3.17(v) the ROI extracted using [16] is 332 X 332, and has 711 background pixels i.e. background is 1% and ROI extracted using

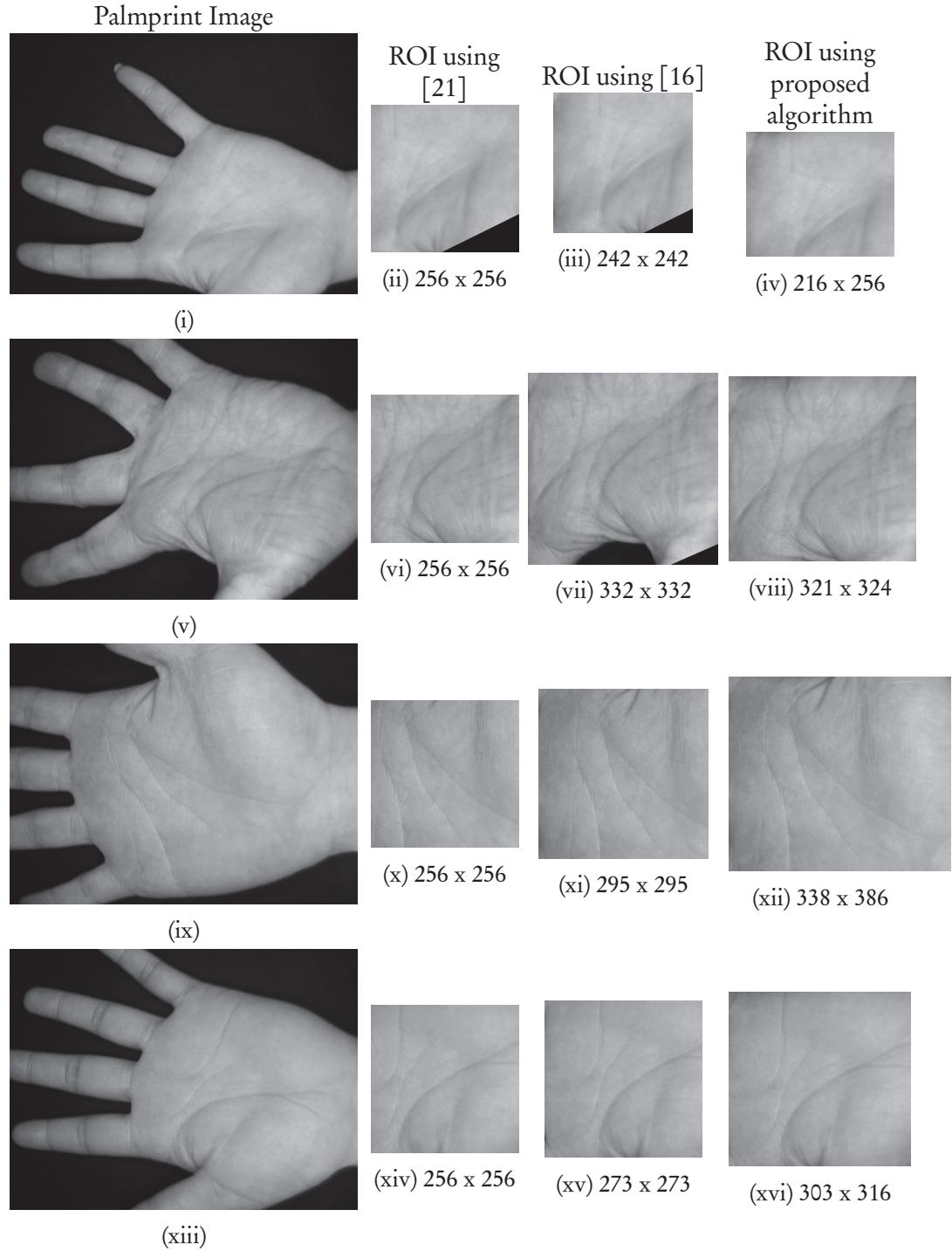


Figure 3.17: The ROIs extracted using [16, 21] and proposed method on CASIA palm-print image database.

Table 3.4: Number of ROIs with background information using proposed approach, static approach [21] and dynamic approach [16] on CASIA palmprint image database

	Static approach [21]	Dynamic approach [16]	Proposed approach
No of ROIs with background information	51	218	0

Table 3.5: Maximum, minimum and average height, width for ROI extraction and percentage of background in ROI using proposed approach, static approach [21] and dynamic approach [16] on CASIA palmprint image database

Property	Minimum			Maximum			Average		
	Static approach [21]	Dynamic approach [16]	Proposed approach	static approach [21]	Dynamic approach [16]	Proposed approach	Static approach [21]	Dynamic approach [16]	Proposed approach
Height	256	172	152	256	365	436	256	273	325
Width	256	172	150	256	365	395	256	273	300
Background %	0	0	0	7	9	0	0.02	0.0713	0

Table 3.6: Maximum, minimum and average time in seconds for dynamic ROI extraction of the proposed approach on CASIA palmprint image database

	Minimum	Maximum	Average
Time in seconds	0.0381	0.54887	0.1478

[21] ROI size is 256 X 256, which has no background pixels over which the proposed approach extracted ROI size is 321 x 324 without unwanted background information maintained. This proves that compared to the fixed size approach [21] and dynamic size approach [16], the proposed algorithm extracts maximum size ROI without background information.

3.5.3 Experiments on IIT Delhi Touchless Palmprint Database

The proposed algorithm was also applied on IIT Delhi touchless palmprint database [19] contains 2769 images captured from 233 individuals in 8bit JPEG image format. The proposed approach extracted ROIs having the minimum, maximum and average widths are 149, 313, and 220 respectively. Minimum, maximum and average heights are 111, 322 and 232 respectively. The ROIs extracted using dynamic approach [16] having the minimum, maximum and average widths (same as heights) are 145, 306 and 215 respectively. The number of ROIs having background using the fixed size approach [21], dynamic approach [16], and the proposed approach are 0, 206, and 0 respectively. It is found that dynamic approach [16] ROI sizes are nearly equivalent to proposed approach and the proposed approach extracts ROIs without background. The analysis of the background information of ROI is given in Table 3.7. The analysis of the ROI sizes and time required to extract ROI are given in Table 3.8 and Table 3.9 respectively.

Results of the proposed algorithm are compared with fixed size ROI [21] extraction algorithm and dynamic size ROI extraction algorithm [16]. The results are depicted in Figure 3.18. It is found that dynamic approach [16] ROI sizes are nearly equivalent to proposed approach and some ROI [16] sizes are more than the proposed approach sizes though the ROIs retain background information. In Figure 3.18(ix) the ROI extracted using [16] is 294 x 294, and it has 3997 background pixels i.e. background is 5% whereas the proposed approach extracted ROI size is 258 x 237 without background information. The experiments demonstrated fixed size ROI [21] covers

small area with valuable information missing. ROI extraction method of [16] is nearly equivalent to our approach but ROIs will retain background information. Thus compared to the fixed size approach [21] and dynamic size approach [16] the proposed algorithm extracts maximum possible region without background information.

Table 3.7: Number of ROIs with background information using proposed approach, static approach [21] and dynamic approach [16] on IIT Delhi touchless palmprint database

	Static approach [21]	Dynamic approach [16]	Proposed approach
No of ROIs with background information	4	206	0

Table 3.8: Maximum, minimum and average Height, Width for ROI extraction and percentage of background in ROI using proposed approach, static approach [21] and dynamic approach [16] on IIT Delhi touchless palmprint database

Property	Minimum			Maximum			Average		
	Static approach [21]	Dynamic approach [16]	Proposed approach	static approach [21]	Dynamic approach [16]	Proposed approach	Static approach [21]	Dynamic approach [16]	Proposed approach
Height	150	145	111	150	306	322	150	215	232
Width	150	145	149	150	306	313	150	215	220
Background %	0	0	0	0.18	17	0	0.0002	0.219	0

Table 3.9: Maximum, minimum and average time in seconds for dynamic ROI extraction of the proposed approach on IIT Delhi touchless palmprint database

	Minimum	Maximum	Average
Time in seconds	0.0408	0.5161	0.1557

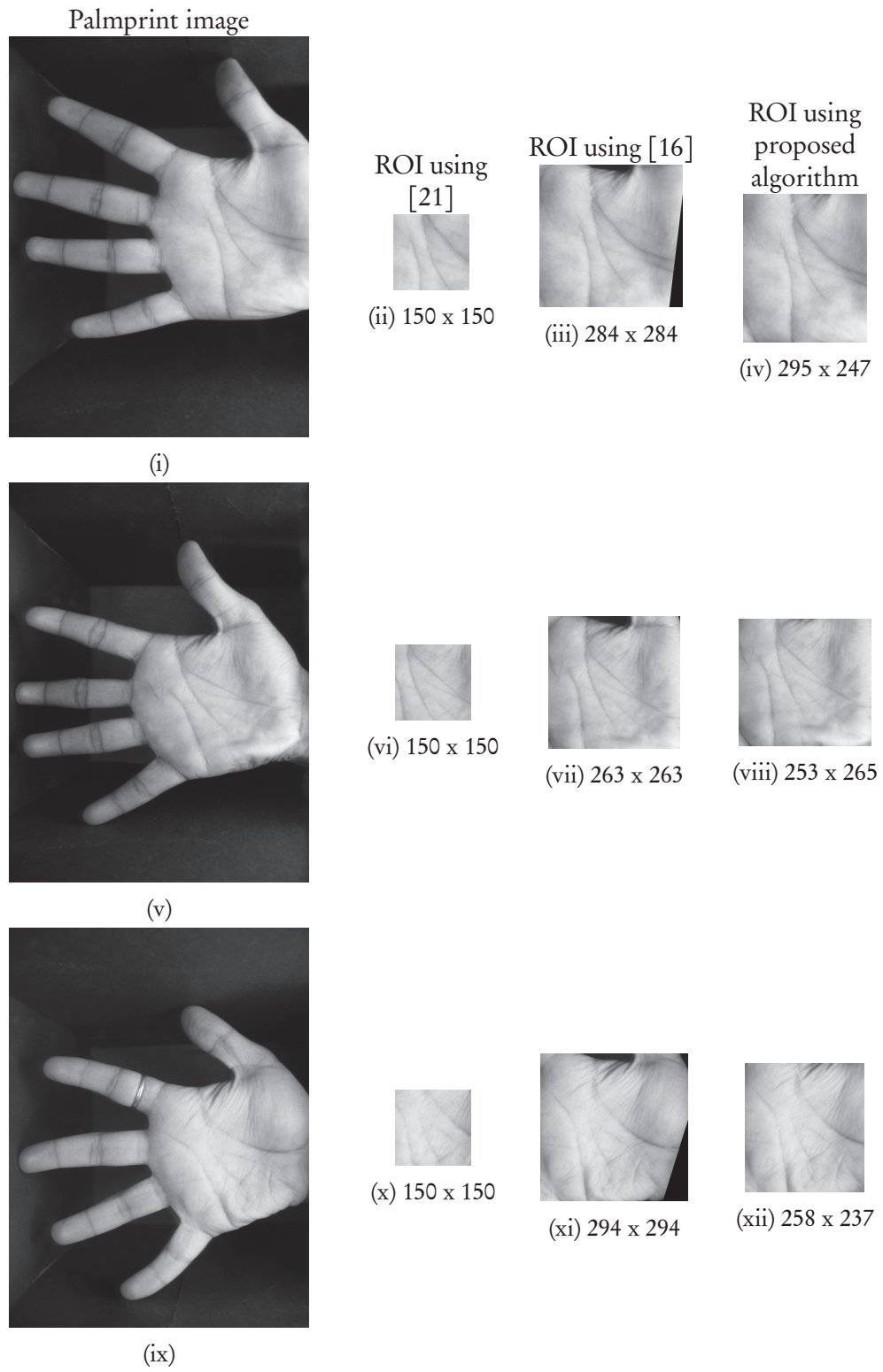


Figure 3.18: The ROIs extracted using [16, 21] and proposed method on IIT Delhi touchless palmprint database.

3.6 Summary

In this chapter, we proposed maximized dynamic ROI extraction approach for palmprints. Mode method is used to perform binarization of the palmprint image. To perform the preprocessing applied the morphological operators on the obtained binarized image. In order to identify the KPs, proposed a KP extraction algorithm using the n-coordinate information of border pixels. These KPs are used to align the palmprint image. The BP and KP information is used to localize the ROI.

Maximize ROI algorithm is proposed to extract maximum possible ROI and in the process, reference point information is obtained. The reference point information will be used to extract the common region of two dynamic ROIs of the same palmprint at the time of verification and identification. The experimental results demonstrated that the proposed approach extracts maximum possible region without background information when compared to the existing fixed [21] and dynamic [16] size ROI extraction techniques on the three databases: (1)The PolyU Palmprint Database, (2)CASIA Palmprint Image Database and (3) IIT Delhi Palmprint Database.

CHAPTER 4

Feature Extraction

Our literature survey in Chapter 2 reveals that the lines and wrinkles are visually distinguishable features of palmprint and these are stable throughout the life time. Thus, line based approaches play a vital role in palmprint recognition. Researchers used the Sobel and Canny edge operators, complete wavelet expansion and directional context modelling, line detectors using 1^{st} and 2^{nd} order derivatives, Modified Finite Radon Transform, internal image seams to extract principal lines. Liu et al. [27] proposed wide line detectors based on the isotropic responses via circular masks and not much research work has been reported using wide principal lines. A sample palmprint image with principal lines such as life line, heart line and head line are shown in Figure 4.1.

Our literature survey also reveals that the statistical features are also distinguishable features of palmprint and these features obtained after perform transformation (Fourier Transform, DCT, Gabor Filter etc.). Thus, statistical features based approaches also play a vital role in palmprint recognition and not much research work has been reported to extract statistical features extracted directly from ROI (without transformations).

The rest of the chapter is organised as follows: details of wide principal line feature extraction is developed in section 4.1. Details of statistical feature extraction is described in section 4.2.

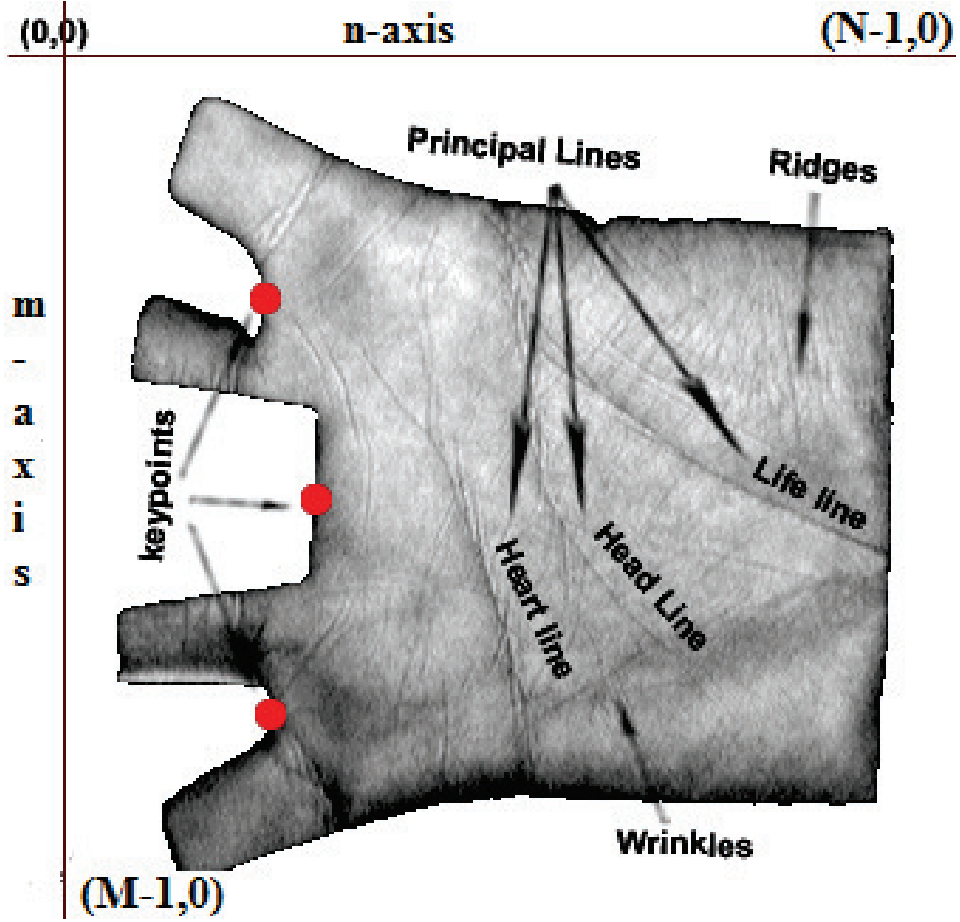


Figure 4.1: Palmprint image labelling with life line, head line and heart line.

4.1 Wide Principal Line Feature Extraction

Finite Radon transform (FRAT) was proposed by Frantisek et al. [132] to extract lines. FRAT of a real function $f(x,y)$ on a finite grid Z_p^2 is defined as

$$FRAT_f(k,l) = \frac{1}{\sqrt{p}} \sum_{(i,j) \in L_{k,l}} f(i,j) \quad (4.1)$$

where p is the size of the grid, k and l represents the slope and intercept of the line respectively.

The Modified Finite Radon Transform (MFRAT) proposed by Hung et al. [22] to

extract line features. MFRAT of real function $f[x, y]$ on the finite grid Z_p^2 is defined as

$$MFRAT_f(k) = \frac{1}{c} \sum_{(i,j) \in L_k} f[i, j] \quad (4.2)$$

where c is a scalar constant and k is the slope of the line.

4.1.1 Mask construction for line and curve extraction

MFRAT [22] can be used only for straight lines with orientation of $\pi/12, 2\pi/12, \dots, 12\pi/12$. However in palmprints, principal lines are not straight and for accuracy purpose they have to be treated as curves. To overcome the limitations of MFRAT, we propose a Wide Principal Line Extractors (WPLE) masks to extract the principal lines. Based on the observation of the palmprint images, we proposed 32 Wide Principal Line Extractors (WPLE) (i.e. C_1, C_2, \dots, C_{32}) to cover straight lines with orientation of $\pi/12, 2\pi/12, \dots, 12\pi/12$ and remaining 20 WPLEs are used to cover curve portion in these orientations. The proposed 32 WPLEs are shown in Figure 4.2 and Figure 4.3. Each extractor size is 14×14 .

The WPLEs C_8 to C_{12} and C_{27} to C_{31} were defined to extract life line pixels of the right hand palmprint image. The WPLEs C_9, C_{10}, C_{27} to C_{30} and C_{32} were defined to extract life line pixels of the left hand palmprint image. The WPLEs C_6 to C_9, C_{22} and C_{23} were defined to extract heart line pixels of the right hand palmprint image. The WPLEs C_3, C_4, C_6, C_{20} to C_{23}, C_{27}, C_{30} and C_{32} were defined to extract heart line pixels of the left hand palmprint image. The WPLEs C_4, C_6 to C_9, C_{22}, C_{23} and C_{28} were defined to extract head line pixels of the right hand palmprint image. The WPLEs $C_8, C_9, C_{21}, C_{23}, C_{27}, C_{30}$ and C_{32} were defined to extract heart line pixels of the left hand palmprint image. The remaining extractors were defined to extract wrinkles.

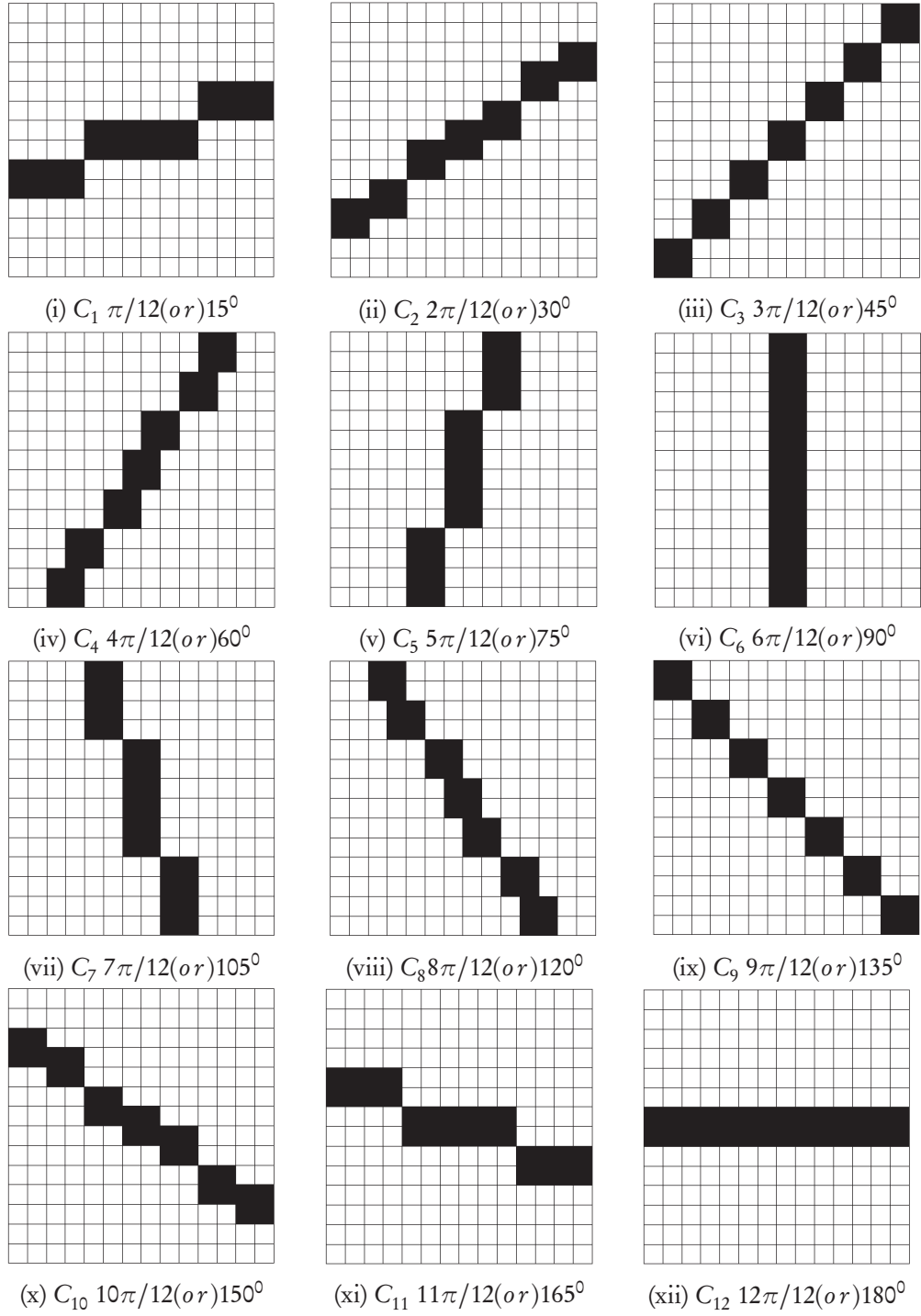
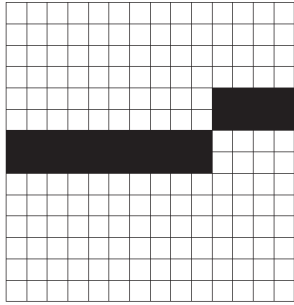
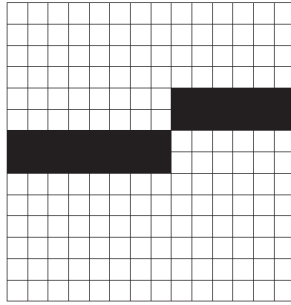


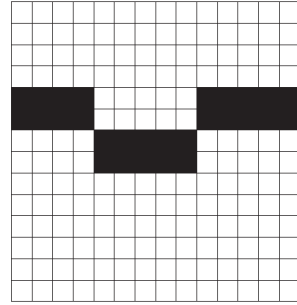
Figure 4.2: Wide Principal Line Extractors with different orientations.



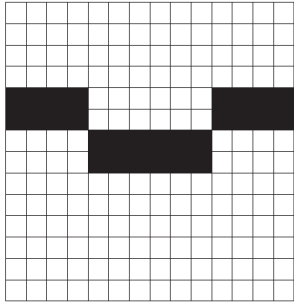
(i) C_{13}



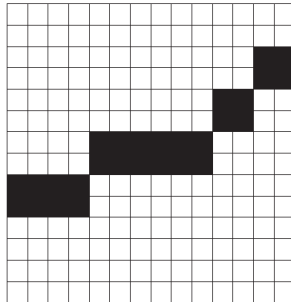
(ii) C_{14}



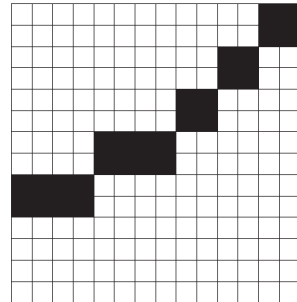
(iii) C_{15}



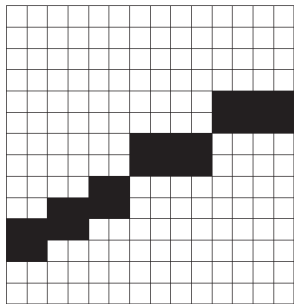
(iv) C_{16}



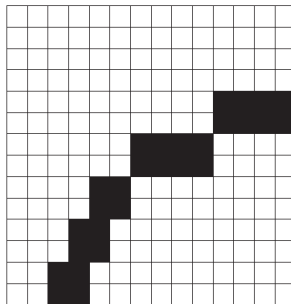
(v) C_{17}



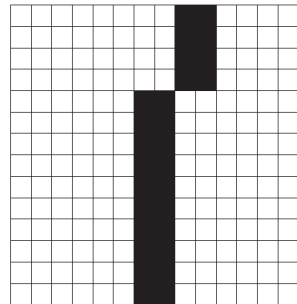
(vi) C_{18}



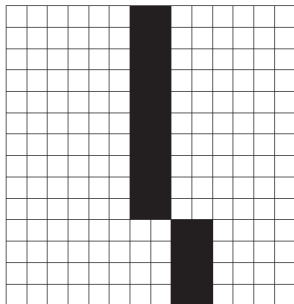
(vii) C_{19}



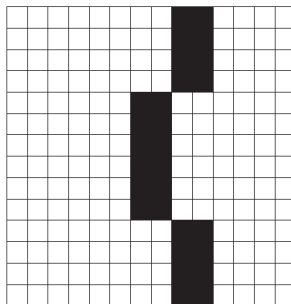
(viii) C_{20}



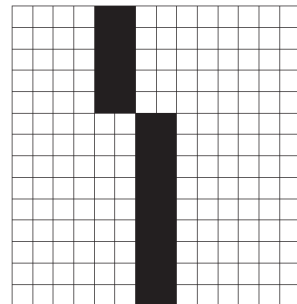
(ix) C_{21}



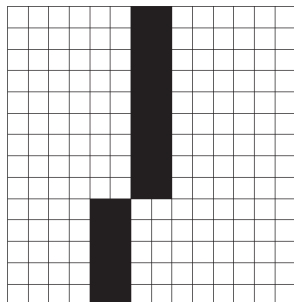
(x) C_{22}



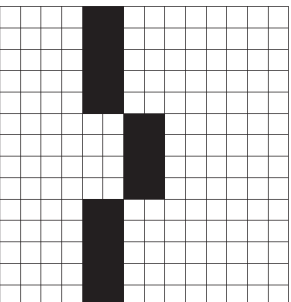
(xi) C_{23}



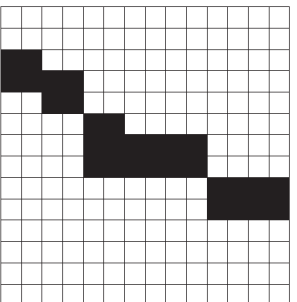
(xii) C_{24}



(xiii) C_{25}



(xiv) C_{26}



(xv) C_{27}

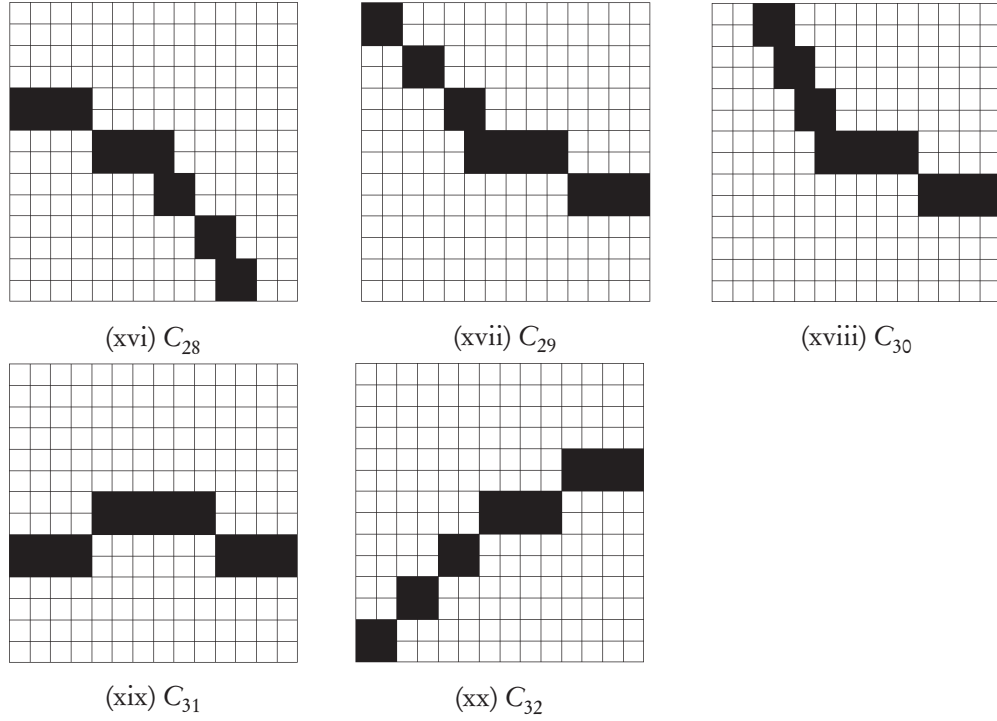


Figure 4.3: Wide Principal Line Extractors to extract curve region.

4.1.2 Energy of ROI

To generate the Wide Principal Line Image (WPLI), energy of ROI is calculated. Hung et al. [22] used the MFRAT to generate the energy image. The proposed approach to calculate the energy of ROI is as follows. Z is a window of size 14×14 , initially it is at the top of the left corner of the ROI. The mean of Z is subtracted from each pixel in Z . The result is named as z' . Wide Principal Line Extractors (WPLE) of a real function z' is named as $wpler$ and it is calculated using equation (4.3). $wpler[C_k]$ represents the sum of the elements of z' where its corresponding elements in C_k is 1.

$$wpler[C_k] = \sum_{(i,j) \in C_k} z'[i,j] \quad \forall k = 1 \dots 32 \quad (4.3)$$

From the $wpler$, the *energy* is calculated by using the equation (4.4).

$$energy = \min(wpler[C_k]) \quad \forall k = 1 \dots 32 \quad (4.4)$$

Initially *Energy_image* size is the size of the ROI (i.e. $u \times v$) all with zeros. Now *energy* value is compared with the corresponding window Z center points in *Energy_image* (i.e. $e(7,7), e(7,8), e(8,7), e(8,8)$), if *energy* value is smaller than existing value then assign the *energy* value in the compared locations. In this way, the energies of all pixels are calculated by moving the window Z to move over the input image (ROI) pixel by pixel from left to right and top to bottom.

For an input ROI image $I(m, n)$ of size $u \times v$, the *Energy_image* is shown below

$$\text{Energy_image} = \begin{vmatrix} e(0,0) & e(0,1) & \dots & e(0,v-1) \\ e(1,0) & e(1,1) & \dots & e(1,v-1) \\ \dots & \dots & \dots & \dots \\ e(u-1,0) & e(u-1,1) & \dots & e(u-1,v-1) \end{vmatrix}$$

The sample ROI images and its corresponding *Energy_images* are shown in Figure 4.4 and 4.5 respectively.

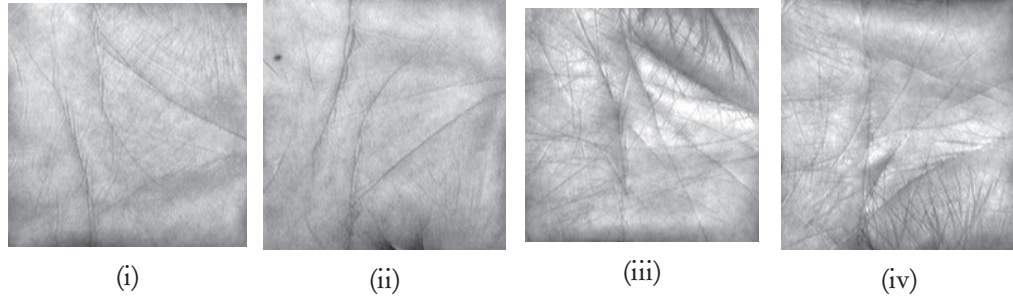


Figure 4.4: Sample ROIs.

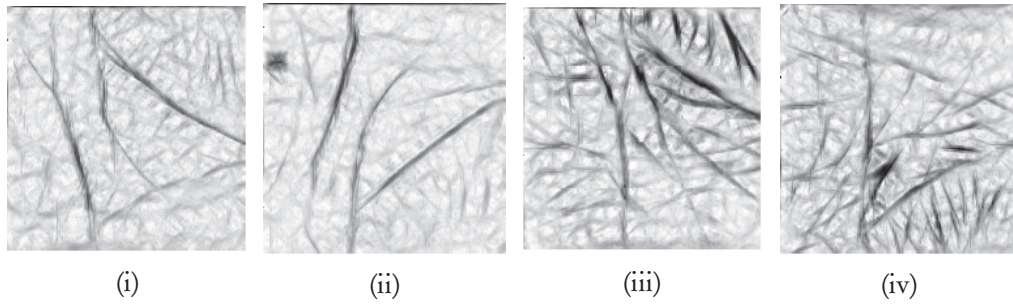


Figure 4.5: Sample *Energy_images*.

4.1.3 Post-processing

Hung et al.[22] extracted 2000 pixels from each ROI as principal line pixels. But in Dynamic ROIs, the ROI size and the number of principal line pixels also varies. Hence, wide principal lines and wrinkles are extracted using equation (4.5) by dynamically selecting a threshold T_1 , which is computed from the Energy_image. Here, the obtained binary image is called as Lines_image.

$$Lines_image(m,n) = \begin{cases} 1 & \text{if } Energy_image(m,n) < T_1 \\ 0 & \text{otherwise} \end{cases} \quad (4.5)$$

The threshold T_1 is chosen as T_2 % of number of pixels in Energy_image is less than T_1 . Based on the experiments T_2 value is determined as 25 and 22.72 for dynamic and static ROIs respectively. The sample Lines_images are shown in Figure 4.6 .

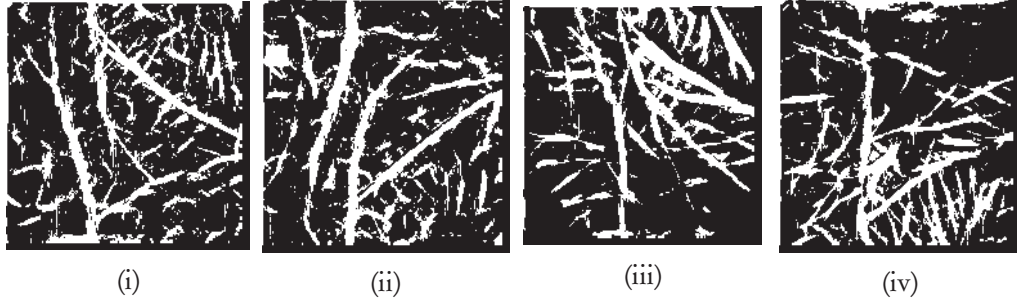


Figure 4.6: Sample Lines_images.

In addition to the principal lines, Lines_image consists of noise pixels. Morphological skeleton operation [133] removes pixels on the boundaries of objects but does not allow objects to break apart. The pixels remaining make up the image skeleton. To eliminate the noise pixels, apply morphological skeleton operation [133] then the obtained is the thinned lines, and the result image is named as skeleton_image. The sample skeleton_images after applying the morphological skeleton operation are shown in Figure 4.7.

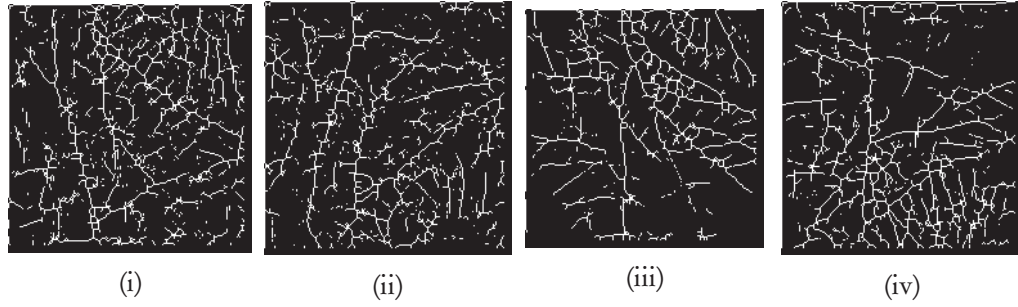


Figure 4.7: Sample skeleton_images after applying the morphological skeleton operation.

Using connected components operation [130] on skeleton_image and by dynamically determining the threshold T_3 , below which these connected components are labelled as noise and discarded the noise pixels. Resulting image is named as thin_line_image. The sample thin_line_images after eliminating noise pixels are shown in Figure 4.8. If T_3 is small, then it is not possible to eliminate all noise pixels. If T_3 is large, then principal line pixels can also be eliminated. Based on the experiments T_3 value is determined as 40 for dynamic and static ROIs.

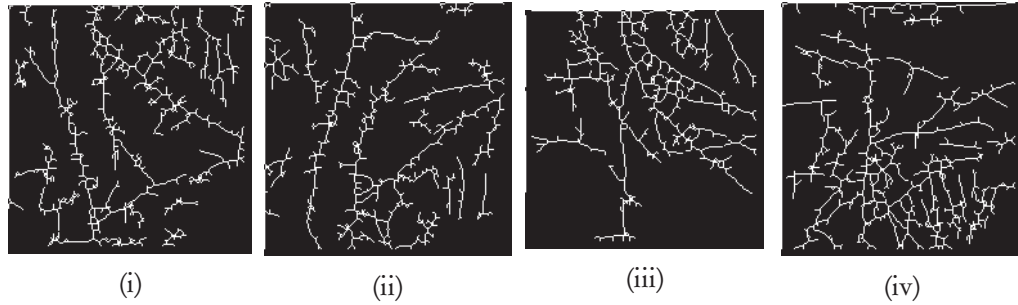


Figure 4.8: Sample thin_line_images after eliminating noise pixels.

The morphological dilate operation [130, 131] gradually enlarge the boundaries of the objects. To obtain Wide Principal Line Image, first apply the morphological dilate operation on thin_line_image with the structuring element which is square type, the result is named as thick_line_image. The size of the structuring element will affect the width of the lines in thick_line_image. The sample images after applying dilate operation with structuring element sizes 2, 3, 4, 5 and 6 are shown in Figures 4.9, 4.10, 4.11, 4.12 and 4.13 respectively. Based on the experiments the size of the structuring

element is determined as 3.

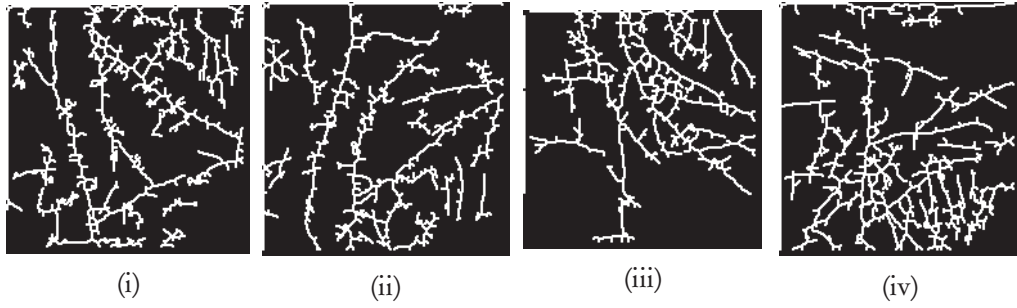


Figure 4.9: Sample thick_line_images after applying dilate operation with structuring element size 2.

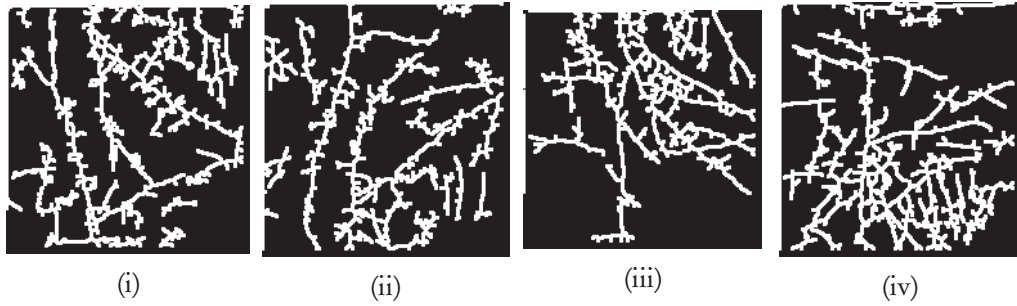


Figure 4.10: Sample thick_line_images after applying dilate operation with structuring element size 3.

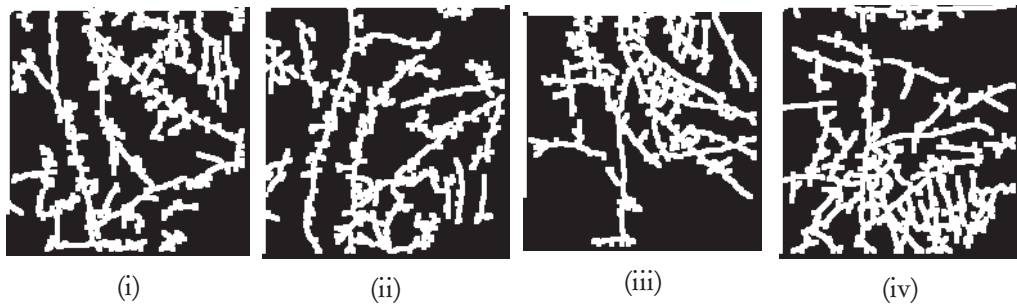


Figure 4.11: Sample thick_line_images after applying dilate operation with structuring element size 4.

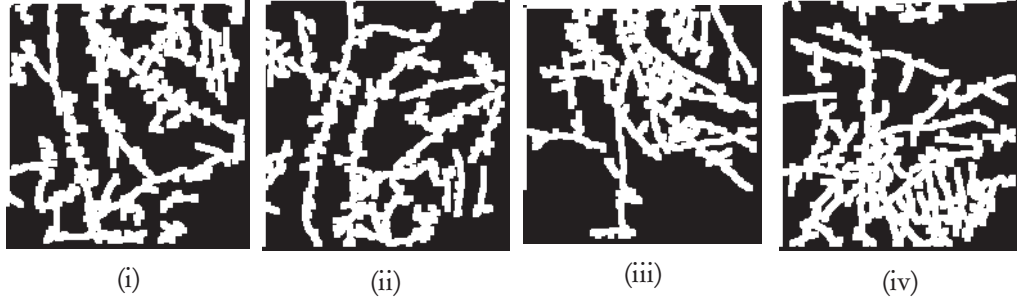


Figure 4.12: Sample thick_line_images after applying dilate operation with structuring element size 5.

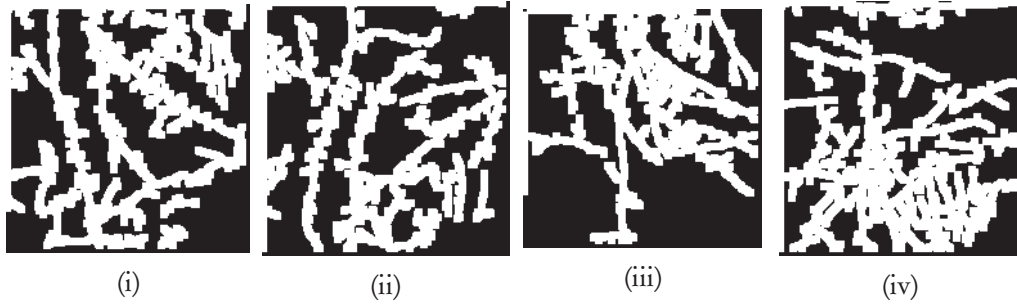


Figure 4.13: Sample thick_line_images after applying dilate operation with structuring element size 6.

Later, apply the logical AND operation between Lines_image and thick_line_image. The result is named as Wide Principal Line Image (WPLI). Sample WPLIs are shown in Figure 4.14. These, wide principal lines are used to retain the high identification accuracy because thin principal lines are similar for different users. But it is observed that this may not happen with wide principal lines.

4.1.4 WPLF extraction algorithm

The step by step procedure to extract WPLI is given at algorithm 4.4. The algorithm 4.4 considers ROI (ri) and thresholds (T_1 , T_3) as input and returns WPLI as output. In this algorithm, apply the WPLEs on ROI(ri) using equations (4.3) and (4.4) to obtain Energy_image. Apply the threshold " T_1 " on Energy_image using equation (4.5) to obtain Lines_image. Apply the morphological skeleton operation [133] on Lines_image to generate the thinned lines image named as skeleton_image. Ap-

ply the connected components operation [130] on `skeleton_image` and the connected components below the threshold " T_3 " are labelled as noise and discard the noise pixels. The result image is named as `thin_line_image`. Apply the morphological dilate [130, 131] on `thin_line_image` with the structuring element which is square type of size 3, the result is named as `thick_line_image`. Apply the logical AND operation between `Lines_image` and `thick_line_image`. The result image is named as Wide Principal Line Image (WPLI). Let ROI size is $M \times N$, then the complexity of the algorithm is $O(MN)$.

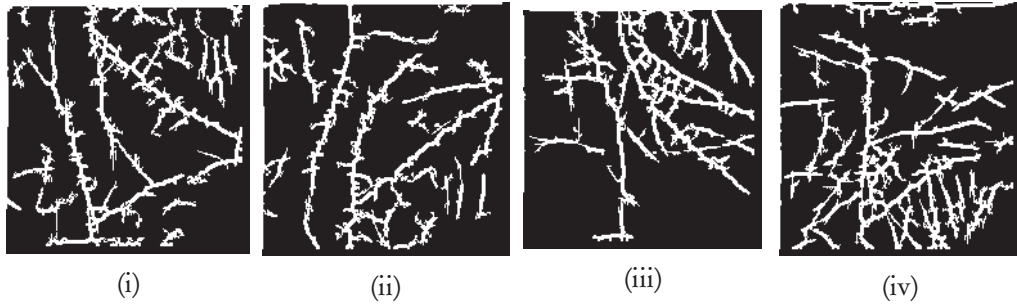


Figure 4.14: Sample WPLIs.

4.1.5 WPLI database generation

For every dynamic ROI in the dynamic ROI database apply the algorithm 4.4 and the result WPLI is stored in WPLI database. The schematic diagram for generation of dynamic WPLI database is shown in Figure 4.15.

Dynamic WPLIs are stored in a folder. To store the reference point information, four two dimensional vectors are defined and these are named as FDX, FDY, SDX, SDY. If the registered WPLI represents the first session i^{th} palm j^{th} image, then it's DX and DY values are stored in i^{th} row of j^{th} column in FDX and FDY respectively. Similarly, if the registered WPLI represents the second session i^{th} palm j^{th} image, then it's DX and DY values are stored in i^{th} row of j^{th} column in SDX and SDY respectively.

Algorithm 4.4 WPLFExtract(ri, T_1 , T_3): To generate Wide Principal Line Image(WPLI)

//Algorithm for generation of Wide Principal Line Image//

Input:

ri : ROI image
 T_1 : Threshold used to generate *Lines_image*
 T_3 : Threshold used to eliminate noise pixels

Output:

WPLI : Wide Principal Line Image

Method:

1. Apply WPLEs on ROI(ri) using equations (4.3) and (4.4) to obtain Energy_image.
2. Apply the threshold " T_1 " on Energy_image using equation (4.5) to obtain Lines_image.
3. Apply the morphological skeleton operation [133] on Lines_image to generate the Thinned lines image named as skeleton_image.
4. Apply the connected components operation [130] on skeleton_image and the connected components below the threshold " T_3 " are labelled as noise and discard the noise pixels. The result image is named as thin_line_image.
5. Apply the morphological dilate [130, 131] on thin_line_image with the structuring element which is square type of size 3, the result is named as thick_line_image.
6. Apply the logical AND operation between Lines_image and thick_line_image. The result image is named as Wide Principal Line Image (WPLI).

Computational Complexity of WPLFExtract	
Let ROI size is M x N	
The complexity of each step from 1 to 6 is	$O(MN)$
Algorithm Complexity: $O(MN)$	

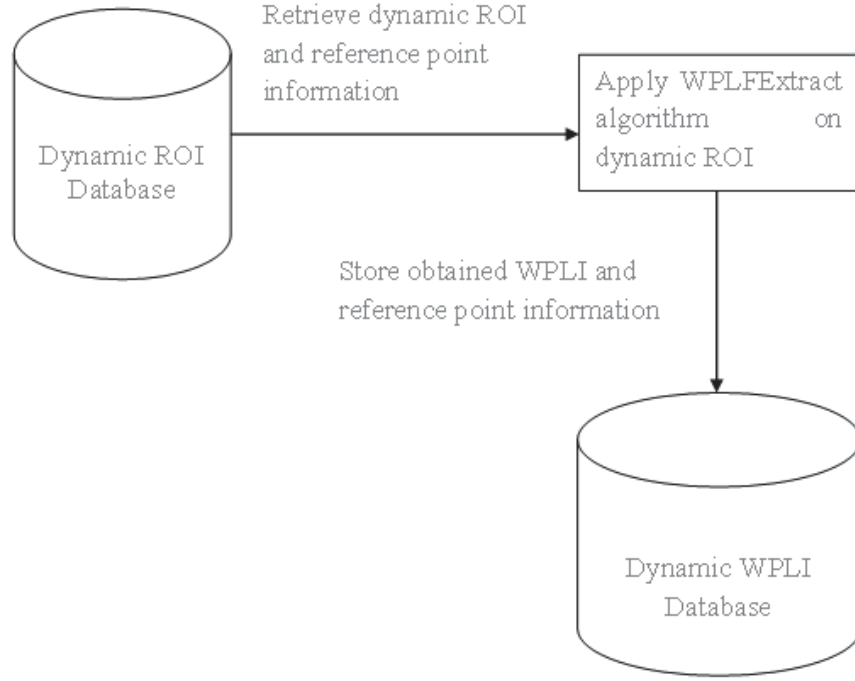


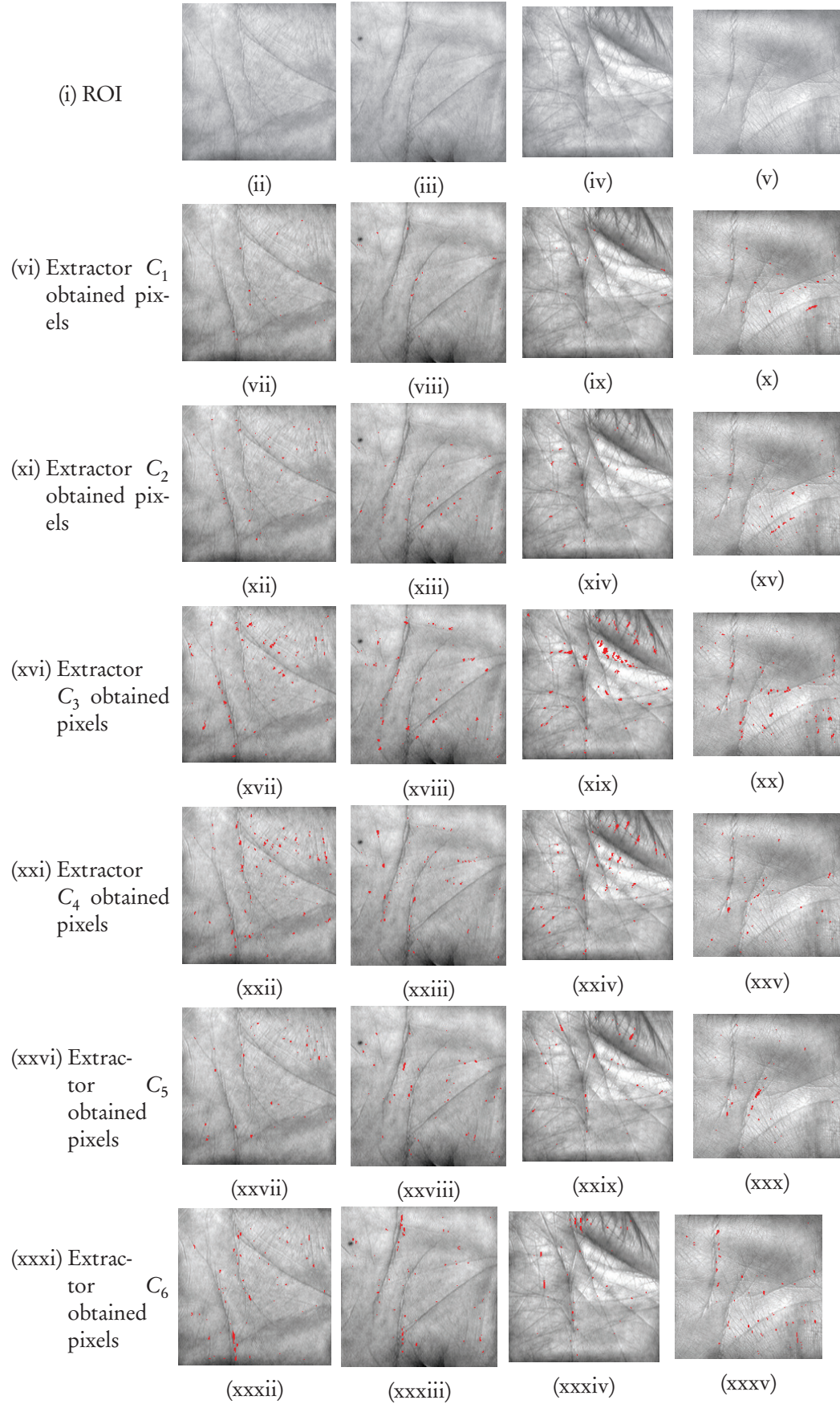
Figure 4.15: Schematic diagram for dynamic WPLI database generation.

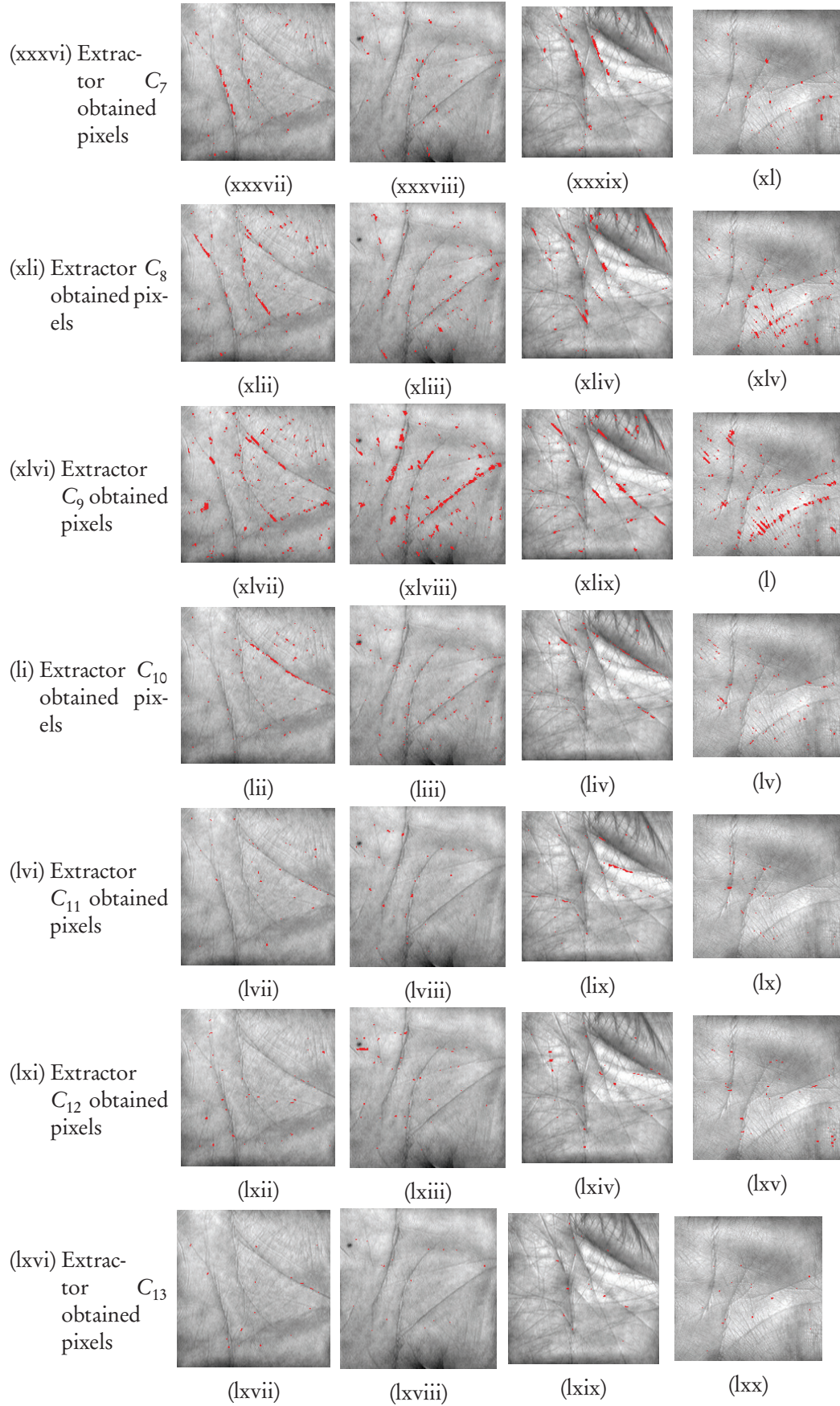
The sample pixels extracted by the WPLEs are shown in Figure 4.16. The average number of pixels extracted by each extractor on the entire dynamic ROI database and number of pixels extracted by each extractor for sample images are shown in Figure 4.17.

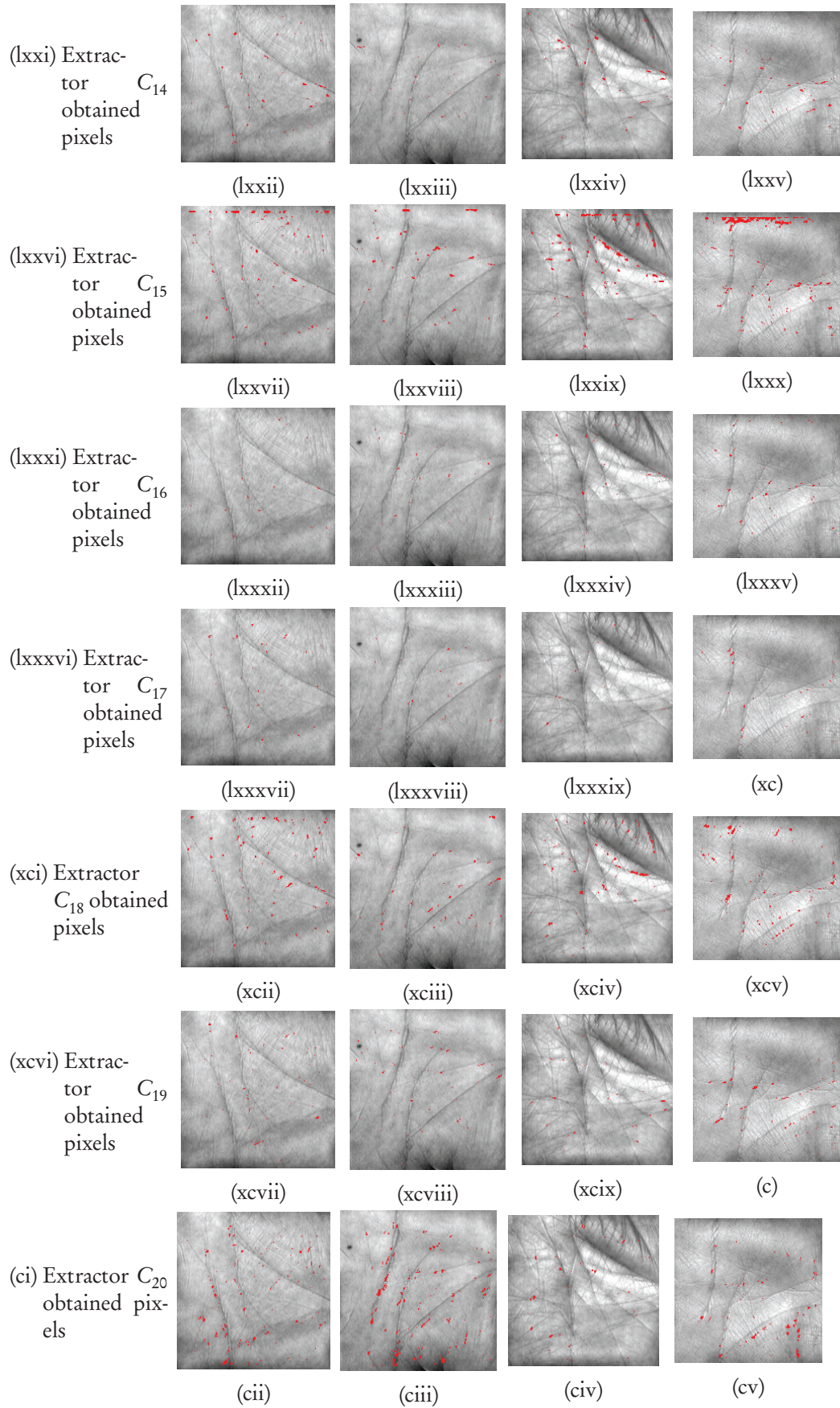
WPLI Extractor	C1	C2	C3	C4	C5	C6	C7	C8	C9	C10	C11	C12	C13	C14	C15	C16	C17	C18	C19	C20	C21	C22	C23	C24	C25	C26	C27	C28	C29	C30	C31	C32
Average Number pixels Extracted by each extractor ROI Name	28	49	172	125	80	101	105	232	460	131	55	64	24	61	234	33	33	149	63	160	108	148	229	104	101	174	402	284	181	184	56	113
Figure 4.16 (ii)	19	48	127	188	57	131	153	300	406	134	24	48	21	81	164	15	35	177	49	174	149	232	320	153	123	142	337	257	201	131	59	114
Figure 4.16 (iii)	16	44	118	74	63	85	93	196	636	90	37	61	14	23	102	18	16	83	52	275	116	120	270	86	105	185	512	222	56	215	26	149
Figure 4.16 (iv)	14	25	304	157	84	70	154	264	397	130	65	57	21	75	290	37	5	135	28	52	65	218	232	114	64	100	266	340	389	135	120	75
Figure 4.16 (v)	59	75	172	69	70	94	88	266	513	102	42	49	18	62	422	63	51	231	111	165	97	119	208	68	95	157	275	118	200	139	58	115

Figure 4.17: Number of pixels (average) extracted using WPLEs on Dynamic ROI database and sample number of values of sample ROIs.

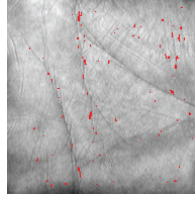
The algorithm 4.4 is applied on each and every image of dynamic ROI database. The maximum, minimum and average time in seconds for WPLF extraction on dynamic ROI database of PolyUPalmprint database are given in Table 4.1.



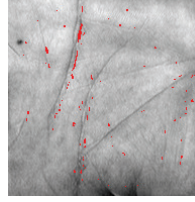




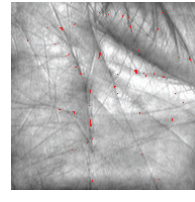
(cvi) Extrac-
tor C_{21}
obtained
pixels



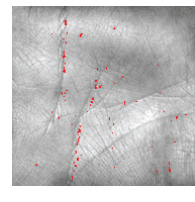
(cvii)



(cviii)

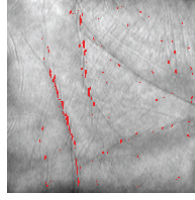


(cix)

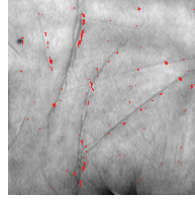


(cx)

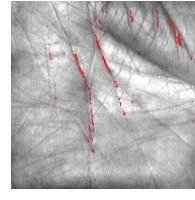
(cxi) Extrac-
tor C_{22}
obtained
pixels



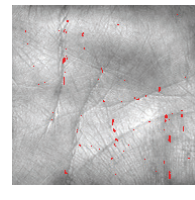
(cxii)



(cxiii)

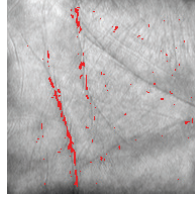


(cxiv)

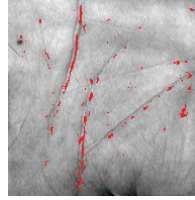


(cxv)

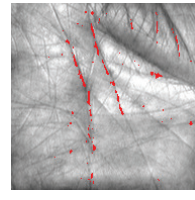
(cxvi) Extrac-
tor C_{23}
obtained
pixels



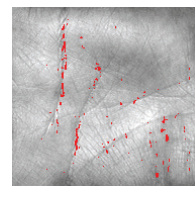
(cxvii)



(cxviii)

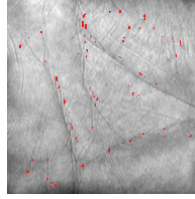


(cxix)

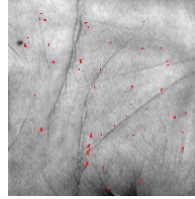


(cxx)

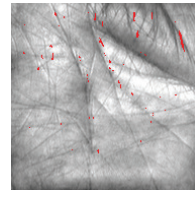
(cxxi) Extrac-
tor C_{24}
obtained
pixels



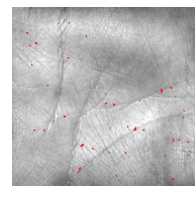
(cxxii)



(cxxiii)

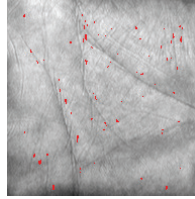


(cxxiv)

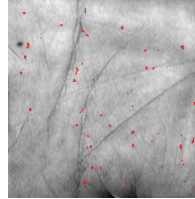


(cxxv)

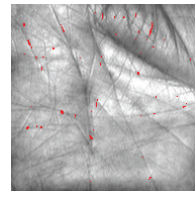
(cxxvi) Extrac-
tor C_{25}
obtained
pixels



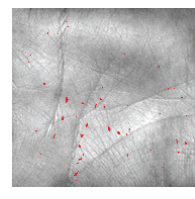
(cxxvii)



(cxxviii)

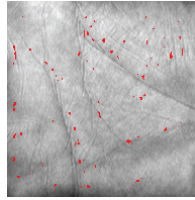


(cxxix)

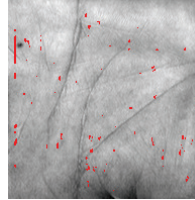


(cxxx)

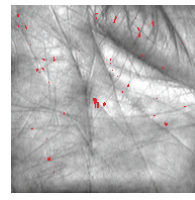
(cxxxvi) Extrac-
tor C_{26}
obtained
pixels



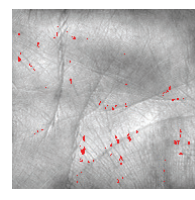
(cxxxvii)



(cxxxviii)

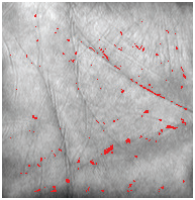


(cxxxiv)

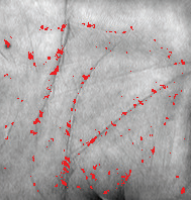


(cxxxv)

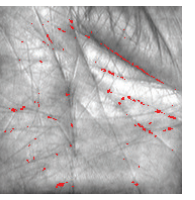
(cxxxvi) Extrac-
tor C_{27}
obtained
pixels



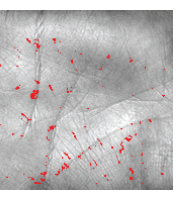
(cxxxvii)



(cxxxviii)



(cxxxix)



(cxl)

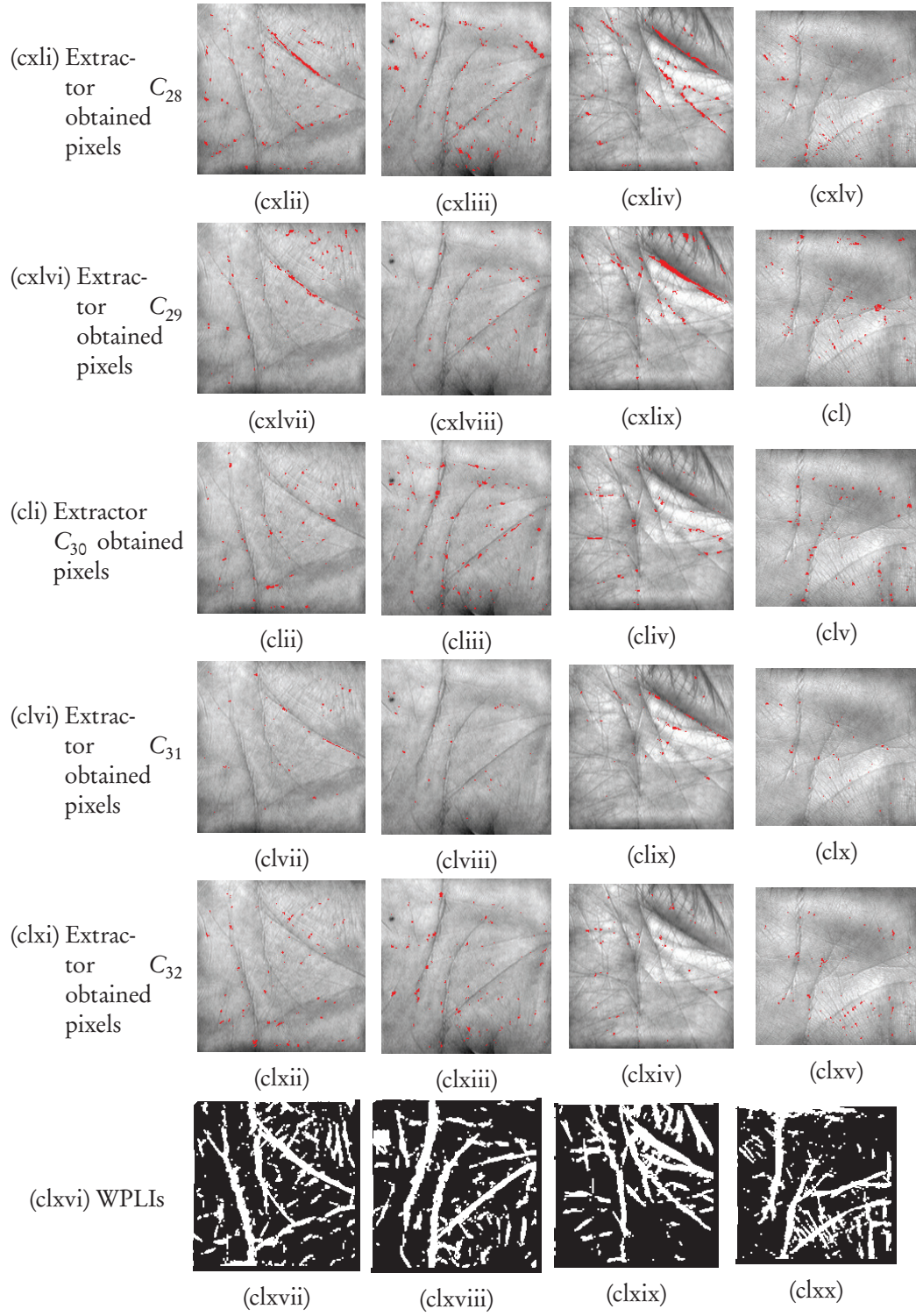


Figure 4.16: Pixels extracted using each extractor of sample images

Table 4.1: Maximum, minimum and average time in seconds for WPLF extraction on dynamic ROI of PolyUPalmprint database

	Minimum	Maximum	Average
Time in Seconds	1.208	4.854	3.127

4.2 Statistical Features Extraction

Our literature survey in Chapter 2 reveals that statistical features are distinguishable in palmprint. Thus statistical feature based approaches play a vital role in palmprint recognition. The present study among the statistical approaches are developed after performing transformations such as DCT, Gabor filter etc. We proposed a statistical feature extraction without applying the transformations on ROIs. The proposed approach to extract the statistical features is as follows:

4.2.1 Segmentation of ROI region into blocks

ROI image is segmented into overlapping segments of 128×128 , 96×96 , 64×64 , 32×32 , 16×16 and 8×8 using overlapping sliding window protocol. Figure 4.18 and Figure 4.19 shows the schematic diagrams for segmenting the Dynamic ROI (190×194). To generate 128×128 segments, window size is taken as 128×128 . Initially it is positioned at the top of the left corner of the ROI. Later, it is moved every time 16 pixels left to right after that 16 pixels top to bottom. If the generated segment size is less than required size then discard that segment.

Number of $k \times k$ segments are generated from the $u \times v$ ROI using equations (4.6) and (4.7), where u and v represents the number of pixels along m and n axis respectively.

$$\text{number of } k \times k \text{ segments} = (1 + \left\lfloor \frac{u-k}{16} \right\rfloor) * (1 + \left\lfloor \frac{v-k}{16} \right\rfloor) \quad \forall k = 32, 64, 96, 128 \quad (4.6)$$

$$\text{number of } k \times k \text{ segments} = \left(\left\lfloor \frac{u}{k} \right\rfloor * \left\lfloor \frac{v}{k} \right\rfloor \right) + \left(\left\lfloor \frac{2*u-k}{2*k} \right\rfloor * \left\lfloor \frac{2*v-k}{2*k} \right\rfloor \right) \quad \forall k = 8, 16 \quad (4.7)$$

20 segments of 128 x 128 are generated from the 194 x 190 ROI. The first 8 segments are surrounded by dotted lines are shown in Figure 4.18. The above approach is applied to generate the segments of size 96 x 96, 64 x 64 and 32 x 32. 42 segments of size 96 x 96 are generated from the 194 x 190 ROI. 72 segments of 64 x 64 are generated from the 194 x 190 ROI. 110 segments of 32 x 32 are generated from the 194 x 190 ROI.

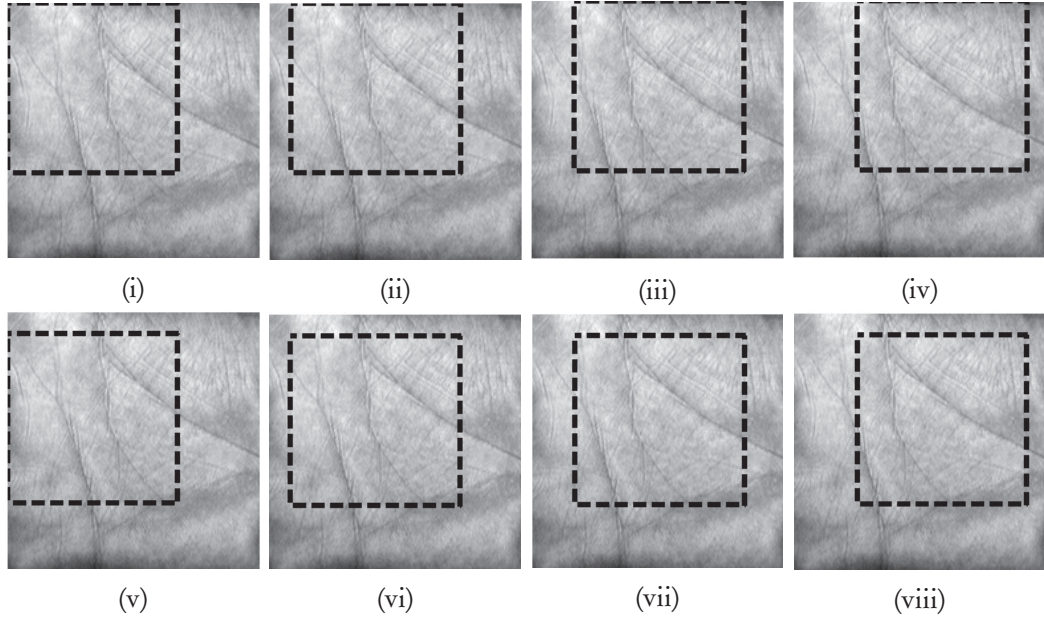


Figure 4.18: Schematic diagrams for segmenting the ROI into 128 x 128.

To generate 16 x 16 segments, window size is taken as 16 x 16. Initially it is positioned on top left corner, it is moved every time 16 pixels left to right later 16 pixels top to bottom. 132 segments of 16 x 16 are generated from the 194 x 190 ROI are shown in Figure 4.19(i). To generate additional (overlapping) segments of 16 x 16 window top left corner at (8, 8), it is moved every time 16 pixels left to right and 16 pixels

top to bottom. 121 segments of 16 x 16 are generated from the 194 x 190 ROI. These segments are surrounded by lines is shown in Figure 4.19(ii).

To generate 8 x 8 segments, window size is taken as 8 x 8. Initially it is positioned at top left corner, it is moved every time 8 pixels left to right later 8 pixels top to bottom. 552 segments of 8 x 8 are generated from the 194 x 190 ROI are shown in Figure 4.19(iii). To generate additional (overlapping) segments of 8 x 8 window is positioned at (4, 4), it is moved every time 8 pixels left to right later 8 pixels top to bottom. 529 segments of 8 x 8 are generated from the 194 x 190 ROI. These segments are surrounded by lines is shown in Figure 4.19(iv). The 194 x 190 ROI is segmented into 1578 segments (blocks).

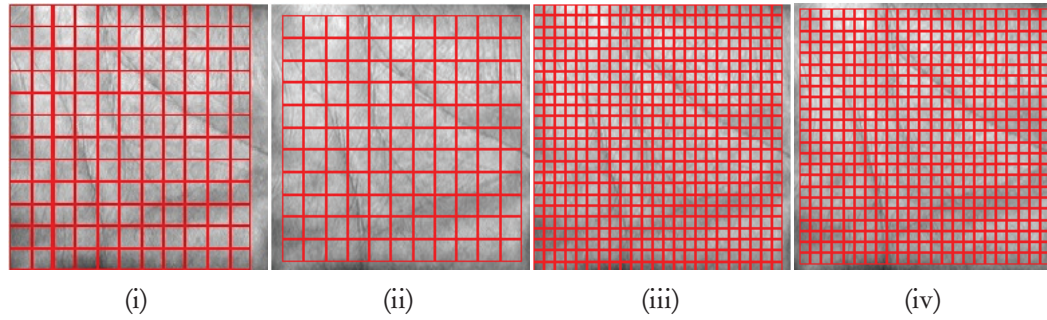


Figure 4.19: Schematic diagrams for segmenting the ROI into (i)&(ii) 16 x 16 (iii)&(iv) 8 x 8 blocks.

4.2.2 Block feature extraction

From each block (segment), standard deviation (SD) and coefficient of variation (CV) using equation (4.8) are calculated. The obtained values, representing the feature vector of respective ROI. The 194 x 190 ROI is segmented into 1578 segments, so its feature vector size is 3156.

$$\text{coefficient of variation of the segment}(CV) = \frac{\text{standard deviation of the segment}}{\text{mean of the segment}} \quad (4.8)$$

4.2.3 Statistical feature extraction algorithm

The step by step procedure to extract the statistical features is explained in the algorithm 4.5. The algorithm takes ROI (or) WPLI as input and returns the feature vector of the input image as output.

Algorithm 4.5 SFExtract(ri , T_1 , T_2): To extract statistical features

//Algorithm for statistical feature extraction//

Input:

ri : Input image

Output:

SFV : Statistical feature vector

Method:

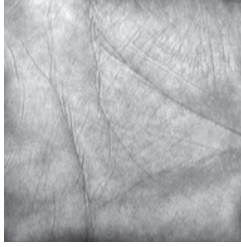

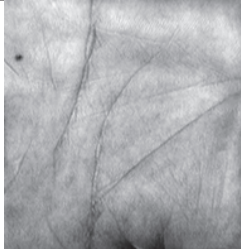

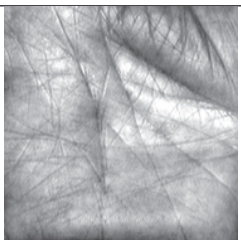

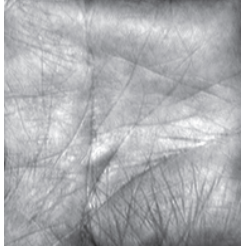

1. Segment the input image into overlapping segments (blocks) of sizes 128×128 , 96×96 , 64×64 , 32×32 , 16×16 and 8×8 .
2. For each segment (block) calculate the standard deviation and coefficient of variation. Store these values into SFV.

Computational Complexity of SFExtract	
Let input image size is $M \times N$	
Steps 1 & 2	$O(MN)$
Algorithm Complexity: $O(MN)$	

The dynamic ROIs and its feature vector sizes are shown in Table 4.2.

The statistical features extraction algorithm 4.5 is also applied on WPLI database. The algorithm takes WPLI as input and returns the statistical feature vector of the WPLI image as output. The dynamic WPLIs and its statistical feature vector sizes are shown in Table 4.2.

Table 4.2: Sample statistical feature vector sizes of dynamic ROIs / WPLIs

Dynamic ROI	Dynamic ROI size	Feature vector size	Dynamic WPLI	Dynamic WPLI size	Feature vector size
	194 x 190	3156		194 x 190	3156
	198 x 193	3338		198 x 193	3338
	186 x 186	2942		186 x 186	2942
	198 x 188	3202		198 x 188	3202

The maximum, minimum and average time in seconds for statistical feature extraction dynamic ROI database of PolyUPalmprint database are given in Table 4.3.

Table 4.3: Maximum, minimum and average time in seconds for statistical feature extraction on dynamic ROI of PolyUPalmprint database

	Minimum	Maximum	Average
Time in Seconds	0.059	0.3885	0.1426

4.3 Summary

In this chapter, we proposed two feature extraction techniques, (1) Wide principal line feature (2) Statistical features. To extract the wide principal lines, we proposed 32 wide principal line extractors, these extractors are used to obtain the energy of the ROI. To enhance the wide principal line features, we applied skeleton, labeling, dilate and logical AND operations. The obtained WPLI are stored in the WPLI database. To generate the statistical features, the ROI images are segmented into overlapping segments. From each segment computed the standard deviation and coefficient of variation as a feature. These generated features are stored as a feature vector.

CHAPTER 5

Verification and identification

Verification is one to one comparison and identification is one to many comparisons. In the early days most of the research is concentrated on palmprint verification only. Now-a-days, most of the research [23, 24, 61, 62, 66, 95, 99, 101] is concentrating on palmprint identification also.

The task of palmprint verification is to calculate the degree of similarity between a query image and a database image. If the matching score is greater than the threshold then the user is a valid user otherwise the user is imposter. At a given threshold, the probability of accepting the imposters is known as the False Acceptance Rate (FAR) and the probability of rejecting a genuine user is known as the False Rejection Rate (FRR). FAR is calculated by comparing every query image with the remaining palms database images (i.e. impostor match) and the percentage of images accepted is considered as FAR. FRR is calculated by comparing every query image with the same palm database images (i.e. genuine match) and the percentage of images rejected is considered as the FRR. FAR and FRR are defined as

$$FAR(\eta) = p(s \geq \eta | \omega_0) = \int_{\eta}^{\infty} p(x | \omega_0) dx \quad (5.1)$$

$$FRR(\eta) = p(s < \eta | \omega_1) = \int_{-\infty}^{\eta} p(x | \omega_1) dx \quad (5.2)$$

Where η is a threshold, ω_0 , ω_1 are the imposter and genuine matching score classes and $p(x | \omega_0)$, $p(x | \omega_1)$ are the probability density functions of the genuine and imposter matching scores respectively.

Equal Error Rate (EER) is represented by a percentage in which the FAR and FRR are equal. Plot the FAR and FRR values of all the thresholds, the intersection of FAR

and FRR is considered as the EER. Receiver Operating Characteristics (ROC) curve of a system illustrates the FRR and FAR of a matcher at all the threshold values. Each point on the ROC curve defines the FRR and the FAR values at a particular threshold. Decidability Index (DI) is the measure of the separability of genuine and imposter matching scores. Decidability Index can be measured as the ratio of the difference between mean values of genuine and imposter matching scores to the square root of the average of the variances of genuine and imposter matching scores.

Decidability Index (DI) is defined as

$$DI = \frac{\mu_1 - \mu_2}{\sqrt{\frac{\sigma_1^2 + \sigma_2^2}{2}}} \quad (5.3)$$

Where μ_1 and μ_2 are the mean values of genuine and imposter matching scores, σ_1 and σ_2 are standard deviation of genuine and imposter matching scores respectively.

The task of identification is used to identify the person from database images. The Correct Identification Rate (CIR) of the system can be measured as the ratio of number of correctly identified palmprint images to the total number of palmprint images in the query set. The CIR of the system can be measured as follows:

$$CIR = \frac{CI}{TT} * 100 \quad (5.4)$$

Where CI is the number of correct identification of palmprint images and TT is the total number of palmprint images in the query set.

In this chapter proposed a palmprint verification and a two-phase palmprint identification approaches. Thread diagram representing the palmprint verification and two-phase palmprint identification is shown in Figure 5.1. Palmprint verification approach is described in section 5.1. Section 5.2 gives a brief account of two-phase palmprint identification.

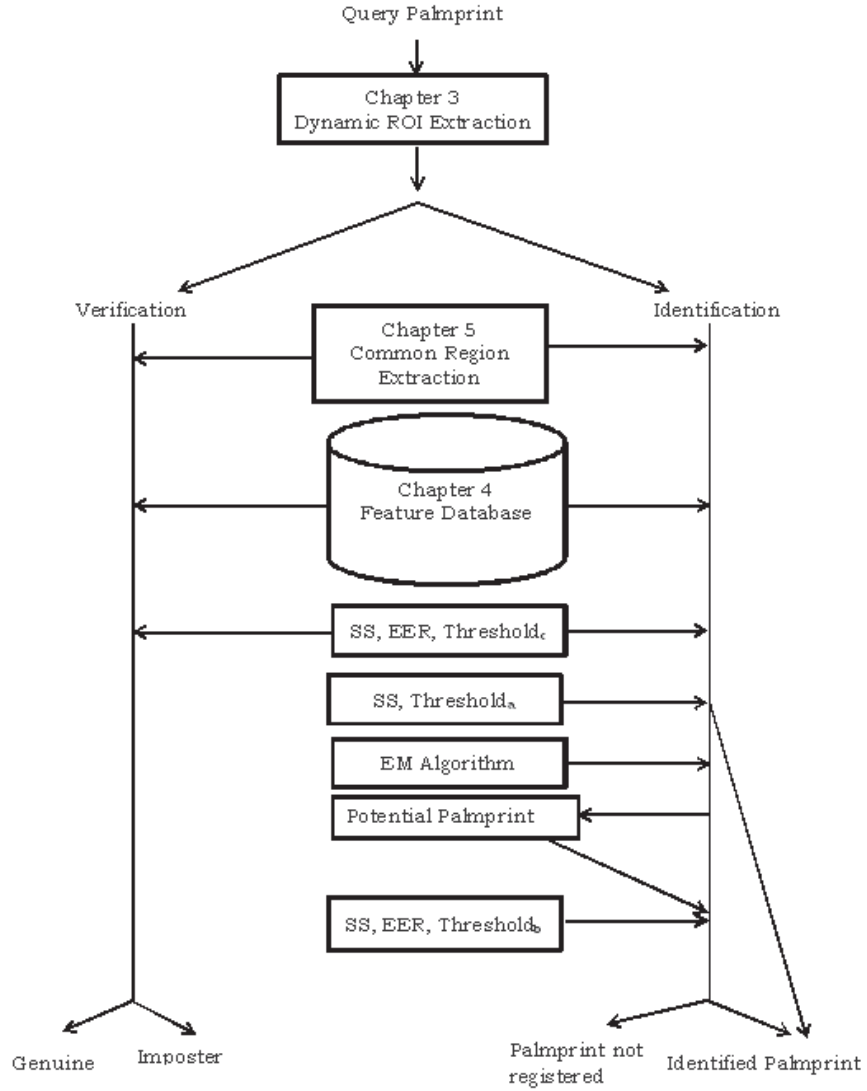


Figure 5.1: Thread diagram representing the palmprint verification and two-phase palmprint identification.

5.1 Palmprint Verification

In palmprint verification query palmprint to be compared with corresponding palmprint database images. If the similarity score is greater than the $threshold_c$ then the query palmprint is considered as genuine otherwise it is considered as imposter. In dynamic ROI extraction, the ROI size is dynamic and based on the availability, it extracts maximum possible ROI. For the same palmprint of different images the ROI sizes may

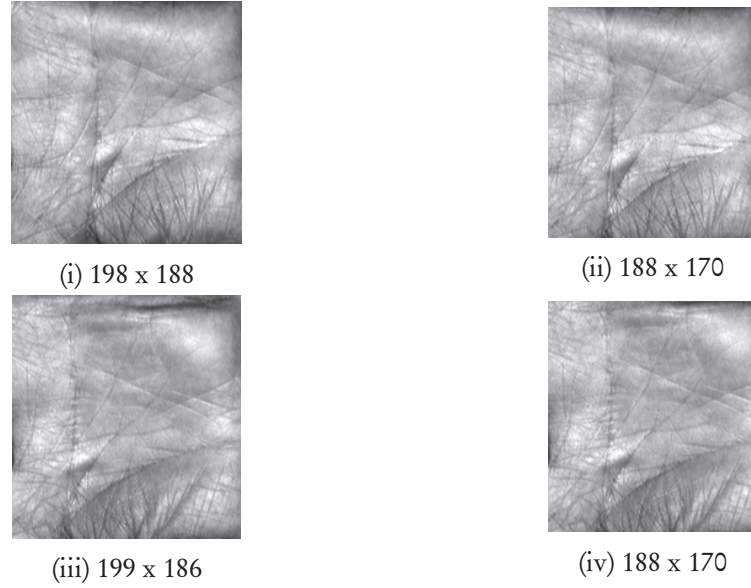


Figure 5.2: Common region of the two dynamic ROIs of the same palm (i)& (iii) dynamic ROIs (ii)& (iv) selected common regions from dynamic ROIs.

vary. Before performing the matching, there is a need to identify the common region between query palmprint ROI and corresponding database palmprint ROI. The step by step procedure to extract common region between query ROI and database ROI is given at algorithm 5.6. The algorithm takes two dynamic ROIs and there reference point information (i.e. DX and DY) as input and returns the common regions of the input ROIs as output.

Let r_1 and r_2 are ROIs of the same palm. r_1 size is 198 x 188, DX and DY values of r_1 are 101 and 19 respectively. r_2 size is 199 x 186, DX and DY values of r_2 are 110 and 37 respectively. r_1 and r_2 are shown in Figure 5.2(i) and Figure 5.2(iii). After applying the algorithm 5.6, the identified common regions are shown in Figure 5.2(ii) and Figure 5.2(iv).

Extract the dynamic ROI and reference point information from the query palmprint using the method discussed in Chapter 3. If the selected feature is WPLF apply algorithm 4.4 on extracted dynamic ROI and the result image is named as query image otherwise extracted dynamic ROI is named as query image. The WPLI database is considered as a database, if the palmprint to be verified using Wide Principal Line

Algorithm 5.6 CommonRegExtract($r_1, r_2, d_{x1}, d_{y1}, d_{x2}, d_{y2}$) : To extract common region of two dynamic ROIs (or) WPLIs

//Algorithm for extraction of common region from dynamic ROIs (or) WPLIs//

Input:

r_1 : First dynamic ROI (or) WPLI
 r_2 : Second dynamic ROI (or) WPLI
 d_{x1} : DX value of r_1
 d_{y1} : DY value of r_1
 d_{x2} : DX value of r_2
 d_{y2} : DY value of r_2

Output:

$r r_1$: Common region portion in r_1
 $r r_2$: Common region portion in r_2

Method: Let r_1 and r_2 sizes are $w_1 \times h_1$ and $w_2 \times h_2$ respectively.

1. Identify the distance of top boundary of the common region from the reference point
 $dd_x \leftarrow \min(d_{x1}, d_{x2})$
2. Identify the distance from the reference point to the left corner of the common region in n-direction
 $dd_y \leftarrow \max(d_{y1}, d_{y2})$
3. Identify the distance between the reference point to the bottom boundary of the common region in m-direction
 $cc \leftarrow \min(w_1 - d_{x1}, w_2 - d_{x2})$
4. Compute the height and width of the common region
 $Height\ y \leftarrow \min(h_1 - dd_y + d_{y1}, h_2 - dd_y + d_{y2})$
 $Width\ x \leftarrow dd_x + cc - 2$
5. Compute the Top left corner of the common region in r_1
 $s_{x1} \leftarrow d_{x1} - dd_x$
 $s_{y1} \leftarrow dd_y - d_{y1}$
6. Compute the Top left corner of the common region in r_2
 $S_{x2} \leftarrow d_{x2} - dd_x$
 $s_{y2} \leftarrow dd_y - d_{y2}$
7. Assign the identified common regions of r_1 and r_2 to $r r_1$ and $r r_2$ respectively.
 $r r_1(1 : x, 1 : y) \leftarrow r_1(S_{x1} + 1 : S_{x1} + x, S_{y1} + 1 : S_{y1} + y)$
 $r r_2(1 : x, 1 : y) \leftarrow r_2(S_{x2} + 1 : S_{x2} + x, S_{y2} + 1 : S_{y2} + y)$
8. Return $r r_1, r r_2$

Computational Complexity of CommonRegExtract	
Let common region size is $M \times N$ then Step 7 Complexity	$O(MN)$
Algorithm Complexity: $O(MN)$	

Features. Identify the common region between query image and database image using the algorithm 5.6. For Wide Principal Line images, similarity score is calculated using equation (5.6).

Let L_1 and L_2 are the database WPLI and query WPLI common regions respectively and their size is $u \times v$, then the matching score (MS) between L_1 and L_2 is defined as

$$MS(L_1, L_2) = \frac{\sum_{i=1}^u \sum_{j=1}^v L_1(i, j) \cdot L_2(i, j)}{\sum_{i=1}^u \sum_{j=1}^v L_1(i, j)} \quad (5.5)$$

$$SS(L_1, L_2) = \max(MS(L_1, L_2), MS(L_2, L_1)) \quad (5.6)$$

The symbol \cdot represents the logical AND operation. If L_1 and L_2 are identical then the matching score will be 1. The matching score will range between 0 and 1.

In statistical feature based palmprint verification, dynamic ROI database is considered as database. Identify the common region between query image and database image using the algorithm 5.6. Compute the statistical feature vectors for the extracted common regions using the algorithm 4.5. The Similarity Score (SS) between the feature vectors of query and database images is calculated using equation (5.9).

To calculate the dissimilarity between query and database images, researchers [63] used the Canberra Distance (CD) [134]. Canberra Distance between j^{th} database image and query image will be calculated using equation (5.7). Where A_i is the i^{th} feature of the query image, $B_{j,i}$ is the i^{th} feature of the j^{th} database image and n_f is the number of values in the feature vector. The Canberra Distance ranges between 0 and n_f . If the two ROIs feature vectors are the same then CD value is zero and the maximum value of CD is n_f . That is, if the verification ROIs belongs to the same palm then CD value is nearer to zero and if the ROIs belongs to the different palms then CD value is nearer to n_f .

$$CD_j = \sum_{i=1}^{n_f} \frac{|A_i - B_{j,i}|}{|A_i| + |B_{j,i}|} \quad (5.7)$$

In dynamic ROIs, the common region among different palm ROIs is smaller than the common region among different palmprint images of the same palm ROIs. So, the number of features extracted for different palms ROIs comparison is less than the number of features extracted for same palm of same person ROIs comparison. Hence, there is a possibility of genuine verification CD value is more than the imposter verification CD value. To overcome this problem, we proposed Dissimilarity Distance (DD). The Dissimilarity Distance (DD) can be calculated using equation (5.8).

$$DD = \frac{1}{u} \sum_{i=1}^u \frac{|A(i) - B(i)|}{|A(i)| + |B(i)|} \quad (5.8)$$

Where A and B are feature vectors of query image and database image respectively. A(i) is the i^{th} feature of the query image, B(i) is the i^{th} feature of the database image and u is the number values in the feature vector. The Dissimilarity Distance ranges between 0 and 1. If the two ROIs feature vectors are the same, then DD value is zero and one of the feature vector is zeros then DD value is one. That is, if the verification ROIs belongs to the same palm then DD value is nearer to zero and if the ROIs belongs to the different palms then DD value is nearer to 1. The similarity score can be calculated using equation (5.9).

$$SS = 1 - DD \quad (5.9)$$

To calculate the $threshold_c$, every database image is compared with remaining all images in the database. If the database image is compared with the same palm database image then the similarity score is considered as genuine similarity score, otherwise, the similarity score is considered as imposter similarity score. Between the genuine and imposter similarity scores identify the EER and its related threshold, i.e. $threshold_c$ using the algorithm 5.7. The algorithm 5.7 considers genuine similarity score vector, imposter similarity score vector, sizes of these vectors as input parameters and returns the EER and threshold as output. The obtained threshold is considered as $threshold_c$. The detailed procedure to identify the threshold is explained in the algorithm 5.7.

The schematic diagram for palmprint verification is shown in Figure 5.3. The step

Algorithm 5.7 EERExtract(ISS , GSS , $ISScount$, $GSScount$) : To identify EER and $threshold_c$ from genuine and imposter similarity scores

//Algorithm for identification of Equal Error Rate (EER) and $Threshold_c$ //

Input:

ISS : Imposter similarity scores vector
 GSS : Genuine similarity scores vector
 $ISScount$: Number of values in ISS
 $GSScount$: Number of values in GSS

Output:

EER : Equal error rate
 $threshold_c$: Threshold at EER

Method:

1. Initialize
 - $mingss \leftarrow \min(GSS)$
 - $maxiss \leftarrow \max(ISS)$
 - $intervals \leftarrow 5000$
 - $lambda \leftarrow (maxiss - mingss) / intervals$
2. Calculate
 for $i = mingss : lambda : maxiss$
 - $FAR(i) \leftarrow (\text{number of } ISS \text{ values} > I) / ISScount$
 - $FRR(I) \leftarrow (\text{number of } GSS \text{ values} < I) / GSScount$
 endfor
3. Find an i such that $\text{abs}(FAR(i) - FRR(i))$ is minimum $\forall i = 1 : intervals$
4. Calculate
 - $EER \leftarrow (FAR(i) + FRR(i)) / 2$
 - $threshold_c \leftarrow mingss + i * lambda$
5. Return EER, $Threshold_c$

Computational Complexity of EERExtract	
Step 1	$O(ISScount + GSScount)$
Step 2	$O(intervals * (ISScount + GSScount))$
Step 3	$O(intervals)$
Algorithm Complexity: $O(intervals * (ISScount + GSScount))$	

by step procedure to perform the palmprint verification is given at algorithm 5.8. The algorithm takes the database, *query palmprint*, *Palmprint_{ID}* and *threshold_c* as inputs and returns the result such as genuine or imposter as output. In this algorithm, extract the dynamic ROI and its reference point information from query palmprint using the method discussed in Chapter 3. Let the palmprint size is $M \times N$ then the complexity of dynamic ROI extraction is $O(MN)$. If the selected feature is WPLF then apply the algorithm 4.4 on query ROI to generate query WPLI. Query WPLI is named as query image otherwise query ROI is named as query image.

Fetch the database images and its reference point information based on *Palmprint_{ID}* from database. For each database image, extract the common region between query image and database image using the algorithm 5.6. If the selected common region size is $M_1 \times N_1$ then its complexity is $O(M_1N_1)$. If the selected feature is SF then extract the statistical features from extracted common regions and calculate the similarity score using equations (5.8) and (5.9) otherwise calculate the similarity score between query WPLI and database WPLI using equations (5.5) and (5.6). The complexity of the similarity score calculation is $O(M_1N_1)$. If the maximum of the calculated similarity scores is greater than *threshold_c* then declare the query image is genuine otherwise declare the query image is an imposter. The value of M_1N_1 is very much smaller than MN , so the algorithm complexity is $O(MN)$.

Algorithm 5.8 PALMVER(*database*, *query palmprint*, *Palmprint_{Id}*, *Threshold_c*):
To perform palmprint verification

//Algorithm for palmprint verification//

Input:

database : Dynamic ROI/WPLI database and Reference point information
query palmprint : Query palmprint image to be verified
Palmprint_{Id} : Identifier of the query palmprint
Threshold_c : Based on the type of feature (SF/WPLF) identified threshold

Output:

Result : Genuine or imposter

Method:

1. Extract the dynamic ROI and its reference point information from query palmprint using the method discussed in Chapter 3.
 2. If the selected feature is WPLF then apply the algorithm 4.4 on query ROI to generate query WPLI. query WPLI is named as query image otherwise query ROI is named as query image.
 3. Fetch the database images and its reference point information based on *Palmprint_{Id}* from database.
 4. For each fetched database image apply the steps 5 and 6.
 5. Identify the common region between query image and database image using the algorithm 5.6.
 6. if feature is statistical features then
 - Compute the statistical feature vectors for the common regions of query image and database image using the algorithm 4.5.
 - Calculate the similarity score between the statistical features of query image and database image using equations (5.8) and (5.9).else
 - Calculate the similarity score between query image and database image using equations (5.5) and (5.6).endif
 7. Assign the maximum of the calculated similarity scores to maxsimscore.
 8. if maxsimscore \geq Threshold_c then
 - *Result* \leftarrow *genuine*else
 - *Result* \leftarrow *imposter*endif
 9. Return *Result*
-

Computational Complexity of PALMVER	
Step 1	$O(MN)$
step 4	$O(M_1N_1)$
step 5	$O(M_1N_1)$
Algorithm Complexity: $O(MN)$	

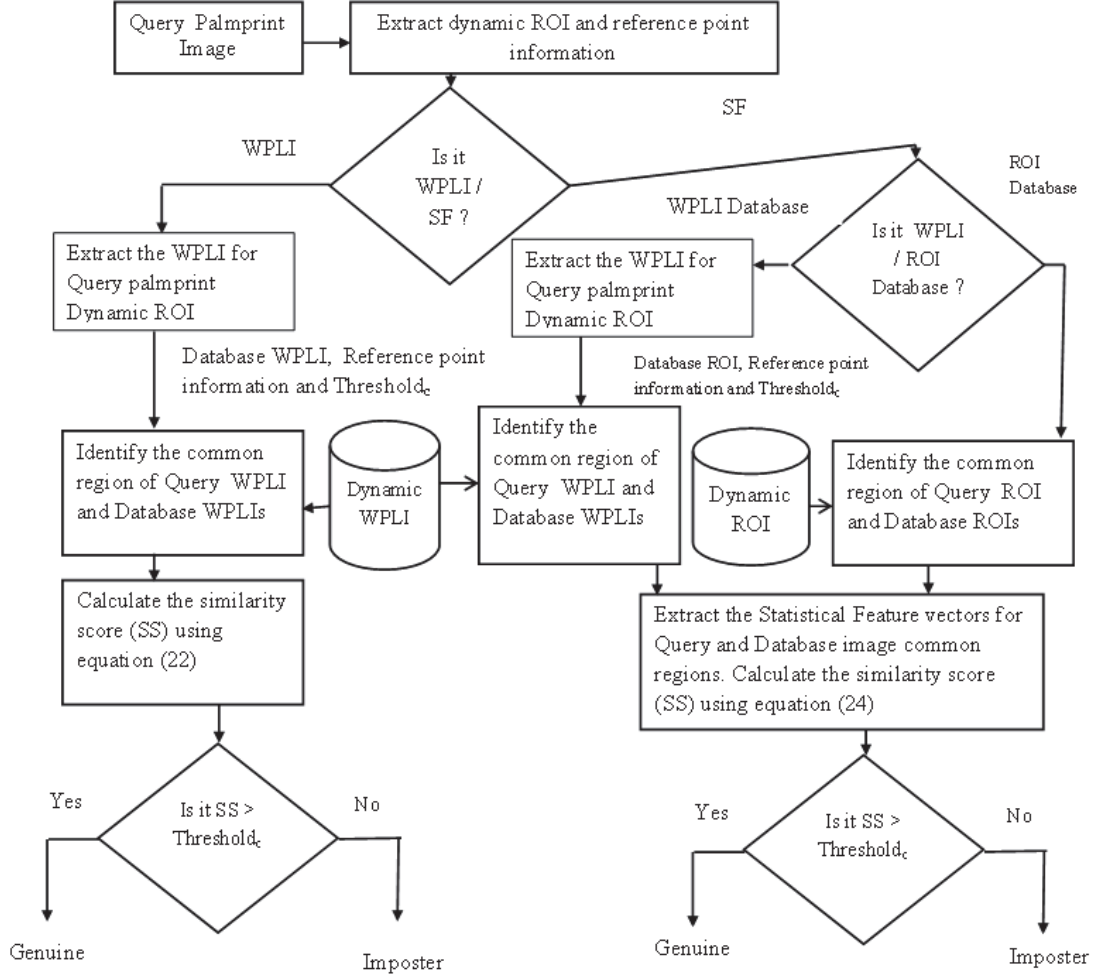


Figure 5.3: Schematic diagram for palmprint verification.

5.2 Two-Phase Palmprint Identification

We proposed a two-phase palmprint identification. In dynamic ROI / WPLI databases, the ROI/WPLI sizes are different. To perform identification the query image is to be compared with all the database images. So for every comparison we need to identify

the common region with query image and database image. To reduce the computation time first we identify the common region of all the database images and extract the feature vectors. In the first phase, identify the query image based on the common region. If the query palmprint is identified then declare identified palmprint, otherwise, EM algorithm [135] is used to identify the potential palmprint set (most similar palmprints). In the second phase, palmprint is identified from the potential palmprint set of the Dynamic ROIs/WPLIs. The detailed procedure is explained in the following subsections.

EM algorithm [135] is an iterative algorithm for parameter estimation. Each iteration calculates the maximum likelihood estimates of the parameter of each Gaussian distribution of the observed data are most likely. The algorithm considers the sorted dissimilarity distances (SDD) vector, number of clusters (C) and number of iterations (IT) as input. Initialization of the parameters as follows. Partition the SDD vector into C clusters. For every i^{th} cluster, calculate the mean μ_i , standard deviation σ_i and assign $1/C$ to α_i .

Each iteration in the EM algorithm follows two steps: E-step and M-step. E-step is an expectation step, estimate the density of given data point, expected value, posterior probability. Assume the probabilistic model of mixed distribution:

$$P(x|\theta) = \sum_{i=1}^C \alpha_i p_i(x|\theta_i) \quad (5.10)$$

Where the parameter $\theta = \{ \alpha_1, \alpha_2, \dots, \alpha_C, \theta_1, \theta_2, \dots, \theta_C \}$

$$\sum_{i=1}^C \alpha_i = 1 \quad (5.11)$$

The function p_i is the density function of Gaussian distribution and parameterized θ_i . The function p_i is defined as follows:

$$p_i(x|\theta_i) = \frac{1}{\sqrt{2\pi\sigma_i^2}} \exp\left(-\frac{(x-\mu_i)^2}{2\sigma_i^2}\right) \quad (5.12)$$

where x is the value of the SDD, $\theta_i = (\mu_i, \sigma_i^2, \alpha_i)$, μ_i, σ_i^2 and α_i are the mean, the vari-

ance and the corresponding mixing parameter for i^{th} Gaussian distribution of the observed data.

Posterior probability is represented by $p(i|x_j, \theta)$ and it is calculated as follows:

$$p(i|x_j, \theta) = \frac{\alpha_i p_i(x_j|\theta_i)}{\sum_{k=1}^C \alpha_k p_k(x_j|\theta_k)} \quad (5.13)$$

In the M-step, update the parameters using the following equations (5.14), (5.15), and (5.16). Let N is the number of values in SDD vector.

$$\alpha_i(t+1) = \frac{\sum_{j=1}^N p(i|x_j, \theta(t))}{N} \quad (5.14)$$

$$\mu_i(t+1) = \frac{\sum_{j=1}^N x_j p(i|x_j, \theta(t))}{\sum_{j=1}^N p(i|x_j, \theta(t))} \quad (5.15)$$

$$\sigma_i^2(t+1) = \frac{\sum_{j=1}^N p(i|x_j, \theta(t)) [x_j - \mu_j]^2}{\sum_{j=1}^N p(i|x_j, \theta(t))} \quad (5.16)$$

Sort the μ , σ^2 and α vectors based on α in ascending order. Threshold (TH) is calculated using the equation (5.17). Consider the palmprint ids whose dissimilarity distances less than TH are considered as most similar palmprints with query image.

$$TH = \frac{\alpha(1) * \mu(1) + \alpha(2) * \mu(2)}{\alpha(1) + \alpha(2)} \quad (5.17)$$

5.2.1 Generation of Feature Database

Identify the size of common region and extraction of the common region from all the database images is essential because to measure the similarity score the feature vectors size must be the same. The step by step procedure to identify the size of the common region, extraction of the common region from all the database images and generation of the FeatureDatabase is given in algorithm 5.9. The algorithm takes dynamic

ROI/WPLI database as input and returns the FeatureDatabase as output. The brief description of the algorithm is as follows: first identifies the size of the common region, its position on the entire database images and extracts the common region from the database images.

The samples of dynamic ROIs and its common regions are shown in Table 5.1. In the given example dynamic ROI images, D_{xa} vector values are 87, 91, 78, 101, 68. D_{ya} vector values are 22, 21, 13, 22, and 21. X_v vector values are 107, 107, 108, 97, and 101. Y_v vector values are 212, 214, 199, 207, and 211. The obtained X_1 , X_2 , Y_{min} , Y_{max} values are 68, 97, 22, and 199 respectively. X and Y values are 165 and 177 respectively.

Apply the algorithm 4.5 on each and every common region to generate a statistical feature vector. These feature vectors are stored for further processing. The feature vectors size is shown in Table 5.1.

The samples of dynamic WPLIs and its common regions are shown in Table 5.2. In the given example WPLI images, D_{xa} vector values are 87, 91, 78, 101, 68. D_{ya} vector values are 22, 21, 13, 19, and 21. X_v vector values are 107, 107, 108, 97, and 101. Y_v vector values are 212, 214, 199, 207, and 211. The obtained X_1 , X_2 , Y_{min} , Y_{max} values are 68, 97, 22, and 199 respectively. X and Y values are 165 and 177 respectively.

The wavelets are widely used for dimensionality reduction and also retain the distinguishable features. To reduce the processing time for identification, we applied wavelets on the common region of WPLIs and generated values are considered as feature vector. Single level two dimensional db4 wavelet decomposition is applied to reduce the dimensionality.

The obtained LL is converted to a vector, and it is considered as a feature vector. The obtained feature vectors are stored for identification. The common region size is 177 x 165, i.e. number of pixels is 29205, after applying the wavelet decomposition the obtained feature vector size is 7912. The feature vector size is shown in Table 5.2. The schematic diagram for FeatureDatabase generation is shown in Figure 5.4.

Algorithm 5.9 FDBGENERATE(database,u): To generate the feature database

//Algorithm for FeatureDatabase generation for database images//

Input:

database: Dynamic ROI/WPLI database and reference point information

u : Number of database images

Output:

FeatureDatabase: Common ROIs feature vectors of database images

Method: For every i^{th} image from the input database execute the steps 1 to 3.

1. Select the i^{th} dynamic ROI and its DX and DY from the dynamic ROI database.

2. Store DX and DY in i^{th} position of D_{xa} and D_{ya} vectors respectively.

3. Let i^{th} dynamic ROI image size is X_i and Y_i .

Compute:

$$X_{rem} \leftarrow X_i - DX$$

$$Y_{rem} \leftarrow Y_i + DY$$

Store X_{rem} , Y_{rem} in X_v and Y_v vectors in i^{th} position respectively.

4. Compute

$$X_1 \leftarrow \min(D_{xa})$$

$$X_2 \leftarrow \min(X_v)$$

$$Y_{min} \leftarrow \max(D_{ya})$$

$$Y_{max} \leftarrow \min(Y_v)$$

$$X \leftarrow X_1 + X_2$$

$$Y \leftarrow Y_{max} - Y_{min}$$

5. For every dynamic ROI, common region size is $X \times Y$.

- The common region top left corner in the dynamic ROI is $(DX - X_1, Y_{min} - DY)$.
- If the database is DynamicROI database then compute the statistical feature vector for the common region otherwise apply the wavelets on the common region to generate feature vector.
- Store the feature vector in FeatureDatabase.

6. Return FeatureDatabase

Computational Complexity of FDBGENERATE	
Let number of database images is u and common region size is M x N	
Steps 1 to 4	$O(u)$
Step 5	$O(uMN)$
Algorithm Complexity: $O(uMN)$	

Table 5.1: Sample images of common region of Dynamic ROI

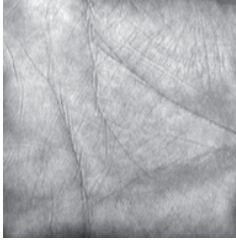
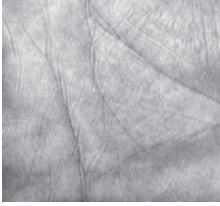
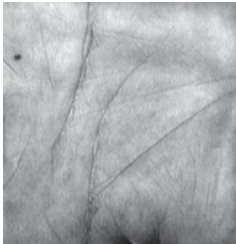
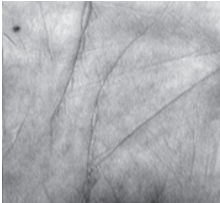
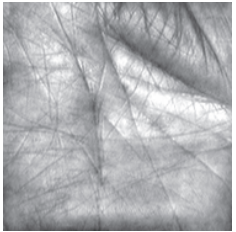
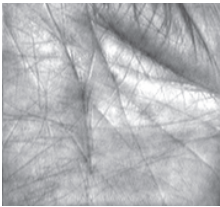
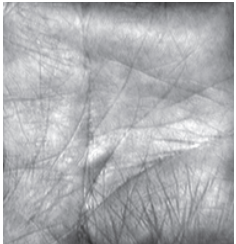
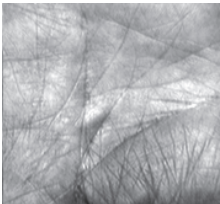
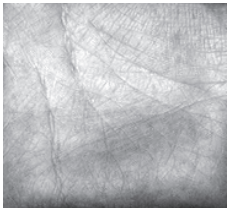
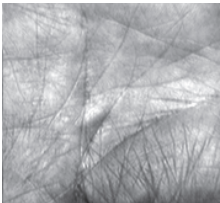









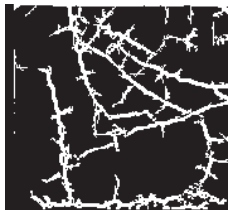
Dynamic ROI	DX	DY	Common region	Feature vector size
 194 x 190	87	22	 165 x 177	2426
 193 x 198	91	21	 165 x 177	2496
 186 x 186	78	13	 165 x 177	2946
 198 x 188	101	19	 165 x 177	2496
 169 x 182	68	21	 165 x 177	2496

Table 5.2: Sample images of common region of WPLI

Dynamic WPLI	DX	DY	Common region	Feature vector size
 194 x 190	87	22	 165 x 177	7912
 198 x 193	91	21	 165 x 177	7912
 186 x 186	78	13	 165 x 177	7912
 198 x 188	101	19	 165 x 177	7912
 169 x 182	68	21	 165 x 177	7912

The parameters required ($threshold_a$, $threshold_b$, C is the number of clusters to be used in EM algorithm [135] etc.), to perform the identification are determined dynamically based on the database palmprint images (Training Set). The step by step procedure to perform the parameter identification is explained in algorithm 5.10.

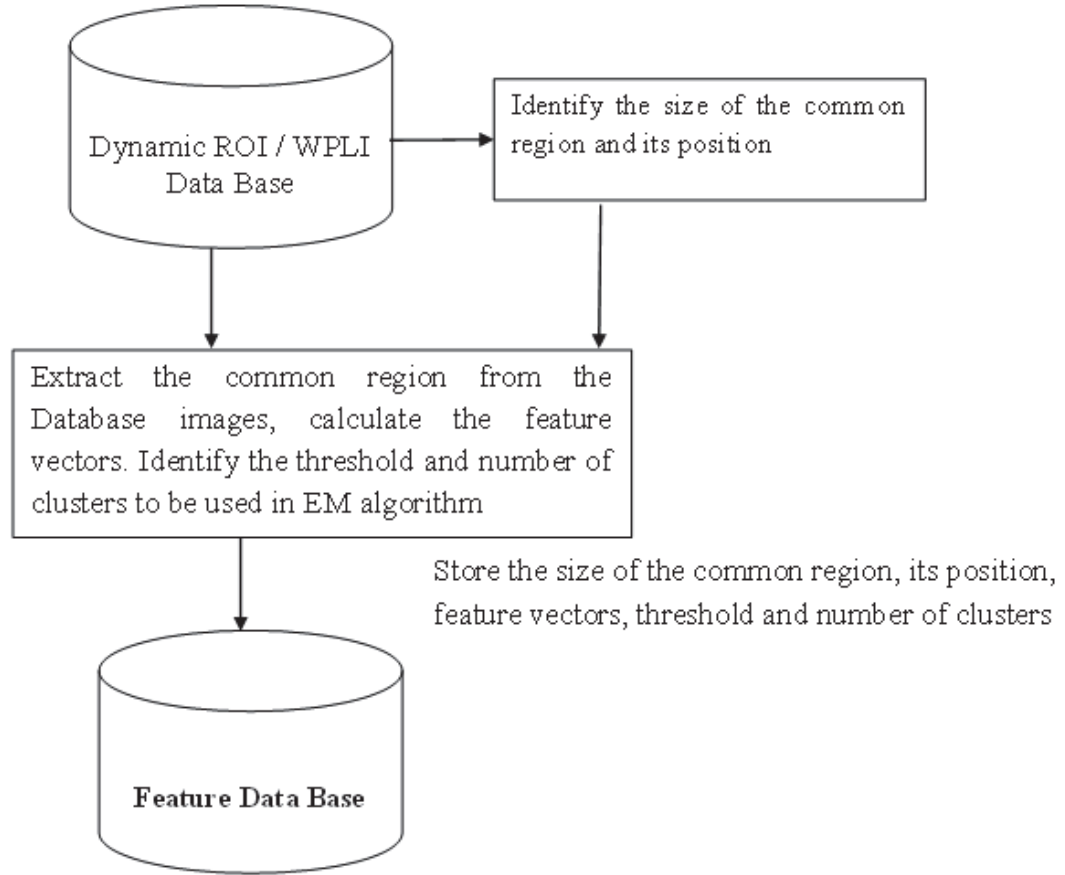


Figure 5.4: Schematic diagram for feature database generation.

The algorithm 5.10, takes the FeatureDatabase as input and returns the values of $threshold_a$, $threshold_b$ and C. Store the values of $threshold_a$, $threshold_b$ and C in the FeatureDatabase. In this algorithm, for every feature vector in the FeatureDatabase, calculate the Dissimilarity Distances with the remaining feature vectors of the database images and identify the minimum Dissimilarity Distances according to palmprint wise. If the minimum Dissimilarity Distance palmprint is same as the query palmprint, then it is considered as a true positive, otherwise it is considered as a false

Algorithm 5.10 ParamID(FeatureDatabase): To identify the parameters, to be used in palmprint identification algorithm

//Algorithm for identification of parameters required for palmprint identification//

Input:

FeatureDatabase : Statistical or WPLI features of database images

Output:

$Threshold_a$: Threshold used in phase 1 to perform identification

$Threshold_b$: Threshold used in phase 2 to perform identification

C : Number of clusters used in EM algorithm [135]

Method:

MDD is a vector. Initially MDD consists of zero number of elements. For every feature vector in the FeatureDatabase apply the steps 1 to 4.

1. Calculate the Dissimilarity Distances with the remaining feature vectors of the database images.
2. Identify the minimum Dissimilarity Distances according to palmprint wise.
3. If the minimum Dissimilarity Distance palmprint is same as the query palmprint, then it is considered as a true positive, otherwise it is considered as a false positive.
4. If it is false positive, then
 - Accumulate the minimum Dissimilarity Distance in MDD vector.
 - Identify the maximum possible value of C when the query palmprint is on the most similar palmprints list. The procedure to identify the C value is as follows:
 - Initialize C=100 (C is the number of clusters).
 - Apply the EM algorithm [135] on palmprint wise minimum Dissimilarity Distances.
 - Accumulate the value of C in CV vector if the query palmprint is on the selected list, otherwise decrease the value of C by 1 and repeat the above step.

Let n_{fp} is the number of false positives. Let sorted minimum Dissimilarity Distance (SMDD) and sorted C values (SCV) are the sorted vectors of MDD and CV.

5. Threshold index (ti) is calculated using the following formula. Threshold (TH) is considered as the ti^{th} value of SMDD and number of clusters (C) is considered as ti^{th} value in SCV.

$$\begin{aligned} ti &\leftarrow \text{ceil}(n_{fp}/10) \\ TH &\leftarrow SMDD(ti) \\ C &\leftarrow SCV(ti) \end{aligned}$$

6. To calculate the $threshold_b$, every database image is compared with the remaining database images of the same palmprint. The smallest value of the matching scores is considered as the $threshold_b$.

7. Return $threshold_a, threshold_b, C$ ¹¹⁴
-

Computational Complexity of ParamID	
Let u is the number of database images v is the size of the feature vector of an image and $M \times N$ is the size of the image	
Step 1	$O(u^2v)$
Steps 2 & 3	$O(u)$
Step 4 EM algorithm	$O(u^2)$
Step 6	$O(u^2MN)$
Algorithm Complexity: $O(u^2MN)$	

positive.

For every false positive, accumulate the minimum Dissimilarity Distance in MDD vector. Identify, the maximum number of clusters having the query palmprint is on the most similar palmprints list, using the EM algorithm [135]. Now, identify the values of $threshold_a$, C consists of number of clusters to be used in EM algorithm.

To calculate the $threshold_b$, every database palmprint image is compared with the remaining database images of the same palmprint. That is, calculate all possible true similarity scores. The smallest value of the true similarity scores is considered as the $threshold_b$.

5.2.2 Palmprint Identification

The block diagram for the palmprint identification is shown in Figure 5.5. The step by step procedure to perform the palmprint identification is explained in algorithm 5.11.

The algorithm 5.11 takes *querypalmprint*, FeatureDatabase, database (ROI / WPLI database) as input and returns the ID of the *querypalmprint*, if the query palmprint is enrolled, otherwise, declare the query palmprint is not registered. Extract the dynamic ROI and reference point information from the query palmprint using the method discussed in Chapter 3.

If the selected feature is WPLF apply algorithm 4.4 on extracted dynamic ROI and the result image is named as query image otherwise extracted dynamic ROI is named

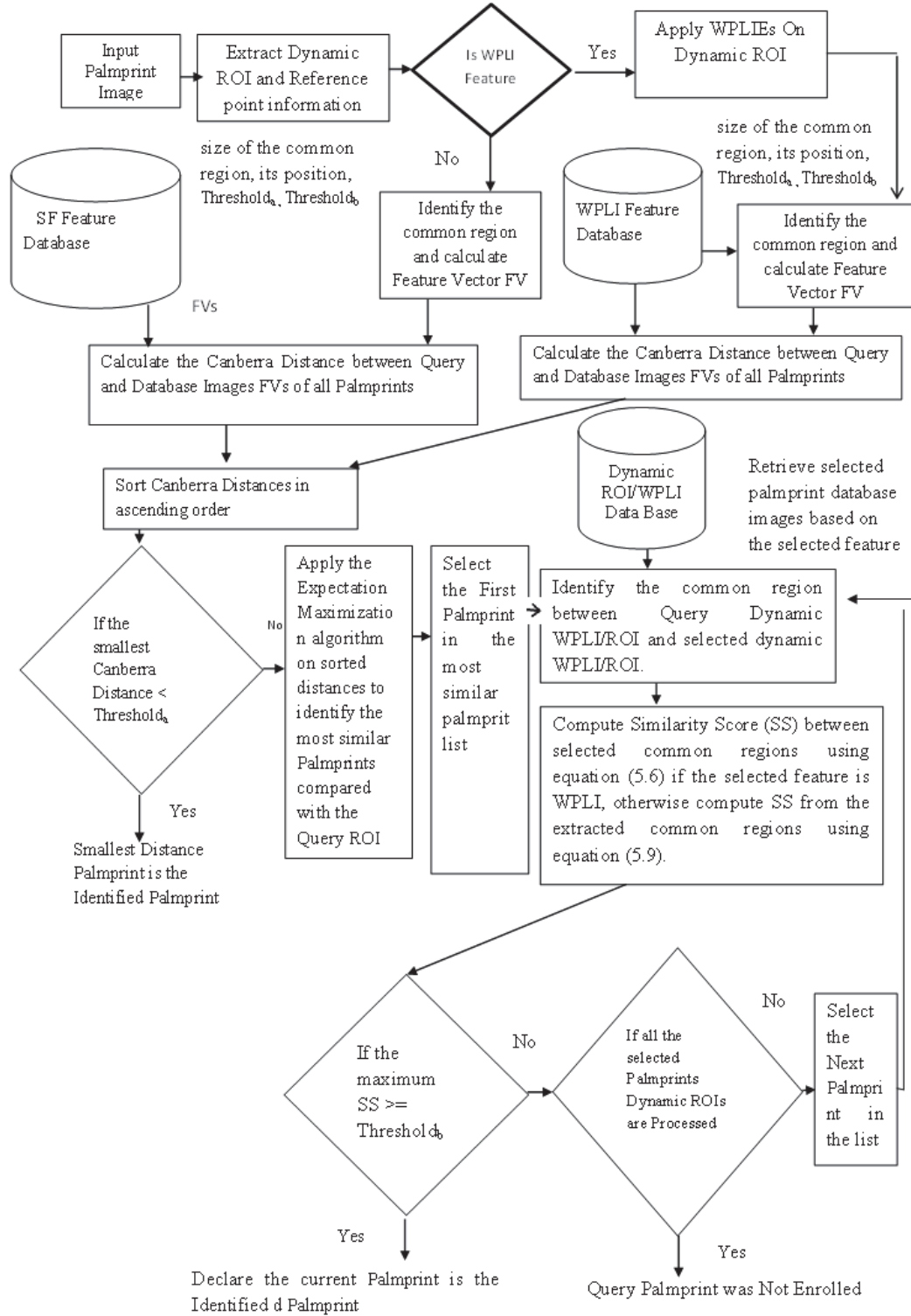


Figure 5.5: Schematic diagram for palmprint identification.

Algorithm 5.11 PalmID(Query Palmprint, FeatureDatabase, database): To identify the palmprint from the database images

//Algorithm for identification of palmprint//

Input:

Query Palmprint : Query palmprint image

FeatureDatabase : Statistical or WPLI features of database images

database: Dynamic ROI/WPLI database and reference point information

Method:

Fetch the $threshold_a$, $threshold_b$ and C from FeatureDatabase

1. Extract the dynamic ROI and reference point information from the query palmprint.
2. If it is WPLI feature based approach apply WPLI feature extractors on extracted dynamic ROI and the result image is named as query image otherwise extracted dynamic ROI is named as query image.
3. Identify the fixed region from the query image based on the reference point information and parameters identified at the time of FeatureDatabase generation.
4. If the database is DynamicROI database then compute the statistical feature vector for the identified fixed region otherwise apply the wavelets on the identified fixed region to generate feature vector.
5. Calculate the Dissimilarity Distances using equation (5.8) between query image feature vector and feature vectors of database images and palmprint wise identify the minimum Dissimilarity Distances.
6. If the smallest distance is less than $threshold_a$ then declare the smallest Dissimilarity Distance palmprint is the identified palmprint and stop the process, otherwise go to Step 7.
7. Apply the EM algorithm [135] on the user wise minimum Dissimilarity Distances calculated at Step 6, to identify most similar palmprints with query image. Select the first similar palmprint images in the database.
8. Calculate the common region between the selected database images and query image using the algorithm 5.6.
9. If it is statistical feature based approach then compute the statistical feature vectors of the extracted common regions. Compute the similarity scores between the feature vectors of the extracted common regions of query image and selected database images using equation (5.9). Otherwise compute the Similarity Scores between the extracted common regions of query image and selected database images using equation (5.6).
10. If the maximum of the similarity scores is greater than or equal to the $threshold_b$ then declare the current database image palmprint is the identified palmprint and stop the process. If all the selected similarity palmprints are processed then declare the query palmprint is not registered and stop the process otherwise select the next similar palmprint images from the database and go to step 8.

Computational Complexity of PalmID	
Let the query palmprint size is $M \times N$ and its extracted dynamic ROI size is $M_1 \times N_1$. u is the number of database images.	
Step 1	$O(MN)$
Steps 2 to 4	$O(M_1N_1)$
Step 5	$O(uM_1N_1)$
Step 6	$O(u^2)$
Steps 8 to 10	$O(M_1N_1)$
Algorithm Complexity: $O(uMN)$	

as query image. Identify the fixed region from the query image based on the reference point information and parameters identified at the time of FeatureDatabase generation. If the database is dynamic ROI database then compute the statistical feature vector for the identified fixed region otherwise apply the wavelets on the identified fixed region to generate feature vector.

Calculate the Dissimilarity Distances using equation (5.8) between query image feature vector and feature vectors of database images and palmprint wise identify the minimum Dissimilarity Distances. Declare the smallest Dissimilarity Distance palmprint is the identified palmprint and stop the process, if the smallest distance is less than $threshold_a$ otherwise apply the EM algorithm on the user wise minimum Dissimilarity Distances, to identify most similar palmprints with query image.

Select the first similar palmprint images in the database. Perform the palmprint verification between the query image and database image is as follows. Calculate the common region between database images and query image using the algorithm 5.6. If it is statistical feature based approach then compute the statistical feature vectors of the extracted common regions. Compute the similarity scores between the feature vectors of the extracted common regions of query image and selected database images using equation (5.9). If the selected feature is WPLF then compute the similarity scores between the extracted common regions of query image and selected database images using equation (5.6).

If the maximum of the similarity scores is greater than or equal to the $threshold_b$

then declare the current database image palmprint is the identified palmprint, and stop the process. If the maximum of the similarity scores is less than $threshold_b$ and all the selected palmprints are processed then declare the query palmprint is not registered and stop the process, otherwise, select the next similar palmprint images from the database and perform the palmprint verification using the above proposed approach. The values of u, M_1N_1 are very much smaller than MN , so the complexity of palmprint identification algorithm is $O(uMN)$.

5.3 Summary

We proposed a common region extraction algorithm to extract the common region between query dynamic ROI and database dynamic ROI based on reference point information. We proposed palmprint verification and two-phase palmprint identification algorithms can be applied on WPLF and SF.

CHAPTER 6

Experimental Design & Analysis

To test the proposed palmprint verification and two-phase palmprint identification algorithms, experiments were performed on the PolyUPalmprint database using wide principal line features and statistical features. The experiments were conducted on a system with an Intel Core i3 processor (2.4 GHz) and 2GB RAM configured with Windows 7 and MATLAB R2012b with image processing toolbox. Section 6.1 gives a brief account of data sets for experiments. Section 6.2 presents experimental results using wide principal line features. Section 6.3 presents experimental results using statistical features on ROI. Section 6.4 presents experimental results using statistical features on WPLI.

6.1 Data Sets

The data sets used by the previous researchers are considered here to compare the performance of the proposed approach. These data sets are given below:

Data set I: The first two samples in the first session and the first sample in the second session of PolyUPalmprint database are regarded as the database images, all the samples are regarded as the query images. Mansoor et al. [23] is also used the same database and query images and obtained CIR was 90.17.

Data set II: The 1st, 6th and 8th samples of the first and second session of PolyUPalmprint database are regarded as the database images. 2nd, 3rd, 4th, 5th and 7th samples of the first and second session of PolyUPalmprint database are regarded as the query images. The number of database images are 2316 and the number of query images are 3855. G.S. Badrinath et al. [95] used the same number of database and query

images and obtained CIR was 99.5. G.S. Badrinath et al. [61, 62] used the same number of database, query images and obtained CIR was 99.937 (without enhancement) and 100 with enhancement.

Data set III: The first 3 samples in the first session of PolyUPalmprint database are regarded as the database images, and the remaining samples of the first session of PolyUPalmprint database are regarded as the query images. The number of database images are 1158 and the number of query images are 2731. Mu et al. [24] used the same number of database, query images and obtained CIR was 99.32.

Data set IV: The 5 samples in the first session of PolyUPalmprint database are regarded as the database images and other samples of the first session are regarded as the query images. The number of database images are 1930 and the number of query images are 1959. Xuan et al. [99, 101] used the same number of database, query images and obtained CIR were 97.377 and 99.02 respectively.

Data set V: Randomly select three samples of each palmprint in the first session to construct database images and use the remaining samples in the first session as query images. The database consists of 1158 palmprint images and query set contains 2731 palmprint images. Zhang et al. [66] used the same number of database and query images.

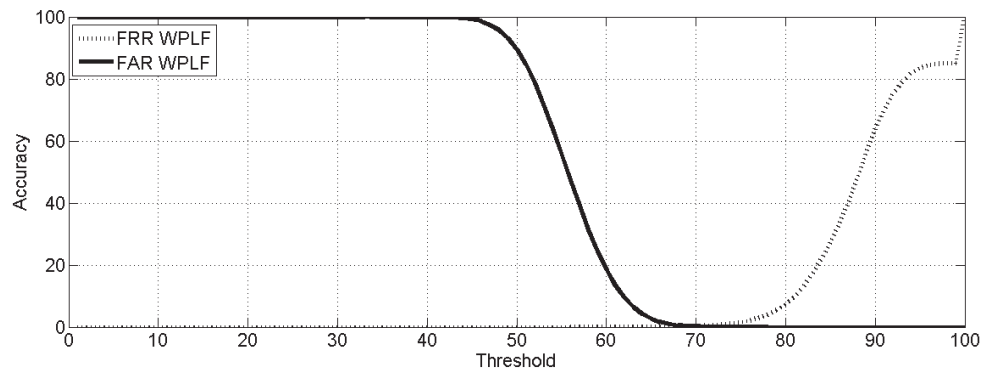
6.2 Experiments using WPLF

6.2.1 Experiments on data set I

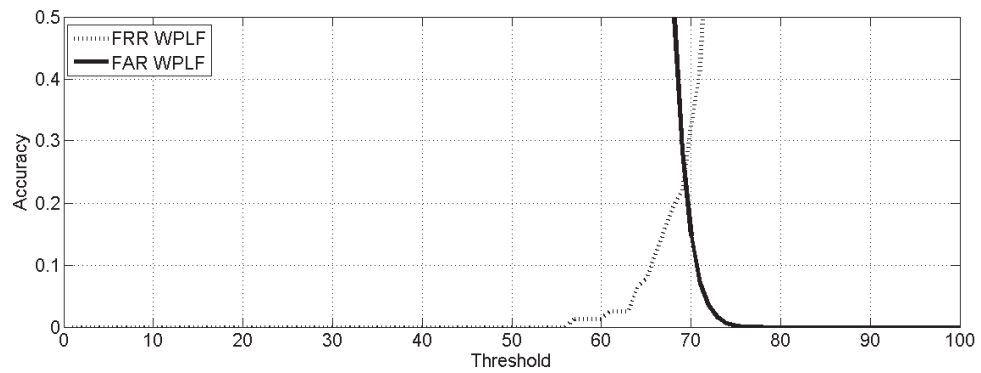
This experiment is conducted to test the identification and verification accuracy of the proposed approach on Data set I.

Palmprint Verification

To calculate the false rejection rate (FRR), every query image is compared the same palm database images. Number of verifications to calculate FRR is 7752. To calculate the false acceptance rate (FAR), every query image is compared with all the remaining palm database images. Number of verifications to calculate FAR is 29,84,520. The false acceptance rate (FAR) and false rejection rate (FRR) are shown in Figure 6.1. Decidability index and equal error rate are given in Table 6.1. Receiver operating characteristic (ROC) curve is given in Figure 6.2. Mansoor et al. [23] used the same number of database and query samples. Clearly the decidability index (DI) is better than existing literature [23] .



(i) Accuracy scaling 0 to 100



(ii) Accuracy scaling 0 to 0.5

Figure 6.1: FAR & FRR representation on data set I using WPLF.

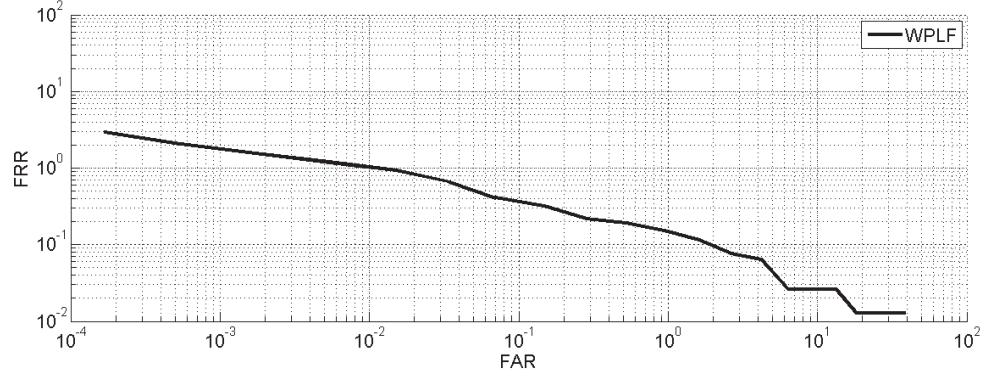


Figure 6.2: ROC curve on data set I using WPLF.

Palmprint Identification

Using the proposed approach, 7694 images are correctly identified, i.e. the CIR is 99.25. The results are represented in Table 6.2. Mansoor et al. [23] obtained the CIR for the same data set was 90.17. Time taken to generate the FeatureDatabase, parameters estimation dynamically based on the database images (training images) and average time for palmprint identification (in seconds) are given in Table 6.3. Clearly the proposed approach obtained better results compared to [23].

Table 6.1: Decidability Index (DI) and Equal Error Rate (EER) analysis using WPLF on PolyUPalmprint database

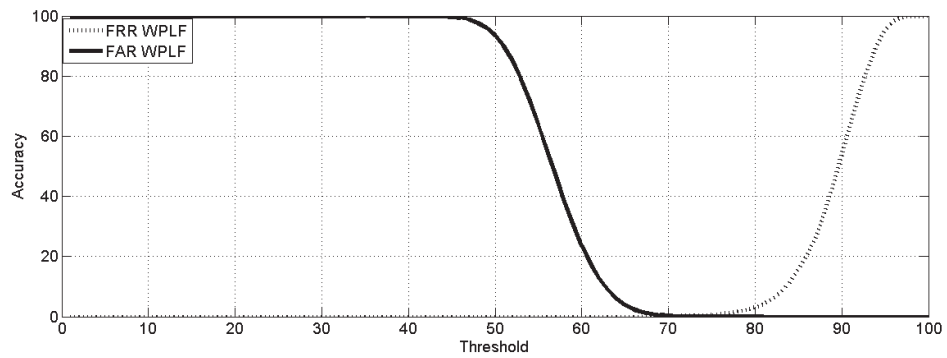
Data Set	Existing Methods			Proposed Approach	
	Author Name	DI	EER	DI	EER
Data set I	Mansoor et al. [23]	2.8914	0.1563	5.799	0.25
Data set II	Badrinath et al. [95]		1.0	7.3719	0.12
	Badrinath et al.[62]	6.265	0.0020		
	Badrinath et al. [61]	7.3521	0.0055		
Data set III	Mu et al. [24]	Not Reported		2.48	0.11
Data set IV	Xuan et al. [99, 101]	Not Reported		7.59	0.03

6.2.2 Experiments on data set II

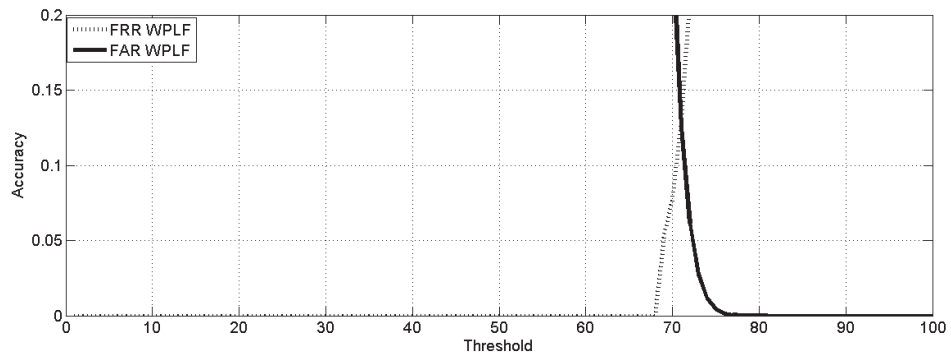
This experiment is conducted to test the identification and verification accuracy of the proposed approach on data set II.

Palmprint Verification

Number of verifications to calculate FRR is 3855. FAR is calculated by comparing the query Wide Principal Line Images of each palm with the remaining other palms database Wide Principal Line Images. Number of verifications to calculate FAR, is 14,84,175. The false acceptance rate (FAR) and false rejection rate (FRR) are shown in Figure 6.3. Decidability index and equal error rate are given in Table 6.1. Receiver operating characteristic (ROC) curve is given in Figure 6.4. Clearly the decidability index is better compared to the existing literature [61, 62].



(i) Accuracy scaling 0 to 100



(ii) Accuracy scaling 0 to 0.2

Figure 6.3: FAR & FRR representation on data set II using WPLF.

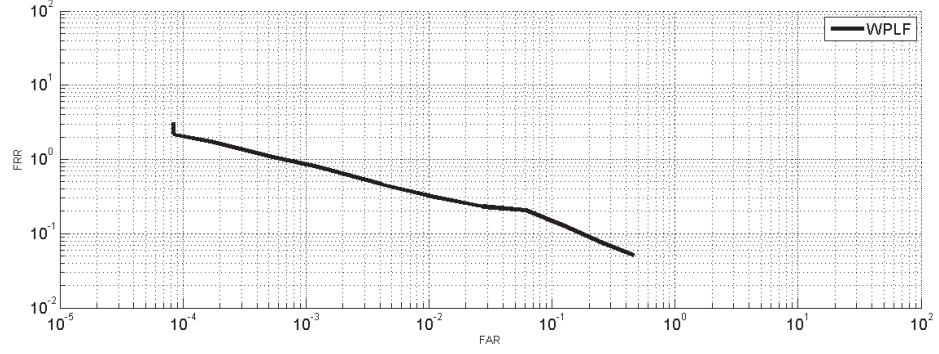


Figure 6.4: ROC Curve on data set II using WPLF.

Palmprint Identification

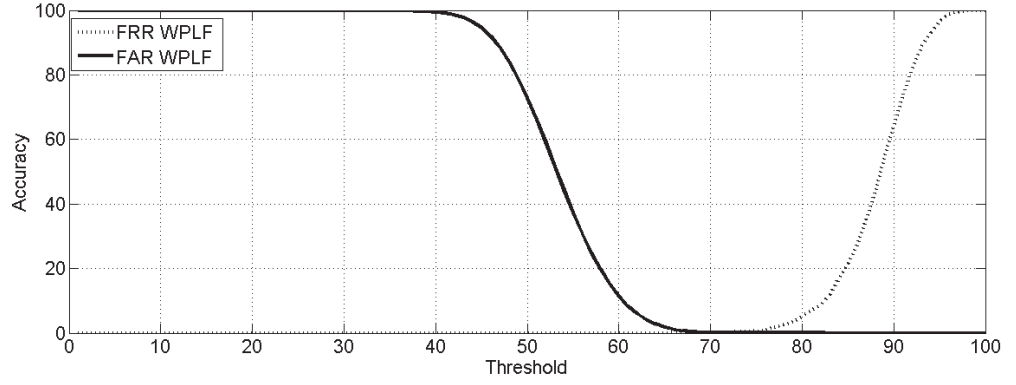
Using the proposed approach 3848 images are correctly identified, i.e. the CIR is 99.818. The results are represented in Table 6.2. Using the Wide Principal Line Images the proposed approach obtained nearly equivalent results compared to [61, 62]. Time taken to generate the FeatureDatabase, parameters estimation dynamically based on the database images (training images) and average time for palmprint identification (in seconds) are given in Table 6.3.

6.2.3 Experiments on data set III

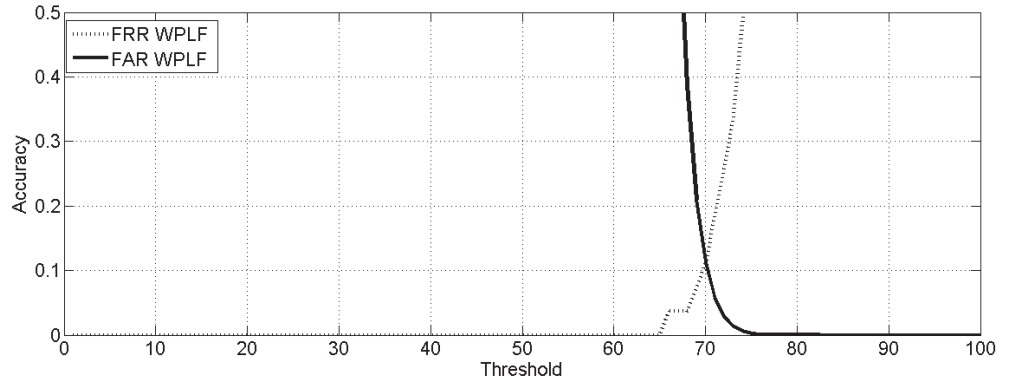
This experiment is conducted to test the identification accuracy of the proposed approach on data set III.

Palmprint Verification

Number of verifications to calculate FRR is 2731. FAR is calculated by comparing the query Wide Principal Line Images of each palm with the remaining other palms database Wide Principal Line Images. Number of verifications to calculate FAR, is 10,51,435. The false acceptance rate (FAR) and false rejection rate (FRR) are shown in Figure 6.5. Decidability index and equal error rate are given in Table 6.1. Receiver operating characteristic (ROC) curve is given in Figure 6.6.



(i) Accuracy scaling 0 to 100



(ii) Accuracy scaling 0 to 0.5

Figure 6.5: FAR & FRR representation on data set III using WPLF.

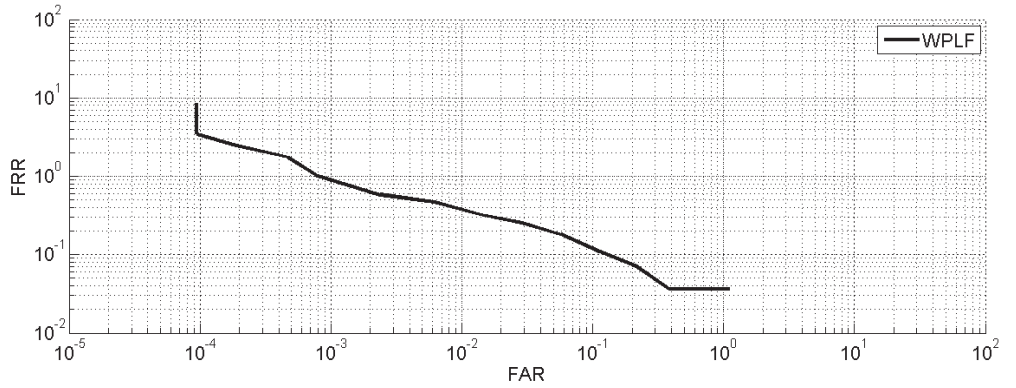


Figure 6.6: ROC Curve on data set III using WPLF.

Palmprint Identification

Using the proposed approach 2719 images are correctly identified, i.e. the CIR is 99.56.

The results are represented in Table 6.2. Mu et al. [24] obtained the CIR for the same

data set is 99.32. Clearly the proposed approach obtained better results compared to [24]. Time taken to generate the FeatureDatabase, parameters estimation dynamically based on the database images (training images) and average time for palmprint identification (in seconds) are given in Table 6.3.

6.2.4 Experiments on data set IV

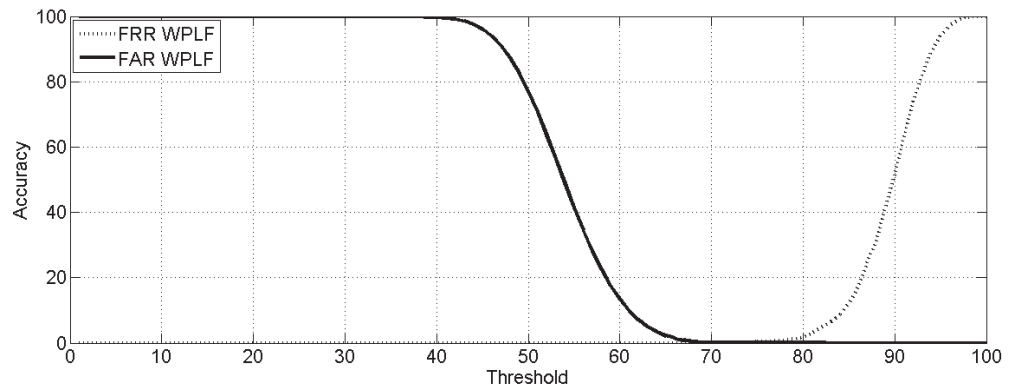
This experiment is conducted to test the identification accuracy of the proposed approach on data set IV.

Palmprint Verification

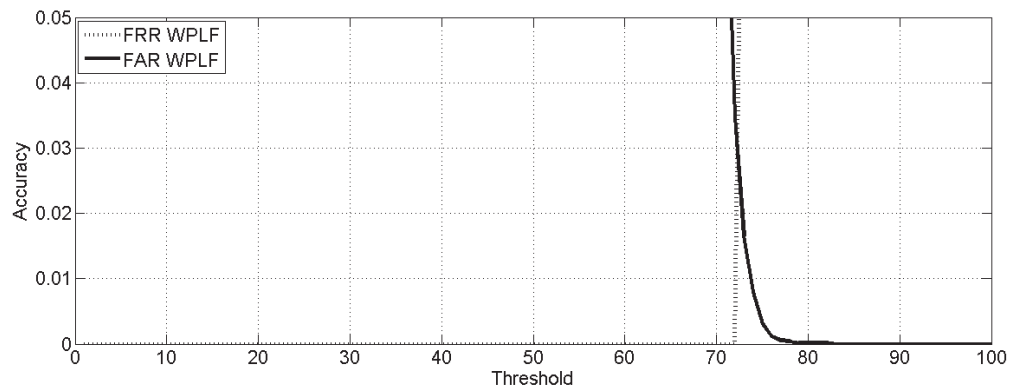
Number of verifications to calculate FRR is 1959. FAR is calculated by comparing the query Wide Principal Line Images of each palm with the remaining other palms database Wide Principal Line Images. Number of verifications to calculate FAR, is 7,54,215. The false acceptance rate (FAR) and false rejection rate (FRR) are shown in Figure 6.7. Decidability index and equal error rate are given in Table 6.1. Receiver operating characteristic (ROC) curve is given in Figure 6.8.

Palmprint Identification

Using the proposed approach 1957 images are correctly identified, i.e. the CIR is 99.897. Xuan et al. [99, 101] obtained CIR for the same data set are 97.377 and 99.02 respectively. Clearly the proposed approach obtained better CIR compared to [99, 101]. Time taken to generate the FeatureDatabase, parameters estimation dynamically based on the database and average time for palmprint identification (in seconds) are given in Table 6.3.



(i) Accuracy scaling 0 to 100



(ii) Accuracy scaling 0 to 0.05

Figure 6.7: FAR & FRR representation on data set IV using WPLF.

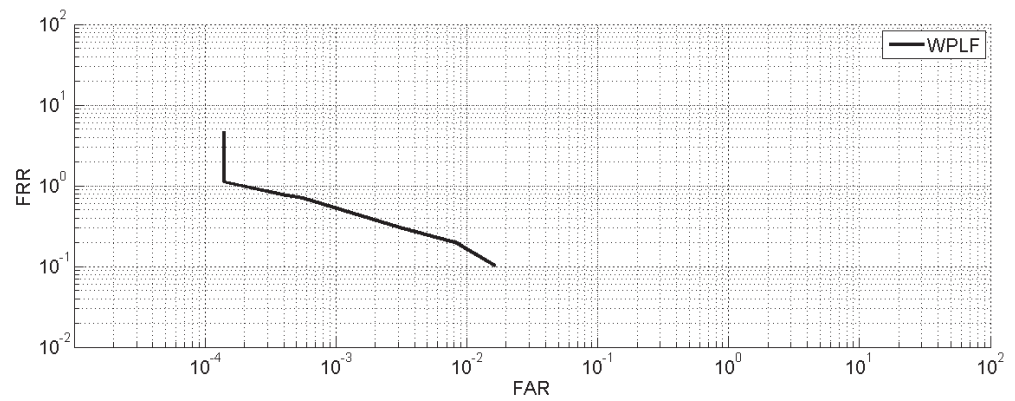


Figure 6.8: ROC Curve on data set IV using WPLF.

Table 6.2: Performance comparison of approaches [23, 24, 61, 62, 95, 99, 101] and proposed approach using WPLF on PolyUPalmprint database

Data set	Existing Methods		CIR of the proposed approach
	Author with reference Number	CIR of existing methods	Dynamic ROI
Data set I	Mansoor et al. [23]	90.17	99.25
Data set II	Badrinath et al. [95]	99.59	99.87
	Badrinath et al. [61, 62]	99.937(without enhancement)& 100 with enhancement	
Data set III	Mu et al. [24]	99.32	99.56
Data set IV	Xuan et al. [99]	97.377	99.897
	Xuan et al. [101]	99.02	

Table 6.3: Time required for identification using WPLF (in seconds)

Data Set	FeatureDatabase generation & Parameter estimation	Identification of query WPLI
Data set I	766.414	0.173
Data set II	2565	0.378
Data set III	813.62	0.1821
Data set IV	1622.94	0.2527

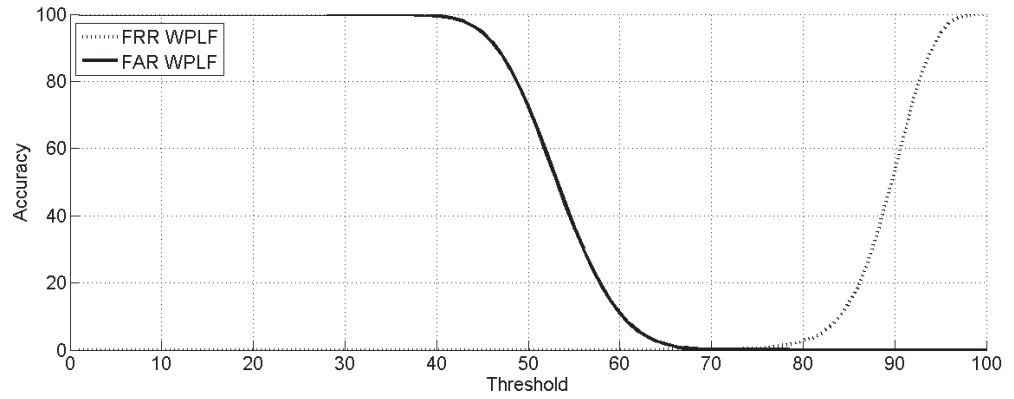
6.2.5 Experiments on data set V

This experiment is conducted to test the identification accuracy of the proposed approach on data set V.

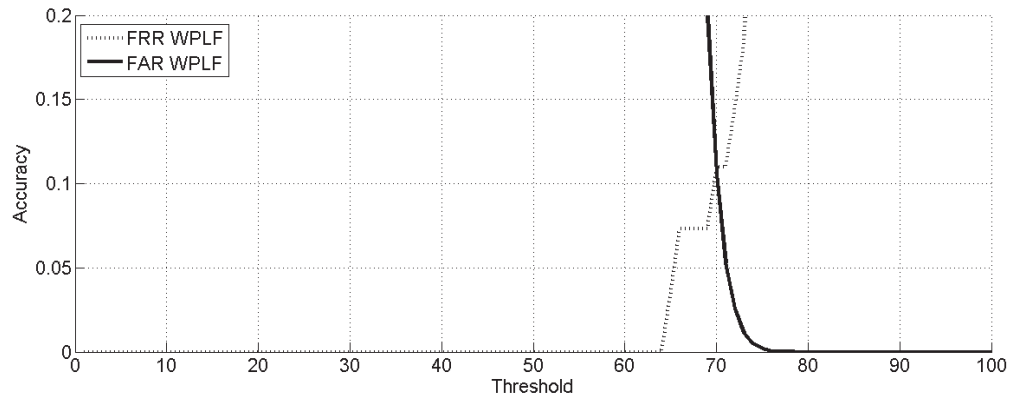
Palmprint Verification

FRR is calculated by comparing the query Wide Principal Line Images of each palm with the same palm database Wide Principal Line Images. Number of verifications to calculate FRR is 2731. FAR is calculated by comparing the query Wide Principal Line Images of each palm with the remaining other palms database Wide Principal Line Images. Number of verifications to calculate FAR, is 10,51,435. The false acceptance rate (FAR) and false rejection rate (FRR) are shown in Figure 6.9. Decidability index

and equal error rate are given in Table 6.4. Receiver operating characteristic (ROC) curve is given in Figure 6.10.



(i) Accuracy scaling 0 to 100



(ii) Accuracy scaling 0 to 0.2

Figure 6.9: FAR & FRR representation on data set V using WPLF.

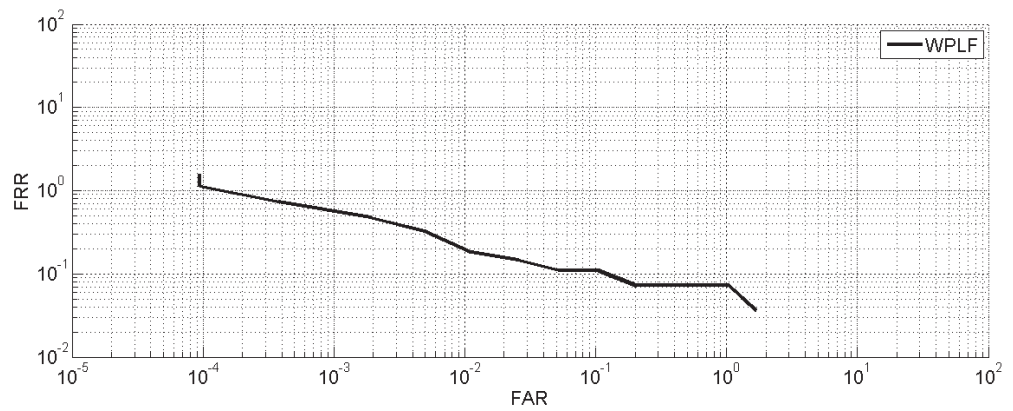


Figure 6.10: ROC Curve on data set V using WPLF.

Table 6.4: Performance comparison of approach [66] and proposed approach using WPLF and SF on Data Set V of PolyUPalmprint database

Author	Feature	EER	DI	CIR
Zhang et al. [66]	CompCode	0.006	Not Reported	100
	OrdiCode	0.005		100
	DogCode	0.023		100
	RLOC	0.022		100
	WLD	0.22		99.97
	Fisherpalms	3.51		99.54
	DCT+LDA	2.716		99.77
Proposed approach	WPLF	0.07	6.77	99.72
	SF (STD)	0.75	5.1	99.77
	SF (CV)	0.6	5.81	99.79
	SF (STD & CV)	0.6	5.63	99.8

Palmprint Identification

Zhang et al. [66] run the experiment 20 times and used the mean to denote the identification performance and robustness of the algorithm. we also run this experiment 20 times and use the mean to denote the identification performance and robustness of the algorithm. The results are represented in Table 6.4.

If identification is performed only for subjects who are present in the enrolment database, the identification is known as closed-set identification. Closed-set identification always returns a non-empty candidate list. While closed-set identification has been studied extensively by researchers, it is rarely used in practice [136]. In open-set identification, some of the identification attempts are made by subjects who are not enrolled. Zhang et al. [66] used the nearest neighbor classification for identification, so it is suitable for only closed-set identification. Our proposed approach results are little bit inferior compared to [66], however our approach is suitable for closed-set as

well as open-set identification.

6.3 Experiments using SF on ROI

6.3.1 Standard deviation as a feature

This experiment is conducted to test the identification accuracy of the proposed approach. For every segment calculated the standard deviation (STD) as a feature.

Palmprint Verification

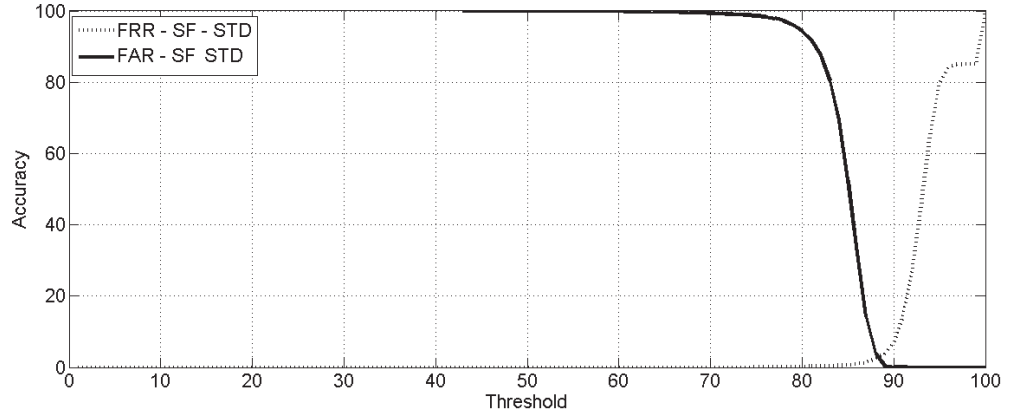
The false acceptance rate (FAR) and false rejection rate (FRR) on data set I are shown in Figure 6.11. Decidability index and equal error rate on data set I are given in Table 6.5. Receiver operating characteristic (ROC) curve on data set I is given in Figure 6.12.

The false acceptance rate (FAR) and false rejection rate (FRR) on data set II are shown in Figure 6.13. Decidability index and equal error rate on data set II are given in Table 6.5. Receiver operating characteristic (ROC) curve on data set II is given in Figure 6.14.

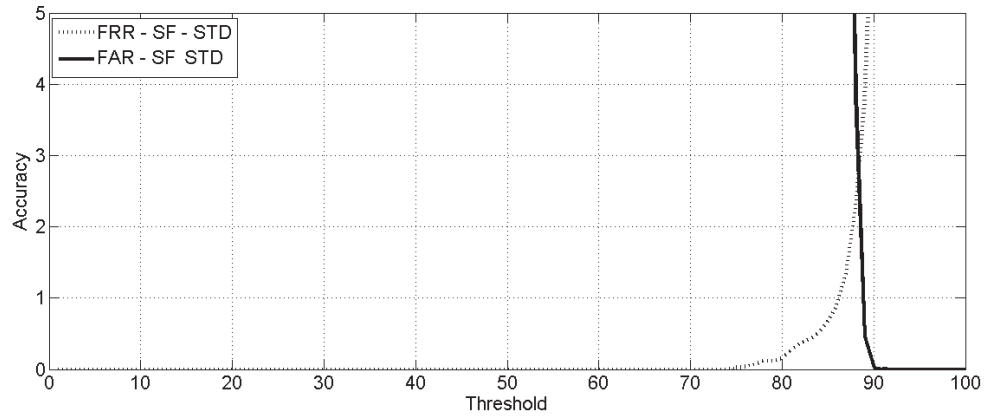
The false acceptance rate (FAR) and false rejection rate (FRR) on data set III are shown in Figure 6.15. Decidability index and equal error rate on data set III are given in Table 6.5. Receiver operating characteristic (ROC) curve on data set III is given in Figure 6.16.

The false acceptance rate (FAR) and false rejection rate (FRR) on data set IV are shown in Figure 6.17. Decidability index and equal error rate on data set IV are given in Table 6.5. Receiver operating characteristic (ROC) curve on data set IV is given in Figure 6.18.

The false acceptance rate (FAR) and false rejection rate (FRR) on data set V are shown in Figure 6.19. Decidability index and equal error rate on data set V are given



(i) Accuracy scaling 0 to 100



(ii) Accuracy scaling 0 to 5

Figure 6.11: FAR & FRR representation on data set I using STD as a feature.

in Table 6.4. Receiver operating characteristic (ROC) curve on data set V is given in Figure 6.20.

Palmprint Identification

On data set I, 7679 images are correctly identified, i.e. the CIR is 99.05. On data set II, 3850 images are correctly identified, i.e. the CIR is 99.87. On data set III, 2726 images are correctly identified, i.e. the CIR is 99.816. On data set IV, 1959 images are correctly identified, i.e. the CIR is 100. On data set V, we run the experiment 20 times and use the mean to denote the identification performance and robustness of the algorithm. The experimental results are shown in Table 6.4 and Table 6.6.

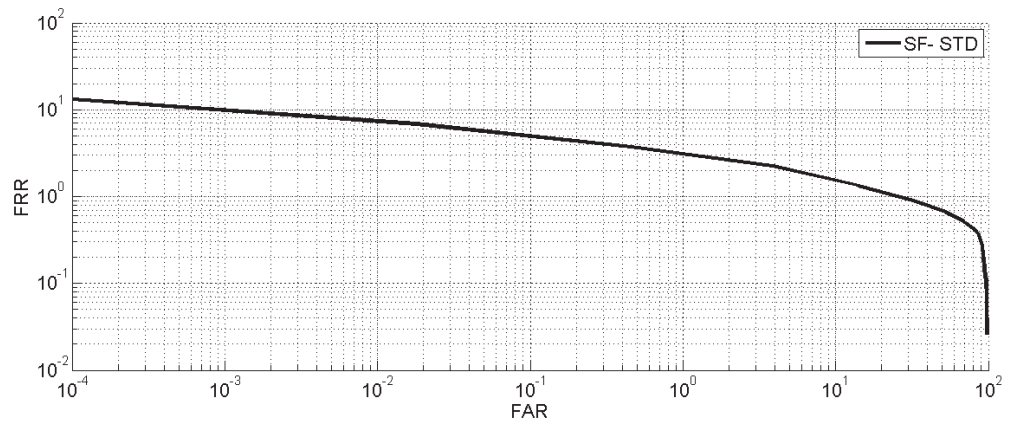
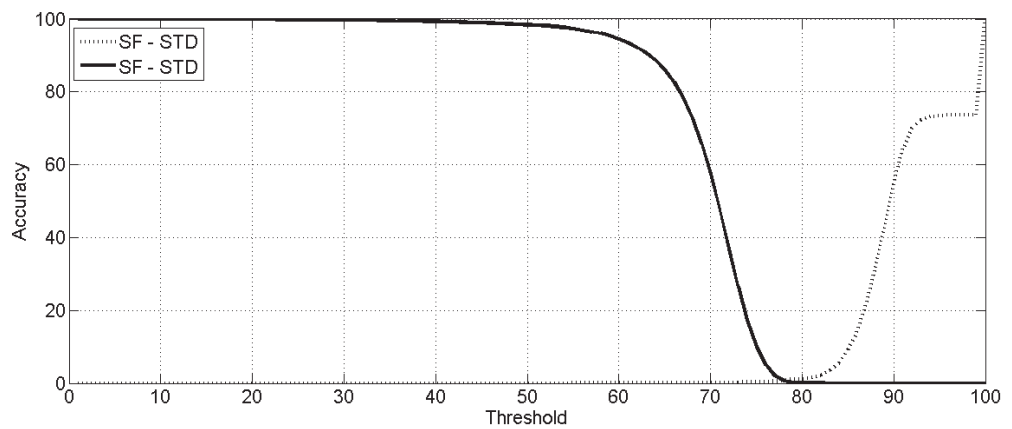
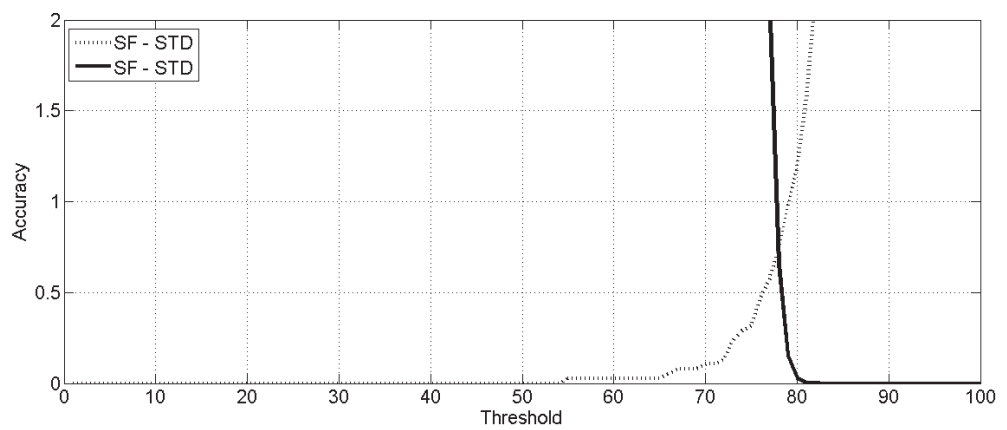


Figure 6.12: ROC curve on data set I using STD as a feature.



(i) Accuracy scaling 0 to 100



(ii) Accuracy scaling 0 to 2

Figure 6.13: FAR & FRR representation on data set II using STD as a feature.

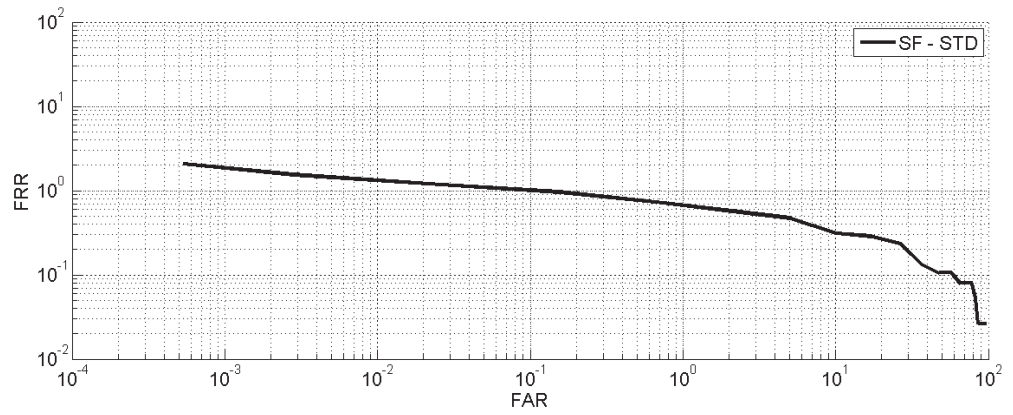
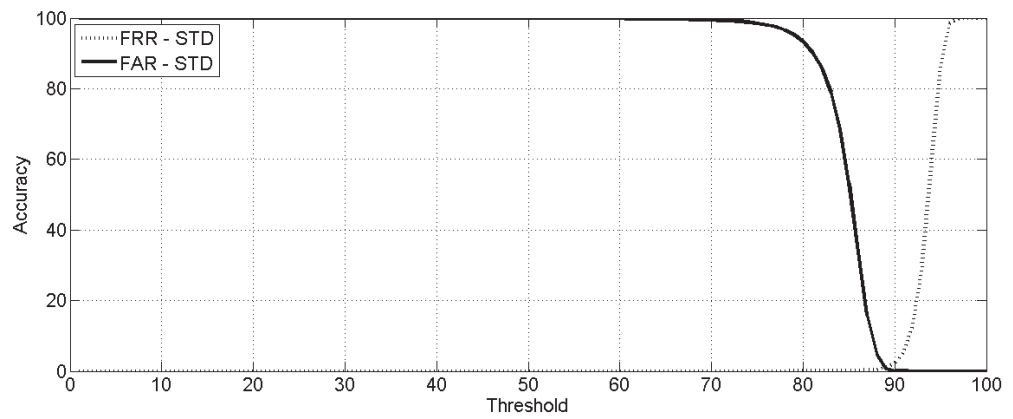
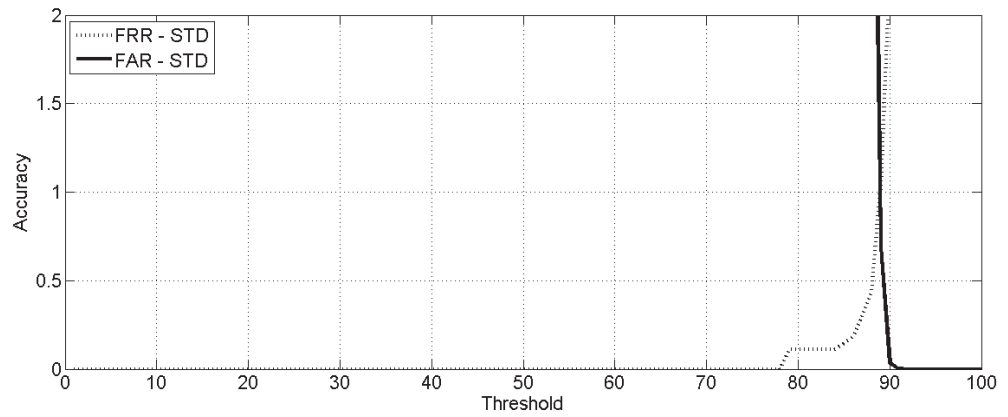


Figure 6.14: ROC curve on data set II using STD as a feature.



(i) Accuracy scaling 0 to 100



(ii) Accuracy scaling 0 to 2

Figure 6.15: FAR & FRR representation on data set III using STD as a feature.

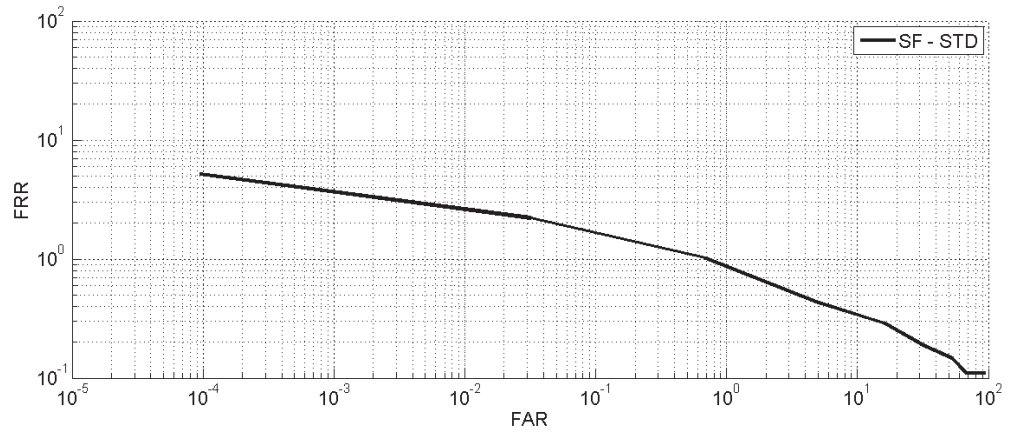
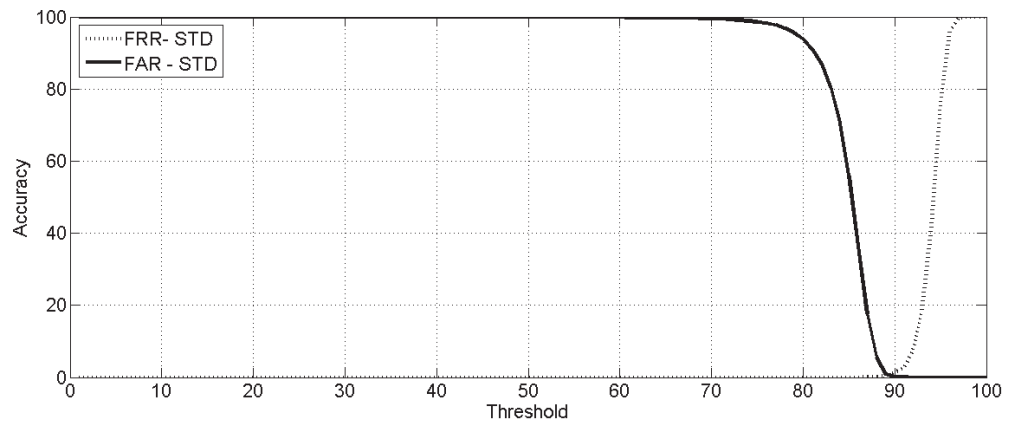
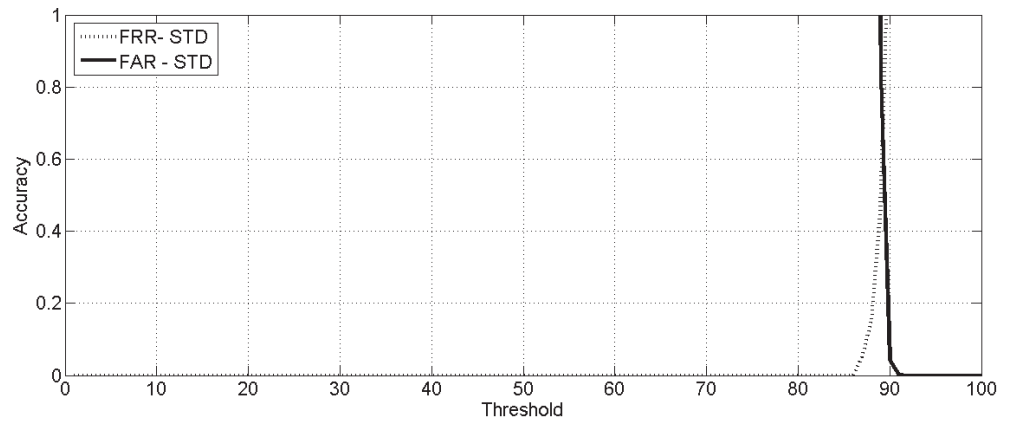


Figure 6.16: ROC curve on data set III using STD as a feature.



(i) Accuracy scaling 0 to 100



(ii) Accuracy scaling 0 to 1

Figure 6.17: FAR & FRR representation on data set IV using STD as a feature.

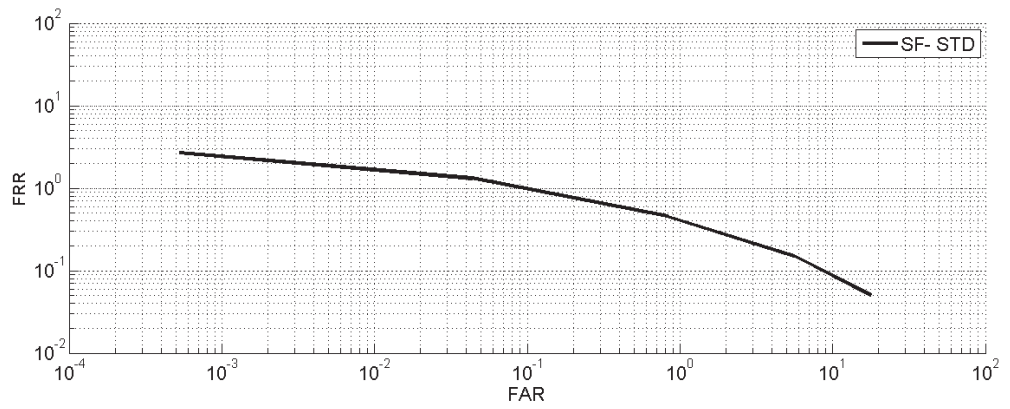
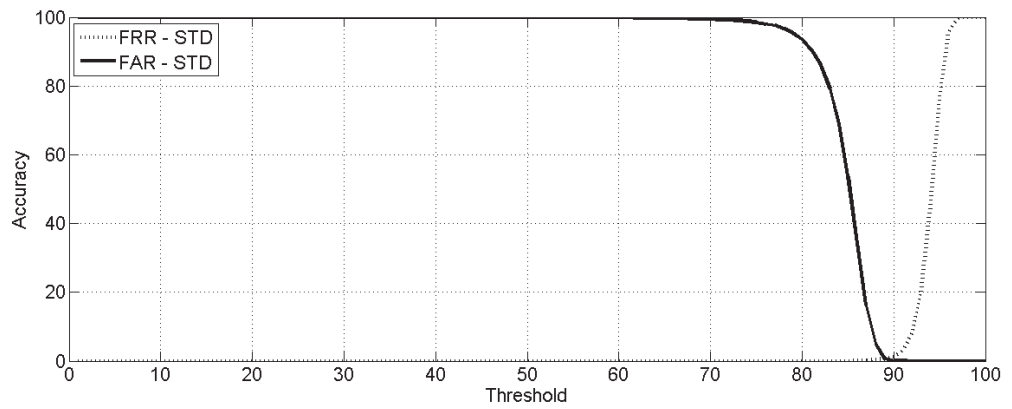
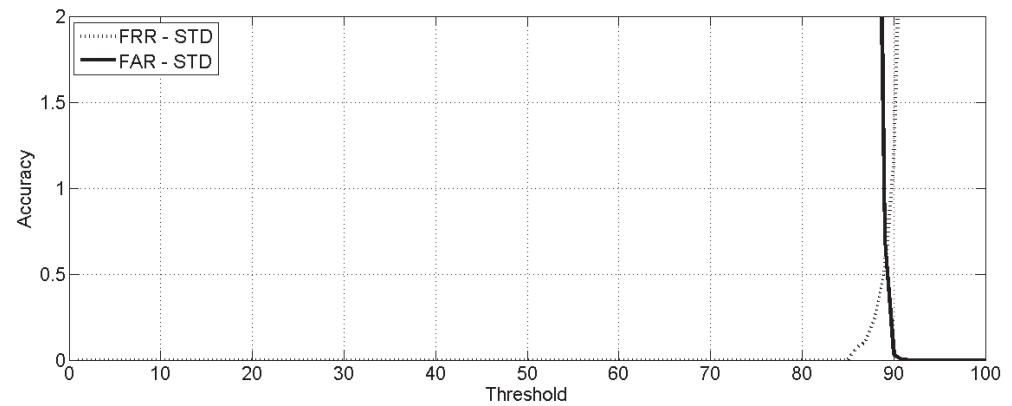


Figure 6.18: ROC curve on data set IV using STD as a feature.



(i) Accuracy scaling 0 to 100



(ii) Accuracy scaling 0 to 2

Figure 6.19: FAR & FRR representation on data set V using STD as a feature.

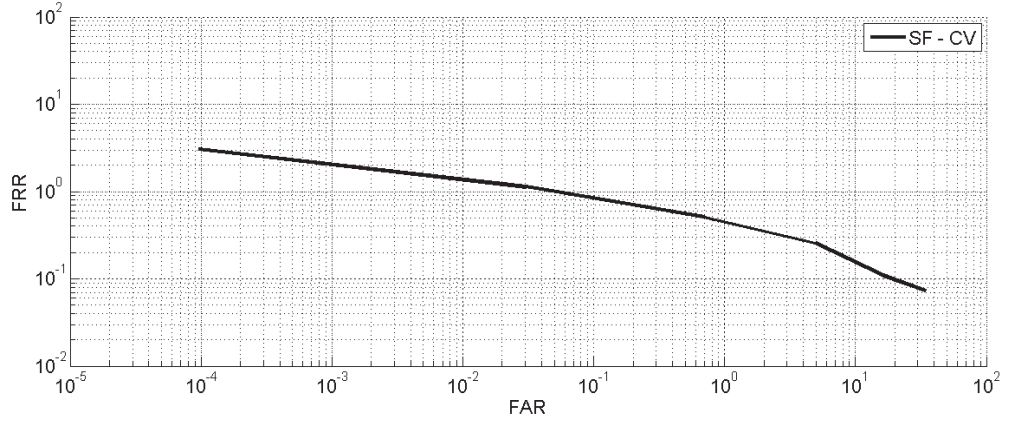


Figure 6.20: ROC curve on data set V using STD as a feature.

Table 6.5: Decidability index (DI) and equal error rate (EER) analysis using SF

Data set	Equal error rate (EER)			Decidability index (DI)		
	STD	CV	STD&CV	STD	CV	STD&CV
Data set I	2.6	2.5	2.5	3.13	3.75	3.44
Data set II	0.9	0.9	0.8	5.08	5.12	5.11
Data set III	0.8	0.8	0.8	3.66	3.55	3.67
Data set IV	0.6	0.5	0.5	3.95	3.8	3.94
Data set V	0.75	0.6	0.6	5.1	5.81	5.63

Time taken to generate the FeatureDatabase, parameters estimation dynamically based on the database images (training images only) and average time for palmprint identification (in seconds) are given in Table 6.7.

Using the standard deviation as a feature vector the proposed approach extract better results compared to existing methods [23, 24, 95, 99, 101].

6.3.2 Coefficient of variation as a feature

This experiment is conducted to test the identification accuracy of the proposed approach. For every segment calculated the coefficient of variation (CV) as a feature.

Table 6.6: Performance comparison (CIR) of approaches [23, 24, 61, 62, 95, 99, 101] and the proposed approach using SF on PolyUPalmprint database

Data set	Existing methods		CIR of proposed approach		
	Author with reference number	CIR of existing methods	STD	CV	STD & CV
Data set I	Atif Bin Mansoor et al.[23]	90.17	99.05	98.826	99.08
Data set II	G.S. Badrinath et al. [95]	99.59	99.87	99.948	99.92
	G.S. Badrinath et al. [61, 62]	99.937(without enhancement)100 with enhancement			
Data set III	Mu et al. [24]	99.32	99.816	99.89	99.89
Data set IV	Xuan et al. [99]	97.377	100	100	100
	Xuan et al. [101]	99.02			

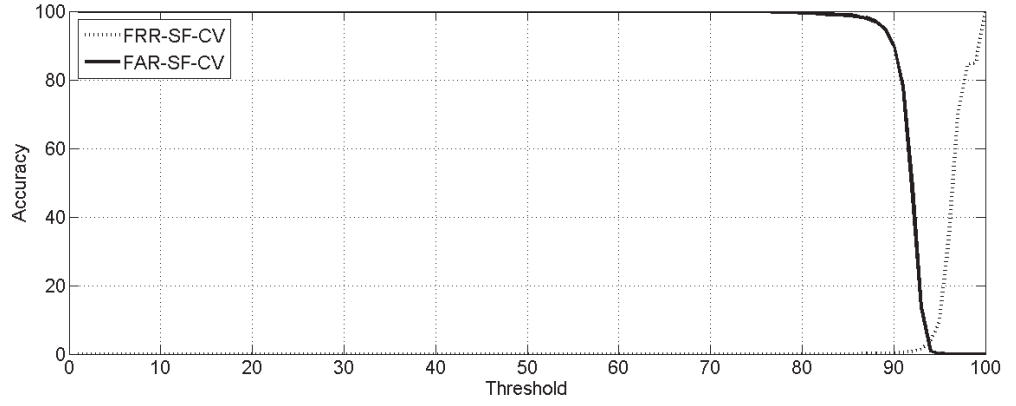
Palmprint Verification

The false acceptance rate (FAR) and false rejection rate (FRR) on data set I are shown in Figure 6.21. Decidability index and equal error rate on data set I are given in Table 6.5. Receiver operating characteristic (ROC) curve on data set I is given in Figure 6.22.

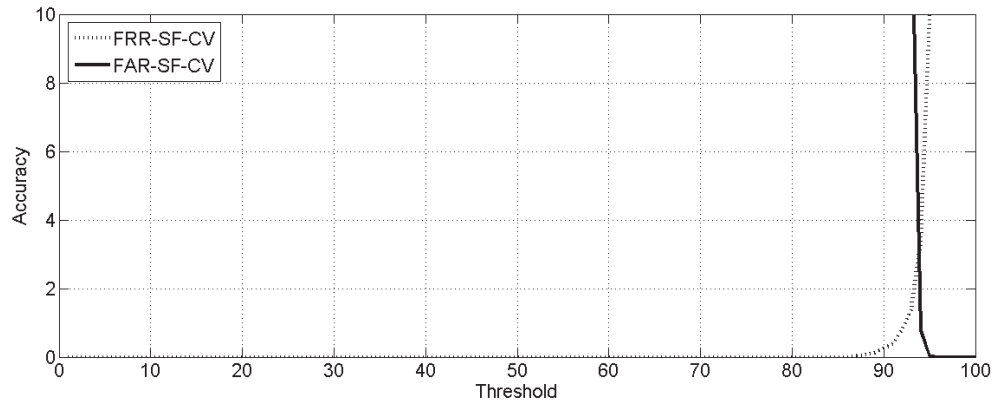
The false acceptance rate (FAR) and false rejection rate (FRR) on data set II are shown in Figure 6.23. Decidability index and equal error rate on data set II are given in Table 6.5. Receiver operating characteristic (ROC) curve on data set II is given in Figure 6.24.

The false acceptance rate (FAR) and false rejection rate (FRR) on data set III are shown in Figure 6.33. Decidability index and equal error rate on data set III are given in Table 6.5. Receiver operating characteristic (ROC) curve on data set III is given in Figure 6.34.

The false acceptance rate (FAR) and false rejection rate (FRR) on data set IV are shown in Figure 6.27. Decidability index and equal error rate on data set IV are given in Table 6.5. Receiver operating characteristic (ROC) curve on data set IV is given in Figure 6.28.



(i) Accuracy scaling 0 to 100



(ii) Accuracy scaling 0 to 10

Figure 6.21: FAR & FRR representation on data set I using CV as a feature.

The false acceptance rate (FAR) and false rejection rate (FRR) on data set V are shown in Figure 6.29. Decidability index and equal error rate on data set V are given in Table 6.4. Receiver operating characteristic (ROC) curve on data set V is given in Figure 6.30.

Palmprint Identification

On data set I, using the dynamic ROI, 7661 images are correctly identified, i.e. the CIR is 98.826. On data set II, using the dynamic ROI, 3854 images are correctly identified, i.e. the CIR is 99.948. On data set III, using the dynamic ROI, 2728 images are correctly identified, i.e. the CIR is 99.89. On data set IV using the dynamic ROI, 1959 images are correctly identified, i.e. the CIR is 100. On data set V, we run the

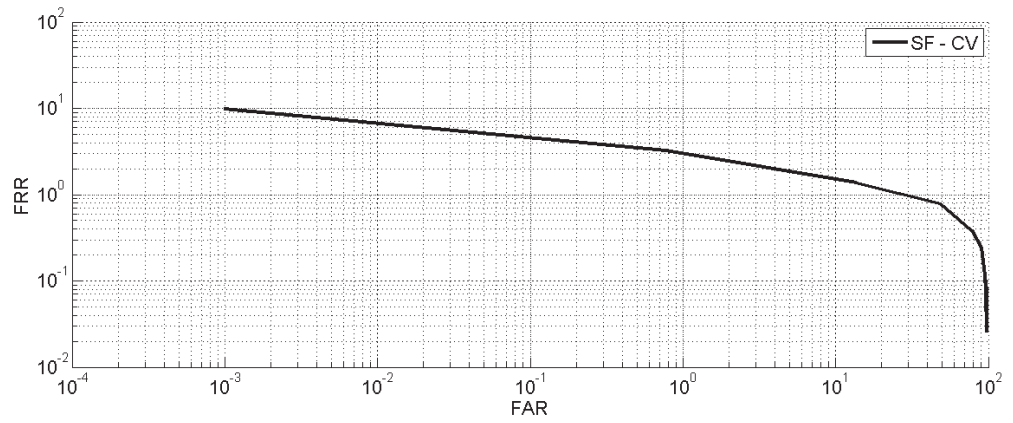
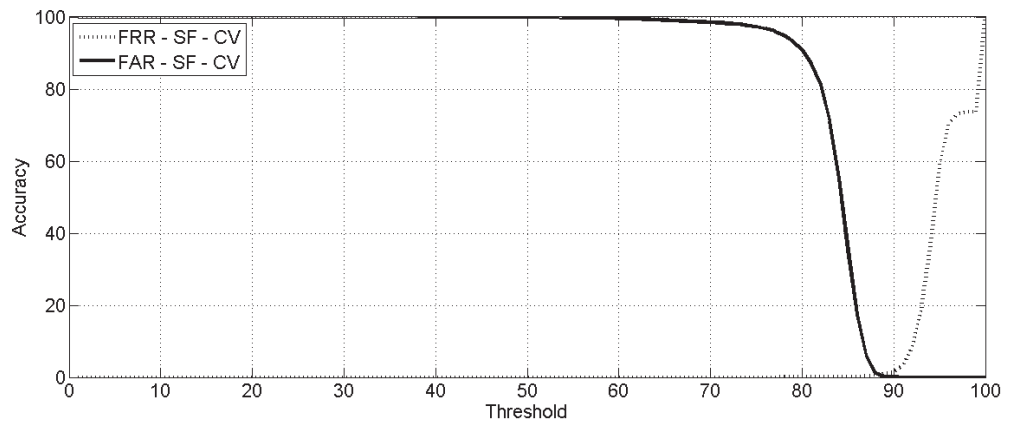
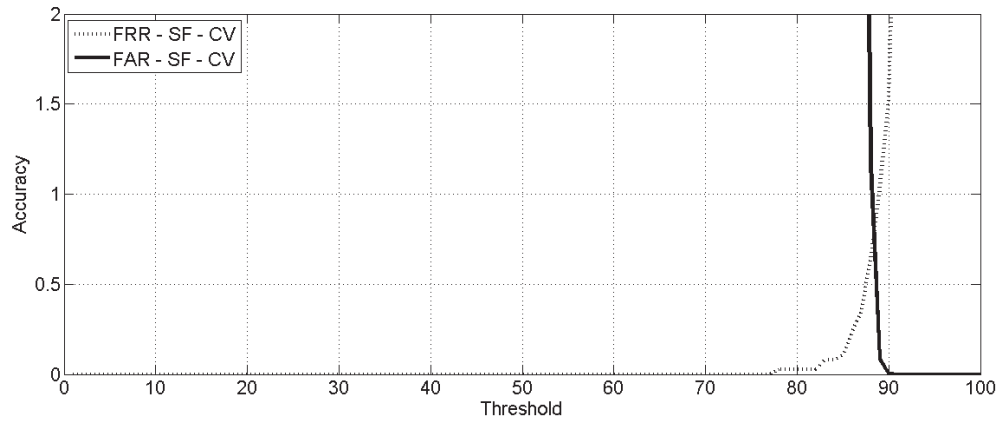


Figure 6.22: ROC curve on data set I using CV as a feature.



(i) Accuracy scaling 0 to 100



(ii) Accuracy scaling 0 to 2

Figure 6.23: FAR & FRR representation on data set II using CV as a feature.

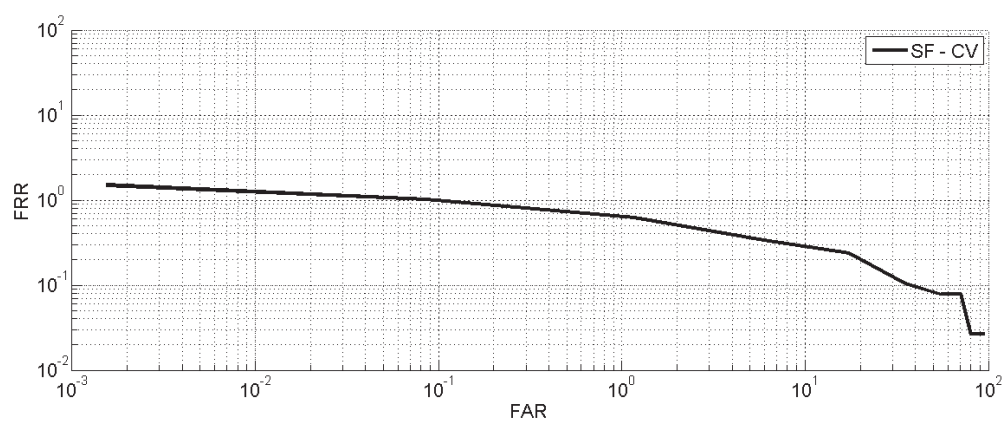
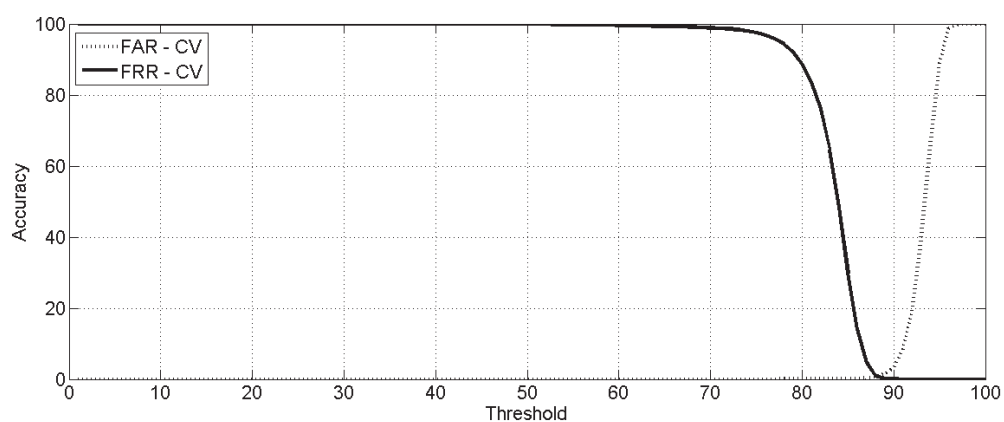
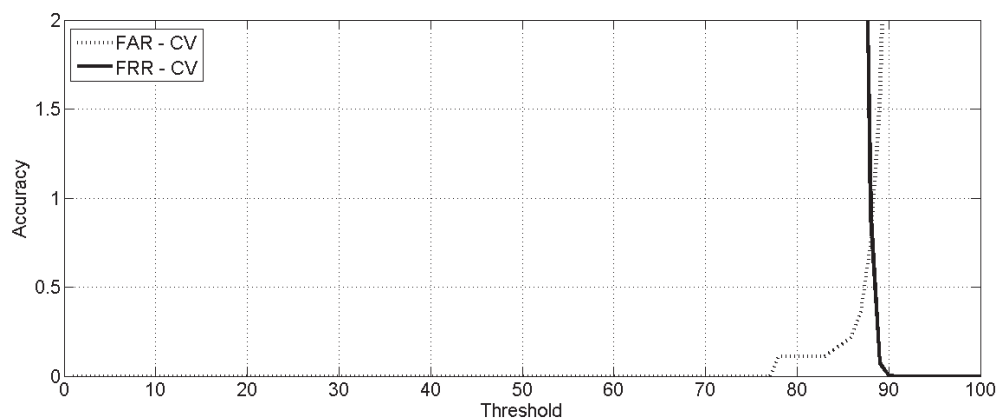


Figure 6.24: ROC curve on data set II using CV as a feature.



(i) Accuracy scaling 0 to 100



(ii) Accuracy scaling 0 to 2

Figure 6.25: FAR & FRR representation on data set III using CV as a feature.

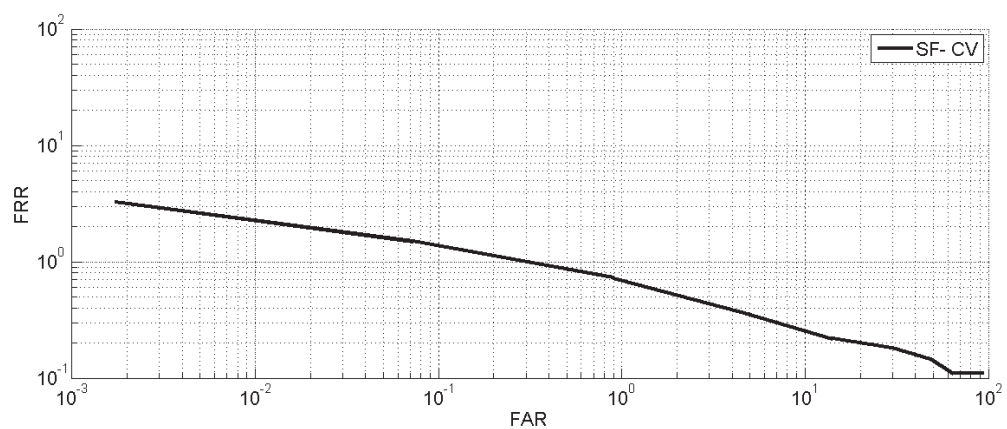
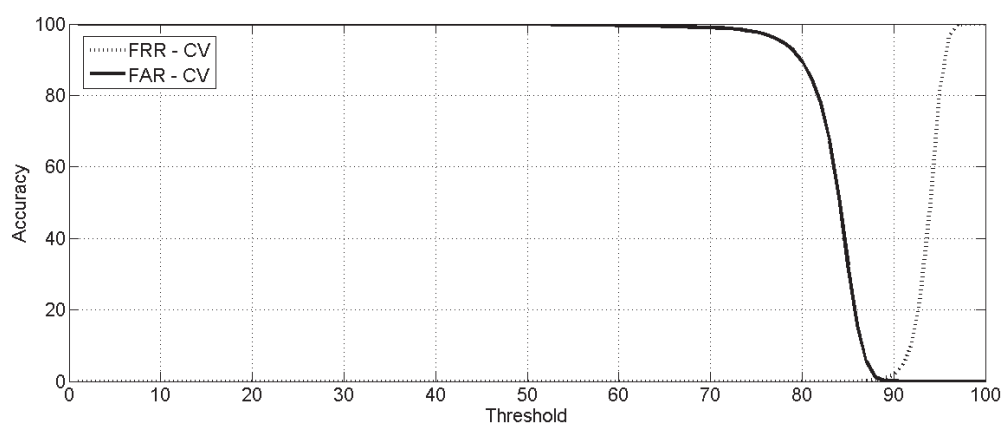
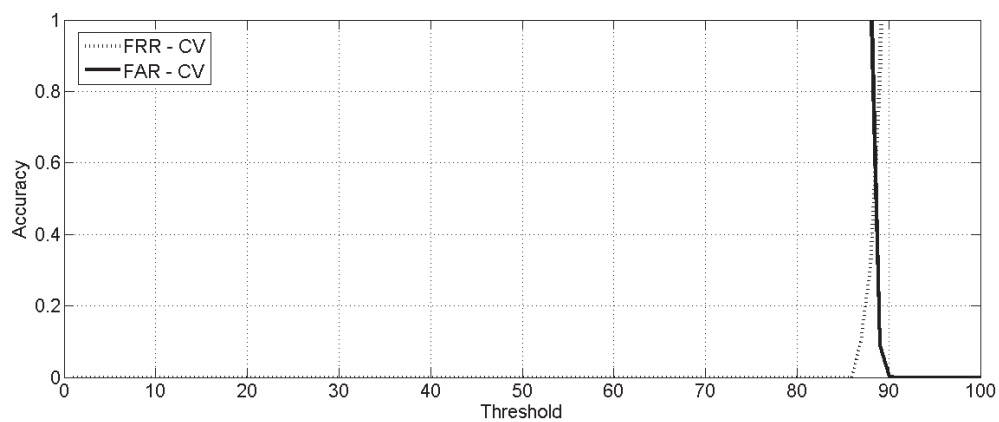


Figure 6.26: ROC curve on data set III using CV as a feature.



(i) Accuracy scaling 0 to 100



(ii) Accuracy scaling 0 to 1

Figure 6.27: FAR & FRR representation on data set IV using CV as a feature.

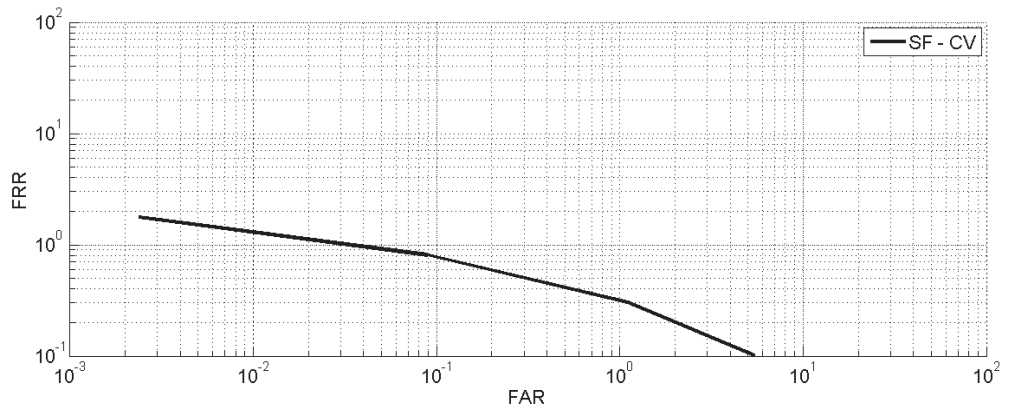
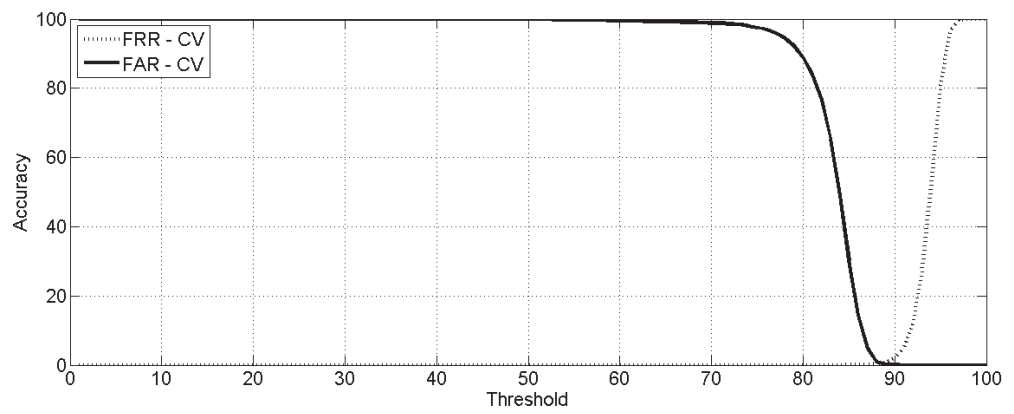
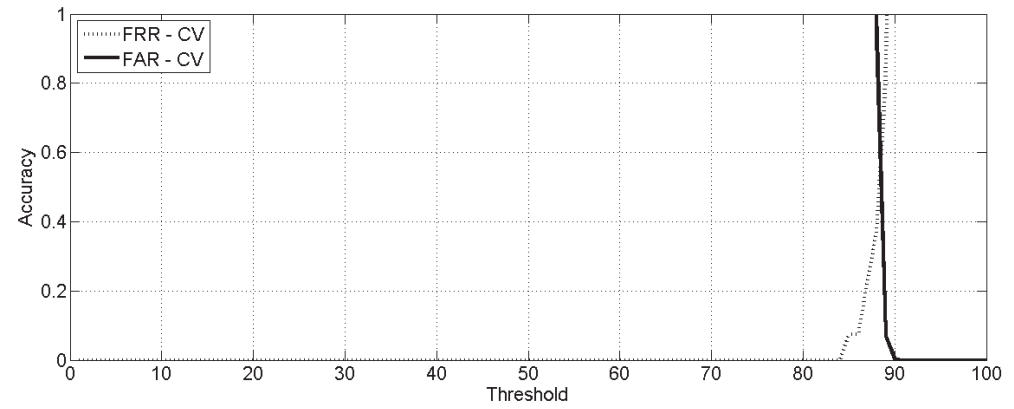


Figure 6.28: ROC curve on data set IV using CV as a feature.



(i) Accuracy scaling 0 to 100



(ii) Accuracy scaling 0 to 1

Figure 6.29: FAR & FRR representation on data set V using CV as a feature.

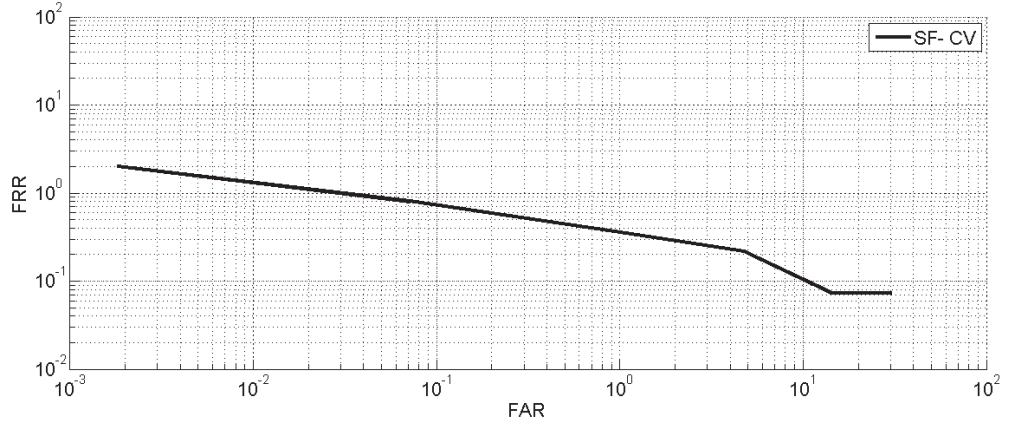


Figure 6.30: ROC curve on data set V using CV as a feature.

experiment 20 times and use the mean to denote the identification performance and robustness of the algorithm. The experimental results are shown in Table 6.4 and Table 6.6.

Time taken to generate the FeatureDatabase, parameters estimation dynamically based on the database and average time for palmprint identification (in seconds) are given in Table 6.7. Using the coefficient of variation as a feature vector the proposed approach extract better results compared to existing methods [23, 24, 95, 99, 101].

6.3.3 Standard deviation and coefficient of variation as features

For every segment calculated the standard deviation (STD) and coefficient of variation (CV) as features.

Palmprint Verification

The false acceptance rate (FAR) and false rejection rate (FRR) on data set I are shown in Figure 6.31. Decidability index and equal error rate on data set I are given in Table 6.5. Receiver operating characteristic (ROC) curve on data set I is given in Figure 6.32.

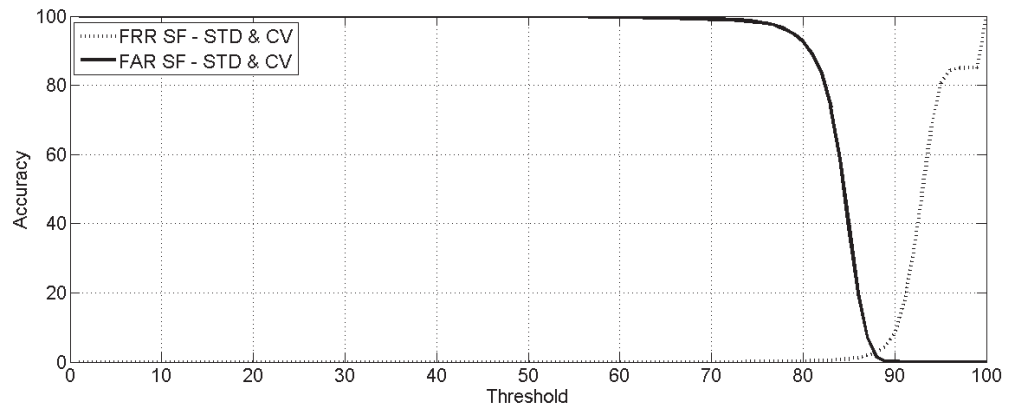
The false acceptance rate (FAR) and false rejection rate (FRR) on data set II are shown in Figure 6.33. Decidability index and equal error rate on data set II are given

in Table 6.5. Receiver operating characteristic (ROC) curve on data set II is given in Figure 6.34.

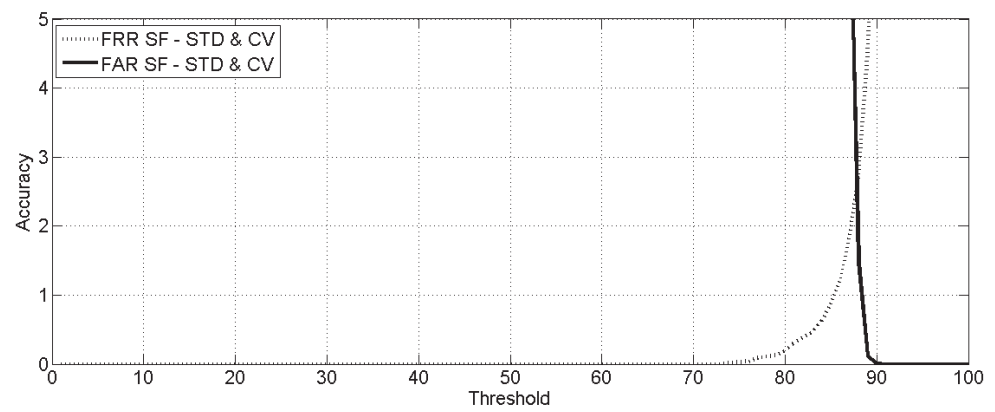
The false acceptance rate (FAR) and false rejection rate (FRR) on data set III are shown in Figure 6.35. Decidability index and equal error rate on data set III are given in Table 6.5. Receiver operating characteristic (ROC) curve on data set III is given in Figure 6.36.

The false acceptance rate (FAR) and false rejection rate (FRR) on data set IV are shown in Figure 6.37. Decidability index and equal error rate on data set IV are given in Table 6.5. Receiver operating characteristic (ROC) curve on data set IV is given in Figure 6.38.

The false acceptance rate (FAR) and false rejection rate (FRR) on data set V are shown in Figure 6.39. Decidability index and equal error rate on data set V are given in Table 6.4. Receiver operating characteristic (ROC) curve on data set V is given in Figure 6.40.



(i) Accuracy scaling 0 to 100



(ii) Accuracy scaling 0 to 5

Figure 6.31: FAR & FRR representation on data set I using STD & CV as a feature.

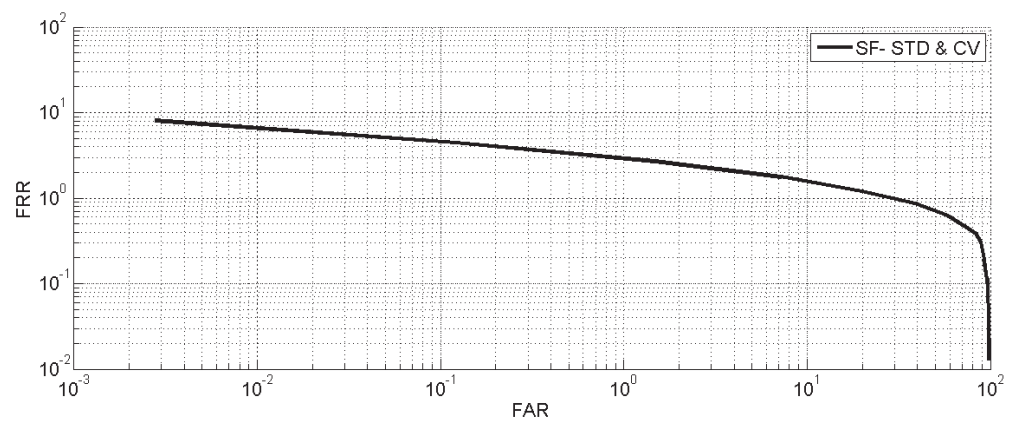
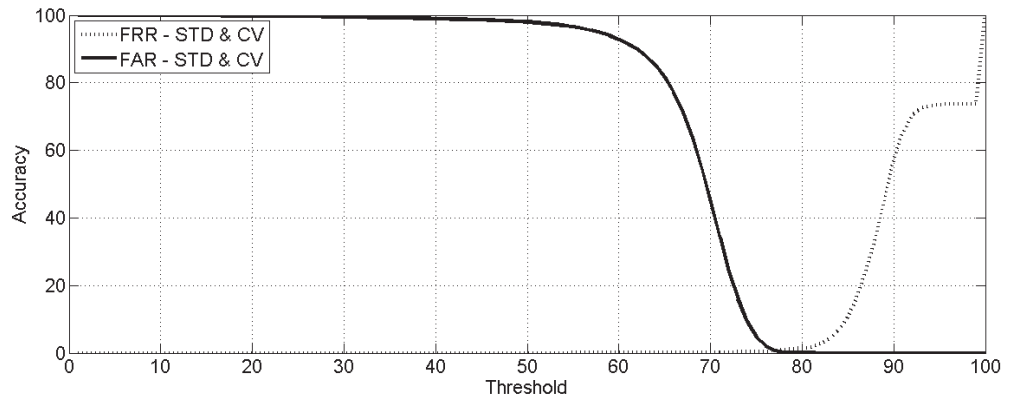
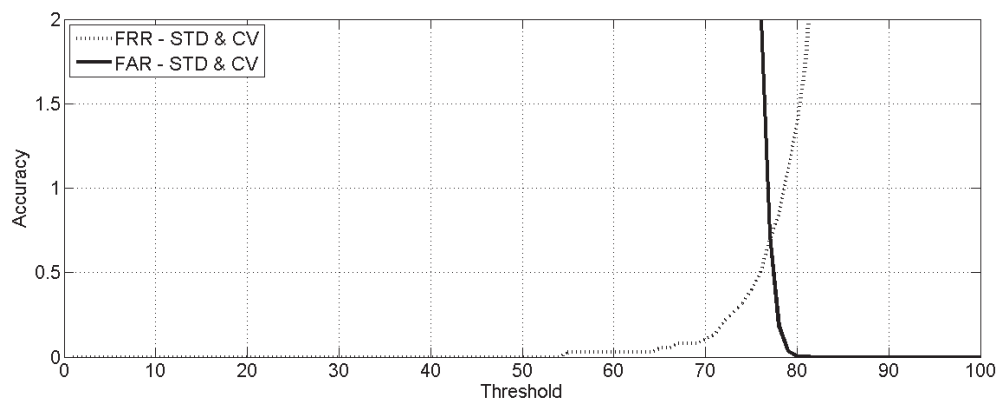


Figure 6.32: ROC curve on data set I using STD & CV as a feature.



(i) Accuracy scaling 0 to 100



(ii) Accuracy scaling 0 to 2

Figure 6.33: FAR & FRR representation on data set II using STD & CV as a feature.

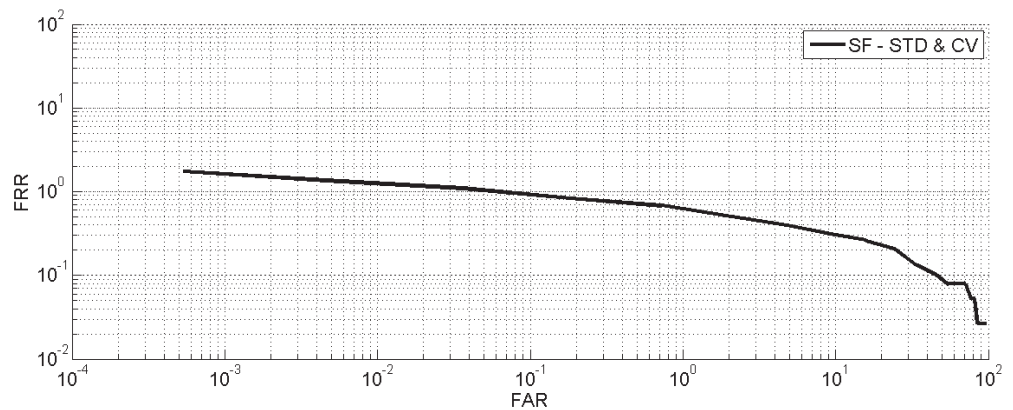
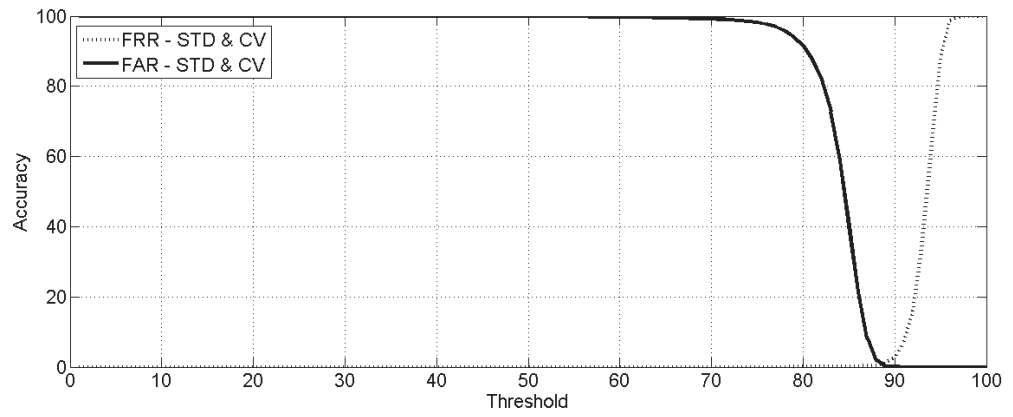
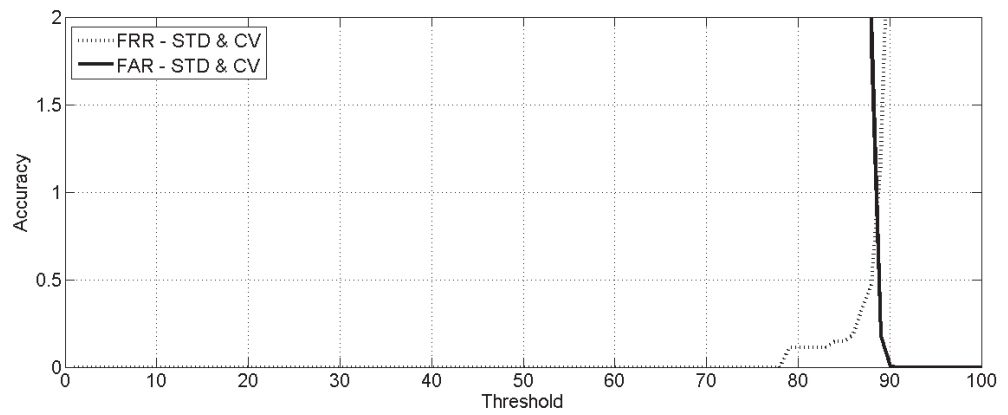


Figure 6.34: ROC curve on data set II using STD & CV as a feature.



(i) Accuracy scaling 0 to 100



(ii) Accuracy scaling 0 to 2

Figure 6.35: FAR & FRR representation on data set III using STD & CV as a feature.

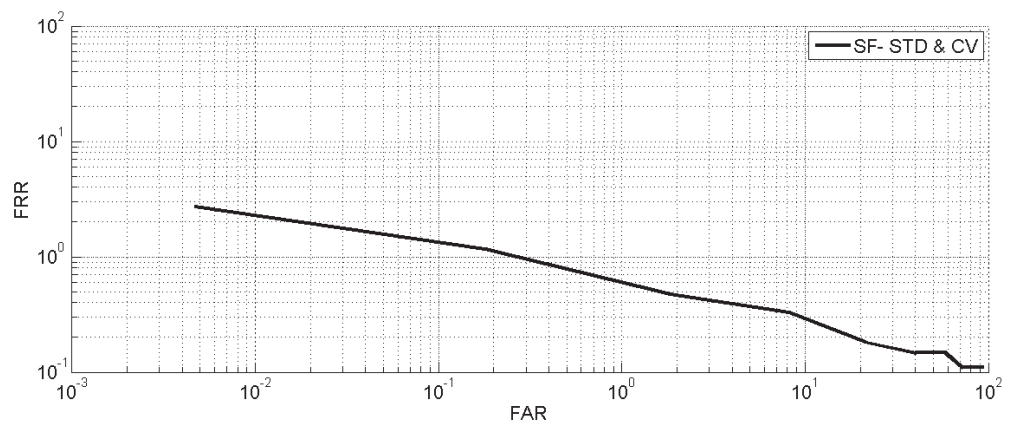
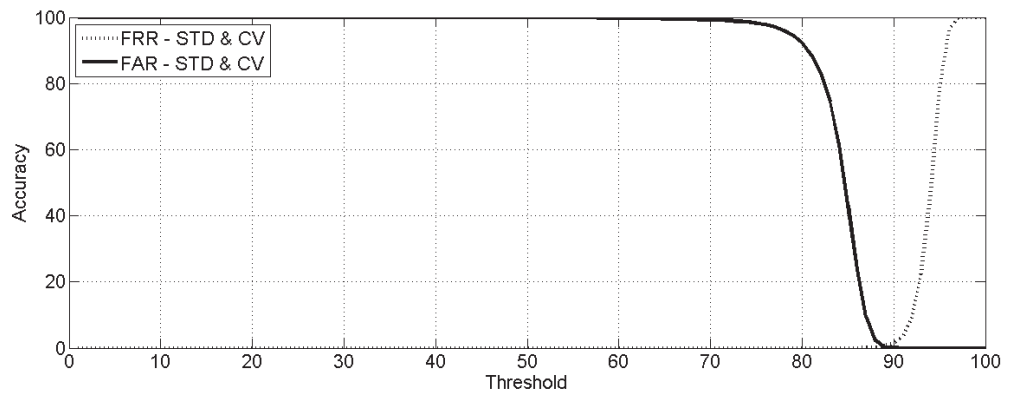
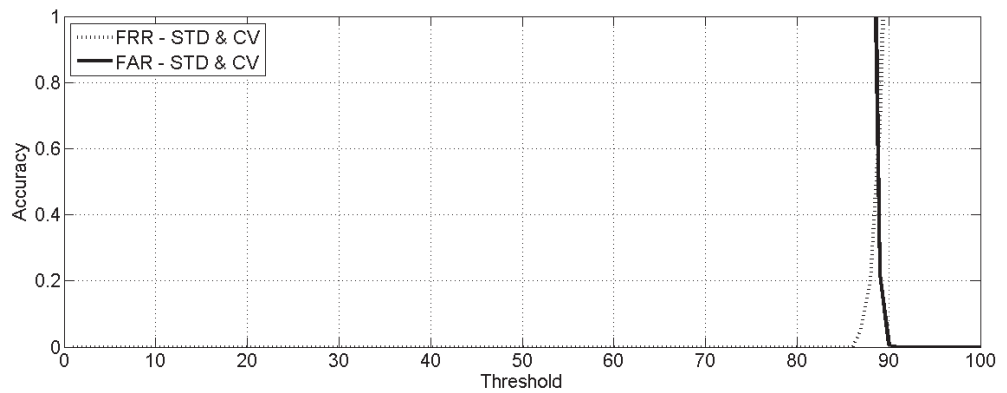


Figure 6.36: ROC curve on data set III using STD & CV as a feature.



(i) Accuracy scaling 0 to 100



(ii) Accuracy scaling 0 to 1

Figure 6.37: FAR & FRR representation on data set IV using STD & CV as a feature.

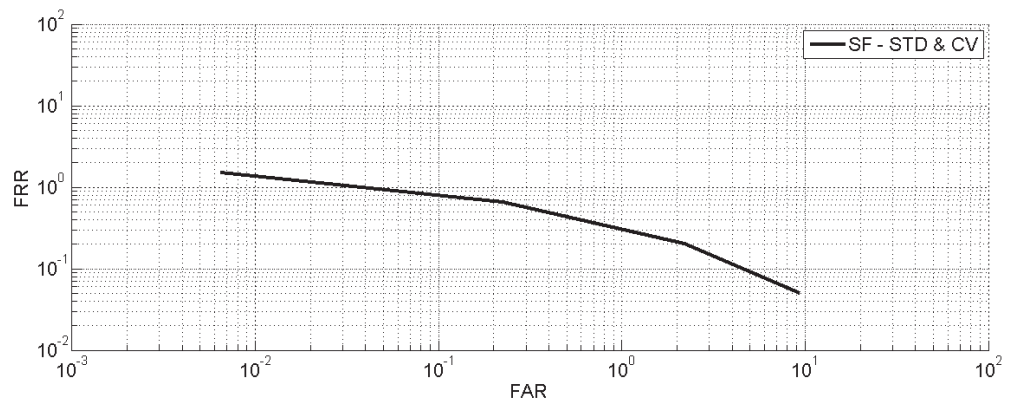
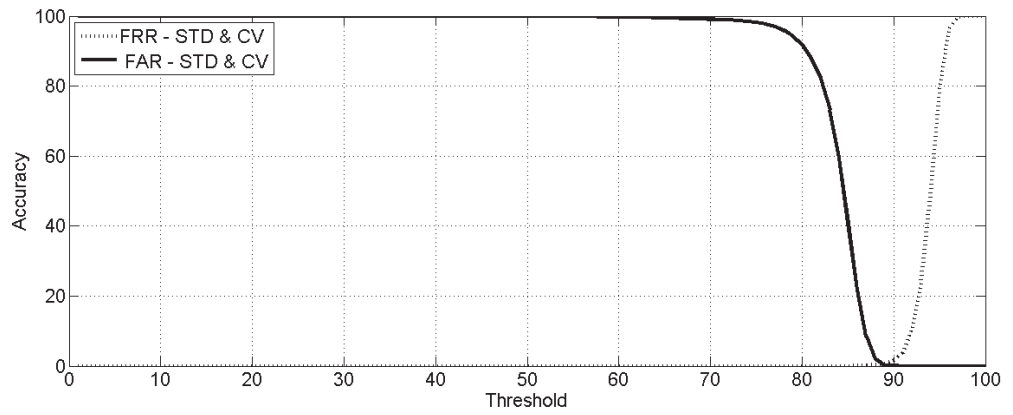
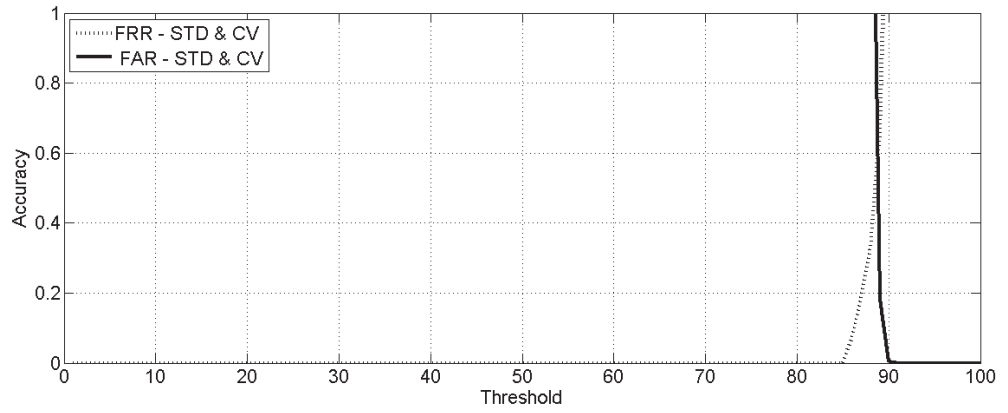


Figure 6.38: ROC curve on data set IV using STD & CV as a feature.



(i) Accuracy scaling 0 to 100



(ii) Accuracy scaling 0 to 1

Figure 6.39: FAR & FRR representation on data set V using STD & CV as a feature.

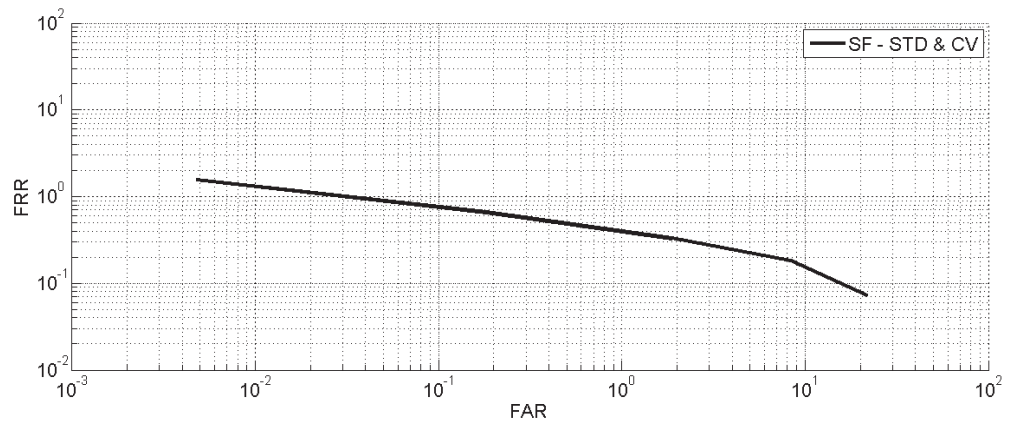


Figure 6.40: ROC curve on data set V using STD & CV as a feature.

Palmprint Identification

On data set I, 7681 images are correctly identified, i.e. the CIR is 99.08. On data set II, 3852 images are correctly identified, i.e. the CIR is 99.922. On data set III, 2728 images are correctly identified, i.e. the CIR is 99.89. On data set IV, 1959 images are correctly identified, i.e. the CIR is 100. On data set V, we run the experiment 20 times and use the mean to denote the identification performance and robustness of the algorithm. The obtained CIR is 99.8. The experimental results are shown in Table 6.4 and Table 6.6.

Time taken to generate the FeatureDatabase, parameters estimation dynamically based on the database images (training images) and average time for palmprint identification (in seconds) is given in Table 6.7. Using the standard deviation and coefficient of variation as a feature vector the proposed approach extract better results compared to existing methods [23, 24, 95, 99, 101].

Table 6.7: Time required for identification using SF (in seconds)

Data set	FeatureDatabase generation & Parameter estimation			Identification of query ROI using statistical features		
	STD	CV	STD&CV	STD	CV	STD&CV
Data set I	1219	1730	1267	0.18	0.22	0.24
Data set II	2838	2932	3905	0.12	0.19	0.22
Data set III	739	637	1059	0.12	0.13	0.18
Data set IV	1966	1812	2643	0.11	0.16	0.19
Data set V	839	953	1004	0.58	0.43	0.54

6.4 Experiments using SF on WPLI

6.4.1 Standard deviation as a feature

This experiment is conducted to test the identification accuracy of the proposed approach using statistical features on WPLI. For every segment calculated the standard deviation (STD) as a feature.

Palmprint Verification

The false acceptance rate (FAR) and false rejection rate (FRR) on data set I are shown in Figure 6.41. Decidability index and equal error rate on data set I are given in Tables 6.8 and 6.9 respectively. Receiver operating characteristic (ROC) curve on data set I is given in Figure 6.42.

The false acceptance rate (FAR) and false rejection rate (FRR) on data set II are shown in Figure 6.43. Decidability index and equal error rate on data set II are given in Tables 6.8 and 6.9 respectively. Receiver operating characteristic (ROC) curve on data set II is given in Figure 6.44.

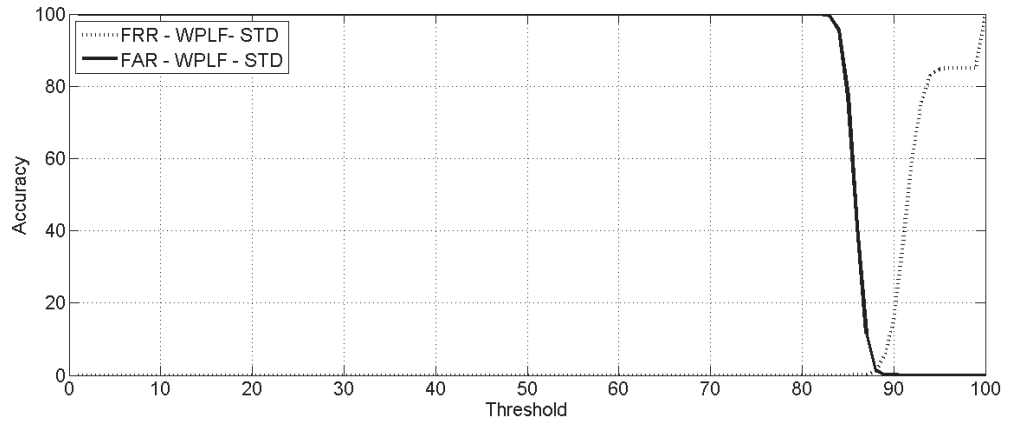
The false acceptance rate (FAR) and false rejection rate (FRR) on data set III are shown in Figure 6.45. Decidability index and equal error rate on data set III are given in Tables 6.8 and 6.9 respectively. Receiver operating characteristic (ROC) curve on data set III is given in Figure 6.46.

The false acceptance rate (FAR) and false rejection rate (FRR) on data set IV are shown in Figure 6.47. Decidability index and equal error rate on data set IV are given in Tables 6.8 and 6.9 respectively. Receiver operating characteristic (ROC) curve on data set IV is given in Figure 6.48.

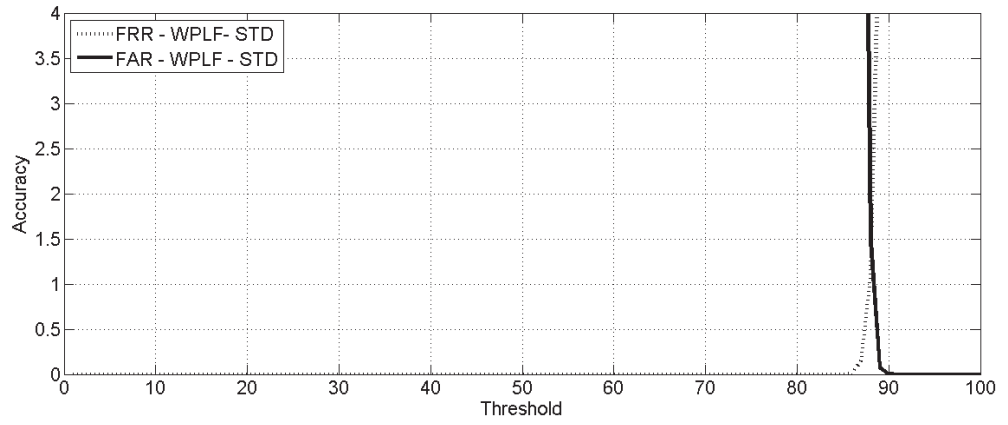
The false acceptance rate (FAR) and false rejection rate (FRR) on data set V are shown in Figure 6.49. Decidability index and equal error rate on data set V are given in Tables 6.8 and 6.9 respectively. Receiver operating characteristic (ROC) curve on data set V is given in Figure 6.50.

Palmprint Identification

On data set I, 7563 images are correctly identified, i.e. the CIR is 97.56. On data set II, 3834 images are correctly identified, i.e. the CIR is 99.45. On data set III, 2695 images are correctly identified, i.e. the CIR is 98.68. On data set IV, 1956 images are correctly identified, i.e. the CIR is 99.846. On data set V, we run the experiment 20



(i) Accuracy scaling 0 to 100



(ii) Accuracy scaling 0 to 5

Figure 6.41: FAR & FRR representation on data set I of WPLI database using STD as a feature.

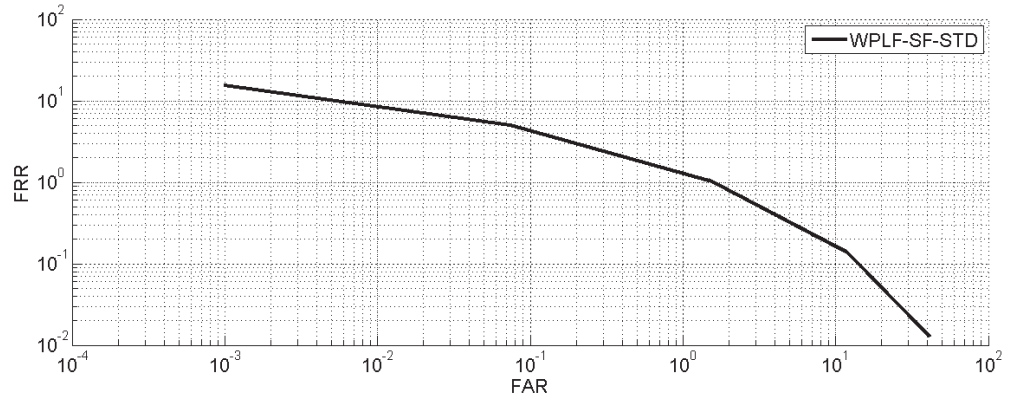
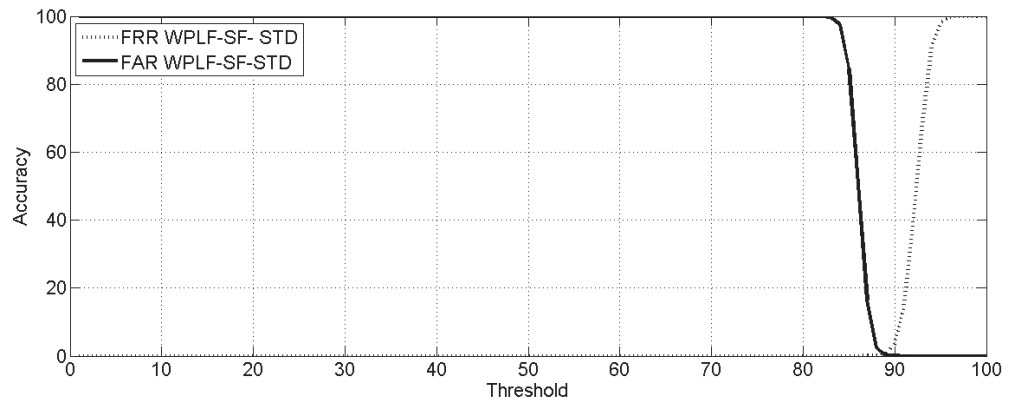
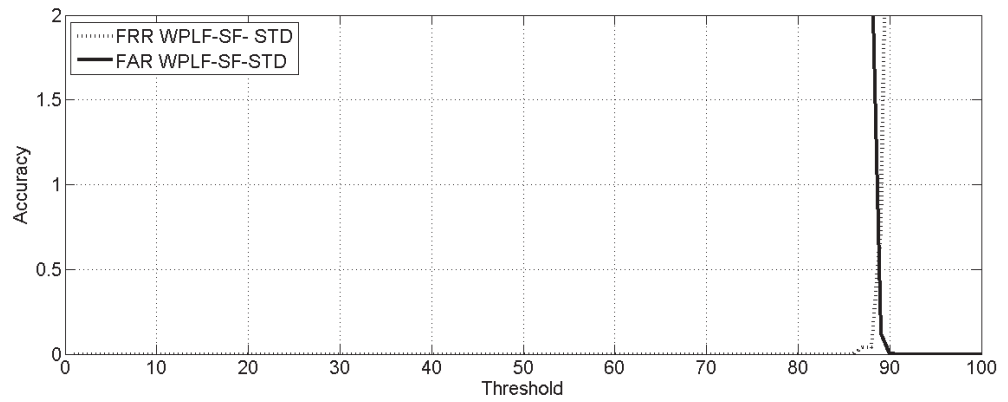


Figure 6.42: ROC curve on data set I of WPLI database using STD as a feature.



(i) Accuracy scaling 0 to 100



(ii) Accuracy scaling 0 to 2

Figure 6.43: FAR & FRR representation on data set II of WPLI database using STD as a feature.

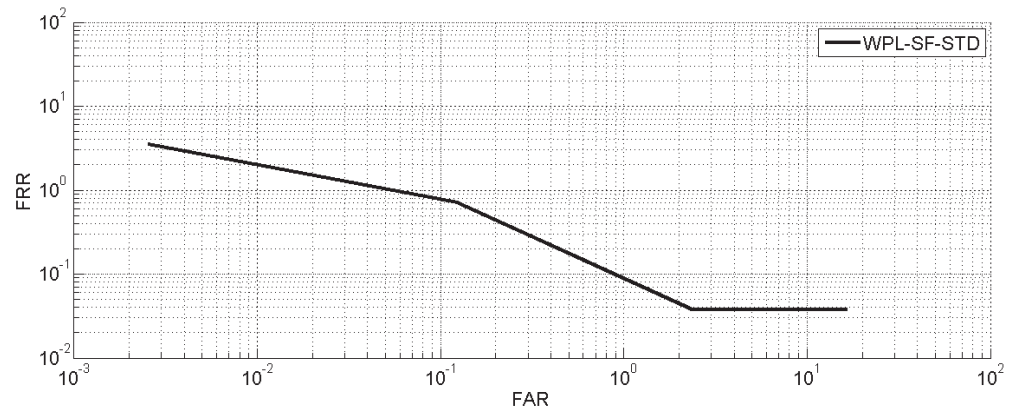
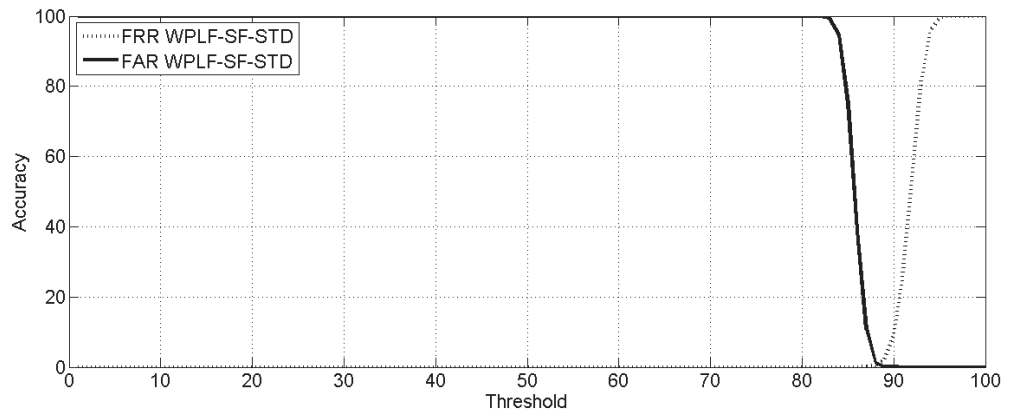
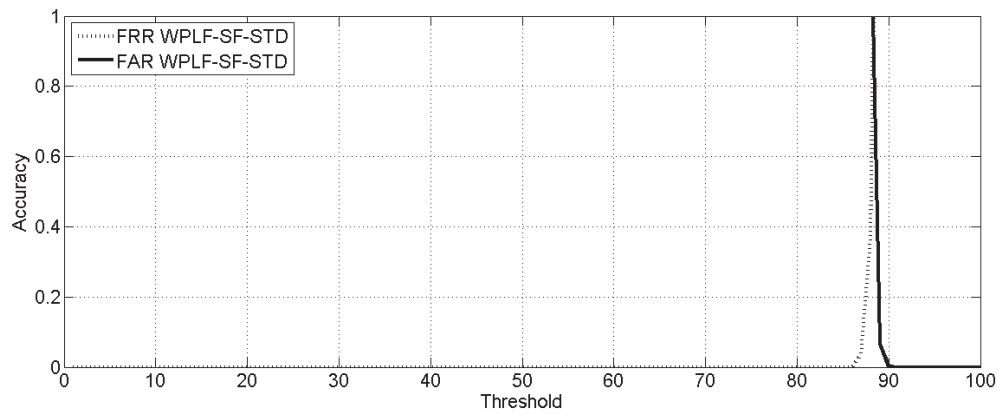


Figure 6.44: ROC curve on data set II of WPLI database using STD as a feature.



(i) Accuracy scaling 0 to 100



(ii) Accuracy scaling 0 to 1

Figure 6.45: FAR & FRR representation on data set III of WPLI database of WPLI database using STD as a feature.

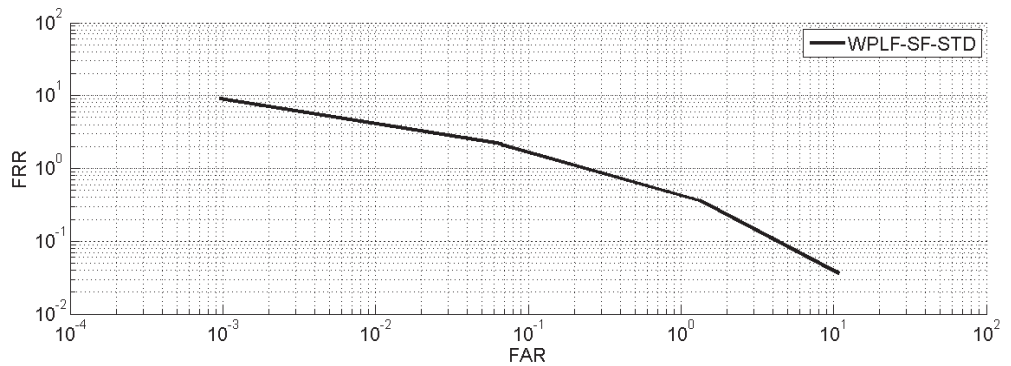
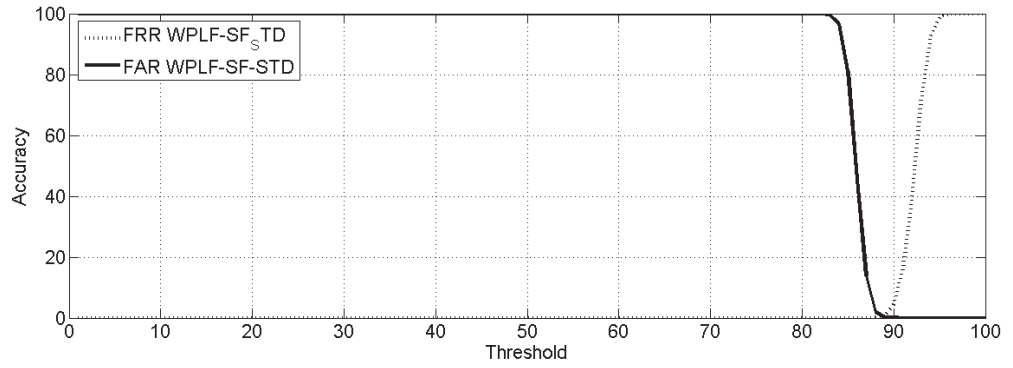
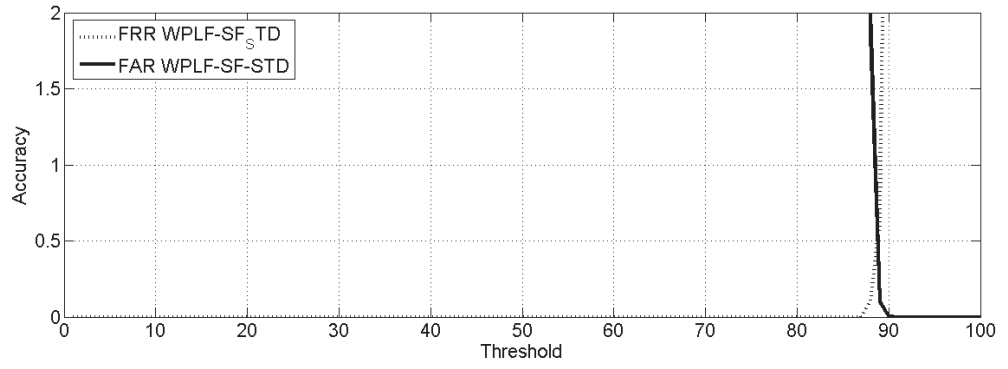


Figure 6.46: ROC curve on data set III of WPLI database using STD as a feature.



(i) Accuracy scaling 0 to 100



(ii) Accuracy scaling 0 to 2

Figure 6.47: FAR & FRR representation on data set IV of WPLI database using STD as a feature.

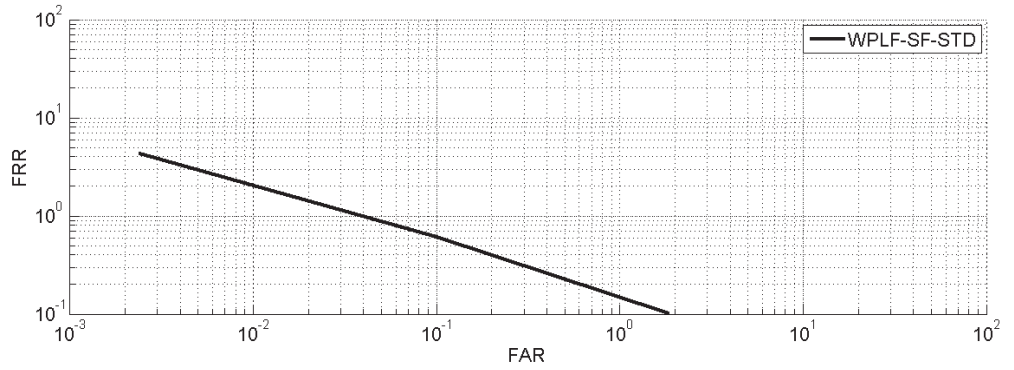
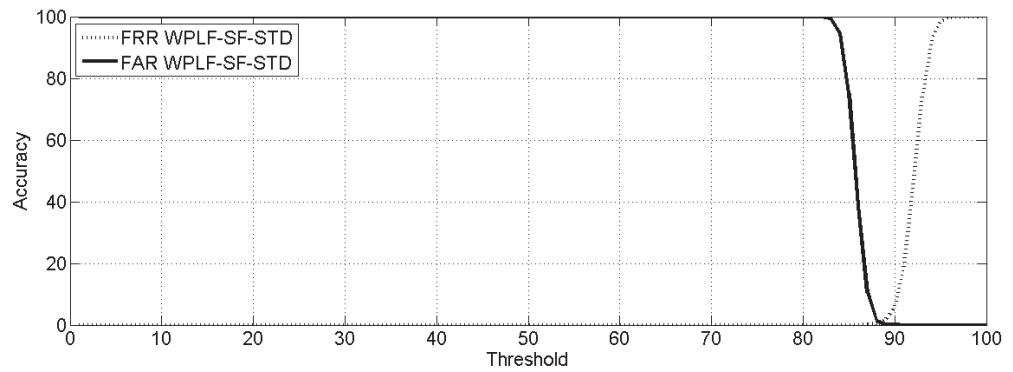
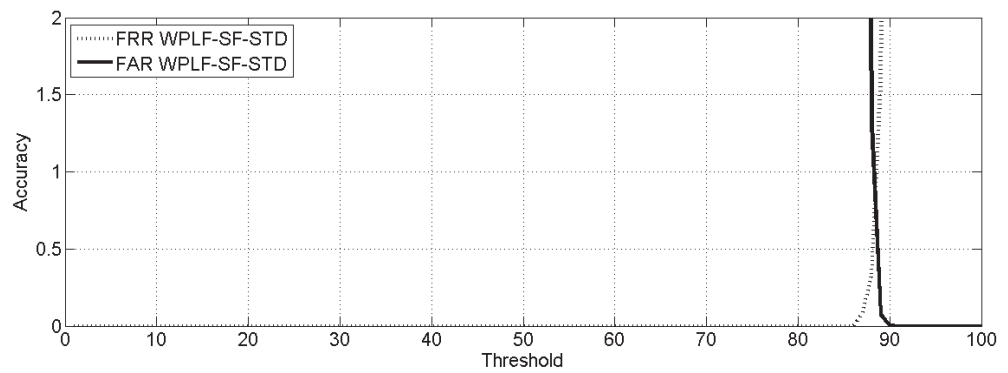


Figure 6.48: ROC curve on data set IV of WPLI database using STD as a feature.



(i) Accuracy scaling 0 to 100



(ii) Accuracy scaling 0 to 2

Figure 6.49: FAR & FRR representation on data set V of WPLI database using STD as a feature.

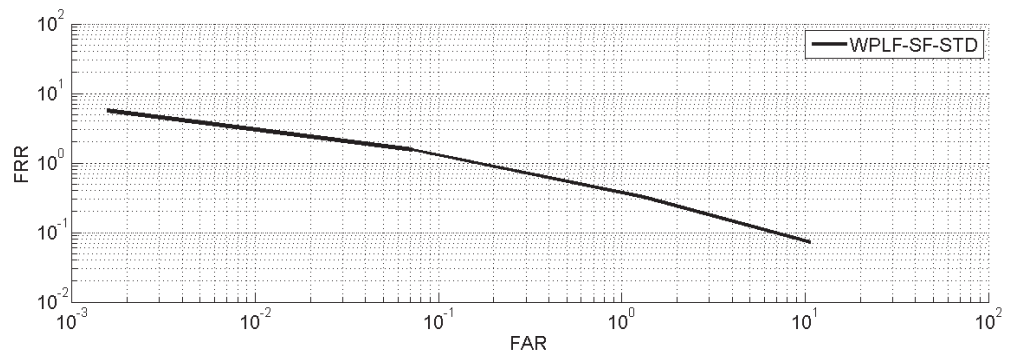


Figure 6.50: ROC curve on data set V of WPLI database using STD as a feature.

times and use the mean to denote the identification performance and robustness of the algorithm. The obtained CIR is 99.2.

The experimental results are shown in Table 6.10. The experimental results shows that, statistical features extracted using standard deviation from ROI database gives better results compared with statistical features extracted using standard deviation from WPLI database. Time taken to generate the FeatureDatabase, parameters estimation dynamically based on the database images (training images only) and average time for palmprint identification (in seconds) are given in Table 6.11.

Table 6.8: Performance (DI) comparison of the proposed approach using SF on ROI and WPLI databases

Data set	SD as a feature		CV as a feature		SD & CV as a feature	
	ROI	WPLI	ROI	WPLI	ROI	WPLI
Data set I	3.13	2.72	3.75	2.92	3.44	2.86
Data set II	5.08	5.48	5.12	6.37	5.11	6.15
Data set III	3.66	5.08	3.55	5.71	3.67	5.58
Data set IV	3.95	5.60	3.8	6.46	3.94	6.26
Data set V	5.1	5.36	5.81	6.08	5.63	5.92

Table 6.9: Performance (EER) comparison of the proposed approach using SF on ROI and WPLI databases

Data set	STD as a feature		CV as a feature		STD & CV as a feature	
	ROI	WPLI	ROI	WPLI	ROI	WPLI
Data set I	2.6	1.2	2.5	0.7	2.5	0.8
Data set II	0.9	0.4	0.9	0.15	0.8	0.2
Data set III	0.8	0.7	0.8	0.4	0.8	0.4
Data set IV	0.6	0.4	0.5	0.15	0.5	0.2
Data set V	0.75	0.7	0.6	0.3	0.6	0.25

Table 6.10: Performance (CIR) comparison of the proposed approach using SF on ROI and WPLI databases

Data set	STD as a feature		CV as a feature		STD & CV as a feature	
	ROI	WPLI	ROI	WPLI	ROI	WPLI
Data set I	99.05	97.56	98.826	98.28	99.08	98.19
Data set II	99.87	99.45	99.948	99.74	99.92	99.79
Data set III	99.816	98.68	99.89	99.01	99.89	99.04
Data set IV	100	99.846	100	99.897	100	99.897
Data set V	99.7	99.2	99.79	99.36	99.8	99.37

6.4.2 Coefficient of variation as a feature

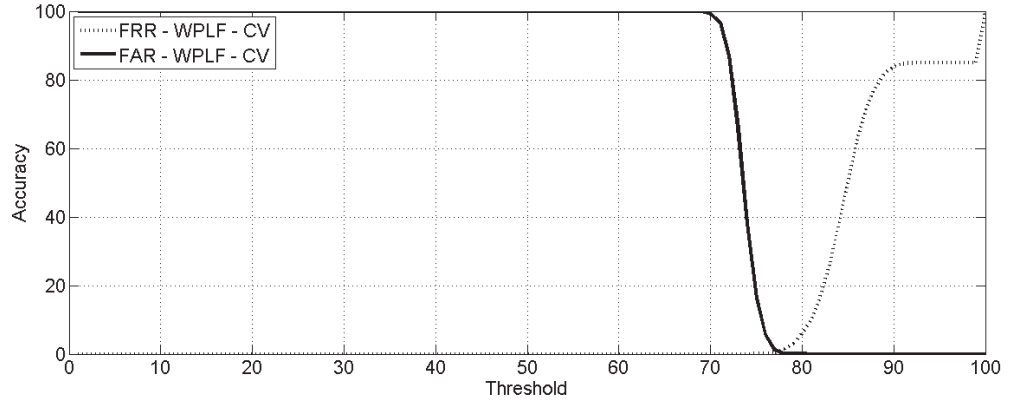
This experiment is conducted to test the identification accuracy of the proposed approach. For every segment calculated the coefficient of variation (CV) as a feature.

Palmprint Verification

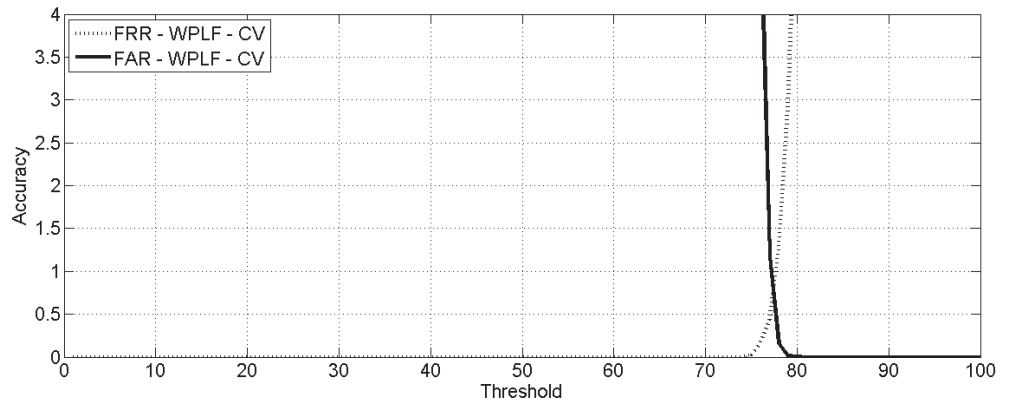
The false acceptance rate (FAR) and false rejection rate (FRR) on data set I are shown in Figure 6.51. Decidability index and equal error rate on data set I are given in Tables 6.8 and 6.9 respectively. Receiver operating characteristic (ROC) curve on data set I is given in Figure 6.22.

The false acceptance rate (FAR) and false rejection rate (FRR) on data set II are shown in Figure 6.53. Decidability index and equal error rate on data set II are given in Tables 6.8 and 6.9 respectively. Receiver operating characteristic (ROC) curve on data set II is given in Figure 6.54.

The false acceptance rate (FAR) and false rejection rate (FRR) on data set III are shown in Figure 6.63. Decidability index and equal error rate on data set III are given in Tables 6.8 and 6.9 respectively. Receiver operating characteristic (ROC) curve on data set III is given in Figure 6.64.



(i) Accuracy scaling 0 to 100



(ii) Accuracy scaling 0 to 10

Figure 6.51: FAR & FRR representation on data set I of WPLI database using CV as a feature.

The false acceptance rate (FAR) and false rejection rate (FRR) on data set IV are shown in Figure 6.57. Decidability index and equal error rate on data set IV are given in Tables 6.8 and 6.9 respectively. Receiver operating characteristic (ROC) curve on data set IV is given in Figure 6.58.

The false acceptance rate (FAR) and false rejection rate (FRR) on data set V are shown in Figure 6.59. Decidability index and equal error rate on data set V are given in Tables 6.8 and 6.9 respectively. Receiver operating characteristic (ROC) curve on data set V is given in Figure 6.30.

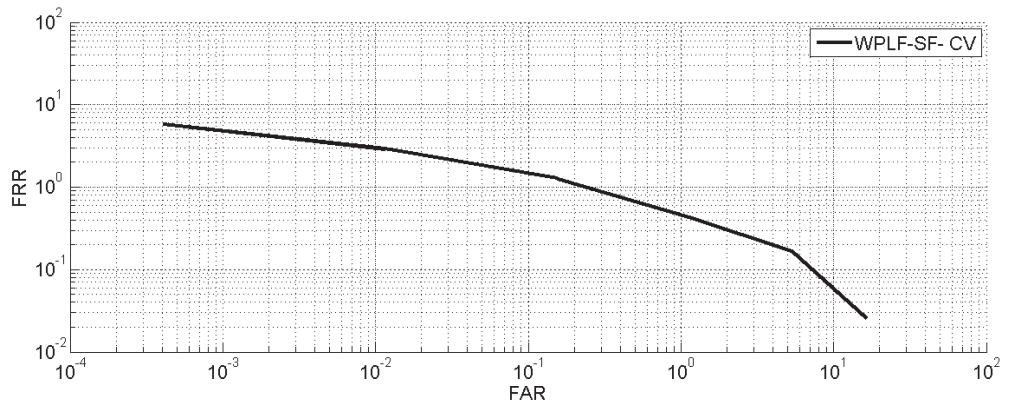
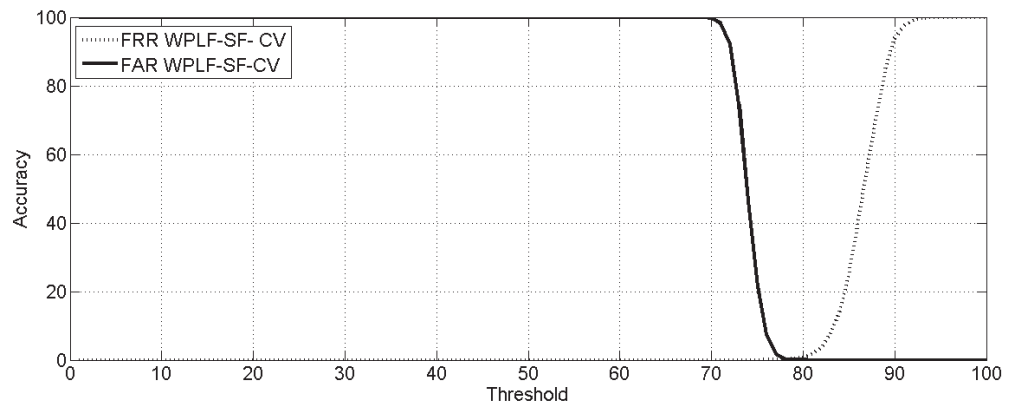
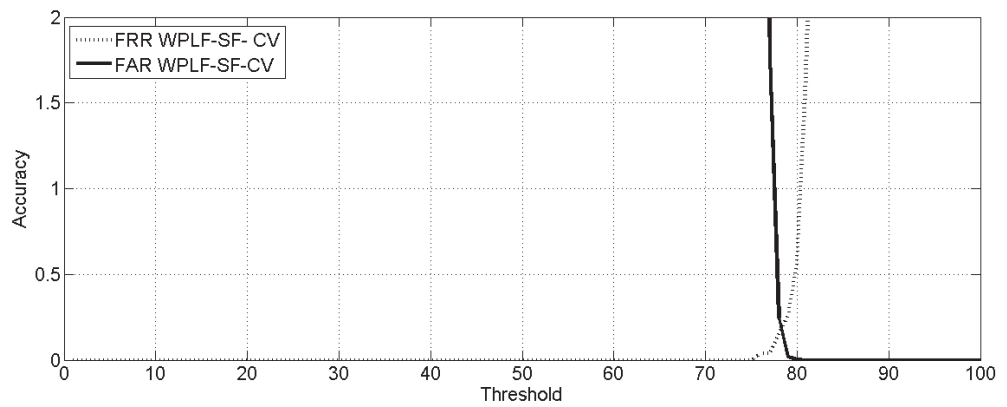


Figure 6.52: ROC curve on data set I of WPLI database using CV as a feature.



(i) Accuracy scaling 0 to 100



(ii) Accuracy scaling 0 to 2

Figure 6.53: FAR & FRR representation on data set II of WPLI database using CV as a feature.

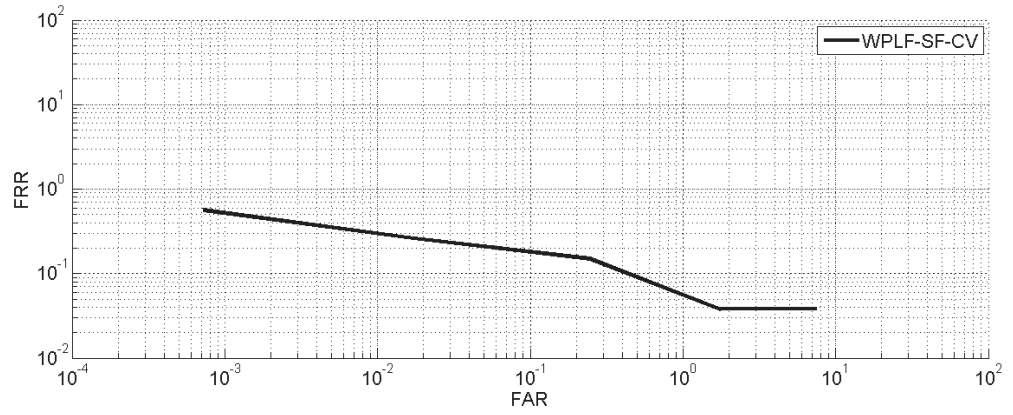
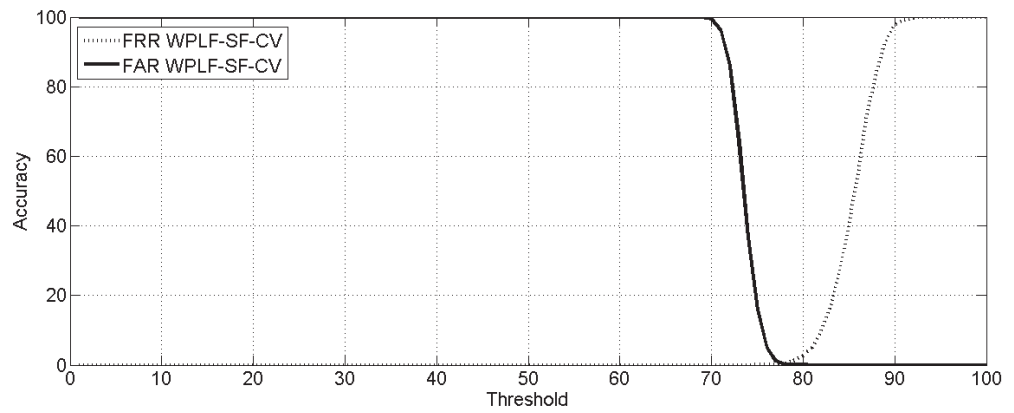
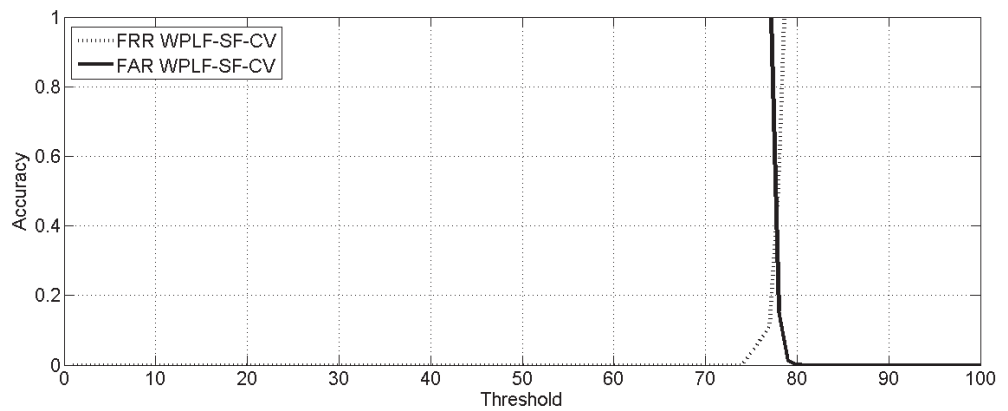


Figure 6.54: ROC curve on data set II of WPLI database using CV as a feature.



(i) Accuracy scaling 0 to 100



(ii) Accuracy scaling 0 to 1

Figure 6.55: FAR & FRR representation on data set III of WPLI database using CV as a feature.

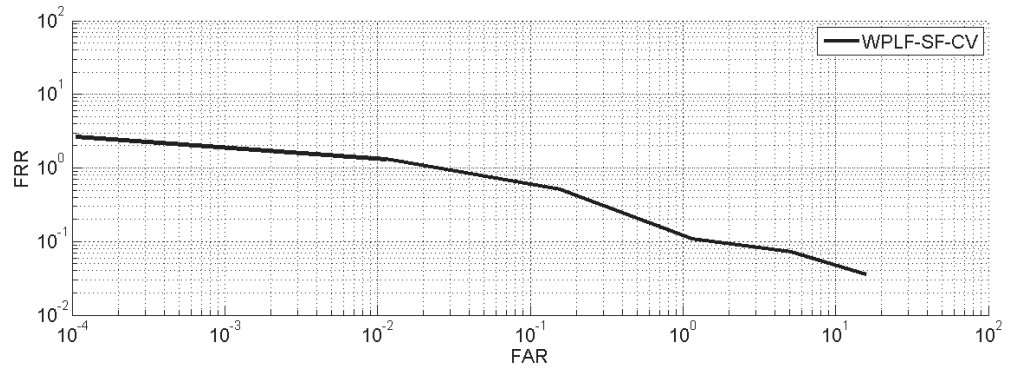
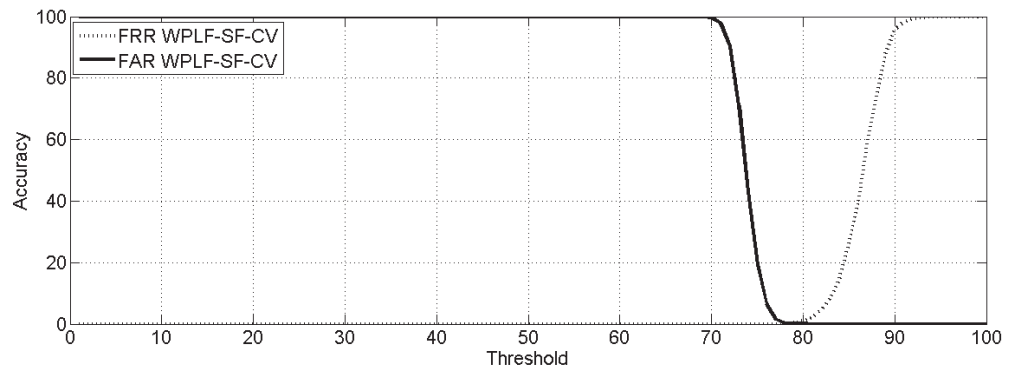
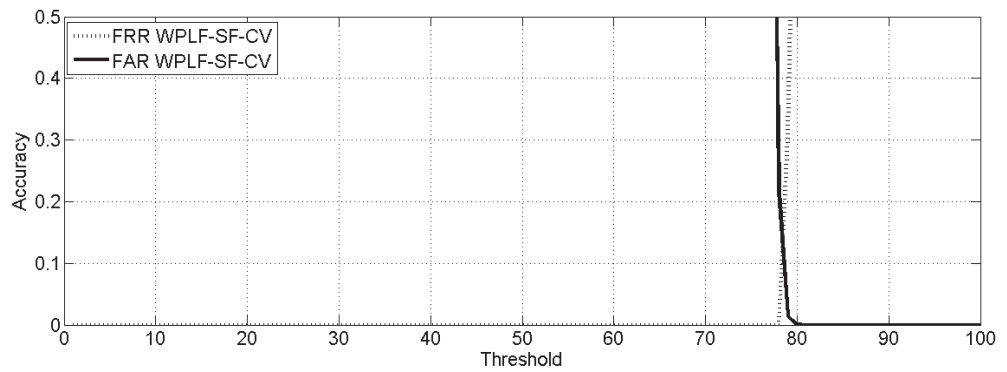


Figure 6.56: ROC curve on data set III of WPLI database using CV as a feature.



(i) Accuracy scaling 0 to 100



(ii) Accuracy scaling 0 to 0.5

Figure 6.57: FAR & FRR representation on data set IV of WPLI database using CV as a feature.

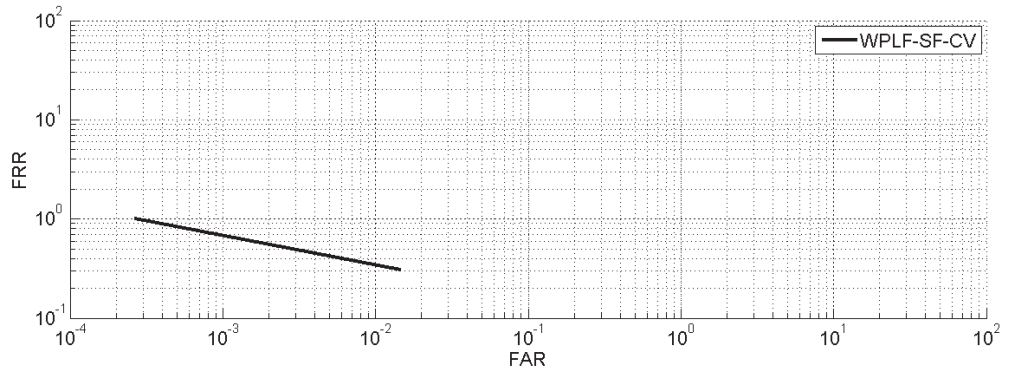
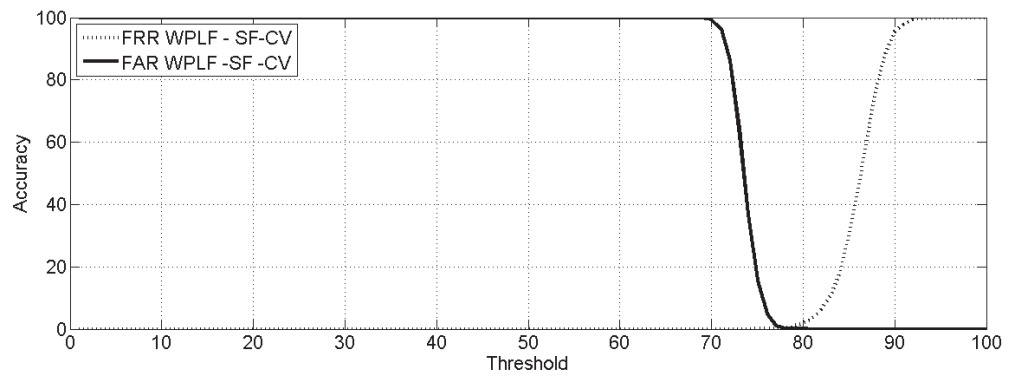
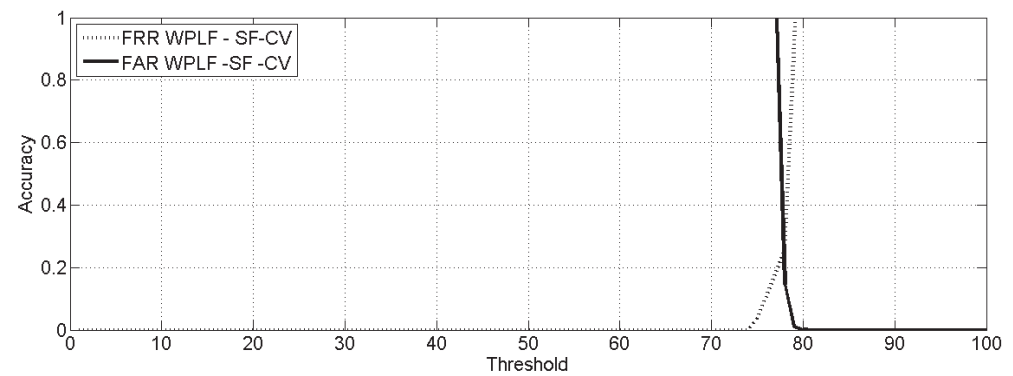


Figure 6.58: ROC curve on data set IV of WPLI database using CV as a feature.



(i) Accuracy scaling 0 to 100



(ii) Accuracy scaling 0 to 1

Figure 6.59: FAR & FRR representation on data set V of WPLI database using CV as a feature.

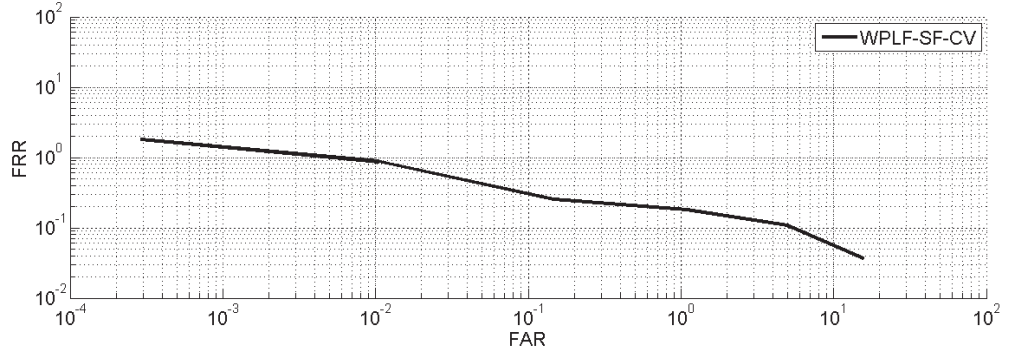


Figure 6.60: ROC curve on data set V of WPLI database using CV as a feature.

Palmpoint Identification

On data set I, 7619 images are correctly identified, i.e. the CIR is 98.28. On data set II, 3845 images are correctly identified, i.e. the CIR is 99.74. On data set III, 2704 images are correctly identified, i.e. the CIR is 99.01. On data set IV, 1957 images are correctly identified, i.e. the CIR is 99.897. On data set V, we run the experiment 20 times and use the mean to denote the identification performance and robustness of the algorithm. The obtained CIR is 99.36. The experimental results are shown in Table 6.10.

The experimental results shows that, statistical features extracted using coefficient of variation from ROI database gives better results compared with statistical features extracted using coefficient of variation from WPLI database. Time taken to generate the FeatureDatabase, parameters estimation dynamically based on the database and average time for palmpoint identification (in seconds) are given in Table 6.11.

6.4.3 Standard deviation and coefficient of variation as features

For every segment calculated the standard deviation (STD) and coefficient of variation (CV) as features.

Palmprint Verification

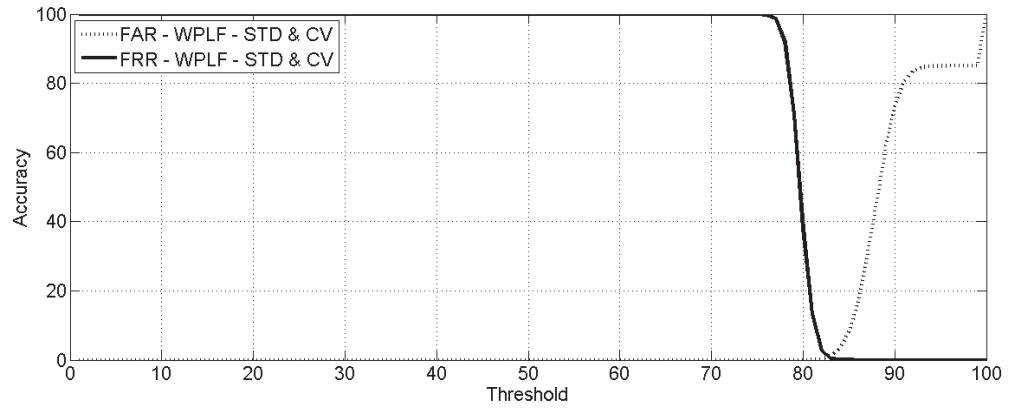
The false acceptance rate (FAR) and false rejection rate (FRR) on data set I are shown in Figure 6.61. Decidability index and equal error rate on data set I are given in Tables 6.8 and 6.9 respectively. Receiver operating characteristic (ROC) curve on data set I is given in Figure 6.62.

The false acceptance rate (FAR) and false rejection rate (FRR) on data set II are shown in Figure 6.63. Decidability index and equal error rate on data set II are given in Tables 6.8 and 6.9 respectively. Receiver operating characteristic (ROC) curve on data set II is given in Figure 6.64.

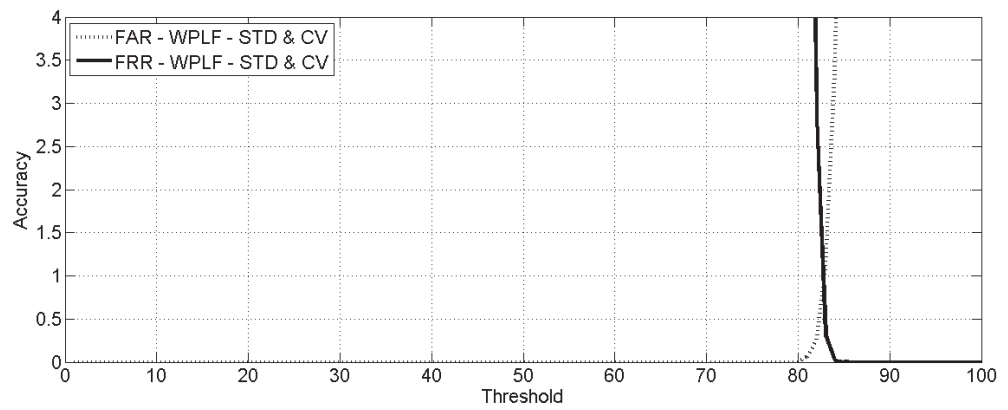
The false acceptance rate (FAR) and false rejection rate (FRR) on data set III are shown in Figure 6.65. Decidability index and equal error rate on data set III are given in Tables 6.8 and 6.9 respectively. Receiver operating characteristic (ROC) curve on data set III is given in Figure 6.66.

The false acceptance rate (FAR) and false rejection rate (FRR) on data set IV are shown in Figure 6.67. Decidability index and equal error rate on data set IV are given in Tables 6.8 and 6.9 respectively. Receiver operating characteristic (ROC) curve on data set IV is given in Figure 6.68.

The false acceptance rate (FAR) and false rejection rate (FRR) on data set V are shown in Figure 6.69. Decidability index and equal error rate on data set V are given in Tables 6.8 and 6.9 respectively. Receiver operating characteristic (ROC) curve on data set V is given in Figure 6.70.



(i) Accuracy scaling 0 to 100



(ii) Accuracy scaling 0 to 4

Figure 6.61: FAR & FRR representation on data set I of WPLI database using STD & CV as a feature.

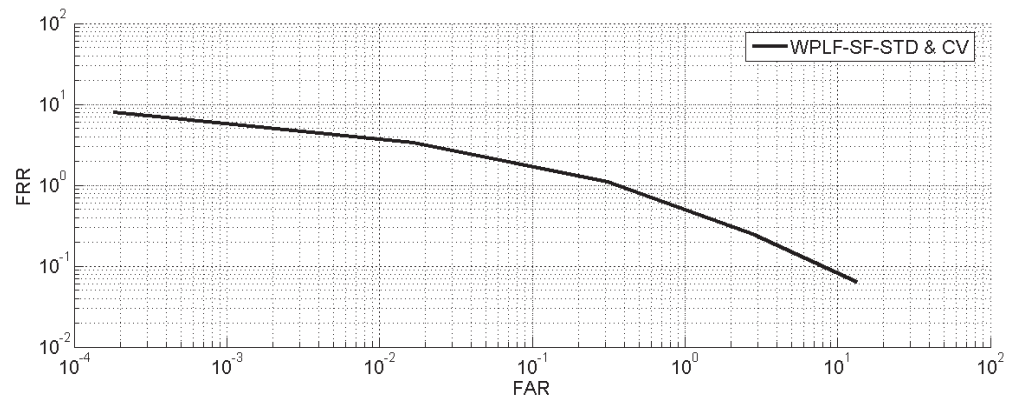
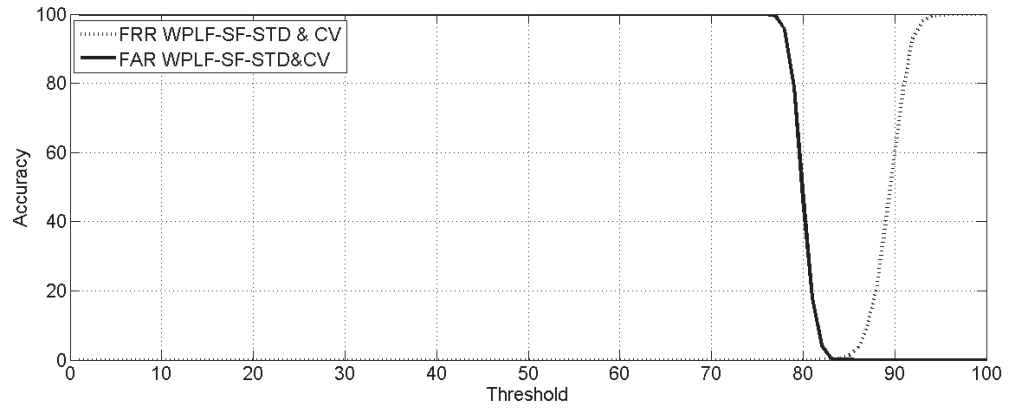
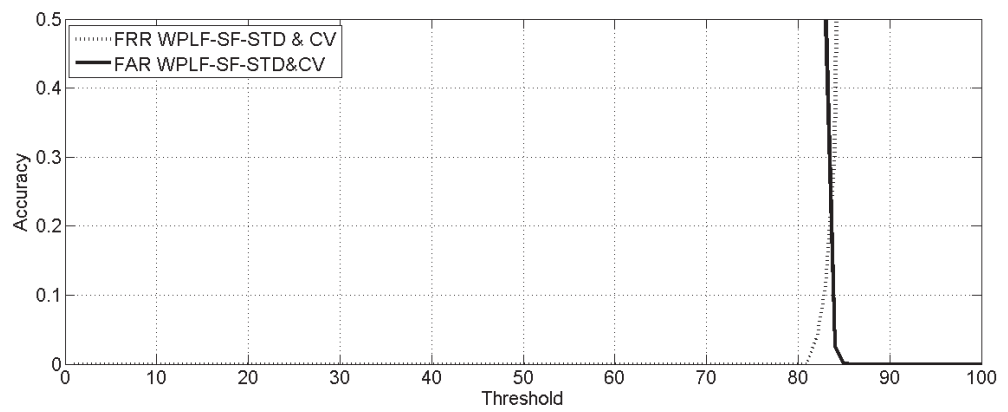


Figure 6.62: ROC curve on data set I of WPLI database using STD & CV as a feature.



(i) Accuracy scaling 0 to 100



(ii) Accuracy scaling 0 to 0.5

Figure 6.63: FAR & FRR representation on data set II of WPLI database using STD & CV as a feature.

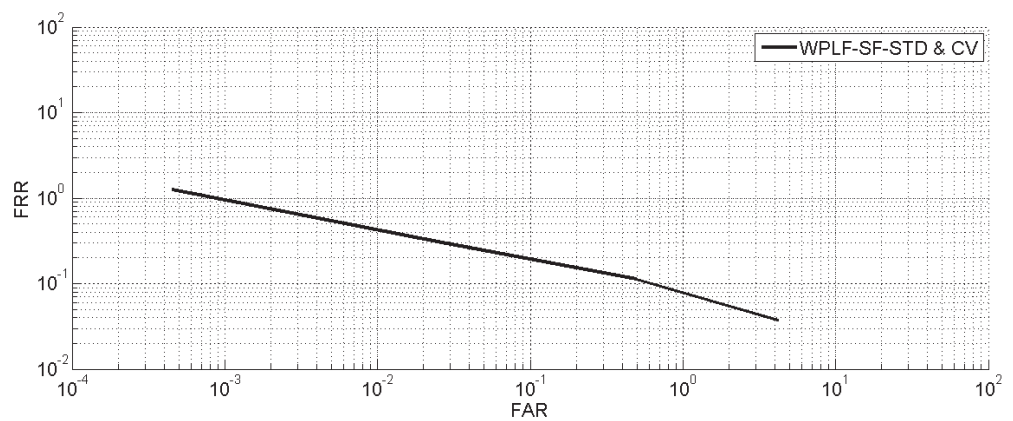
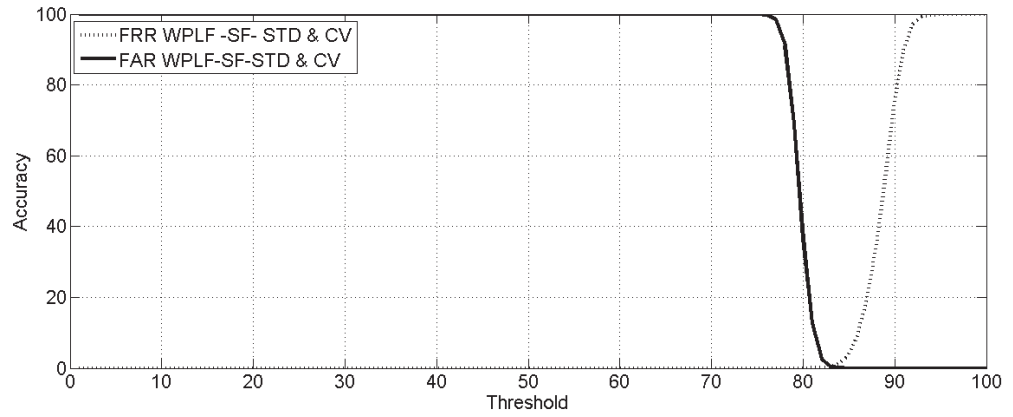
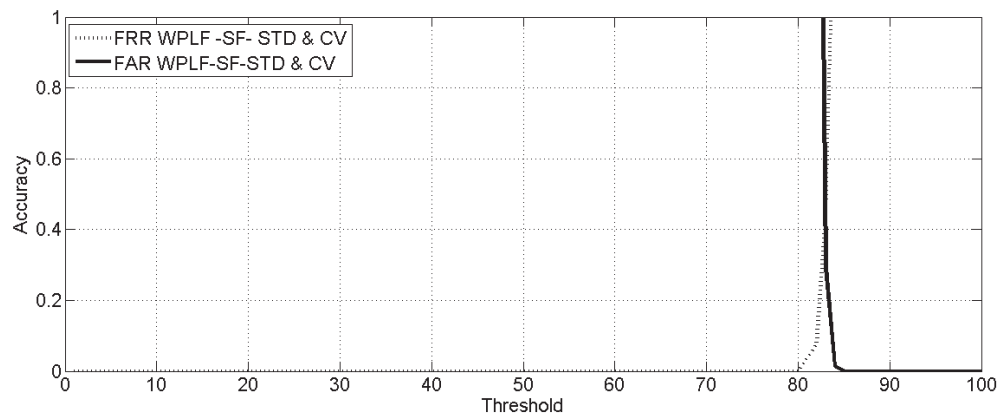


Figure 6.64: ROC curve on data set II of WPLI database using STD & CV as a feature.



(i) Accuracy scaling 0 to 100



(ii) Accuracy scaling 0 to 1

Figure 6.65: FAR & FRR representation on data set III of WPLI database using STD & CV as a feature.

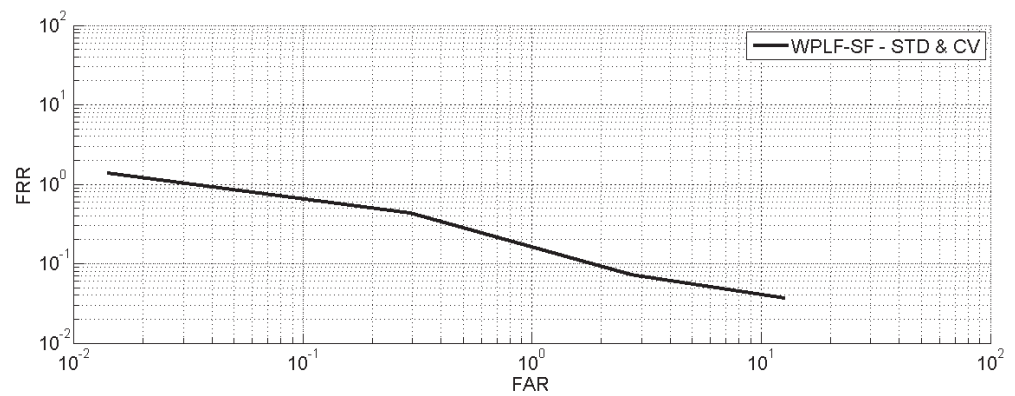


Figure 6.66: ROC curve on data set III of WPLI database using STD & CV as a feature.

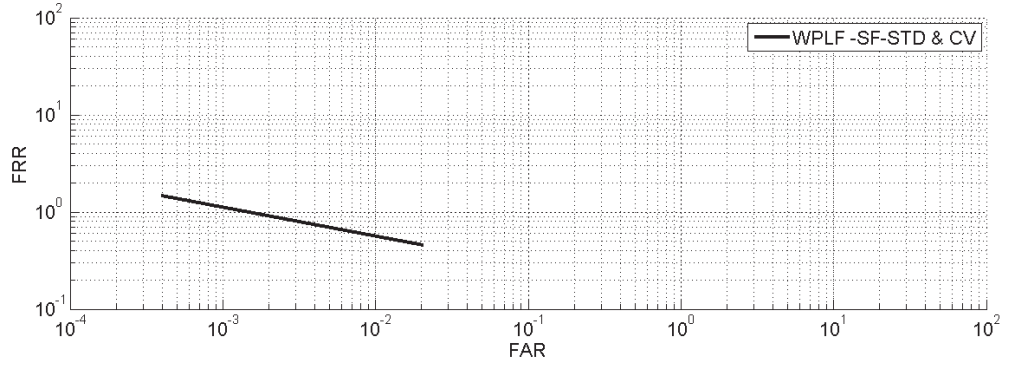
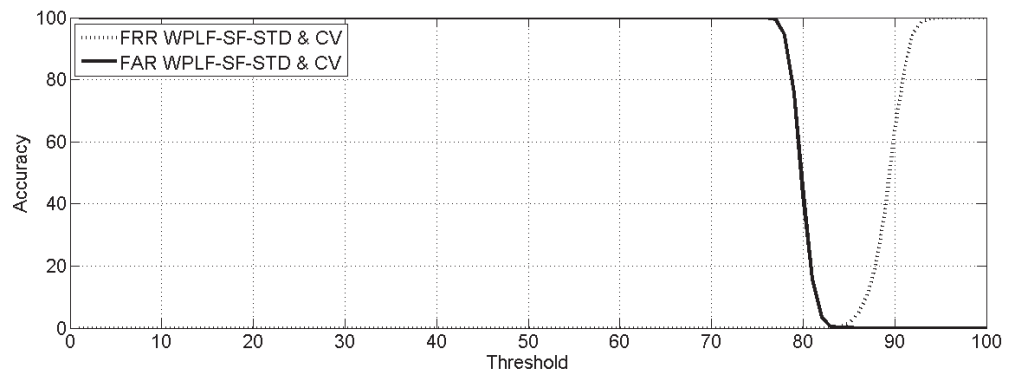
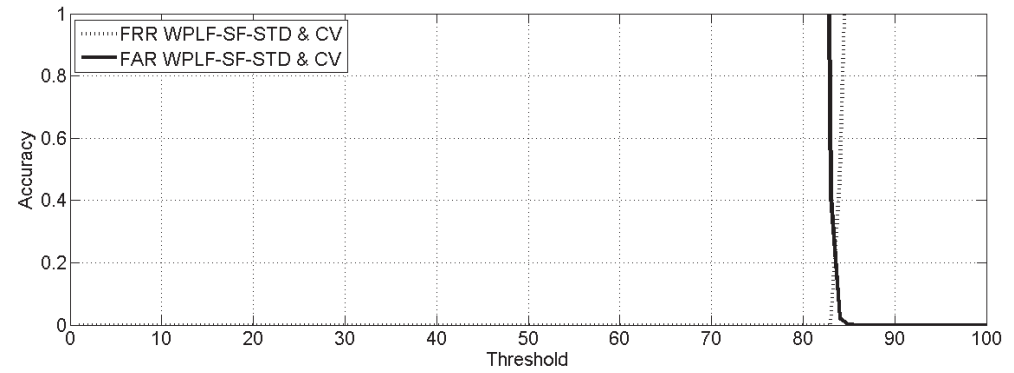


Figure 6.68: ROC curve on data set IV of WPLI database using STD & CV as a feature.



(i) Accuracy scaling 0 to 100

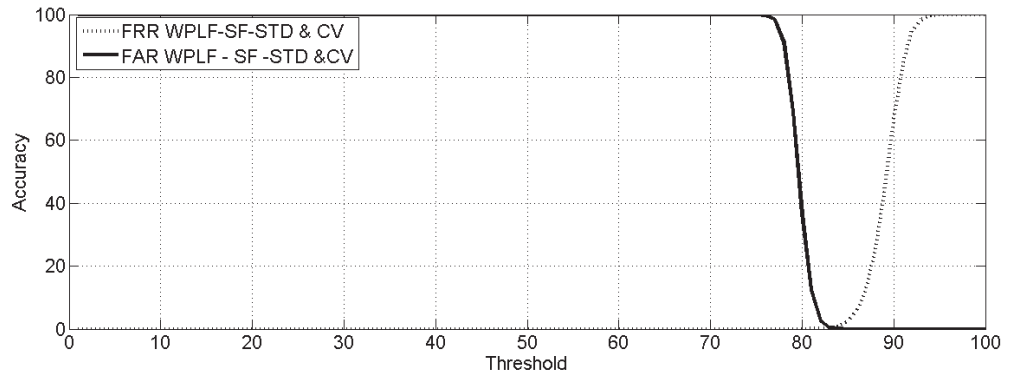


(ii) Accuracy scaling 0 to 1

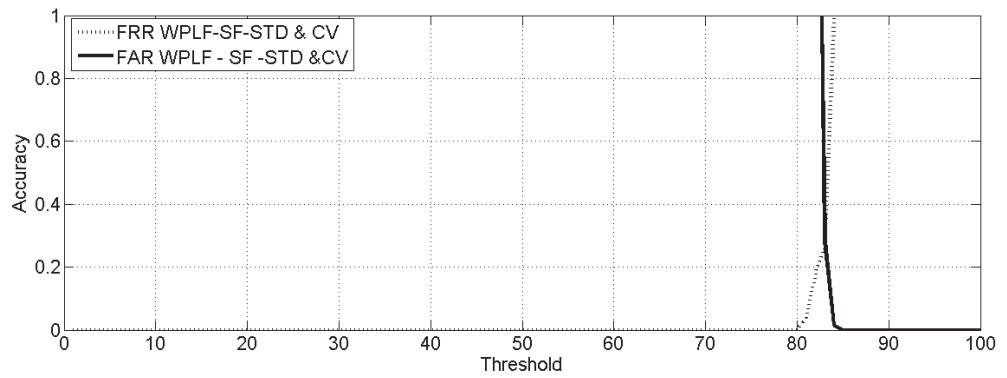
Figure 6.67: FAR & FRR representation on data set IV of WPLI database using STD & CV as a feature.

Palmprint Identification

On data set I, 7612 images are correctly identified, i.e. the CIR is 98.19. On data set II, 3847 images are correctly identified, i.e. the CIR is 99.79. On data set III, 2705



(i) Accuracy scaling 0 to 100



(ii) Accuracy scaling 0 to 1

Figure 6.69: FAR & FRR representation on data set V of WPLI database using STD & CV as a feature.

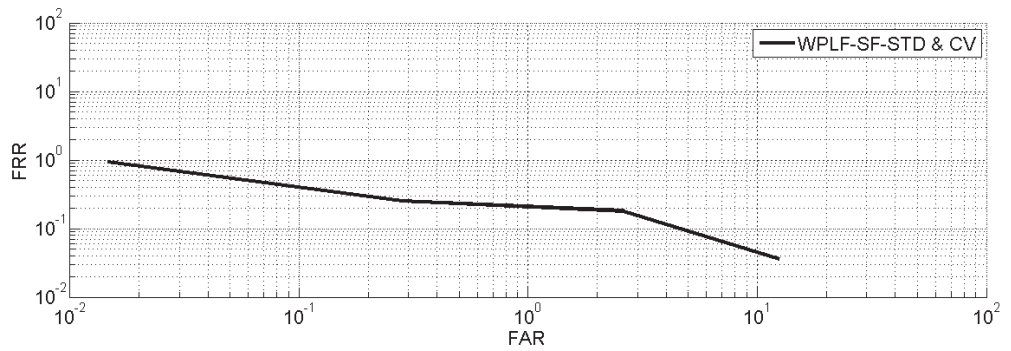


Figure 6.70: ROC curve on data set V of WPLI database using STD & CV as a feature.

images are correctly identified, i.e. the CIR is 99.04. On data set IV, 1957 images are correctly identified, i.e. the CIR is 99.897. On data set V, we run the experiment 20 times and use the mean to denote the identification performance and robustness of the algorithm. The obtained CIR for dynamic WPLI is 99.37. The experimental results are shown in Table 6.10.

The experimental results shows that, statistical features extracted using standard deviation and coefficient of variation from ROI database gives better results compared with statistical features extracted using standard deviation and coefficient of variation from WPLI database. Time taken to generate the FeatureDatabase, parameters estimation dynamically based on the database images (training images) and average time for palmprint identification (in seconds) is given in Table 6.11.

Table 6.11: Time required for identification on WPLI using SF (in seconds)

Data set	FeatureDatabase generation & Parameter estimation			Identification of query WPLI using statistical features		
	STD	CV	STD&CV	STD	CV	STD&CV
Data set I	1128	1411	1327	0.18	0.15	0.14
Data set II	2782	3110	4215	0.17	0.13	0.15
Data set III	637	839	902	0.18	0.11	0.11
Data set IV	2634	6616	2886	0.21	0.17	0.18
Data set V	878	996	984	0.2	0.34	0.37

6.5 Summary

In this chapter we conducted the experiments to prove the effectiveness of the proposed approach. We used the datasets used by the previous researchers [23, 24, 95, 99, 101].

From the experimental results of identification and verification, it can be concluded that the discrimination of wide principal line images and statistical features

are strong and the proposed approach yields a better performance in terms of the CIR and EER compared with existing approaches [23, 24, 95, 99, 101].

.

CHAPTER 7

Conclusions and Future Directions

7.1 Conclusion

In our present work, we have proposed palmprint identification through dynamic ROI. In order to identify the key points, the n-coordinate information of border pixels is used. These key points are used to align the palmprint. The border pixel information is used to localize the ROI. The MaximizeROI algorithm is proposed to extract maximum possible ROI and in the process, reference point information is obtained. Experimental results demonstrated that the proposed approach extracts maximum possible region without background information when compared to the existing fixed [21] and dynamic [16] size ROI extraction techniques on the PolyUPalmprint database.

A set of wide principal line extractors are devised. Later these wide principal line extractors are used to extract the wide principal lines from ROI. To enhance the WPLF, applied the skeleton, dilate and logical AND operators. The obtained WPLIs are stored in the WPLI database. We also proposed statistical feature extraction. The ROI images are segmented into overlapping sub blocks. Later, from each sub block the standard deviation and coefficient of variation are calculated as features. We proposed a common region extraction algorithm based on reference point information from database and query images. We proposed palmprint verification and two-phase palmprint identification algorithms can be applied on WPLF and SF.

The experimental results on verification show that of wide principal line features out performs compared with statistical features. The experimental results also show that the proposed WPLE can extract wide principal lines from palmprints effectively.

From the experimental results of identification, it can be concluded that the discrimination of wide principal lines is also strong and the proposed approach yields a better performance in terms of the correct identification rate compared with existing approaches [23, 24, 61, 62, 66, 95, 99, 101].

From the experimental results on identification using statistical features, it can be understood that the standard deviation and coefficient of variation individually produced good results as compared to previous reported works. It was also observed that CIR can be improved when both the features are applied in combination. From the experimental results it can be concluded that the discrimination of statistical features such as standard deviation and coefficient of variation was strong and the proposed approach yields a better performance in terms of the correct identification rate compared with existing approaches [23, 24, 61, 62, 95, 99, 101].

7.1.1 Papers Published

1. Hemantha Kumar Kalluri, Munaga.V.N.K. Prasad, Arun Agarwal, Dynamic ROI Extraction Algorithm for Palmprints, Third International Conference on Advances in Swarm Intelligence (ICSI 2012), Part II, LNCS 7332, pp. 217-227, 2012.
2. Hemantha Kumar Kalluri, Munaga.V.N.K. Prasad, Arun Agarwal, Palmprint Identification Based on Wide Principal Lines, International Conference on Advances in Computing, Communications and Informatics (ICACCI-2012), pp. 918-924, 2012.
3. Hemantha Kumar Kalluri, Munaga.V.N.K. Prasad, Arun Agarwal, Palmprint Identification and Verification based on wide principal lines through Dynamic ROI, Accepted by International Journal of Biometrics.
4. Homogeneous Two-Phase palmprint identification (to be communicated).

7.2 Future Directions

In future, following directions are suggested:

1. Security and Privacy: to enhance the security and privacy, cancelable palmprint templates to be used. Cancelable templates may be created for palmprint images, and the proposed system to be tested using cancelable templates.
2. Touchless acquisition of palmprints and recognition: proposed approach is tested on PolyUPalmprint database. The proposed approach (verification/identification) to be tested on touchless palmprint databases.
3. Scalability Analysis: proposed approach is tested on PolyUPalmprint database consisting of 7752 images. Proposed system may be tested using large databases, like UIDAI database.
4. Multimodal identification: At the time of palmprint acquisition it is possible to acquire hand geometry, fingerprints and palm vein. So it is possible to design a system using the features of palmprint, hand geometry, fingerprints and palm vein. By using the fusion the system performance may improve (i.e. CIR and DI may increase and EER may decrease).

REFERENCES

- [1] D. Zhang, Palmprint authentication, Kluwer Academic Publishers, 2004.
- [2] D. Zhang, Automated Biometrics: Technologies and Systems, Kluwer Academic Publishers, 2000.
- [3] A. K. Jain, P. Flynn and A. A. Ross, Handbook of Biometrics, Springer Science, Business Media, LLC, 2008.
- [4] K. Jain, R. P. W. Duin and J. Mao, "Statistical pattern recognition: a review," IEEE Transactions on Pattern Analysis and Machine Intelligence, vol. 22, no. 1, pp. 4-37, 2000.
- [5] M. N. Murthy and V. S. Devi, Pattern Recognition an Algorithmic Approach, Springer, Universities Press, 2011.
- [6] A. R. Webb, K. D. Copsey, Statistical Pattern Recognition, 3rd Edition, Wiley Publishers, 2011.
- [7] M. G. Thomson, Syntactic and Structural Pattern Recognition Theory and Applications, World Scientific, vol. 7, 1990.
- [8] S. Robert, Pattern Recognition Statistical, structural and Neural approaches, John Wilkey sons, inc.
- [9] C. M. Bishop, Neural networks for pattern recognition, Clarendon Press, Oxford, 1995.
- [10] D. Maltoni, D. Maio, A. K. Jain and S. Prabhakar, Handbook of Fingerprint Recognition, Springer-verlog, 2009.

- [11] A. K. Jain, A. A. Ross, K. Nanda Kumar, Introduction to Biometrics, Springer Science+Business Media, LLC, 2011.
- [12] B. Yegnanarayana, Artificial Neural Networks, Prentice - Hall, India, 2007.
- [13] R. Brunelli and T. Poggio, "Face recognition: features versus templates," IEEE Transactions on Pattern Analysis and Machine Intelligence, vol. 15, no. 10, pp. 1042-1052, 1993.
- [14] A. Kong, D. Zhang and M. Kamel, "A survey of palmprint recognition," Pattern recognition, vol. 42, no. 7, pp. 1408-1418, 2009.
- [15] W. K. Kong and Z. David, "Palmprint texture analysis based on low-resolution images for personal authentication," in 16th International Conference on Pattern Recognition, pp.807-810, 2002
- [16] J. Kong, Y. Lu, S. Wang, M. Qi and H. Li, "A two stage neural network-based personal identification system using handprint," Neurocomputing, vol. 71, no. 4-6, pp. 641-647, 2008.
- [17] "PolyUPalmprint Database," Honkong Polytechnique University, [Online]. Available: <http://www.comp.polyu.edu.hk/biometrics>
- [18] "CASIA Palmprint Image Database," Center for Biometrics and Security Research, [Online]. Available: "<http://biometrics.idealtest.org/>".
- [19] "IIT Delhi Touch Less Palmprint Database, " IIT Delhi [Online]. Available: http://web.iitd.ac.in/ajaykr/Database_Palm.html.
- [20] D. Zhang, W. K. Kong, J. You and M. Wong, "Online palmprint identification," IEEE Transactions on Pattern Analysis and Machine Intelligence, vol. 25, no. 9, pp. 1041-1050, 2003.
- [21] C.L. Lin, T. C. Chuang and K. C. Fan, "Palmprint verification using hierarchical decomposition," Pattern Recognition, vol. 38, no. 12, pp. 2639-2652, 2005.

- [22] D. S. Huang, W. Jia and D. Zhang, "Palmprint verification based on principal lines," *Pattern Recognition*, vol. 41, no. 4, pp. 1316-1328, 2008.
- [23] A. B. Mansoor, H. Masood, M. Mumtaz and S. A. Khan, "A feature level multimodal approach for palmprint identification using directional subband energies," *Journal of Network and Computer Applications*, vol. 34, no. 1, pp. 159-171, 2011.
- [24] M. Mu, Q. Ruan and S. Guo, "Shift and gray scale invariant features for palmprint identification using complex directional wavelet and local binary pattern," *Neurocomputing*, vol. 74, no. 17, pp. 3351-3360, 2011.
- [25] L. Zhang and D. Zhang, "Characterization of palmprints by wavelet signatures via directional context modeling," *IEEE Transactions on Systems, Man, and Cybernetics- Part B* , vol. 34, no. 3, pp. 1335-1347, 2004.
- [26] X. Wu, D. Zhang and K. Wang, "Palm line extraction and matching for personal authentication," *IEEE Transactions on Systems, Man, and Cybernetics- Part A: Systems and Humans*, vol. 36, no. 5, pp. 978-987, 2006.
- [27] L. Liu, D. Zhang and J. You, "Detecting wide lines using isotropic nonlinear filtering," *IEEE Transactions on Image Processing*, vol. 16, no. 6, pp. 1584-1595, 2007.
- [28] C. C. Han, H. L. Cheng, C. L. Lin and K. C. Fan, "Personal authentication using palm-print features," *Pattern Recognition*, vol. 36, no. 2, pp. 371-381, 2003.
- [29] H. K. Choge, T. Oyama, S. Karungaru, S. Tsuge and M. Fukumi, "A circle-based region of interest segmentation method for palmprint recognition," in *ICROS-SICE international joint conference*, pp. 4993-4997, 2009.
- [30] S. Y. Kung , S. H. Lin and M. Fang, "A neural network approach to face / palm recognition," in *Neural networks for signal processing*, Cambridge, MA, pp. 323-332, 1995.

- [31] W. W. Boles and S. Y. T. Chu, "Personal identification using images of the human palm," in IEEE TENCON - Speech and Image Technologies for Computing and Telecommunications , pp. 295-298, 1997.
- [32] J. Doi and M. Yamanaka, "Personal authentication using feature points on finger and palmar creases," in 32nd Applied Imagery Pattern Recognition Workshop, pp. 282-287, 2003.
- [33] W. Shu and D. Zhang, "Automated personal identification by palmprint," Optical Engineering, vol. 37, no. 8, pp. 2359-2362, 1998.
- [34] N. Duta, A. K. Jain and K. V. Mardia, "Matching of palmprints," Pattern Recognition Letters, vol. 23, no. 23, pp. 477-485, 2002.
- [35] A. W. K. Kong, D. Zhang and G. Lu, "A study of identical twin's palmprints for personal verification," Pattern Recognition, vol. 39, no. 11, pp. 2149-2156, 2006.
- [36] J. You, W. K. Kong, D. Zhang and K. H. Cheung, "On hierarchical palmprint coding with multiple features for personal identification in large databases," IEEE Transactions on Circuits and Systems for Video Technology, vol. 14, no. 2, pp. 234-243, 2004.
- [37] G. Feng, K. Dong, D. Hu and D. Zhang, "When faces are combined with palmprints: a novel biometric fusion strategy," in International Conference on Biometric Authentication (ICBA), pp. 701-707, 2004.
- [38] X. Wu, K. Wang and D. Zhang, "Palmprint authentication based on orientation code matching," in 5th International Conference on Audio and Video based Biometric Person Authentication, pp. 555-562, 2005.
- [39] A. W. K. Kong and D. Zhang, "Feature-level fusion for effective palmprint authentication," in International Conference on Biometric Authentication (ICBA), pp. 761-767, 2004.

- [40] X. Wu, D. Zhang and K. Wang, "A palmprint cryptosystem," in International Conference on Advances in Biometrics," pp. 1035-1042, 2007.
- [41] X. Wu, D. Zhang, K. Wang and N. Qi, "Fusion of palmprint and iris for personal authentication," in 3rd International Conference on Advanced Data Mining and Applications, pp. 466-475, 2007.
- [42] L. Zhang, Z. Guo, Z. Wang and D. Zhang, "Palmprint verification using complex wavelet transform," in IEEE International Conference on Image Processing, pp. 417-420, 2007.
- [43] J. Lu, Y. Zhao, Y. Xue and J. Hu, "Palmprint recognition via locality preserving projections and extreme learning machine neural network," in 9th International Conference on Signal Processing, pp. 2096-2099, 2008.
- [44] A. Kong, D. Zhang and M. Kamel, "Palmprint identification using feature-level fusion," Pattern Recognition, vol. 39, pp. 478-487, 2006.
- [45] W. Jia, B. Ling, K. W. Chau and L. Heutte, "Palmprint identification using restricted fusion," Applied Mathematics and Computation, vol. 205, no. 2, pp. 927-934, 2008.
- [46] X. Y. Jing, Y. F. Yao, D. Zhang, J. Y. Yang and M. Li, "Face and palmprint pixel level fusion and Kernel DCV-RBF classifier for small sample biometric recognition," Pattern Recognition, vol. 40, no. 11, pp. 3209-3224, 2007.
- [47] Z. Q. Zhao, D. S. Huang and W. Jia, "Palmprint recognition with 2DPCA+PCA based on modular neural networks," Neurocomputing, vol. 71, no. 1-3, pp. 448-454, 2007.
- [48] A. Kong, D. Zhang and M. Kamel, "Three measures for secure palmprint identification," Pattern Recognition, vol. 41, no. 4, pp. 1329-1337, 2008.
- [49] Y. Xu, D. Zhang and J. Y. Yang, "A feature extraction method for use with bimodal biometrics," Pattern Recognition, vol. 43, no. 3, pp. 1106-1115, 2010.

- [50] J. Xu and J. Yang, "A nonnegative sparse representation based fuzzy similar neighbor classifier," *Neurocomputing*, vol. 99, pp. 76-86, 2013.
- [51] Y. Xu, Z. Fan, M. Qiu, D. Zhang and Z. Y. Yang, "A sparse representation method of bimodal biometrics and palmprint recognition experiments," *Neurocomputing*, vol. 103, pp. 164-171, 2013.
- [52] A. Kumar, D. C. M. Wong, H. C. Shen and A. K. Jain, "Personal verification using palmprint and hand geometry biometric," in *4th International Conference on Audio and video based Biometric Person Authentication*, 2003.
- [53] X. Wu, K. Wang and D. Zhang, "HMMs Based Palmprint Identification," in *ICBA, LNCS 3072*, pp. 775-781, 2004.
- [54] X. Pan and Q. Q. Ruan, "A modified preprocessing method for palmprint recognition," in *8th International Conference on Signal Processing*, 2006
- [55] P. Shang and T. Li, "Multifractal characteristics of palmprint and its extracted algorithm," *Applied Mathematical Modelling*, vol. 33, no. 12, pp. 4378-4387, 2009.
- [56] F. Yue, W. Zuo, D. Zhang and K. Wang, "Orientation selection using modified FCM for competitive code-based palmprint recognition," *Pattern Recognition*, vol. 42, no. 11, pp. 2841-2849, 2009.
- [57] J. Chen, Y. S. Moon, M. F. Wong and G. Su, "Palmprint authentication using a symbolic representation of images," *Image and Vision Computing*, vol. 28, no. 3, pp. 343-351, 2010.
- [58] T. Connie, A. T. B. Jin, M. G. K. Ong and D. N. C. Ling, "An automated palmprint recognition system," *Image and Vision Computing*, vol. 23, no. 5, pp. 501-515, 2005.
- [59] T. Savic and N. Pavesic, "Personal recognition based on an image of the palmar surface of the hand," *Pattern Recognition*, vol. 40, no. 11, pp. 3152-3163, 2007.

- [60] G.K. O. Michael, T. Connie and A. B. J. Teoh, "Touch-less palmprint biometrics: novel design and implementation," *Image and Vision Computing*, vol. 26, no. 12, pp. 1551-1560, 2008.
- [61] G. S. Badrinath and P. Gupta, "Stockwell transform based palm-print recognition," *Applied Soft Computing*, vol. 11, no. 7, pp. 4267-4281, 2011.
- [62] G. S. Badrinath and P. Gupta, "Palmprint based recognition system using phase-difference information," *Future Generation Computer Systems*, vol. 28, no. 1, pp. 287-305, 2012.
- [63] M. P. Dale , M. A. Joshi and N. Gilda, "Texture based palmprint identification using DCT features," in *Seventh International Conference on Advances in Pattern Recognition*, pp. 221-224, 2009.
- [64] J. GUO, Y. LIU and W. YUAN, "Palmprint recognition using local information from a single image per person," *Journal of Computational Information Systems*, vol. 8, no. 8, pp. 3199-3206, 2012.
- [65] D. Zhang and W. Shu, "Two novel characteristics in palmprint verification: datum point invariance and line feature matching," *Pattern Recognition*, vol. 32, no. 4, pp. 691-702, 1999.
- [66] D. ZHANG, W. ZUO and F. YUE, "A comparative study of palmprint recognition algorithms," *ACM Computing Surveys*, vol. 44, no. 1, pp. 2.1-2.37, 2012.
- [67] X. Q. Wu, K. Q. Wang and D. Zhang, "Wavelet based palmprint recognition," in *first international conference on machine learning and cybernetics*, pp. 1253-1257, 2002.
- [68] X. Wu and K. Wang, "A novel approach of palm-line extraction," in *Third International Conference on Image and Graphics (ICIG'04)*, 2004.
- [69] X. Wu, D. Zhang, K. Wang and B. Huang, "Palmprint classification using principal lines," *Pattern Recognition*, vol. 37, no. 10, pp. 1987-1998, 2004.

- [70] X. Wu, K. Wang and D. Zhang, "Palmprint recognition using directional line energy feature," in 17th International Conference on Pattern Recognition, 2004.
- [71] A. Negi, B. Panigrahi, M. V. K. Prasad and M. Das, "A palmprint classification scheme using heart line feature extraction," in 9th International Conference on Information Technology, 2006.
- [72] T. Cook, R. Sutton and K. Buckley, "Automated flexion crease identification using internal image seams," Pattern Recognition, vol. 43, no. 3, pp. 630-635, 2010.
- [73] X. Pan and Q. Q. Ruan, "Palmprint recognition using Gabor-based local invariant features," Neurocomputing, vol. 72, no. 7-9, pp. 2040-2045, 2009.
- [74] M. Mu and Q. Ruan, "Mean and standard deviation as features for palmprint recognition based on Gabor filters," International Journal of Pattern Recognition and Artificial Intelligence, vol. 25, pp. 491-512, 2011.
- [75] W. K. Kong, D. Zhang and W. Li, "Palmprint feature extraction using 2-D gabor filters," Pattern Recognition, vol. 36, no. 10, pp. 2339-2347, 2003.
- [76] G. Lu, D. Zhang and K. Wang, "Palmprint recognition using eigenpalms features," Pattern Recognition Letters, vol. 24, no. 9-10, pp. 1463-1467, 2003.
- [77] Y. H. Pang, T. Connie, A. T. B. Jin and D. N. C. Ling, "Palmprint authentication with zernike moment invariants," in 3rd IEEE International Symposium on Signal Processing and Information Technology, pp. 199-202, 2003.
- [78] G.M. Lu, K. Q. Wang and D. Zhang, "Wavelet based independent component analysis for Palmprint identification," in Third International Conference on Machine Learning and Cybernetics, pp. 3547-3550, 2004.
- [79] Y. Li, K. Wang and D. Zhang, "Palmprint recognition based on translation invariant zernike moments and modular neural network," in Second International Conference on Advances in Neural Networks, pp.177-182, 2005.

- [80] W. Zuo, D. Zhang and K. Wang, "Bidirectional PCA with assembled matrix distance metric for image recognition," IEEE Transactions on Systems, Man, and Cybernetics- Part B: Cybernetics, vol. 36, no. 4, pp. 863-872, 2006.
- [81] G. Feng, D. Hu, D. Zhang and Z. Zhou, "An alternative formulation of kernel LPP with application to image recognition," Neurocomputing, vol. 69, no. 13-15, pp. 1733-1738, 2006.
- [82] X. Wang, H. Gong, H. Zhang, B. Li and Z. Zhuang, "Palmprint identification using boosting local binary pattern," in The 18th International Conference on Pattern Recognition, 2006.
- [83] L. Shang, D. S. Huang, J. X. Du and C. H. Zheng, "Palmprint recognition using FastICA algorithm and radial basis probabilistic neural network," Neurocomputing, vol. 69, no. 13-15, pp. 1782-1786, 2006.
- [84] D. Hu, G. Feng and Z. Zhou, "Two-dimensional locality preserving projections (2DLPP) with its application to palmprint recognition," Pattern Recognition, vol. 40, no. 1, pp. 339-342, 2007.
- [85] G. Y. Chen and W. F. Xie, "Pattern recognition with SVM and dual-tree complex wavelets," Image and Vision Computing, vol. 25, no. 6, pp. 960-966, 2007.
- [86] X. Pan and Q. Q. Ruan, "Palmprint recognition using Gabor feature-based $(2D)^2$ PCA," Neurocomputing, vol. 71, no. 13-15, pp. 3032-3036, 2008.
- [87] H. Masood, M. Mumtaz, M. A. A. Butt, A. B. Mansoor and S. A. Khan, "Wavelet based palmprint authentication system," in International Symposium on Biometrics and Security Technologies, 2008.
- [88] X. Pan and Q. Q. Ruan, "Palmprint recognition with improved two-dimensional locality preserving projections," Image and Vision Computing, vol. 26, no. 9, pp. 1261-1268, 2008.

- [89] M. A. Butt, H. Masood, M. Mumtaz, A. B. Mansoor and S. A. Khan, "Palmprint identification using Contourlet transform," in *2nd IEEE International Conference on Biometrics: Theory, Applications and Systems*, 2008.
- [90] L. Nanni and A. Lumini, "Wavelet decomposition tree selection for palm and face authentication," *Pattern Recognition Letters*, vol. 29, no. 3, pp. 343-353, 2008.
- [91] A. W. K. Kong and D. Zhang, "Competitive Coding Scheme for Palmprint Verification," in *17th International Conference on Pattern Recognition*, 2004.
- [92] M. Wan, Z. Lai, J. Shao and Z. Jin, "Two-dimensional local graph embedding discriminant analysis (2DLGEDA) with its application to face and palm biometrics," *Neurocomputing*, vol. 73, no. 1-3, pp. 197-203, 2009.
- [93] C. L. Su, "Palm-print recognition by matrix discriminator," *Expert Systems with Applications*, vol. 36, no. 7, pp. 10259-10265, 2009.
- [94] G. Y. Chen and B. Kegl, "Invariant pattern recognition using Contourlets and AdaBoost," *Pattern Recognition*, vol. 43, no. 3, pp. 579-583, 2010.
- [95] G. S. Badrinath, N. K. Kachhi and P. Gupta, "Verification system robust to occlusion using low-order Zernike moments of palmprint sub-images," *Telecommun Syst*, vol. 47, pp. 275-290, 2011.
- [96] F. Yue, W. Zuo, D. Zhang and B. Li, "Fast palmprint identification with multiple templates per subject," *Pattern Recognition Letters*, vol. 32, no. 8, pp. 1108-1118, 2011.
- [97] B. Zhang, Y. Gao and H. Zheng, "Local kernel feature analysis (LKFA) for object recognition," *Neurocomputing*, vol. 74, no. 4, pp. 575-579, 2011.
- [98] Z. Lai, M. Wan, Z. Jin and J. Yang, "Sparse two-dimensional local discriminant projections for feature extraction," *Neurocomputing*, vol. 74, no. 4, pp. 629-637, 2011.

- [99] W. Xuan , L. Li and W. Mingzhe, "Palmprint verification based on 2D-gabor wavelet and pulse-coupled neural network," *Knowledge-Based Systems*, vol. 27, pp. 451-455, 2012.
- [100] H. Imtiaz and S. A. Fattah, "A wavelet-based dominant feature extraction algorithm for palmprint recognition," *Digital Signal Processing*, vol. 23, no. 1, pp. 244-258, 2013.
- [101] W. Xuan, L. Junhua and W. Minghe, "On-line fast palmprint identification based on adaptive lifting wavelet scheme," *Knowledge-based systems*, vol. 42, pp. 68-73, 2013.
- [102] G. Y. Chen, T. D. Bui and A. Krzyzak, "Palmprint classification using dual-tree complex wavelets," in *IEEE International Conference on Image Processing*, pp. 2645-2648, 2006.
- [103] Y. Wang, Q. Ruan and X. Pan, "Palmprint recognition method using dual-tree complex wavelet transform and local binary pattern histogram," in *Intelligent Signal Processing and Communication Systems*, pp. 646-649, 2007.
- [104] W. Zuo, H. Zhang, D. Zhang and K. Wang, "Post-processed LDA for face and palmprint recognition: what is the rationale," *Signal Processing*, vol. 90, no. 8, pp. 2344-2352, 2010.
- [105] Z. Guo, W. Zuo, L. Zhang and D. Zhang, "A unified distance measurement for orientation coding in palmprint verification," *Neurocomputing*, vol. 73, no. 4-6, pp. 944-950, 2010.
- [106] J. Lu and Y. P. Tan, "Improved discriminant locality preserving projections for face and palmprint recognition," *Neurocomputing*, vol. 74, no. 18, pp. 3760-3767, 2011.
- [107] J. Yin, Z. Liu, Z. Jin and W. Yang, "Kernel sparse representation based classification," *Neurocomputing*, vol. 77, no. 1, pp. 120-128, 2012.

- [108] T. Connie , A. Teoh, M. Goh and D. Ngo, "PalmHashing: a novel approach for cancelable biometrics," *Information Processing Letters*, no. 1, vol. 93, pp. 1-5, 2005.
- [109] F. Yue, W. Zuo, "Consistency analysis on orientation features for fast and accurate palmprint identification," *Information Sciences*, vol. 268, pp. 78-90, 2014.
- [110] D. Hong, Z. Pam, X. Wu, "Improved differential box counting with multi-scale and multi-direction: A new palmprint recognition method," *Optical*, vol. 125, no. 15, pp. 4154-4160, 2014.
- [111] X.Wu, Q. Zhao, W. Bu, "A SIFT-based contactless palmprint verification approach using iterative RANSAC and local palmprint descriptors," *Pattern Recognition*, vol. 47, no. 10, pp. 3314-3326, 2014.
- [112] Guo, W. Zhou, Y. Wang, "Palmprint recognition algorithm with horizontally expanded blanket dimension," *Neurocomputing*, vol. 127, no. 15, pp. 152-160, 2014.
- [113] S. Ribaric, D. Ribaric and N. Pavesic, "Multimodal biometric user-identification system for network-based applications," *Vision, Image and Signal Processing, IEE Proceedings*, vol. 150, no. 6, pp. 409-416, 2003.
- [114] C. C. Han, "A hand-based personal authentication using a coarse-to-fine strategy," *Image and Vision Computing*, vol. 22, no. 11, pp. 909-918, 2004.
- [115] C. Poon, D. C. M. Wong and H. C. Shen , "Personal identification and verification: fusion of palmprint representations," in *International Conference on Biometric Authentication (ICBA)*, pp. 782-788, 2004.
- [116] Q. Li, Z. Qiu and D. Sun , "Feature-level fusion of hand biometrics for personal verification based on Kernel PCA," in *International Conference on Biometrics*, pp. 744-750, 2005.

- [117] A. Kumar and D. Zhang, "Personal authentication using multiple palmprint representation," *Pattern Recognition*, vol. 38, no. 10, pp. 1695-1704, 2005.
- [118] S. Ribaric and I. Fratric, "A biometric identification system based on eigenpalm and eigenfinger features," *IEEE transactions on pattern analysis and machine intelligence*, vol. 27, no. 11, pp. 1698-1709, 2005.
- [119] A. Kumar, D. C. Wong, H. C. Shen and A. K. Jain, "Personal authentication using hand images," *Pattern Recognition Letters*, vol. 27, no. 13, p. 1478-1486, 2006.
- [120] R. M. Haralick and L. G. Shapiro , *Computer and Robot Vision*, Addison-Wesley, 1991.
- [121] A. Kumar and D. Zhang, "Personal recognition using hand shape and texture," *IEEE transactions on image processing*, vol. 15, no. 8, pp. 2454-2461, 2006.
- [122] L. Shang, D. S. Huang, J. X. Du and Z. K. Huang , "Palmprint recognition using ICA based on winner-take-all network and radial basis probabilistic neural network," in *Third international conference on Advances in Neural Networks*, pp. 216-221, 2006.
- [123] F. Yang, B. Ma, Q. X. Wang, D. Yao, C. Fang, S. Zhao and X. Zhou, "Information fusion of biometrics based-on fingerprint, hand-geometry and palm-print," in *IEEE Workshop on Automatic Identification Advanced Technologies*, pp. 247-252, 2007.
- [124] Y. F. Yao, X. Y. Jing and H. S. Wong, "Face and palmprint feature level fusion for single sample biometrics recognition," *Neurocomputing*, vol. 70, no. 7-9, pp. 1582-1586, 2007.
- [125] J. G. Wang, W. Y. Yau, A. Suwandy and E. Sung, "Person recognition by fusing palmprint and palm vein images based on Laplacianpalm representation," *Pattern Recognition*, vol. 41, no. 5, pp. 1514-1527, 2008.

- [126] J. Bhatnagar and A. Kumar, "On estimating performance indices for biometric identification," *Pattern Recognition*, vol. 42, no. 9, pp. 1803-1815, 2009.
- [127] D. Zhang, Z. Guo, G. Lu, L. Zhang, Y. Liu and W. Zuo, "Online joint palmprint and palmvein verification," *Expert Systems with Applications*, vol. 38, no. 3, pp. 2621-2631, 2011.
- [128] M. Sonka, V. Hlavac and R. Boyle, *Image Processing, Analysis, and Machine Vision*, Books/cole publishing company, 1999.
- [129] K. Wang, J. Liao, X. Wu and H. Zhang, "Recognize a special structure in palmprint for palm medicine," in *Twentieth IEEE international symposium on computer-based medical systems (CBMS'07)*, 2007.
- [130] Haralick, Robert M., and Linda G. Shapiro, *Computer and Robot Vision*, Volume I, Addison-Wesley, 1992.
- [131] R. C. Gonzalez, R. E. Woods, S. L. Eddins, *Digital Image Processing Using MATLAB*, Gatesmark Publishing, 2009.
- [132] F. Matus, J. Flusser, "Image representations via a Finite Radon Transform," *IEEE Transactions on Pattern analysis and Machine Intelligence*, vol. 15, no 10, 1993.
- [133] L. Lam, S-W. Lee, C. Y. Suen, "Thinning methodologies - a comprehensive survey", *IEEE Transactions on Pattern Analysis and Machine Intelligence*, vol. 14, no. 9, 1992.
- [134] G. Jurman, S. Riccadonna, R. Visintainer and C. Furlanello, "Canberra distance on ranked lists," in *Advances in Ranking NIPS*, 2009.
- [135] T. K. Moon, *The Expectation-Maximization Algorithm*, *IEEE Signal Processing Magazine*, vol.13, no. 6, pp. 47-60, 1996.
- [136] A. K. Jain, P. Flynn, Arun A. Ross, *Handbook of Biometrics*, Springer Science Business Media, LLC, 2008.